



Novel Syntheses of Porphyrazine-Phthalocyanine Hybrids

Norah Mohammad Almanei

This thesis is submitted in partial fulfilment of the requirements of the degree of Doctor of Philosophy at the University of East Anglia.

2024

©This copy of the thesis has been supplied on condition that anyone who consults it is understood to recognise that its copyright rests with the author and that no quotation from the thesis, nor any information derived therefrom, may be published without the author's prior written consent.

Declaration

The research described in this thesis is, to the best of my knowledge, original and my own work except where due reference has been made.

Norah Almanei
2024

I dedicate this thesis to my dear mother and my loving family.

Abstract

Porphyrazines Pzs, are intermediate structures between phthalocyanines and porphyrines, each bearing the same core but with phthalocyanines having benzo-fusion on each pyrrolic unit. Phthalocyanine and porphyrin hybrids, where mixtures of C and N bridges exist, have received significant attention over recent years, in part due to the synthetic breakthroughs achieved by our group at UEA. However, C/N hybrid systems are still rare, and C/N porphyrazine-phthalocyanine hybrids (mixed C/N bridges and partial benzo-fusion) are unknown, to the best of our knowledge.

The research by the Cammidge group has reported a new synthetic pathway involving the use of an AB dimer intermediate (formed from an aminoisoindoline and phthalonitrile) for the synthesis of *meso*-aryl tetrabenzotriazaporphyrins TBTAPs. In this study, we have employed a similar synthetic strategy to investigate and develop new porphyrazine hybrid derivatives. The synthesis described in Chapter 2 is based on the formation of key AB dimer intermediates from *trans*-2,3-diphenyldinitrile derivatives starting materials, which are reacted with aminoisoindoline precursors. This dimer undergoes self-condensation in the presence of a Magnesium or Zinc template to give mixtures of M-porphyrazine complexes (unsymmetrical and symmetrical Pzs ABBA, ABBB-Ar, ABBB-N and BBBB), which were isolated and purified.

The work culminated in the successful synthesis, purification, and characterisation of a wide array of porphyrazine hybrids using NMR spectroscopy, MALDI-TOF mass spectrometry, X-ray crystallography, and UV-Vis absorption spectroscopy, and experimental details are recorded in Chapter 3. Of particular note is the first direct observation of benzyl elimination during macrocyclization. While this step has been inferred from other syntheses of related hybrids, the observation of a mono-benzofused, all-N hybrid proves this process can operate under the reaction conditions.

Access Condition and Agreement

Each deposit in UEA Digital Repository is protected by copyright and other intellectual property rights, and duplication or sale of all or part of any of the Data Collections is not permitted, except that material may be duplicated by you for your research use or for educational purposes in electronic or print form. You must obtain permission from the copyright holder, usually the author, for any other use. Exceptions only apply where a deposit may be explicitly provided under a stated licence, such as a Creative Commons licence or Open Government licence.

Electronic or print copies may not be offered, whether for sale or otherwise to anyone, unless explicitly stated under a Creative Commons or Open Government license. Unauthorised reproduction, editing or reformatting for resale purposes is explicitly prohibited (except where approved by the copyright holder themselves) and UEA reserves the right to take immediate 'take down' action on behalf of the copyright and/or rights holder if this Access condition of the UEA Digital Repository is breached. Any material in this database has been supplied on the understanding that it is copyright material and that no quotation from the material may be published without proper acknowledgement.

Table of Contents

Abstract	iii
Table of Contents	iv
List of Abbreviations.....	viii
Acknowledgements	xi
Chapter 1: Introduction	1
1.1 History of porphyrin.	2
1.2 Structure of porphyrin.....	2
1.3 Synthesis of porphyrin.	3
1.3.1 Synthesis of <i>meso</i> and β -substituted porphyrins.....	4
1.3.1.1 From benzaldehyde and pyrrole (the Rothmund method).....	4
1.3.1.2 The Adler synthesis.....	4
1.3.1.3 Lindsey method.....	5
1.3.1.4 Synthesis of symmetrically beta-substituted porphyrins.....	5
1.4 Spectroscopic properties of porphyrins.....	6
1.4.1 UV-Vis spectroscopy.....	6
1.4.2 ^1H NMR spectroscopy.	7
1.5 History of phthalocyanine and terabenzotriazaporphyrin.	8
1.5.1 Synthesis of phthalocyanine.	9
1.5.1.1 From phthalonitrile 1.11	10
1.5.1.2 From phthalic anhydride 1.12 and urea.....	11
1.5.1.3 From 1, 3-diiminoisindoline 1.13	11
1.5.1.4 From phthalimide 1.14	12
1.5.1.5 From phthalic acid 1.16	13
1.5.1.6 Synthesis of metal-free phthalocyanine using sodium alkoxides... 13	
1.5.2 Synthesis of tetrabenzotriazaporphyrin (TBTAP).	14
1.5.2.1 Synthesis of TBTAP using mixed cyclization of phthalonitrile, methylenephthalimidine, and phthalimidine acetic acid.	14
1.5.2.2 Synthesis of TBTAP by mixed cyclization reaction of phthalimidine derivatives.	14
1.5.2.3 Synthesis of TBTAP using Grignard reagents.	15
1.5.2.4 Using aminoisindoline precursors.....	17
1.5.2.5 Synthesis of TBTAP using aminoisindoline dimer (AB dimer). . 18	
1.6 History of porphyrazine.	19
1.6.1 Synthesis of symmetrical and unsymmetrical porphyrazines (Pzs).....	21
1.6.1.1 Synthesis of symmetrical porphyrazines (Pzs).	22
1.6.1.2 Synthesis of unsymmetrical porphyrazine (porphyrazine/ phthalocyanine) complexes.....	26
1.7 Properties of phthalocyanines/porphyrazines.	34
1.7.1 Electronic absorption spectroscopy.	34
1.8 Applications.	37
1.8.1 Photodynamic therapy (PDT) applications.....	37
1.8.2 Antimicrobial applications in PDT.....	38
1.8.3 Catalytic applications.....	40
1.8.4 Solar energy conversion and dye applications.....	41

1.9	Aim of the project.....	43
Chapter 2: Results and Discussion		44
2.1	Introduction.....	45
2.2	Synthesis of [20-(4-methoxyphenyl)-tetrabenzob[<i>b, g, q, l</i>]-5, 10, 15-triaza-porphyrinato] magnesium “ <i>meso</i> -(4-methoxyphenyl) TBTAP Mg)” from aminoisoindoline.....	46
2.2.1	Synthesis of <i>o</i> -Bromobenzamidinium 2.3	46
2.2.2	Synthesis of (<i>Z</i>)-1-(4-methoxyphenylmethylene)-1 <i>H</i> -isoindol-3-amine 2.4	47
2.2.3	Synthesis of [20-(4-methoxyphenyl)-tetrabenzob[<i>b, g, q, l</i>]-5, 10, 15-triazaporphyrinato] magnesium 2.6	49
2.3	Synthesis of porphyrazine Mg hybrids from dinitrile derivatives.....	51
2.3.1	Synthesis of bis-(4-methoxyphenyl)-dicyanoethylene 2.8	51
2.3.2	Synthesis of octa(4-methoxyphenyl) porphyrazine Mg (II) 2.9	53
2.4	Synthesis of porphyrazine hybrids from aminoisoindoline (A) and dinitrile (B) derivatives.....	57
2.4.1	Self-condensation mechanism for aminoisoindoline forming dimers.....	59
2.5	Employing a reactive “ <i>cis</i> ” intermediate.....	63
2.5.1	Synthesis of dimethoxypyrrole intermediate derivative 2.13	63
2.5.2	Synthesis of ethylenedioxy pyrrole intermediate derivative 2.16	68
2.6	Syntheses of porphyrazine hybrids from (AB dimer) intermediate.....	69
2.6.1	Synthesis of 4-methoxyphenyl-substituted AB dimer intermediate 2.17	70
2.6.2	Synthesis of Mg-porphyrazine hybrids from novel AB intermediates.....	70
2.6.3	Characterization of the prepared target hybrids.....	76
2.6.4	Synthesis of Zn-porphyrazine hybrids from (AB dimer) intermediate.....	83
2.6.5	Synthesis of 4-methoxyphenyl-substituted Zn-Pz/Pc hybrids from dimer 2.17	84
2.6.6	Results and yields.....	87
2.7	Synthesis of (Zn)-porphyrazine/phthalocyanine hybrids – varying the β -aryl substituents.....	87
2.7.1	Synthesis of <i>t</i> -butyl-substituted dinitrile 2.23	87
2.7.2	Synthesis of <i>t</i> -butyl phenyl-substituted (AB dimer) 2.27	88
2.7.3	Synthesis of <i>t</i> -butyl phenyl Pz/Pc hybrids.....	92
2.7.4	Synthesis of isopropoxyphenyl substituted dinitrile 2.24	96
2.7.5	Synthesis of isopropoxyphenyl substituted (AB dimer) 2.35	99
2.7.6	Synthesis of Zn-Pz/Pc hybrids (4-isopropoxyphenyl-substituted) from dimer 2.35	102
2.8	Synthesis of Zn-Pz/Pc hybrids with different <i>meso</i> -aryl substituent.....	106
2.8.1	Synthesis of (<i>Z</i>)-1-(4-thiophenylmethylene)-1 <i>H</i> -isoindol-3-amine 2.42	107
2.8.2	Synthesis of 4-methoxyphenyl-substituted (AB dimer) with 4-thiophenylmethylene)-1 <i>H</i> -isoindol-3-amine 2.45	109
2.8.3	Synthesis of Zn-porphyrazine hybrids with <i>meso</i> -thiophene substitution from dimer 2.45	112
2.9	Electronic absorption spectra of porphyrazine hybrids.....	117
2.10	Suggested mechanisms of formation of porphyrazine hybrids.....	120
2.11	Conclusion.....	124
Chapter 3: Experimental		126
3.1	General methods.....	127
3.2	Synthesis of 2-bromobenzamidinium hydrochloride 2.3	128
3.3	Synthesis of 2-(4-isopropoxyphenyl) acetonitrile 2.34	129
3.4	Synthesis of 2-[(trimethylsilyl)ethynyl] thiophene 2.44	130

3.5	Synthesis of aminoisoindoline derivatives.....	131
3.5.1	Synthesis of (Z)-1-(4-methoxybenzylidene)-1 <i>H</i> -isoindol-3-amine 2.4	131
3.5.2	Synthesis of (Z)-1-(4- thiophenylmethylene)-1 <i>H</i> -isoindol-3-amine 2.42	132
3.6	Synthesis of substituted dinitriles.	133
3.6.1	Synthesis of 4-methoxyphenyl substituted dinitrile 2.8	133
3.6.2	Synthesis of 2,2-dimethoxy-3,4-bis(4-dimethoxyphenyl)-5-amino-2 <i>H</i> -pyrrole 2.13	134
3.6.3	Synthesis of 5-imino-3,4-bis(4-methoxyphenyl)-1 <i>H</i> -pyrrol-2-one 2.14	134
3.6.4	Synthesis of 5-imino-3,4-bis(4-methoxyphenyl)-1 <i>H</i> -pyrrol-2-dioxolane 2.16	135
3.6.5	Synthesis of <i>t</i> -butylphenyl substituted dinitrile 2.23	136
3.6.6	Synthesis of Isopropoxyphenyl substituted dinitrile 2.24	137
3.7	Dimeric condensation products of aminoisoindoline derivatives with substituted dinitriles.	138
3.7.1	Condensation products of aminoisoindoline 4 with 4-methoxyphenyl dinitrile 2.8	138
3.7.1.1	Dimer 2.17	138
3.7.1.2	Dimer 2.18	139
3.7.2	Condensation products of aminoisoindoline 4 with <i>t</i> -butylphenyl substituted dinitrile 2.23	140
3.7.2.1	Dimer 2.27	140
3.7.2.2	Dimer 2.28	141
3.7.3	Condensation products of aminoisoindoline 4 with isopropoxyphenyl substituted dinitrile 2.24	142
3.7.3.1	Dimer 2.35	1433
3.7.3.2	Dimer 2.36	143
3.7.3.3	Free-metal porphyrzine hybrid (H ₂ -ABBB-N) 2.37	144
3.7.4	Condensation products of aminoisoindoline 2.42 with 4-methoxyphenyl substituted dinitrile 2.8	145
3.7.4.1	Dimer 2.45	145
3.7.4.2	Dimer 2.46	146
3.8	Synthesis of [20-(4-methoxyphenyl) -tetrabenz[<i>b, g, q, l</i>]-5,10,15 triazaporphyrinato] magnesium 2.6	147
3.9	Synthesis of octa(4-methoxyphenyl) porphyrzine Mg (II) complex 2.9	148
3.10	Synthesis of porphyrzine hybrids from dimer 2.17	149
3.10.1	Synthesis of Mg-porphyrzine hybrids from dimer 2.17	149
3.10.1.1	Mg- <i>meso</i> -(4-methoxyphenyl) ABBA Pz/Pc hybrid 2.11	150
3.10.1.2	Mg- <i>meso</i> -(4-methoxyphenyl) ABBB-Ar Pz/Pc hybrid 2.10	151
3.10.1.3	Mg-ABBB-N Pz/Pc complex 2.19	152
3.10.2	Synthesis of Zn-porphyrzine hybrids from dimer 2.17	153
3.10.2.1	Zn- <i>meso</i> -(4-methoxyphenyl) ABBA Pz/Pc hybrid 2.20	154
3.10.2.2	Zn-ABBB-N Pz/Pc complex 2.22	155
3.11	Synthesis of Zn-porphyrzine hybrids from dimer 2.27	156
3.11.1	Zn- <i>meso</i> -(4-methoxyphenyl) ABBA Pz/Pc hybrid Pz/Pc 2.29	157
3.11.2	Zn-ABBB-N Pz/Pc complex 2.31	158
3.12	Synthesis of Zn-porphyrzine hybrids from dimer 2.35	159
3.12.1	Zn- <i>meso</i> -(4-methoxyphenyl) ABBA Pz/Pc hybrid 2.38	160
3.12.2	Zn-ABBB-N Pz/Pc complex 2.40	161
3.12.3	Porphyrzine complex Zn-BBBB 2.41	162
3.13	Synthesis of Zn-porphyrzine hybrids from dimer 2.45	163
3.13.1	Zn- <i>meso</i> -(4-thiophene) ABBA Pz/Pc hybrid 2.47	164
3.13.2	Zn- <i>meso</i> -(4-thiophene) ABBB-Ar Pz/Pc hybrid 2.48	165
3.13.3	Porphyrzine complex Zn-BBBB 2.49	166

References.....	167
Appendices	177

List of Abbreviations

Ar	Aryl
BINAP	2,2'-bis(diphenylphosphino)-1,1'-binaphthyl
Br	Broad
Bu	Butyl
DABCO	1,4-Diazabicyclo- [2.2.2]-octane
DBU	1,8-diazabicyclo [5.4.0] undec-7-ene
DDQ	2,3-dichloro-5,6-dicyanobenzoquinone
DCM	Dichloromethane
Diglyme	Diethylene glycol dimethyl ether
DMF	Dimethylformamide
DMSO	Dimethylsulfoxide
DSSCs	Dye-sensitised solar cells
δ	Chemical shift in ppm
BINAP	2,2'-Bis(diphenylphosphino)-1,1'-binaphthalene
d	Doublet
dd	Doublet of doublets
DCM	Dichloromethane
DMF	Dimethyl formamide
DMSO	Dimethyl sulfoxide
DBTAPs	Dibenzotriazaporphyrins
dt	Doublet of triplets
ϵ	Extinction coefficient
eq	Equivalent

HOMO	Highest occupied molecular orbital
Hz	Hertz
IR	Infrared
<i>J</i>	Coupling constant in NMR spectroscopy
L	Ligand
LUMO	Lowest unoccupied molecular orbital
MS	Mass spectrometry
<i>m/z</i>	Mass-to-charge
MALDI	Matrix assisted laser desorption ionisation.
MBTAP	Monobenzotriazaporphyrins
Me	Methyl
MHz	Megahertz
M (in structures)	Metal (any)
<i>m</i>	Multiplet
MALDI-TOF	Matrix-assisted laser desorption/ionization (time of flight)
MHz	Megahertz
m.p.	Melting point
MS	Mass spectrometry
Mwt	Molecular weight
nm	Nanometres
NMR	Nuclear Magnetic Resonance
OMe	Methoxy
OPVs	Organic photovoltaics
Pc	Phthalocyanine
Pe	Pentane

PDT	Photodynamic therapy
ppm	Parts per million
pm	Picometre
ppm	Parts per million
PACT	Photodynamic antimicrobial chemotherapy
PS	Photosensitiser
Pz	Porphyrazine
q	Quartet
r.t	Room temperature
ROS	Reactive oxygen species
λ	Wavelength
s	Singlet
t	Triplet
TAP	Tetraazaporphyrins
TBTAP	Tetrabenzotriazaporphyrin
TPP	Tetraphenyl porphyrin
THF	Tetrahydrofuran
TFA	Trifluoroacetic acid
TLC	Thin Layer Chromatography
tt	Triplet of triplets
UV-Vis	Ultraviolet

Acknowledgements

My first and deepest thanks go to Allah for granting me the strength and ability to conduct this study and for easing the challenges of years of exile from my family and home during my time in the UK. I also wish to express profound gratitude to my supervisor, Professor Andrew Cammidge. This thesis would not have been possible without his invaluable support and guidance. I feel very lucky to have had such a superb supervisor, whose stimulating motivation, insightful feedback, and constant support provided a safe and encouraging environment as I navigated my journey as a doctoral candidate.

I would also like to extend my thanks to Dr. Isabelle Fernandes for her time, advice, support, and kindness, and to Dr. David Hughes for the X-ray crystallography service.

My deepest gratitude goes to my family, especially my mother, sisters and brothers, for their unwavering support and belief in me. Their love, pride and encouragement have been a constant source of strength and motivation, driving me to work hard and achieve my best.

I also like to acknowledge the past and current members of Cammidge's group for their camaraderie and for creating a friendly working environment. I especially want to thank Dr. Faeza Alkorbi, Dr. Norah Alsaiari, Dr. Jacob Gretton, and Dr. Ibtesam Mashnoy.

I am very grateful to Qassim University for providing me the opportunity to pursue my studies in the UK and to the Embassy of Saudi Arabia for their funding during my PhD degree.

Finally, I would like to thank the Saudi Culture Bureau and Qassim University for fully funding this research.

CHAPTER 1:

Introduction

1.1 History of porphyrin

The word "porphyrin" stems from an ancient Greek word "porphura", meaning purple colour.¹ Porphyrin has a macrocyclic structure comprising four pyrrole rings connected to methine groups.² It is a fluorescent dye that occurs naturally in various biological systems, including the particular pair of chlorophylls in the photosynthetic reaction centre (RC), hemes, and cyano-cobalamine (vitamin B₁₂), where it serves various biological functions (Figure 1.1). These "pigments of life" possess specific characteristics such as their ability to coordinate, exhibit redox-active behaviours, and light harvesting.^{3,4}

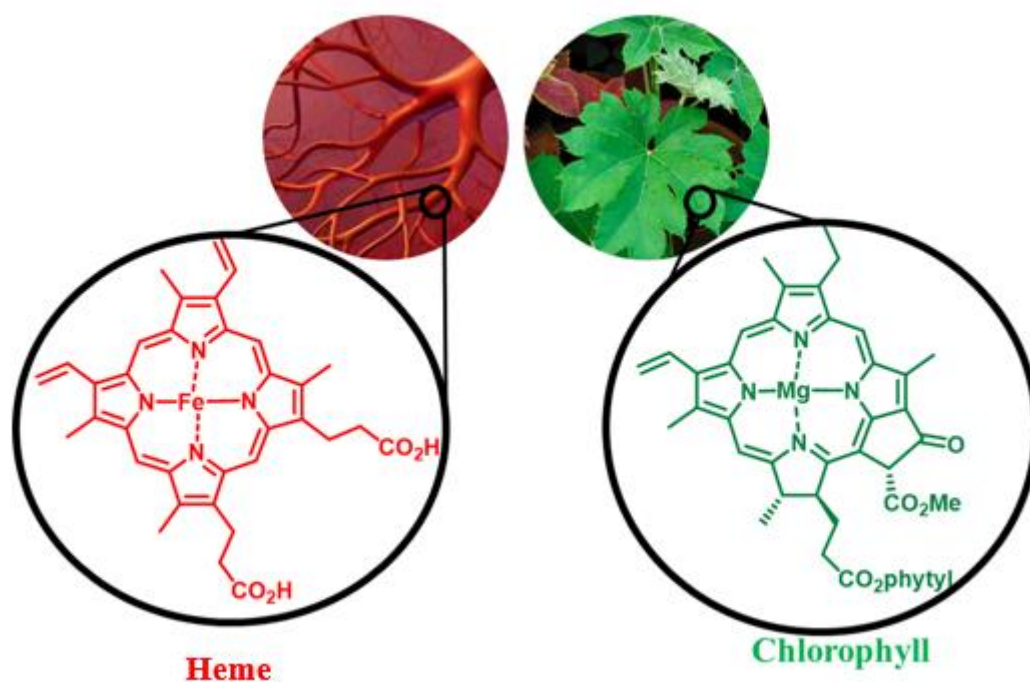


Figure 1.1: Heme and chlorophyll structures.

In 1912, Küster proposed the macrocyclic structure of porphyrin, but it was not accepted because it was believed that a giant ring would be too unstable.¹ However, the significance of porphyrin derivatives like heme and chlorophyll in biology has led to many synthetic studies over the years, some of which have been recognised with Nobel prizes.^{5, 6} For example, Willstätter in 1915 for efforts in establishing the constitution of chlorophylls, Hans Fischer in 1930 for haemin synthesis, and R. B. Woodward in 1965 for innovative progress in the area of organic synthesis, including complete preparation of the chlorophyll.⁷

1.2 Structure of porphyrin

Although porphyrin dyes possess 22 π -electrons, only 18 are found in the aromatic system, following Hückel's rule of aromaticity ($4n+2=18$, where $n=4$). Fischer introduced the

nomenclature system, which starts by numbering the β -carbons in pyrrole rings beginning from number 1 to 8. The bridging carbon atoms were abbreviated using Greek symbols α , β , γ , and δ .

Although the Fischer system effectively names simple porphyrins, it is challenging for multi-substituted β and *meso*-positions in porphyrin derivatives. To solve this problem, the IUPAC developed a more systematic naming scheme in 1979, which was finalised in 1987.¹ This new system assigns numbers to all atoms, including the nitrogen atoms, enabling the naming of various porphyrin derivatives, such as unmetalled porphyrin, porphyrin complexes, cyclic porphyrins (with compressed or expanded ring system), and porphyrins containing other fused rings. (Figure 1.2).⁸

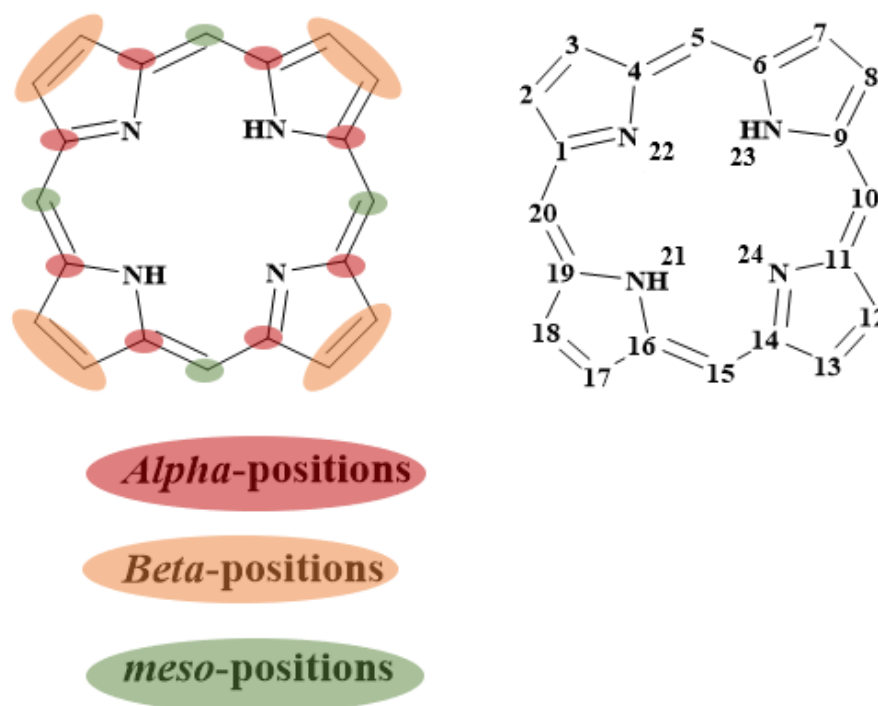


Figure 1.2: The numbering system for porphyrins according to Fischer (alpha, beta and - *meso*-positions) and the IUPAC system of porphyrins.

1.3 Synthesis of porphyrin

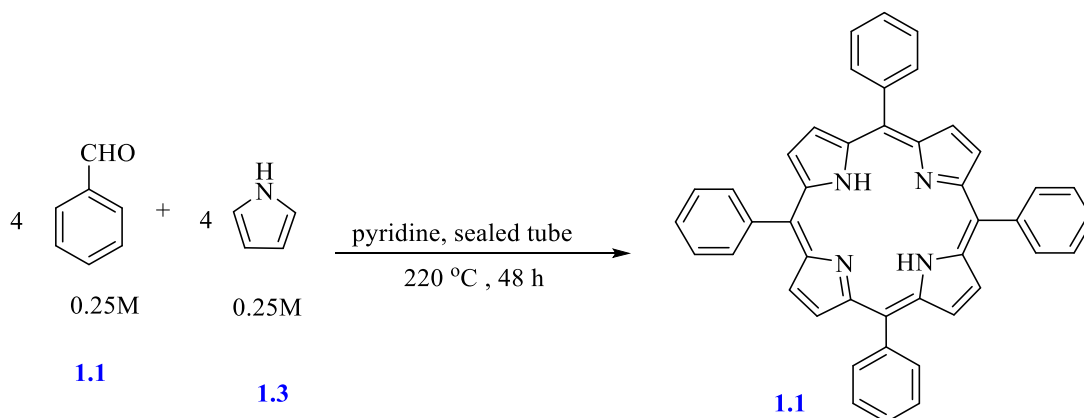
Multiple approaches are available for synthesising porphyrins, which generally involve using pyrroles and aldehydes. The final product will vary based on the specific pyrrole and aldehyde precursors used, allowing for the creation of β and *meso*-substituted porphyrins. Various metal salts such as Zinc (Zn), Copper (Cu), Nickel (Ni), and Tin (Sn) form metal complexes with the porphyrin ligand *via* the substitution of core protons (H^+) of porphyrins.⁹

1.3.1 Synthesis of *meso* and β -substituted porphyrins

The following discussion explores the preparation of porphyrins. *Meso*-substituted porphyrins have been prepared using Rothmund, Adler, and Lindsey methods.

1.3.1.1 From benzaldehyde and pyrrole (the Rothmund method)

Rothmund accomplished the first synthesis of 5,10,15,20-tetraphenylporphyrin **1.1** in 1936 by combining benzaldehyde **1.2** and pyrrole **1.3** in a 4:4 molar ratio with pyridine, heating the mixture at 220 °C for 48 h in a sealed tube. The 5,10,15,20-tetraphenylporphyrin was obtained in a low yield of 9% as deep-purple needles. The process is illustrated in Scheme 1.1. However, the Rothmund synthesis had significant drawbacks, including low and inconsistent yields and the need for harsh reaction conditions, which only a tiny selection of unreactive aldehydes could withstand.¹⁰ The substitution nature of the phenyl ring in the Rothmund reaction is a key determinant of the yield of *meso*-substituted porphyrin **1.1**.¹¹



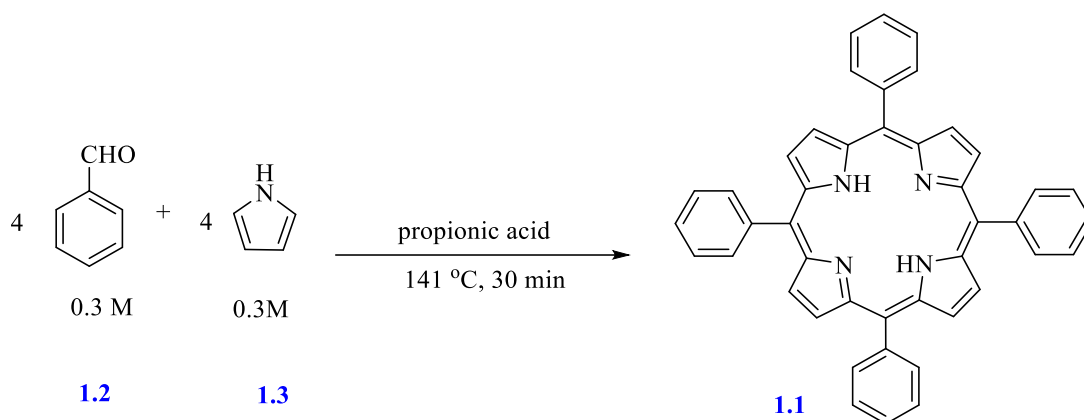
Scheme 1.1: The Rothmund synthesis of *meso*-substituted porphyrin.

1.3.1.2 The Adler synthesis

Adler modified the Rothmund reaction, producing a more efficient method for producing tetraphenylporphyrin under milder conditions. This preparation was achieved by mixing benzaldehyde and pyrrole at low concentrations, then refluxing the mixture in propionic acid (at 141 °C) for 30 min. in the presence of air. Upon cooling, porphyrin crystals were obtained through filtration, resulting in a better yield of 20%. The use of propionic acid as a solvent enabled Adler to avoid the need for sealed bombs, which was a significant obstacle to the Rothmund method. Furthermore, the Adler reaction could be scalable because the simple reaction conditions are suitable for many aldehydes.

The Adler method is generally more effective than the Rothmund method but still has certain drawbacks. For instance, the reaction was unsuccessful when using benzaldehydes that

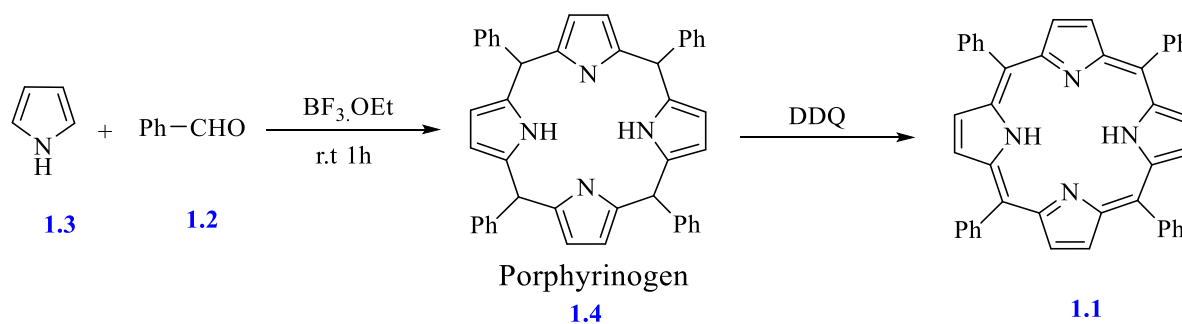
contained acid-sensitive functional groups, and purification issues arose due to the use of propionic acid (since some porphyrins did not recrystallize from the solvent). Consequently, the yields obtained were sometimes low (Scheme 1.2).^{12,13}



Scheme 1.2: Adler synthesis of *meso*-substituted porphyrin.

1.3.1.3 Lindsey method

Lindsey's research team has optimized the reaction between pyrrole and aryl aldehyde to produce many tetra-arylporphyrin derivatives with excellent yields. This reaction is a one-pot synthesis method that occurs in two steps, in diluted solutions and the presence of BF_3 -etherate Lewis acid catalyst to form the porphyrinogen followed by the oxidation of this intermediate to porphyrin using 2,3-dichloro-5,6-dicyanobenzoquinone (DDQ) (Scheme 1.3).¹⁴

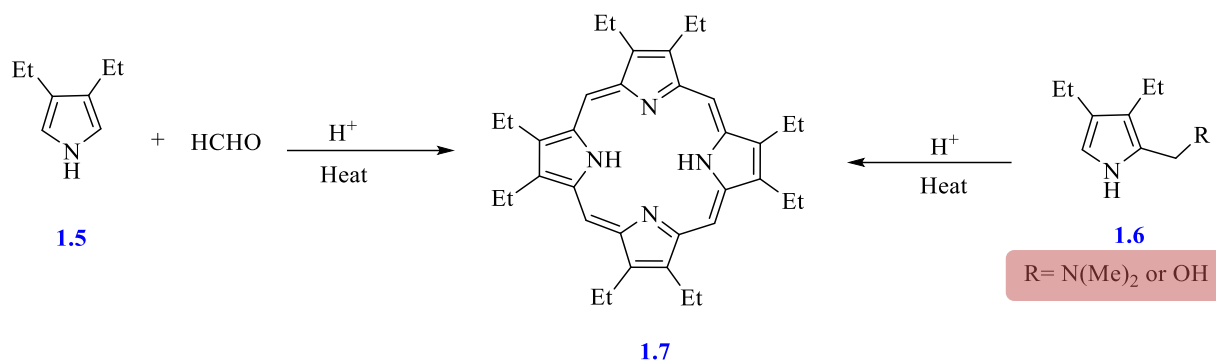


Scheme 1.3: Lindsey's method for synthesizing *meso*-substituted porphyrins.

1.3.1.4 Synthesis of symmetrically beta-substituted porphyrins

Two methods are available to produce porphyrins with symmetrically substituted at beta-positions. Using the synthesis of 2,3,7,8,12,13,17,18-octaethyl porphyrin (OEP) as an example, the first method involves tetramerization of 3,4-diethylpyrrole **1.5** in the presence of formaldehyde and a specific acid catalyst, which produces OEP **1.7** via a cyclization reaction.¹⁵ The second method involves tetramerization of 2-substituted pyrroles with a CH_2R group,

where "R" is a good leaving group, under acidic conditions to obtain **1.7** in a high yield (Scheme 1.4).^{16, 17}



Scheme 1.4: Synthesis of *beta*-substituted porphyrins.

1.4 Spectroscopic properties of porphyrins

The diverse chemical and physical properties of porphyrin molecules are determined by their specific structural features. All porphyrins have a distinct colour and can absorb light within Vis. and UV regions of the electromagnetic spectrum. Some porphyrins may also demonstrate luminescence, paramagnetism, photoconduction, or semi-conductivity, while others possess photosensitizing or catalytic activities. Researchers from various fields have expressed interest in understanding the underlying principles responsible for this wide range of porphyrin properties.¹⁸

1.4.1 UV-Vis spectroscopy

Many previous studies reported that porphyrins possessed intense colour due to the highly conjugated π -electron systems, making it possible to study their characteristics through UV-Vis absorption spectra.¹⁹ These spectra are characterized by two electronic absorption bands at near-ultraviolet and the other in visible wavelength (λ) regions. These absorption bands correspond to the electronic transitions. The UV Absorption Soret or B band absorption occurs at λ 380-500 nm by electronic transition from the ground state to the second excited state ($S_0 \rightarrow S_2$) depending on the β - or *meso*-substitution. The *Q*-bands, due to a weak transition to the first excited state ($S_0 \rightarrow S_1$), appeared at λ 500-750 nm. The good optical properties of porphyrins, caused by the conjugated system, including the 18 π -electrons, enables spectroscopic monitoring of metal complexation, for example. The substituent position can control the position of the spectral bands and the intensity of the *Q*-band (Figure 1.3).²⁰

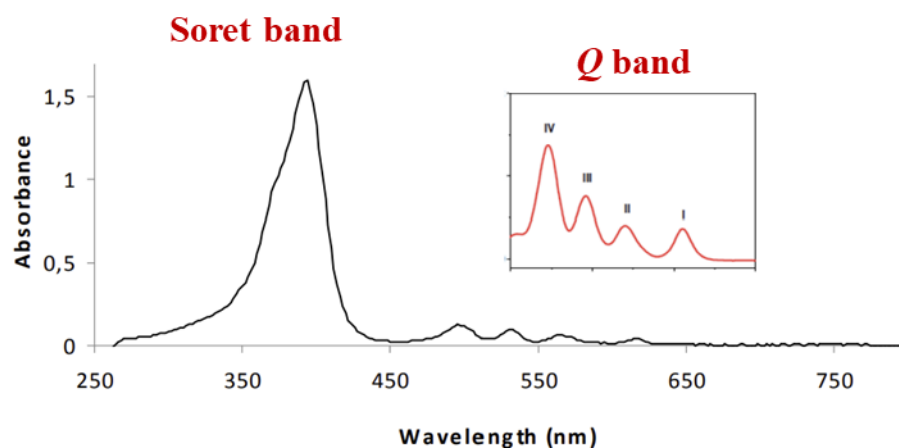


Figure 1.3: The electronic absorption spectra of 5,10,15,20-tetraphenylporphyrin **1.1** (the Soret and *Q*-regions).²⁰

1.4.2 ^1H NMR spectroscopy

Numerous studies detailing the NMR spectra of porphyrins have been published. These spectra are easier to interpret than one might anticipate, as the different protons have wide resonance frequency ranges, and no spin-spin interaction exists between groups at various positions on the ring. Consequently, it is a valuable tool for clarifying the structure of porphyrins and related compounds.²¹ The ^1H NMR spectra of porphyrins validate their distinctive aromaticity. The β -pyrrole and *meso*-H are de-shielded by the diamagnetic ring current. Moreover, the protons of the internal N-H are shifted up-field because of the ring current's shielding effect (Figure 1.4).²²

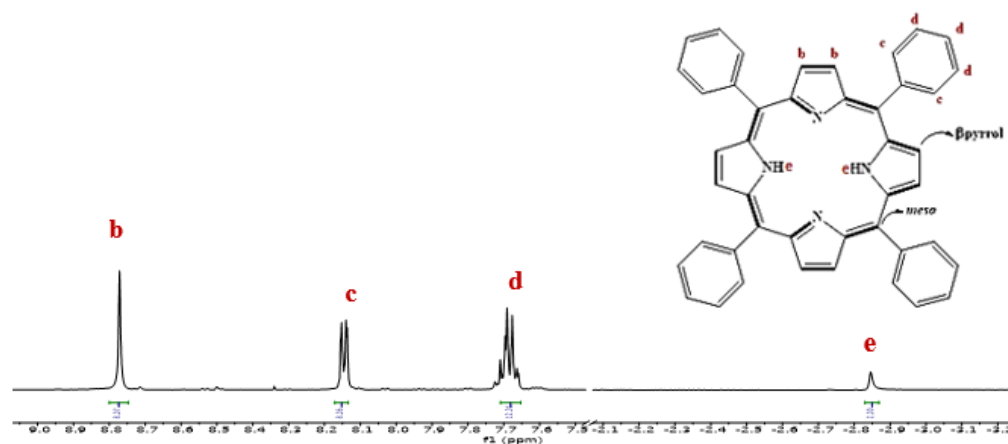


Figure 1.4: ^1H NMR spectrum of 5,10,15,20- tetraphenylporphyrin **1.1**.

1.5 History of phthalocyanine and terabenzotriazaporphyrin

Von Braun and Tscherniac stumbled upon a vibrant metal-free phthalocyanine (Pc) in 1907 while preparing *ortho*-cyano benzamide from phthalimide as a side product.²³ This accidental discovery marked the first instance of phthalocyanine detection at the beginning of the last century. In 1927, de Diesbacha and von der Weid, from Fribourg University, prepared a dark solid copper derivative during cyanation of *o*-dibromobenzene in refluxing pyridine by CuCN.²⁴ The phthalocyanine's structure was not initially explored until 1929.

Two workers at Scottish Dyes Ltd.²⁵ examined a sample of iron phthalocyanine, which was produced as a by-product during the conversion of phthalic acid to phthalimide, and discovered its exceptional thermal stability towards acids and bases, as well as its insolubility. This sample was investigated by Reginald P. Linstead, a young lecturer at Imperial College, London, to determine its complete structure. Linstead *et al.* performed chemical analysis, including elemental analysis and molecular weight determination, using the elevation in boiling point, and oxidation that disintegrated these macrocyclic molecules into phthalimide to identify the structure of the unmetalled phthalocyanine.²⁶

The structure was later verified by J. M. Robertson's X-ray diffraction. Phthalocyanine was one of the first compounds examined using X-ray diffraction.²⁷ Linstead named it "phthalocyanine," including the abbreviations "phthal" and "cyanine" derived from the Greek words "naphtha" (rock oil) and (blue) respectively (Figure 1.5).²⁸

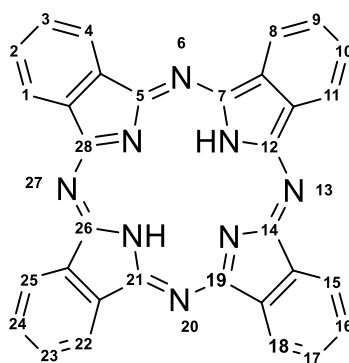


Figure 1.5: The numbering system of phthalocyanine structures H₂Pc.

When a nitrogen atom in phthalocyanine was substituted with one sp²-hybridized carbon atom, it resulted in a hybrid structure that exhibits an intermediate nature between phthalocyanine and tetrabenzoporphyrin. This hybrid's structure is called tetrabenzotriazaporphyrin TBTAP **1.9**. Figure 1.6 shows metal complexes of Pc, TBTAP and tetrabenzoporphyrin (TBP) **1.10**.

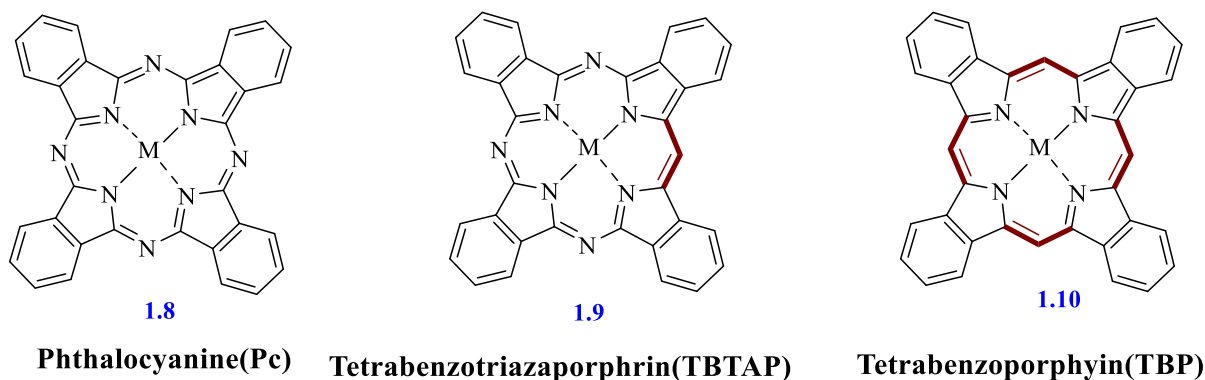


Figure 1.6: Structures of phthalocyanine **1.8**, tetrabenzotriazaporphyrin TBTAP **1.9** and tetrabenzoporphyrin TBP **1.10**.

The tetrabenzotriazaporphyrin (TBTAP) derivatives are attractive because of the synergistic properties of both systems and they offer innovative possibilities in macrocyclic chemistry.²⁹ Quantum chemical calculations of frontier molecular orbitals showed that TBTAP has a similar molecular orbital system to phthalocyanine but with a slightly more significant energy gap (ΔE) between energy levels of the highest occupied molecular orbital (E_{HOMO}) and the lowest unoccupied molecular orbital (E_{LUMO}), resulting in a small shift of the absorption in the visible region. However, the most significant difference is the presence of a *meso*-carbon atom, which makes unique chemistry available that is impossible in the phthalocyanine series. By functionalizing the *meso*-position, it is possible to create new TBTAP structures with new functionality, such as attaching the macrocycle to surfaces or constructing complex multi-macrocyclic systems.^{29, 30}

1.5.1 Synthesis of phthalocyanine

The introduction of phthalocyanine pigments in 1935 significantly departed from the traditional use of dyes as colourants. Phthalocyanines (Pc) are highly significant organic pigments in blue and green shades with exceptional ability to provide strong colour and withstand stability to photodegradation, weather, chemicals, and solvents.²⁹ Initially, phthalocyanines are created in organic solvents and form relatively large single crystals, reaching sizes of up to 100 μm . These pigments find utility in various industries, including paints, coatings (black and white shading), plastics, printing inks, and spin dyeing. Phthalocyanine metal complexes can be synthesised from Pc ligand with almost any metal in the periodic table.³¹

The economic, ecological, and optical considerations contribute to the preference for more stable phthalocyanine complexes, specifically those involving Fe, Zn, Co, and Pt. These

complexes exhibit stability and generally retain the original hue of phthalocyanine.³² Since the pioneering work conducted by Linstead and colleagues in the 1930s, the formation of phthalocyanine metal complexes and similar compounds has typically involved condensation reactions using precursor materials like phthalonitriles, 1,3-diiminoisoindolines, phthalic anhydrides, phthalimides, or phthalamides (Figure 1.7).³³ Free-base phthalocyanines are commonly obtained by demetallation of alkali metal complexes, although direct synthesis from precursors is occasionally feasible, particularly in the instance of 1,3-diiminoisoindolines.³⁴

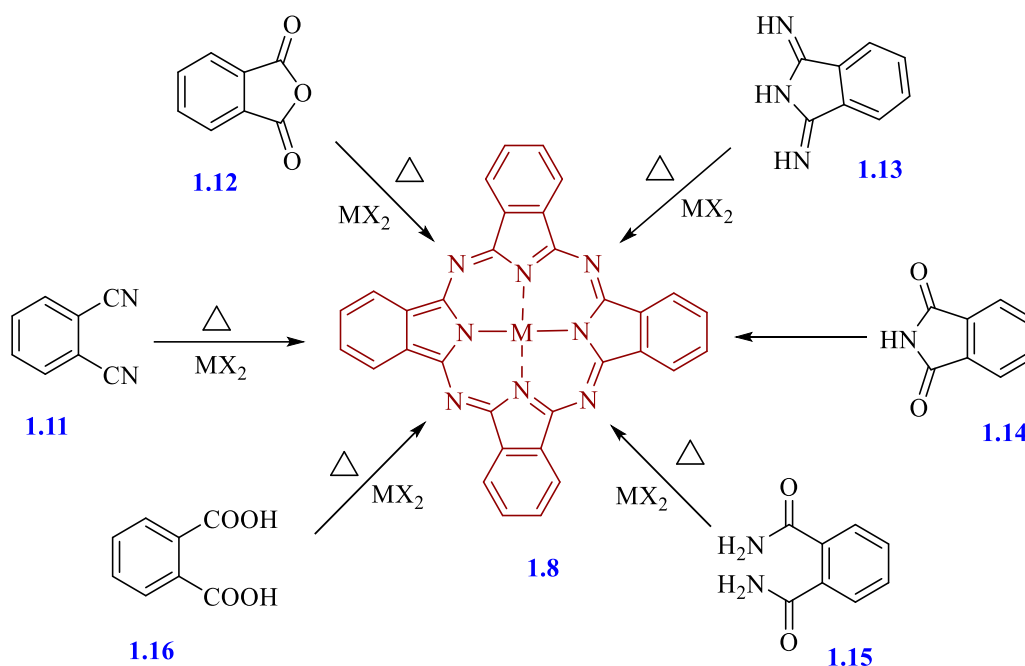
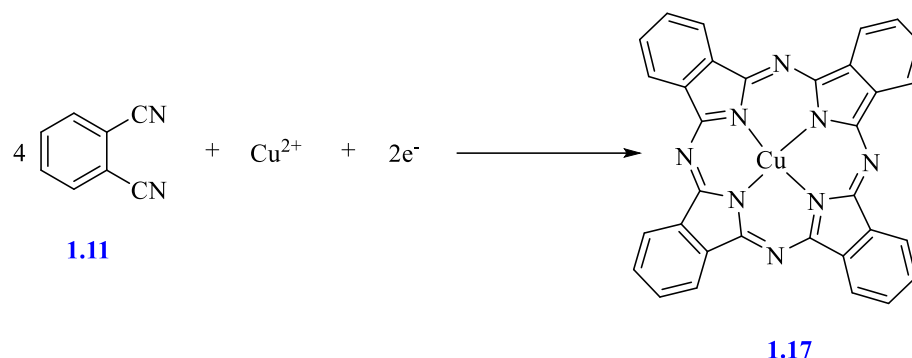


Figure 1.7: Phthalocyanine is synthesised from different precursors, including phthalonitriles **1.11**, phthalic anhydrides **1.12**, 1,3-diiminoisoindolines **1.13**, phthalimides **1.14**, phthalamides **1.15**, and phthalic acid **1.16**. In the case of phthalic acid and its derivatives, a source of NH_3 , typically urea, is required.

1.5.1.1 From phthalonitrile **1.11**

The initial laboratory procedure consisted of heating phthalonitrile with copper bronze or copper salts at high temperatures of 200 °C to 240 °C in copper pans. The reaction can be performed either in the absence or in the presence of a solvent. The metal source can be copper, copper halides, or copper alkoxides. Usually, the reaction occurs in a solvent at 180 °C or by heating a mixture of solid reactants to 300 °C with a highly exothermic reaction. The phthalonitrile method is considered the more refined approach, as it yields relatively pure copper phthalocyanine while minimizing the formation of side products. This procedure is

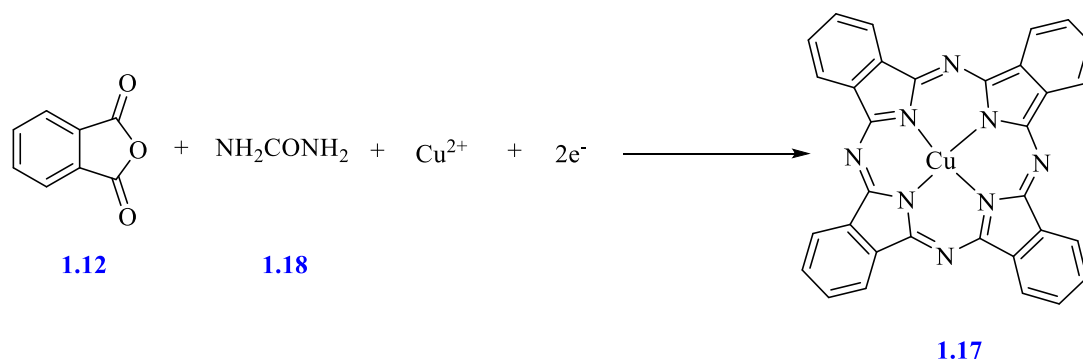
limited by the higher economic costs of phthalonitrile compared to phthalic anhydride (Scheme 1.5). Subsequently, many metals and metal salts have been used equally successfully.^{32, 35}



Scheme 1.5: Preparation route of phthalocyanine from phthalonitrile **1.11**.

1.5.1.2 From phthalic anhydride **1.12** and urea

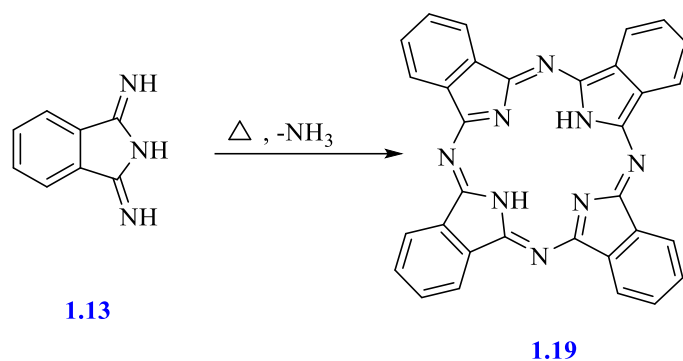
This is the industrial method for the production of copper phthalocyanine pigments due to its high productivity, cost-effective large-scale production techniques, and the availability of cheap precursors. The phthalic anhydride, urea, and CuCl mixture, at a molar ratio of 4:16:1, respectively, are heated in the presence of an ammonium molybdate catalyst. The synthesis can be conducted either with solvents like trichlorobenzene, nitrobenzene, or kerosene at 200 °C or in dry conditions at 300 °C (Scheme 1.6).^{32, 36}



Scheme 1.6: Synthesis of phthalocyanine from phthalic anhydride **1.12** and urea.

1.5.1.3 From 1,3-diiminoisoindoline **1.13**

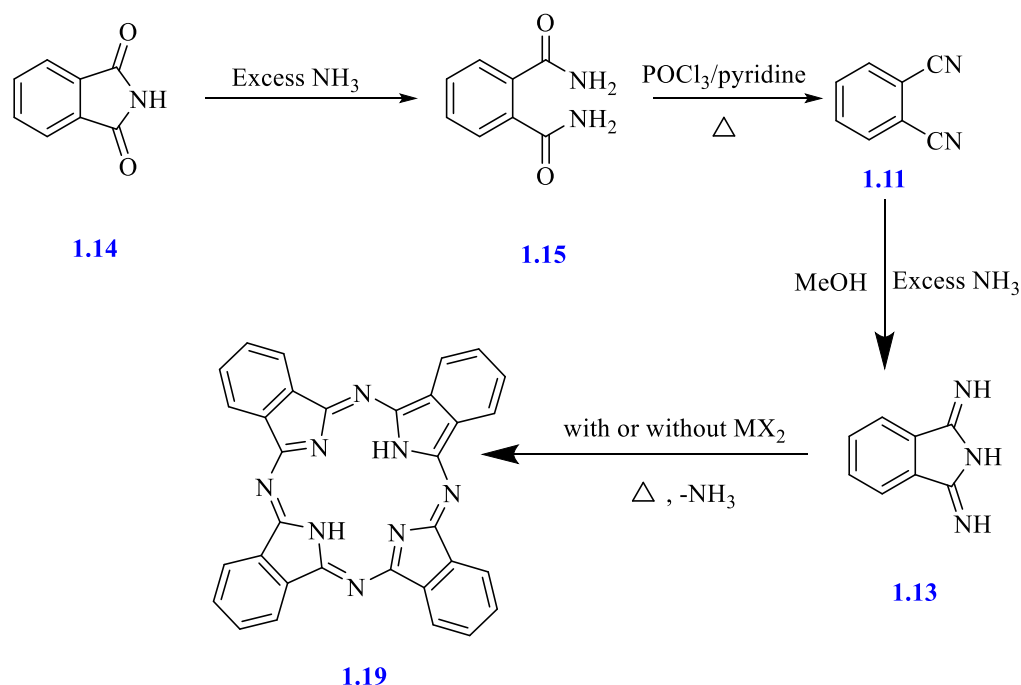
The self-condensation reaction of imidines, where the ammonia molecule is eliminated, can result in the formation of a phthalocyanine structure, regardless of whether the imidine is saturated, unsaturated, or aromatic. The formation of metal-free phthalocyanine requires the presence of hydrogen donors and occurs with significant yields on heating di-iminoisoindoline. On the other hand, when imidines are heated with metal salts or metals, mild conditions are sufficient to produce metal phthalocyanines (Scheme 1.7).³⁷



Scheme 1.7: Synthesis of phthalocyanine from 1,3-diiminoisoindoline **1.13**.

1.5.1.4 From phthalimide **1.14**

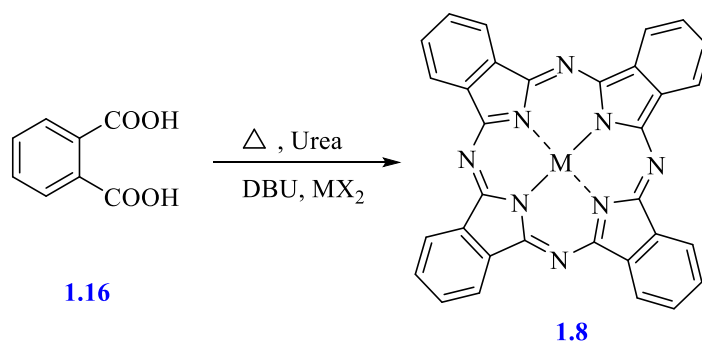
The transformation of imide **1.14** into amide **1.15** can be carried out using a significant excess of concentrated ammonia solution. To convert **1.15** into *o*-dinitriles, phosphorus oxychloride in pyridine was applied at 60 °C, resulting in a 65% yield. The process for obtaining 1,3-diiminoisoindolenes **1.13** was achieved by passing a stream of ammonia gas through a methanolic solution of **1.11**. Boiling **1.13** in dimethylaminoethanol gives the metal-free phthalocyanine **1.19** with a 60% yield. The metallic phthalocyanine was prepared with a 55% yield by reacting a four-fold excess of **1.13** with metal halides (Scheme 1.8).³⁸



Scheme 1.8: Synthesis of phthalocyanine from phthalimides **1.14**.

1.5.1.5 From phthalic acid 1.16

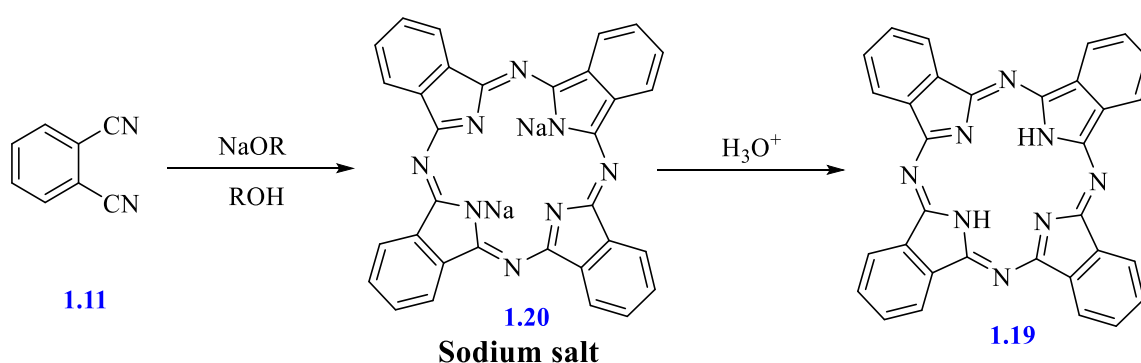
Phthalocyanine metal complexes can be synthesised by directly reacting phthalic acid derivatives with urea and metal halides like CoCl_2 , and ZnCl_2 in the presence of 1,8-diazabicyclo[5,4,0]undec-7-ene (DBU) at 210°C until complete fusion of the reaction mixture. The resulting product is washed with water to remove unreacted species and then dried to yield the phthalocyanine metal complex (Scheme 1.9).³⁹



Scheme 1.9: Synthesis of phthalocyanine from phthalic acid in the presence of DBU as a catalyst.

1.5.1.6 Synthesis of metal-free phthalocyanine using sodium alkoxides

The predominant method for producing metal-free phthalocyanine involves the reaction of alkaline or alkaline earth metal alkoxides with phthalonitrile or diiminoisoindoline. The initial product obtained is the alkali metal salt of phthalocyanine, which is later demetallized using mineral acids. Alternatively, anhydrous sodium polysulfide can be utilized as a substitute for sodium alkoxides in this process (Scheme 1.10).^{32, 40}



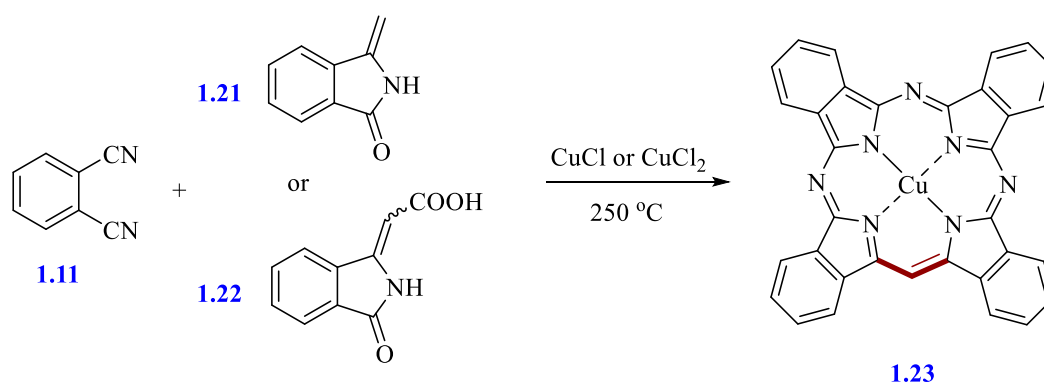
Scheme 1.10: Synthesis of metal-free phthalocyanine 1.19 using sodium alkoxides.

1.5.2 Synthesis of tetrabenzotriazaporphyrin (TBTAP)

Helberger reported the first successful synthesis, achieved through their initial reaction between o-halogenoacetophenone and cuprous cyanide. This reaction formed a substance known as Cu-TBTAP **1.23**.^{41, 42}

1.5.2.1 Synthesis of TBTAP using mixed cyclization of phthalonitrile, methylenephthalimidine, and phthalimidine acetic acid

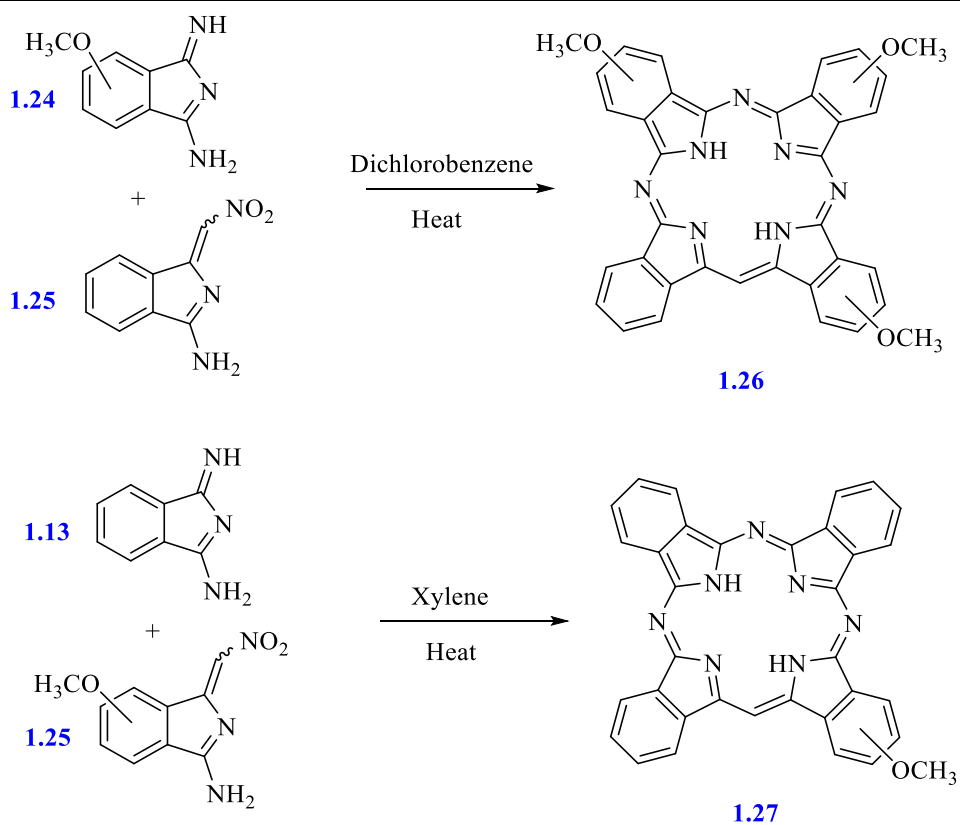
When an equal amount of phthalonitrile was reacted with methylenephthalimidine or phthalimidineacetic acid at 250 °C, either in fusion or in the presence of chloronaphthalene solvent, in the presence of a copper salt, a substantial amount of a green chromophore was obtained. This chromophore was characterized as Cu-TBTAP using different spectroscopic methods of analysis. Furthermore, when a 3:1 ratio of phthalonitrile to phthalimidine acetic acid was used, a significantly higher yield (approximately 70%) of Cu-TBTAP was reported. (Scheme 1.11).^{41, 43}



Scheme 1.11: Synthesis of Cu-TBTAP by mixed cyclization between a phthalonitrile **1.11** and methylenephthalimidine **1.21** or its precursors.

1.5.2.2 Synthesis of TBTAP by mixed cyclization reaction of phthalimidine derivatives

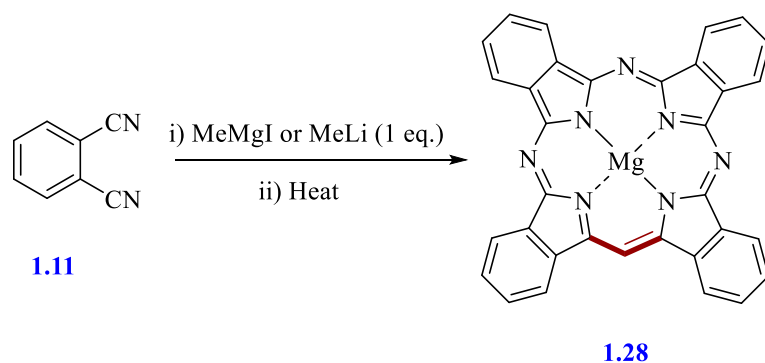
During the late 1980s, indications of renewed enthusiasm for synthesizing TBTAP materials emerged. Researchers acknowledged the potential of mixed cyclization, initially proposed by Dent, and a Bayer patent introduced nitrophthalimidine as an alternative precursor in such mixed cyclization (Scheme 1.12).⁴⁴



Scheme 1.12: Nitrophthalimidine was employed as a substitute precursor in mixed cyclization to produce substituted TBTAPs.

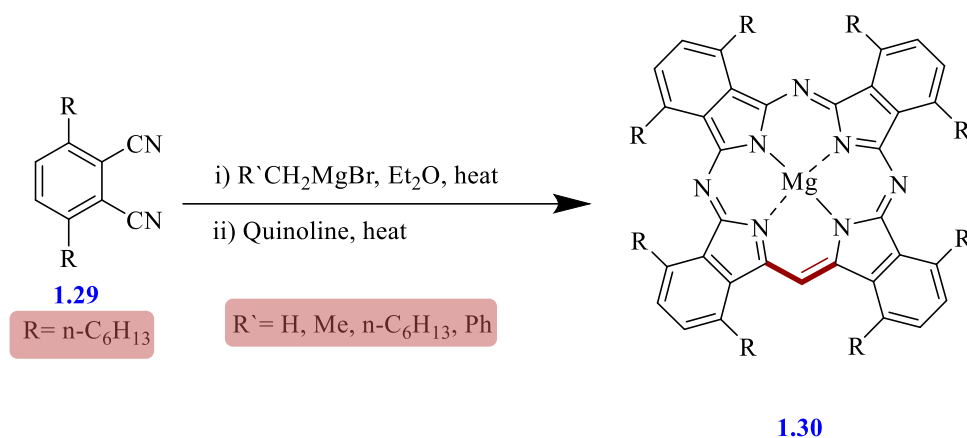
1.5.2.3 Synthesis of TBTAP using Grignard reagents

Phthalonitrile underwent a process involving the reaction with methyl magnesium iodide in a cold ether solution. Subsequently, the resulting intermediate was subjected to additional heating in a high-boiling solvent like quinoline. This led to the formation of Mg-TBTAP, with an approximate yield of 40%. After acid treatment, the magnesium was removed, enabling the incorporation of other metals such as Cu, Zn, Li, and Fe (Scheme 1.13).⁴⁵



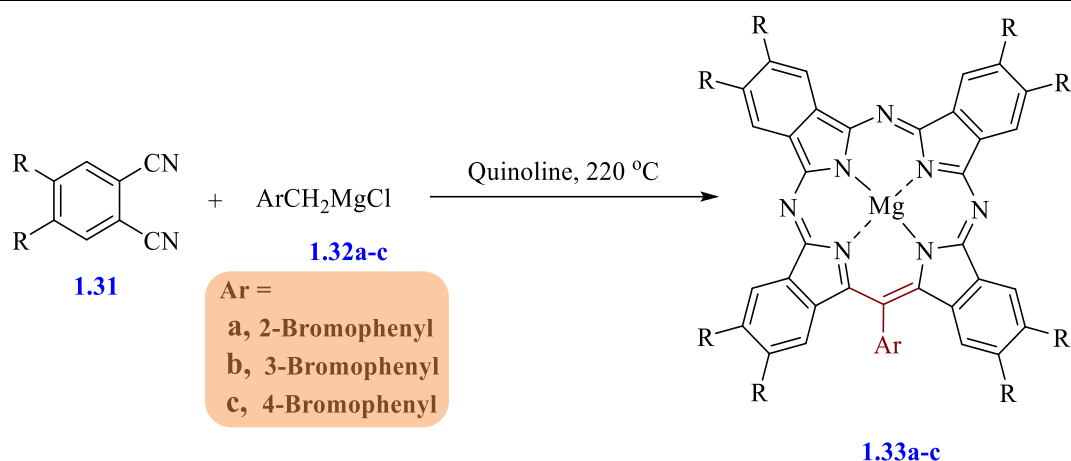
Scheme 1.13: Linstead's first synthesis of Mg-TBTAP by the reaction of phthalonitrile **1.11** with Grignard reagents.

In 2011, Cammidge's group adopted Leznoff's procedure⁴⁶ to introduce the phenyl or alkyl substituents at the *meso*-position of TBTAPs. Their work focused on the synthesis of non-peripherally substituted (n-C₆H₁₃)₈ TBTAP **1.30** from 3,6-dihexyl phthalonitrile **1.29** as shown in Scheme 1.14. However, all trials consistently resulted in the isolation of the same TBTAP **1.30**, which was unsubstituted at the *meso*-position. This observation led to the conclusion that substituents cannot be accommodated at the *meso*-position due to steric hindrance when employing 3,6-disubstituted phthalonitriles.⁴⁷



Scheme 1.14: Using Grignard reagents to prepare the non-peripherally substituted TBTAP analogues.

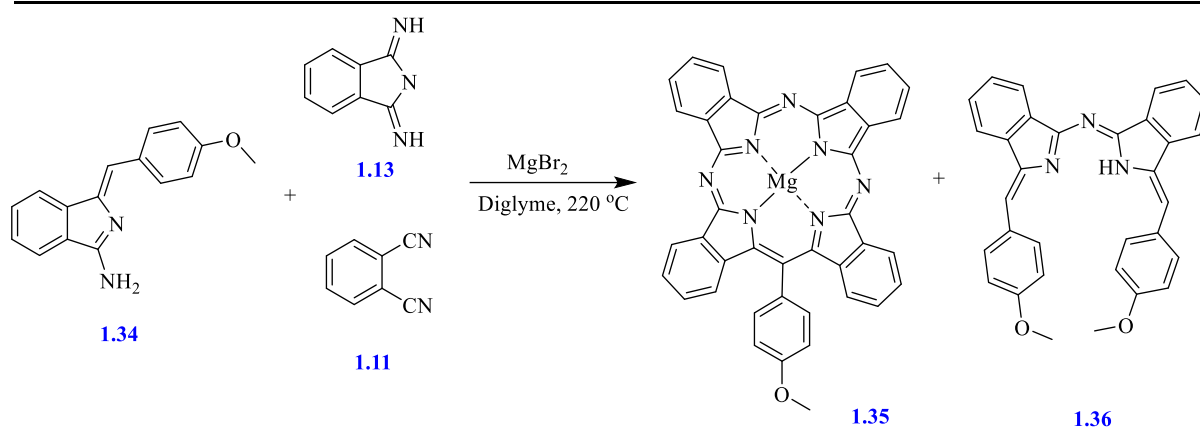
Alharbi *et al.* investigated the formation of novel TBTAPs featuring aryl substituents at the *meso*-position through a series of experiments that utilised improved synthetic strategies. This approach involved employing phthalonitrile derivatives and Grignard reagents, which Leznoff reported,⁴⁶ particularly with benzyl magnesium chloride. TBTAP derivatives **1.33a-c** were synthesised *via* a reaction between phthalonitrile and an isomeric series of 2-, 3- and 4-bromobenzyl magnesium chlorides **1.32a-c**. In addition, to improve the solubility of the resulting TBTAPs, the group explored the reaction of 4,5-disubstituted phthalonitriles with 2-bromobenzyl magnesium chloride **1.32a**. Although the synthesis of these TBTAPs from phthalonitrile derivatives was relatively straightforward, the final product was isolated in low yields (Scheme 1.15).⁴⁸



Scheme 1.15: Synthesis of *meso*-aryl Mg-TBTAP by the reaction of phthalonitrile **1.31** derivatives with benzyl Grignard reagents.

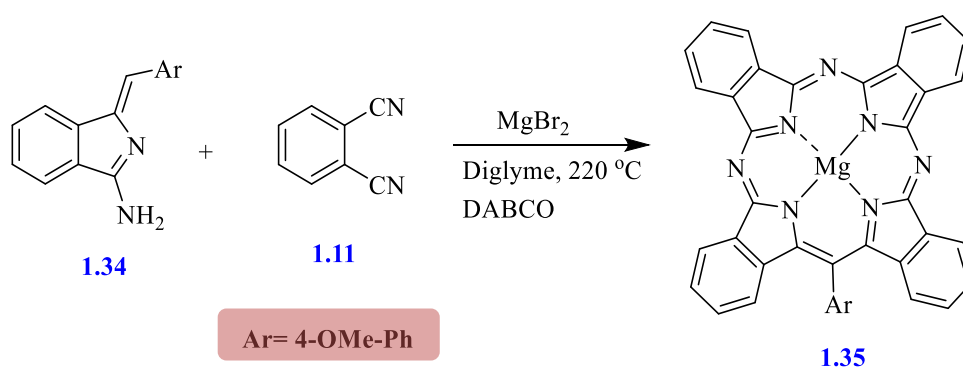
1.5.2.4 Using aminoisoindoline precursors

Cambridge *et al.* continued their investigation into identifying appropriate *meso* carbon donors for the synthesis of TBTAPs with aryl substituents at the *meso*-position. They introduced a modern synthetic approach that resulted in a significant yield of *meso*-phenyl TBTAPs and prevented the formation of further side products. This strategy involved the synthesis of an aminoisoindoline derivative, which facilitated the inclusion of an aryl bearing *meso* carbon atom, following the procedure demonstrated by Hellal *et al.*⁴⁹ In the initial attempt, the reaction employed aminoisoindoline **1.34** and diiminoisoindoline **1.13** in high boiling organic solvents, with MgBr_2 as a template ion (Scheme 2.16). However, significant yields of self-condensation products of starting materials resulted (azadipyrromethene **1.36**), and including formation of phthalocyanine. To address this, the reaction was modified by replacing diiminoisoindoline **1.13** with a less reactive precursor phthalonitrile **1.11**. This led to the successful development of a versatile and high yielding synthesis of *meso*-aryl substituted TBTAPs.^{30, 48}



Scheme 1.16: The utilisation of an aminoisindoline precursor for the formation *meso*-aryl TBTAPs.

The synthesis of TBTAP hybrids has been further optimised, particularly in reducing the formation of azadipyrromethene. The modification involved the slow addition of aminoisindoline, where a 1:1 equiv. solution of aminoisindoline **1.34** and phthalonitrile **1.11** was added to a solution of phthalonitrile (3 equiv.) in hot diglyme. Additionally, (1,4-diazabicyclo [2.2.2] octane) DABCO was introduced to the reaction. They observed that aminoisindoline initially coordinated with the central core of the Mg-TBTAP, but the addition of DABCO displaces the aminoisindoline and facilitates the complete reaction of the starting material. This optimisation resulted in an improved yield of TBTAPs to ~40% (Scheme 2.17).⁴⁸

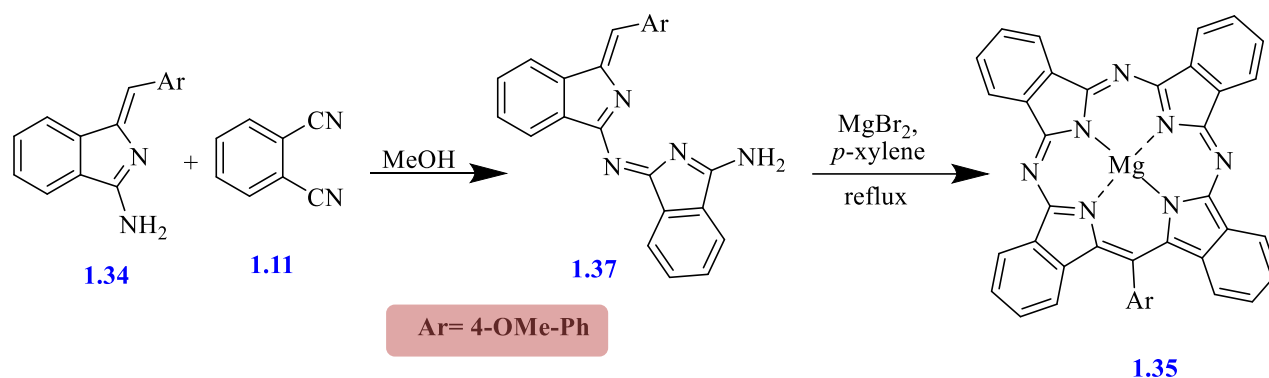


Scheme 1.17: The further optimised synthesis of TBTAP hybrids from aminoisindolines.

1.5.2.5 Synthesis of TBTAP using aminoisindoline dimer (AB dimer)

The Cammidge group's recent research has explored a novel approach aimed at selectively achieving high yields of Mg-TBTAPs by modifying both the experimental conditions and starting materials. This new method involved the synthesis of novel intermediate (AB dimers) **1.37** and their derivatives, obtained through a new synthesis route. The dimers

were formed by condensing aminoisoindoline **1.34** with phthalonitrile **1.11**. Refluxing this dimer in *p*-xylene as solvent replacement of diglyme with 0.5 equiv. MgBr₂ for 3 h resulted in the formation of Mg-TBTAPs **1.35** with excellent yields of ~ 40%.⁵⁰ This procedure presents a significant progression in the synthesis of the parent Mg-TBTAP structure, offering equally high yields under mild reaction conditions (Scheme 1.18).



Scheme 1.18: Synthesis of Mg-TBTAP from intermediate AB dimer **1.37**.

1.6 History of porphyrazine

Porphyrazines, or tetraazaporphyrins are tetrapyrrole macrocycles like porphyrin but with nitrogen atoms in the *meso*-positions. They differ from phthalocyanines in that their β -positions are not benzo-fused and can undergo substitution reactions. While they may not as yet have gained the same level of recognition as porphyrins or phthalocyanines, modifying the β -positions of the pyrrole rings with different substituents is a known valuable pathway to tailoring their properties (Figure 1.8).⁵¹

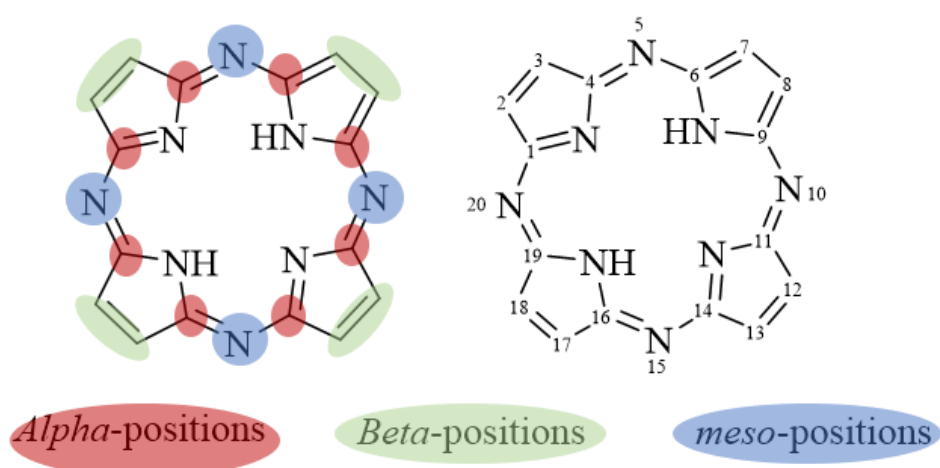


Figure 1.8: Numbering system for porphyrazine H₂Pz structures.

The molecular structure of porphyrazine ligand H_2Pz and its β -substituted $H_2Pz R_8$ and β,β -annulated $H_2Pz(Het)_4$ derivatives are illustrated in Figure 1.9.⁵¹

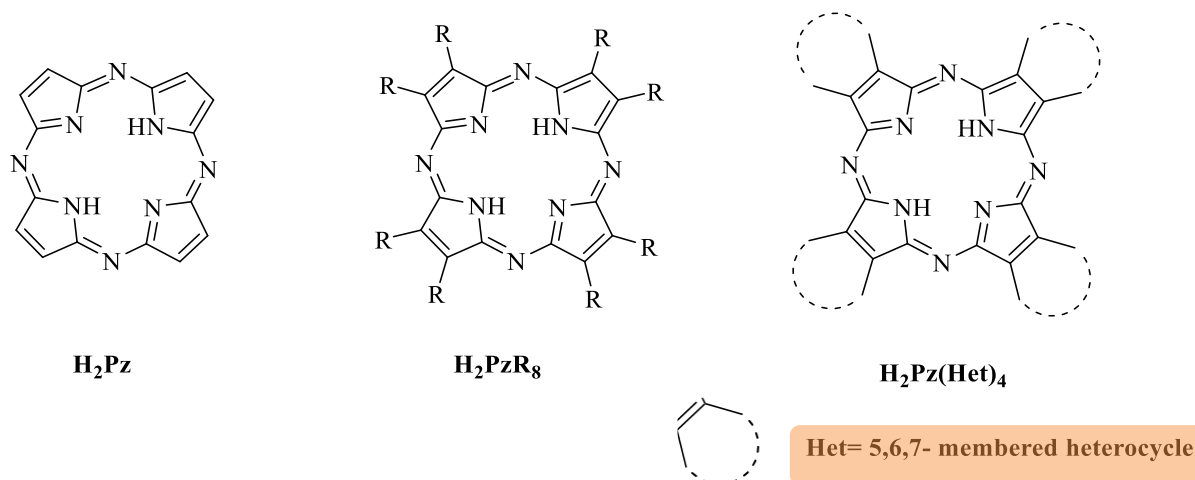
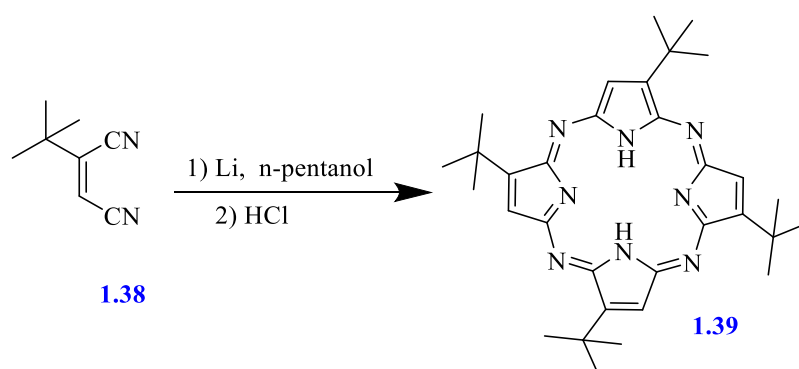


Figure 1.9: The compositions of porphyrazine and its derivatives.

Until today, limited research has been conducted on porphyrazine macrocycles in general. However, they have garnered increasing attention over the past two to three decades.⁵² The early synthesis by R. P. Linstead and colleagues made a groundbreaking discovery by synthesizing simple porphyrazines using a widely used method called template macrocyclization.⁵³ Subsequently, Luk'yanets *et al.* utilized the Linstead protocol to synthesise tetra-*t*-butylporphyrazines **1.39** from 1,2-dicyano-3,3-dimethyl-1-butene (Scheme 1.19).⁵⁴



Scheme 1.19: Macrocyclization of 1,2-dicyano-3,3-dimethyl-1-butene, using the Linstead protocol.⁵⁵

Nonetheless, the significant advancement in the synthesis and structural investigation of novel groups of porphyrazine macrocycles was achieved through the collaborative efforts of A. G. M. Barrett and B. M. Hoffman and coworkers. for the successful preparation of a substantial number of β -substituted porphyrazines.^{52,56}

1.6.1 Synthesis of symmetrical and unsymmetrical porphyrazines (Pzs)

Symmetrical Pzs are generally easier to synthesise and purify. Their preparation involves the cyclotetramerization of dicyanitrile precursors in the presence of a suitable metal salt to yield metalloporphyrazines (M-Pzs), which can then be demetalated. In contrast, synthesising unsymmetrical porphyrazines presents greater challenges using traditional methods. These unsymmetrical Pzs are produced through the cyclotetramerisation of differently substituted dicyanitriles precursors, which result in porphyrazine complexes with varying structural configurations such as AAAB, ABAB, BBBB and ABAB, as shown in Figure 1.10. The challenge arises from the nature of cyclotetramerisation, which tends to form a mixture of regioisomers and side products, complicating purification and resulting in a low yield. Despite these challenges, unsymmetric Pzs often exhibit unique electronic and other properties, making them highly valuable for applications in molecular electronics and photodynamic therapy.⁵⁷

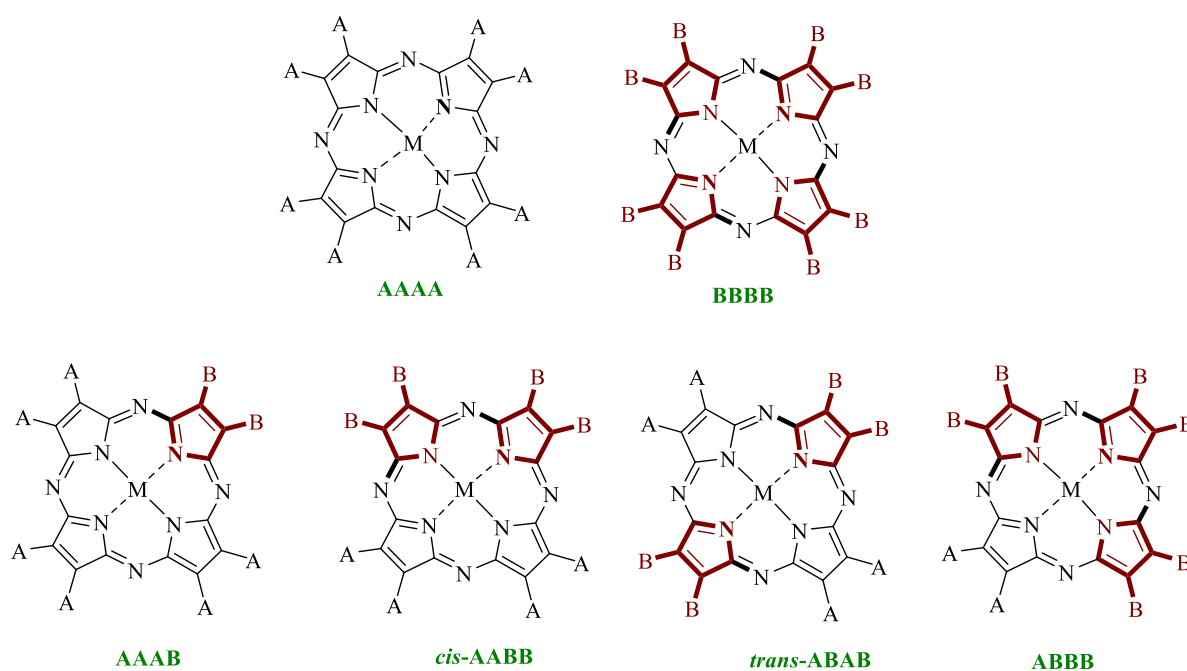


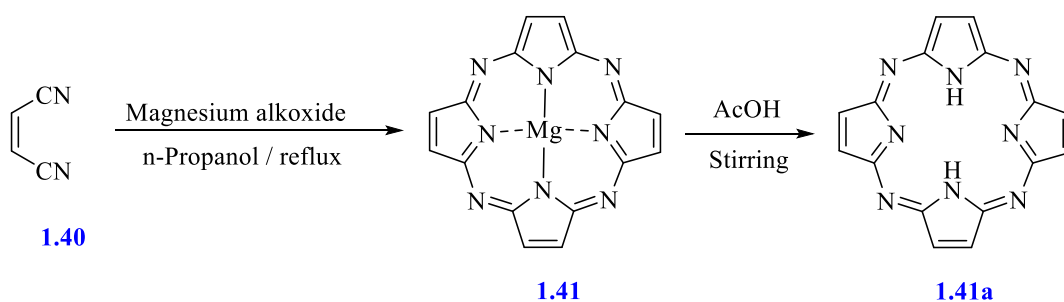
Figure 1.10: The molecular structure of symmetrical and unsymmetrical Pzs.

In the literature there are only a few methods for synthesizing unsymmetrical substituted Pz, mainly due to the scarcity of suitable synthetic intermediates. These intermediates are often unstable and offer a limited range of substitution patterns. Additionally, their utilization does not provide acceptable yields of unsymmetric macrocycles.⁵⁸ However, the most employed synthetic method for phthalocyanines or porphyrazines with two types of substitutions, A and B, involves the crossover cyclotetramerization of phthalonitrile, maleic dinitrile, diiminoisindoline, or diiminopyrroline precursors with different substitution. The resulting products usually showed a mixture compounds, which could be unsymmetrical substituted

tetraazaporphyrins (AAAB, AABB, ABAB, and ABBB tetraazaporphyrins) or symmetric macrocycles designated as AAAA and BBBB Pz. However, obtaining and isolating the desired unsymmetrical compound involves a challenging chromatographic separation process, which is not always feasible, and results in low yields.⁵⁹

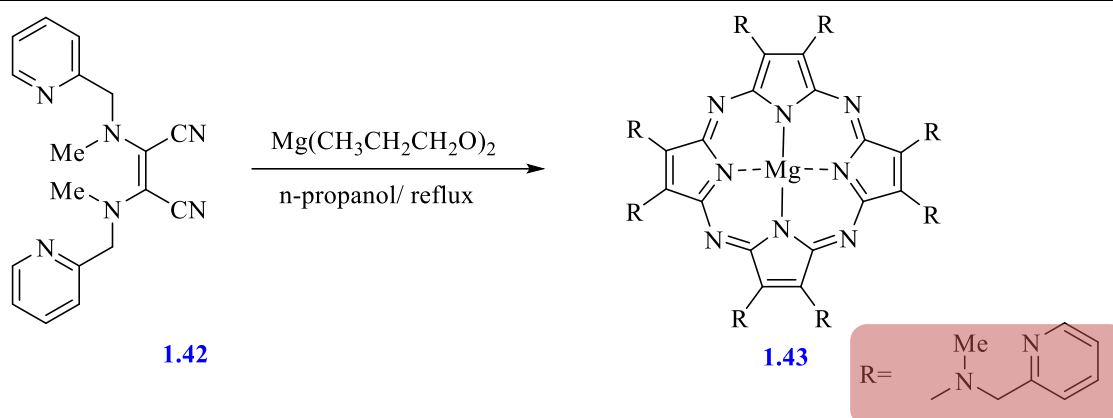
1.6.1.1 Synthesis of symmetrical porphyrazines (Pzs)

R. Patrick Linstead prepared the parent porphyrazine in 1937.⁶⁰ However, challenges were encountered due to the tendency of maleic dinitrile, the starting material, for isomerization or decomposition. When heated it decomposes rapidly under alkaline conditions, resulting in a low yield of porphyrazine.⁵³ However, this issue can be overcome by employing magnesium templated cyclization by using magnesium propoxide in *n*-propyl alcohol followed by stirring the formed magnesium-porphyrazine **1.41** in glacial acetic acid to yield symmetrical metal-free porphyrazine **1.41a** with a satisfactory yield (Scheme 1.20).^{53, 60}



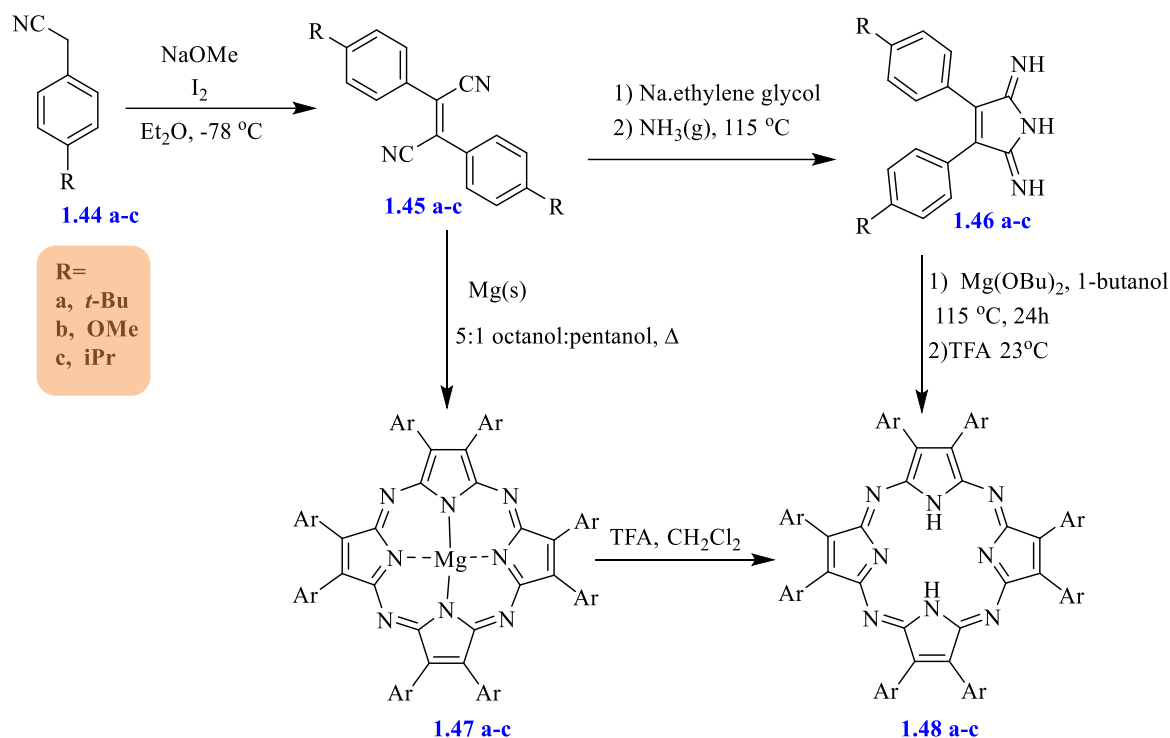
Scheme 1.20: Synthesis of symmetrical porphyrazine from maleic dinitrile **1.40**.

Furthermore, synthesising octa-substituted porphyrazine involved reacting the maleic dinitrile derivatives with magnesium alkoxide at high temperatures in the appropriate alcohol under heating. Typically, either *n*-butanol or *n*-propanol is employed as the alcohol, with the specific choice determined by optimising the reaction temperature. The process begins by combining magnesium turnings with a crystal of iodine and dry propanol, followed by heating. This results in the creation of magnesium alkoxide. Next, the mixture is treated with dinitrile derivative such as **1.42** and heated again, in this case producing porphyrazine **1.43** with a yield of 13% (Scheme 1.21).⁶¹



Scheme 1.21: Synthesis of β -octa-substituted symmetrical porphyrazine **1.43**.

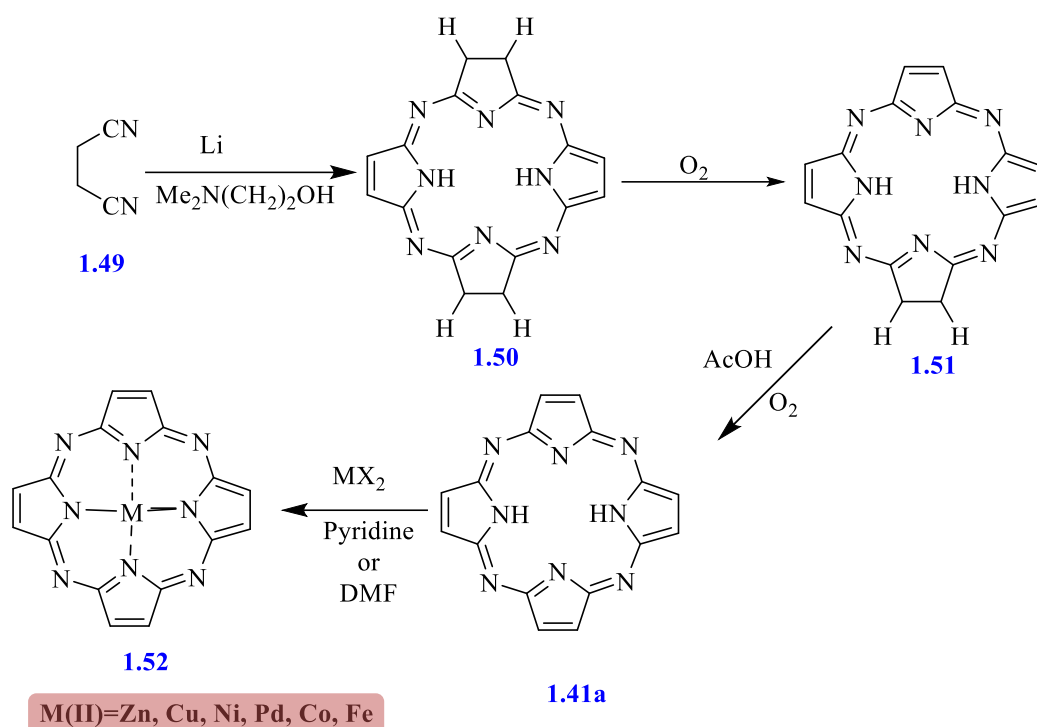
Synthesising symmetrical octaarylporphyrazines can also be achieved starting from fumaronitriles, and involves starting from preparation of the fumaronitrile precursor itself through the oxidative coupling of substituted phenylacetonitrile, e.g. **1.44 a-c**. 4-R-phenylacetonitrile ($R = t\text{-Bu}$, MeO, or *i*-Pr) reacts with excess NaOMe in the presence of I_2 , forming the fumaronitrile product **1.45 a-c**.^{62,63} After that, the two methods for synthesizing metal-free porphyrazine were applied as shown in Scheme 1.22. The first method involves converting the fumaronitrile starting material into pyrroline-2,5-diimine derivatives **1.46a-c**, which requires a high-temperature reaction in the presence of ethylene glycol as a solvent and an excess of ammonia gas. The pyrroline **1.46a-c** is subsequently cyclized with the magnesium template method in butanol to form symmetrical Pz **1.47a-c**. Demetallation is achieved by acid treatment of Pz with an excess of TFA. However, this method has disadvantages as it requires the use of large quantities of highly reactive and toxic $\text{NH}_3(\text{g})$.⁶⁴



Scheme 1.22: Synthesis of symmetrical porphyrazine from fumaronitrile **1.45** derivatives.

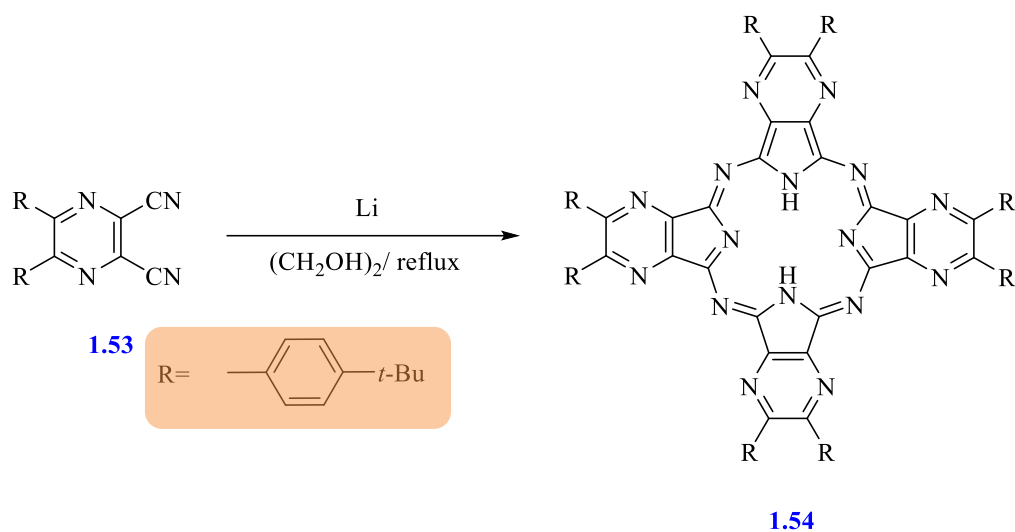
The second method involves direct cyclization of the fumaronitrile **1.45 a-c** without the need for preparing the pyrroline precursor. The cyclization of the fumaronitrile occurs in a mixture of 1-octanol and 1-pentanol (5:1) at a high temperature of 180 °C, using the magnesium template to give the formation of magnesium-porphyrazine **1.47 a-c**. This method was optimized for large-scale synthesis using 5-7 g of fumaronitrile, whereas the pyrroline method has a maximum scale of approximately 1g. Similarly, the demetallated porphyrazine was obtained by stirring in TFA. Additionally, the reaction time for this method is approximately 2-3 days compared to the pyrroline method, which takes from one to two weeks.⁶⁴

The symmetrical porphyrazines can also be synthesised by refluxing succinonitrile with lithium N,N-di-methyl-amino-ethylate in the presence of alcohol and air bubbling. This first affords the reduced form tetraazabacteriochlorin **1.50** and tetraazachlorin **1.51** derivatives, respectively. Oxidation of these reduced forms by heating them in AcOH at 80 °C gave **1.41a** with a low yield. Refluxing **1.41a** in pyridine or DMF with metal chlorides affords the corresponding metal symmetrical porphyrazines (Scheme 1.23).⁶⁵



Scheme 1.23: Synthesis of symmetrical porphyrazine from succinonitrile **1.49**.

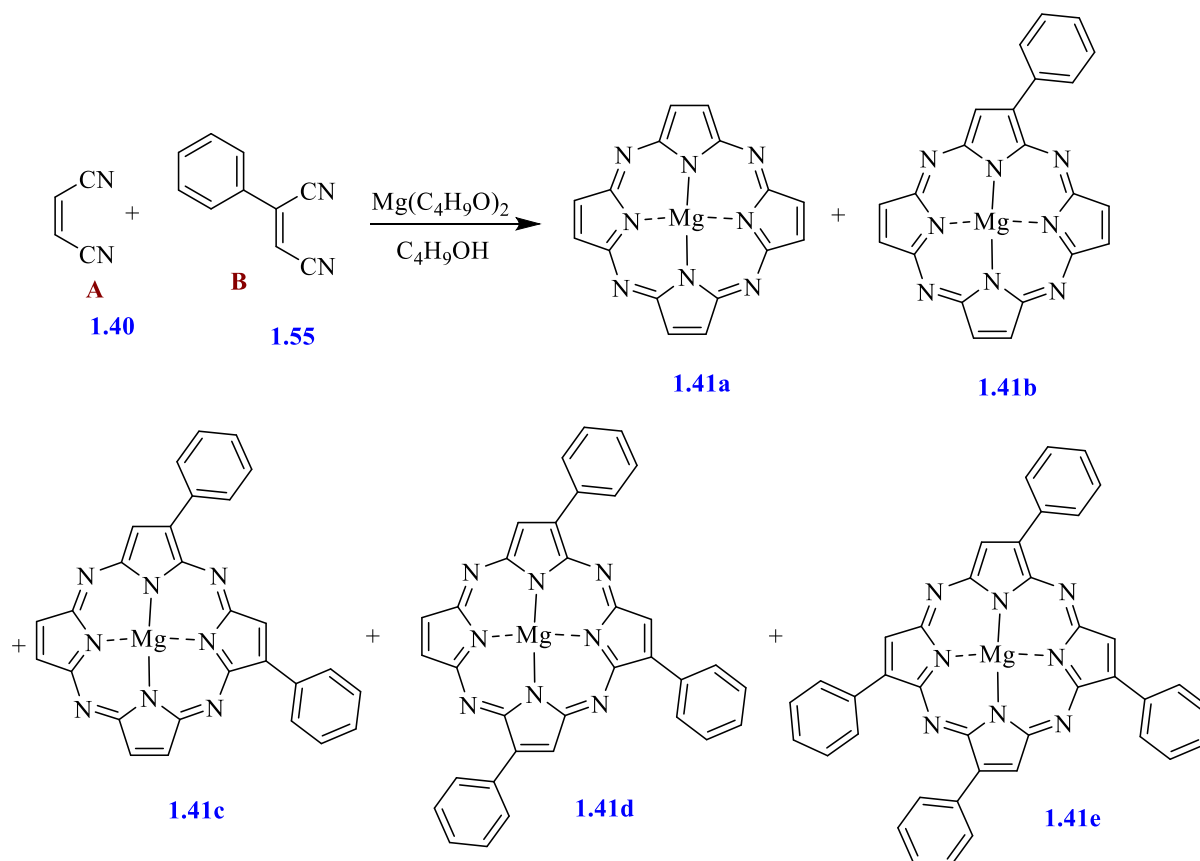
An alternative approach for synthesizing porphyrazine derivatives that are more closely related to Pcs with high nitrogen content involved heating lithium in ethylene glycol followed by adding a derivative of 2, 3-dicyanopyrazine **1.53** to the solution. The obtained reaction mixture was heated for 3 h under reflux and then cooled. After the reaction was completed, the resulting green precipitate underwent purification through column chromatography to afford Pz **1.54** (Scheme 1.24).⁶⁶



Scheme 1.24: Synthesis of symmetrical porphyrazine from 2,3-dicyanopyrazine substituents 1.53.

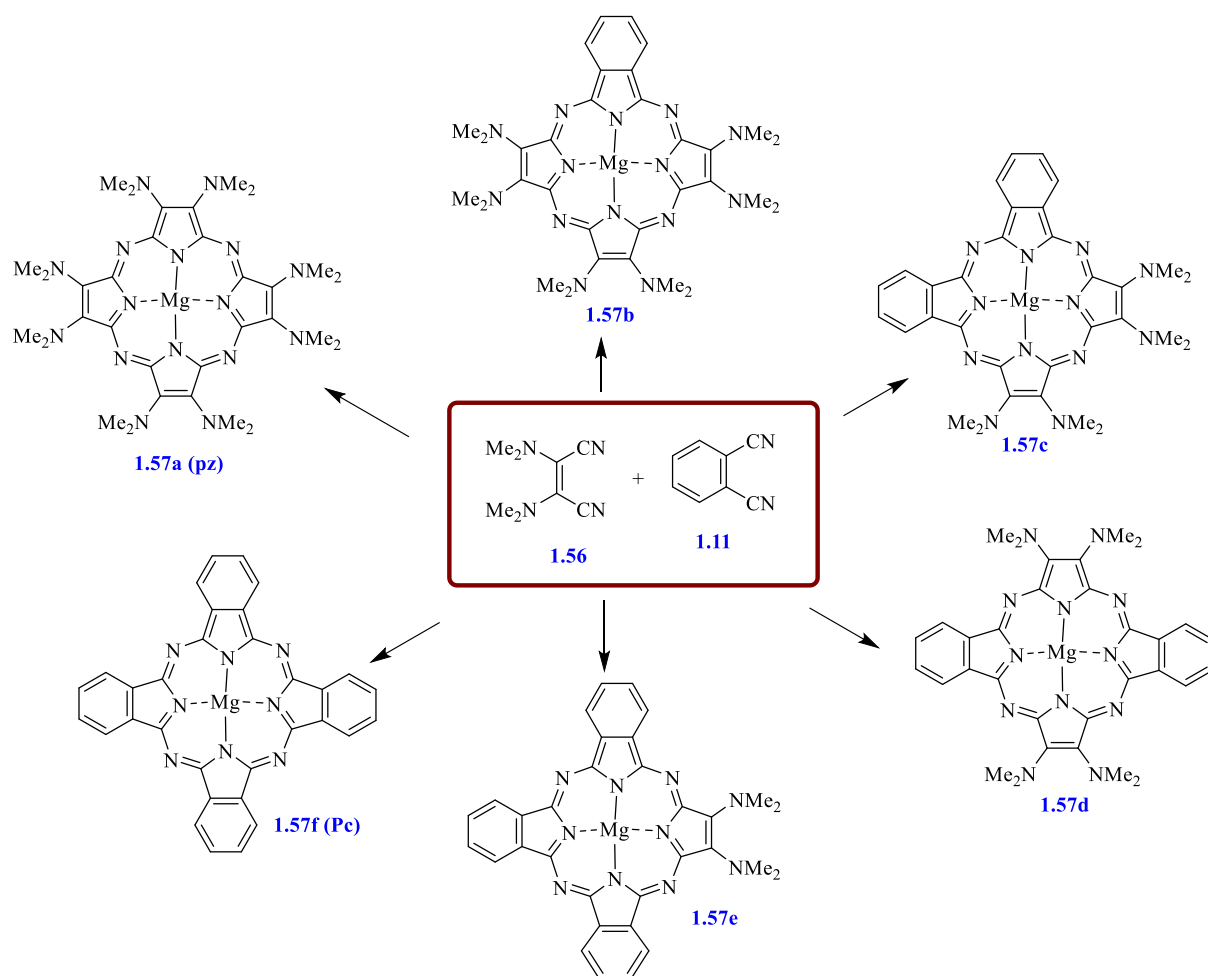
1.6.1.2 Synthesis of unsymmetrical porphyrazine (porphyrazine/phthalocyanine) complexes

The cyclotetramerization of maleic dinitrile derivatives with various substituted dicarbonitrile precursors resulted in the formation of several unsymmetrical Pz hybrids. For example, the reaction with phenylmaleic dinitrile, performed via template condensation in the presence of magnesium butoxide in butanol under reflux conditions, gives a mixture of Mg-porphyrazine with different numbers of phenyl substituents (Scheme 1.25). The best conditions for the reaction were determined to be a 1:1 ratio of maleic dinitrile and monophenyl-maleic dinitrile, along with a cyclization time of 15 minutes. When one of these starting materials dominates the reaction mixture, more tetraazaporphyrin or tetraphenyltetraazaporphyrin is produced compared with the other products. The short synthesis time is attributed to the high reactivity of maleic dinitrile, which decomposes when heated at high temperatures for a long time. The resulting dark green mixture of five tetraazaporphyrins hybrids **1.41a-e** was separated using column chromatography.⁶⁷



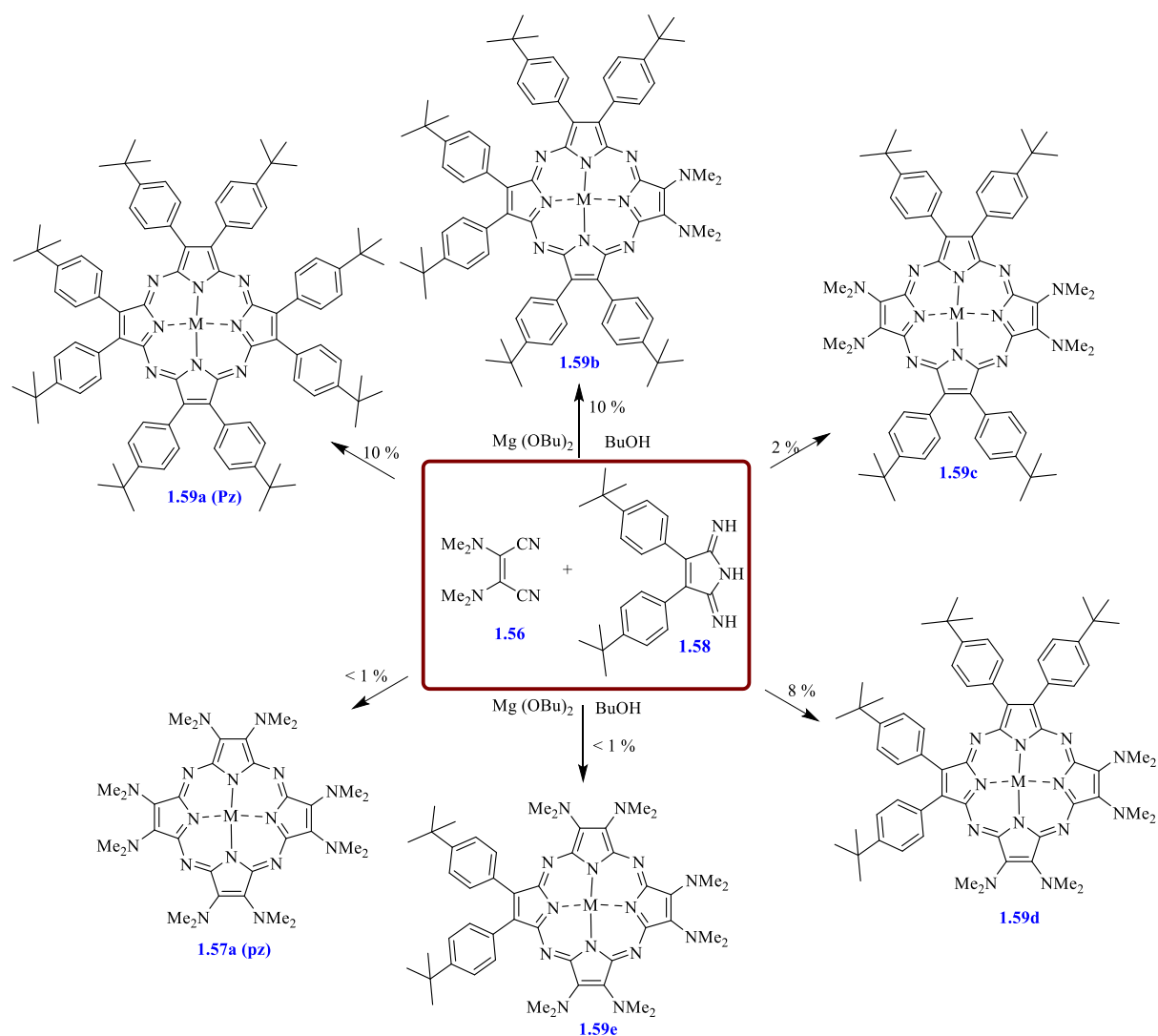
Scheme 1.25: Synthesis of unsymmetrical porphyrazine from maleic dinitrile **1.40**.

Additionally, the bis(dimethylamino)maleic dinitrile **1.56** was co-cyclised with 1,2-dicyanobenzene **1.11** using a magnesium template, following the conditions described by Linstead,⁵³ to produce unsymmetrical porphyrazines with two, four, and six bis(dimethylamino) substituents (Scheme 1.26). Initially, magnesium was stirred in butanol under nitrogen for 24 h. After that, the starting materials **1.56** and **1.11** were added to the resulting suspension of magnesium butoxide, and the reaction mixture was refluxed for 3 days to form a blue-black residue. By employing a molar ratio of 25:1 between the starting materials (**1.56**:**1.11**), a mixture of Pzs **1.57a** and **1.57b** was formed through macrocyclization. Alternatively, when the macrocyclization reaction was conducted using a 3:1 molar ratio, another mixture of complexes **1.57c**, **1.57d**, **1.57e**, and Mg Pc **1.57f** was formed.⁶⁸



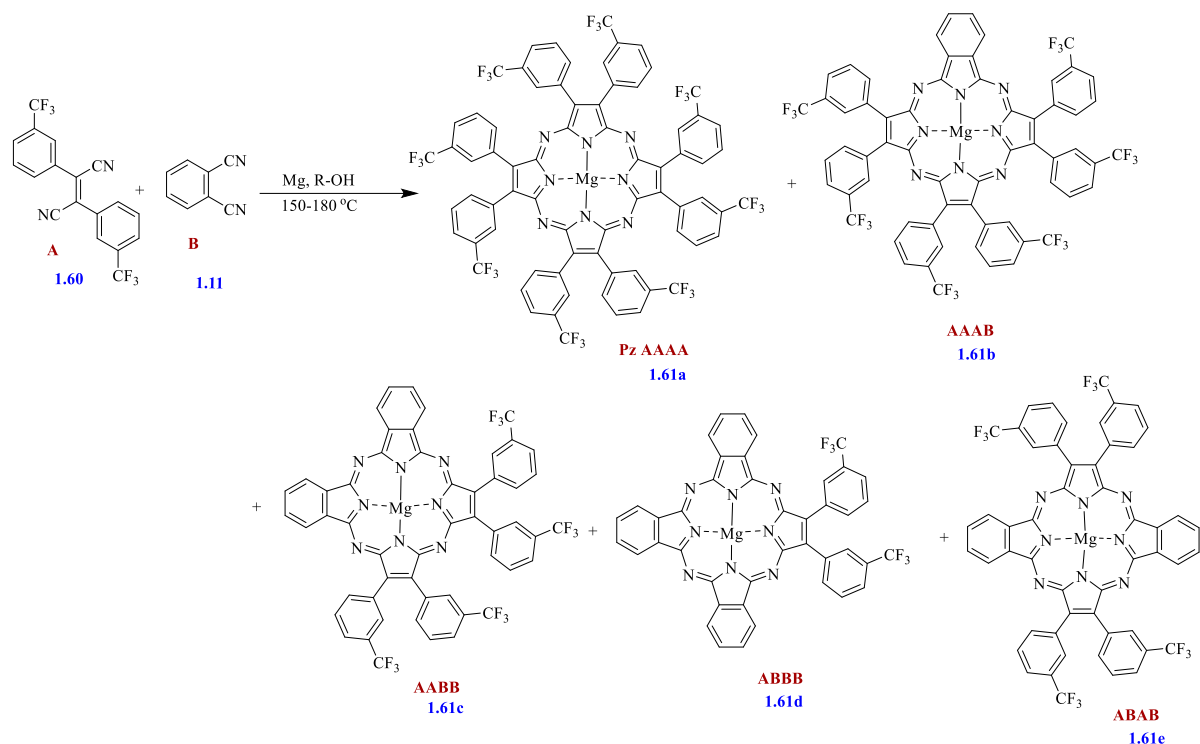
Scheme 1.26: Synthesis of unsymmetrical Pz from reaction maleic dinitrile with phthalonitrile **1.11**.

Furthermore, the reaction of maleic dinitrile derivative **1.56** with pyrroline-2,5-diimine **1.58** derivatives in the suitable alcohol gives a mixture of six different symmetrical or unsymmetrical porphyrazines. In Scheme 1.27 the porphyrazines were prepared by utilizing a magnesium alkoxide templated macrocyclization reaction in a refluxing alcohol solvent.^{69, 60} The reactivity, solubility, and relative molar ratio of maleic dinitrile factor into the yield of each porphyrazine. The demetallated form of the porphyrazine can be acquired through acidic conditions.⁷⁰



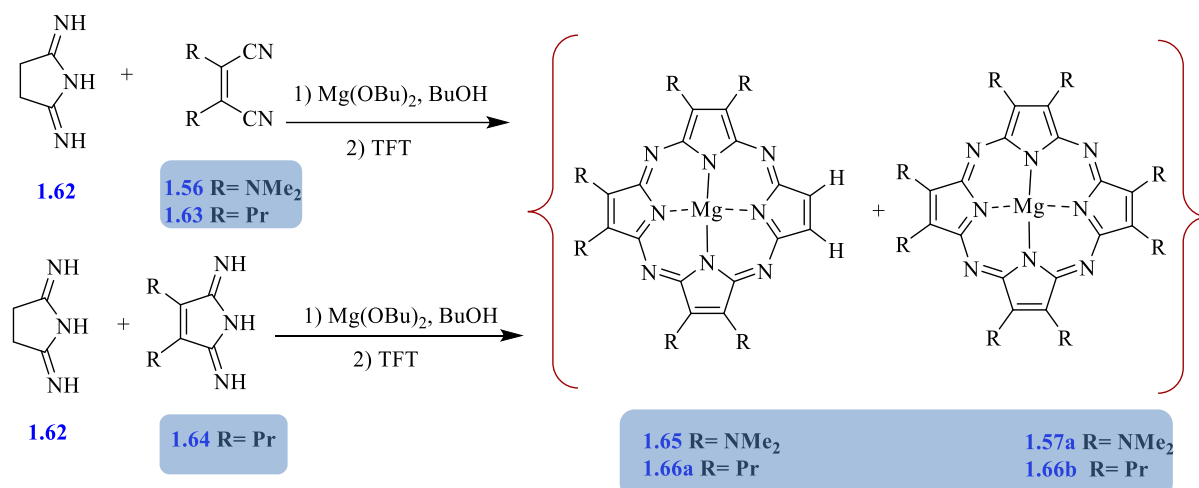
Scheme 1.27: Synthesis of six different porphyrazines through the reaction of maleic dinitrile derivative with pyrroline-2,5-diimine derivatives.

Fumaronitrile derivatives can also be employed to synthesise unsymmetrical Pzs complexes. This was achieved through the reaction of bis-(*m*-trifluoromethylphenyl) fumaronitrile **1.60** with phthalonitrile **1.11** in the presence of template using magnesium alkoxides in alcohol at high boiling point (Scheme 1.29). Upon mixing **1.60** and **1.11** at a 1:1 ratio, six products (Pz AAAA, Pc BBBB, AAAB, ABAB, AABB, and ABBB) were obtained and subsequently separated by column chromatography.⁷¹



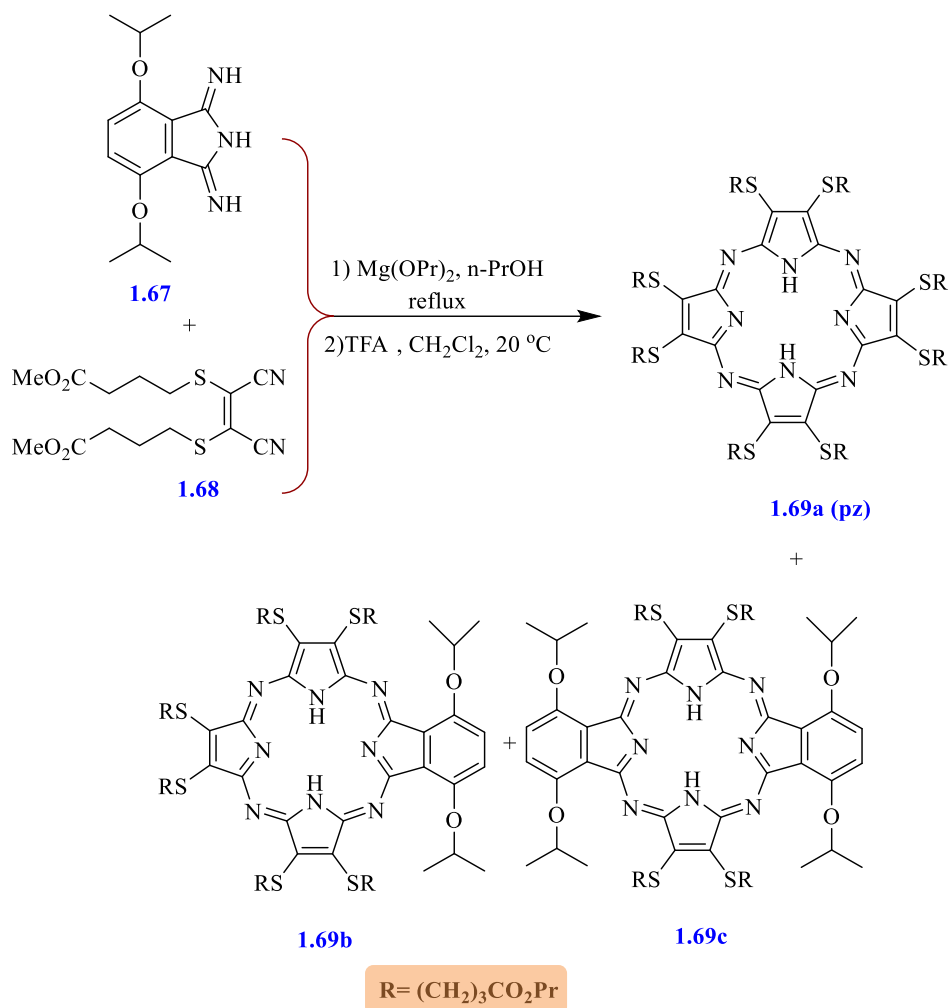
Scheme 1.28: Synthesis of unsymmetrical porphyrazines from fumaronitrile derivatives.

Nie *et al* also synthesised unsymmetrical porphyrazines with three substituted pyrroles at the periphery and one unsubstituted pyrrole. For the synthesis of these complexes of porphyrazines, they employed two methods, as shown in Scheme 1.29. The first method discussed earlier involved the reaction between maleic dinitrile derivatives **1.56** and 2,5-diiminopyrrolidine **1.62** using the co-macrocyclization approach. The product contained the unsymmetrical and the symmetrical porphyrazine **1.65** and **1.57a**, respectively. The second method, also described by the same research group, utilized the reaction of 3.5 equivalents of pyrroline-2,5-diimine derivatives **1.64** with 2,5-diiminopyrrolidine **1.62** via Linstead crossover macrocyclisation. This second method yielded higher amounts of the desired unsymmetrical porphyrazines **1.66a** to the co-cyclization of maleic dinitrile.⁷²



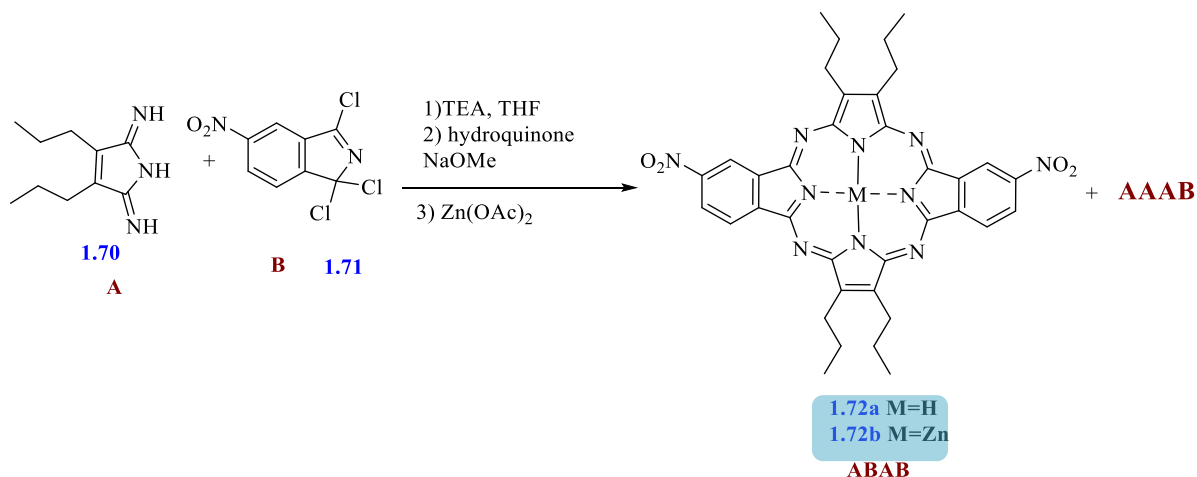
Scheme 1.29: Synthesis of porphyrazine complexes from diiminopyrroline **1.62**.

By utilizing diiminoisindolines derivatives and the Linstead crossover macrocyclization method, the unsymmetrical porphyrazines can be obtained. 1-Imino-4,7-bis(1-methylethoxy)-1H-isindole-3-amine **1.67** was subjected to a reaction with dimethyl 6,7-dicyano-5,8-dithia-6(Z)-dodecenedioate **68** in a ratio of 1:6 (**1.67**: **1.68**). This reaction resulted in the formation of Pz AAAB **1.69 b** and *trans* pz AABB **1.69 c** with yields of 5% and 7% respectively. Additionally, a trace amount of Pz AAAA **1.69 a** was detected. There was no formation of *cis*-Pz AABB and Pz BBBB. The high ratio of **1.68** to **1.67** was necessary due to the significantly higher reactivity of compound **1.68** compared to diiminoisindoline **1.67** (Scheme 1.30).⁷³



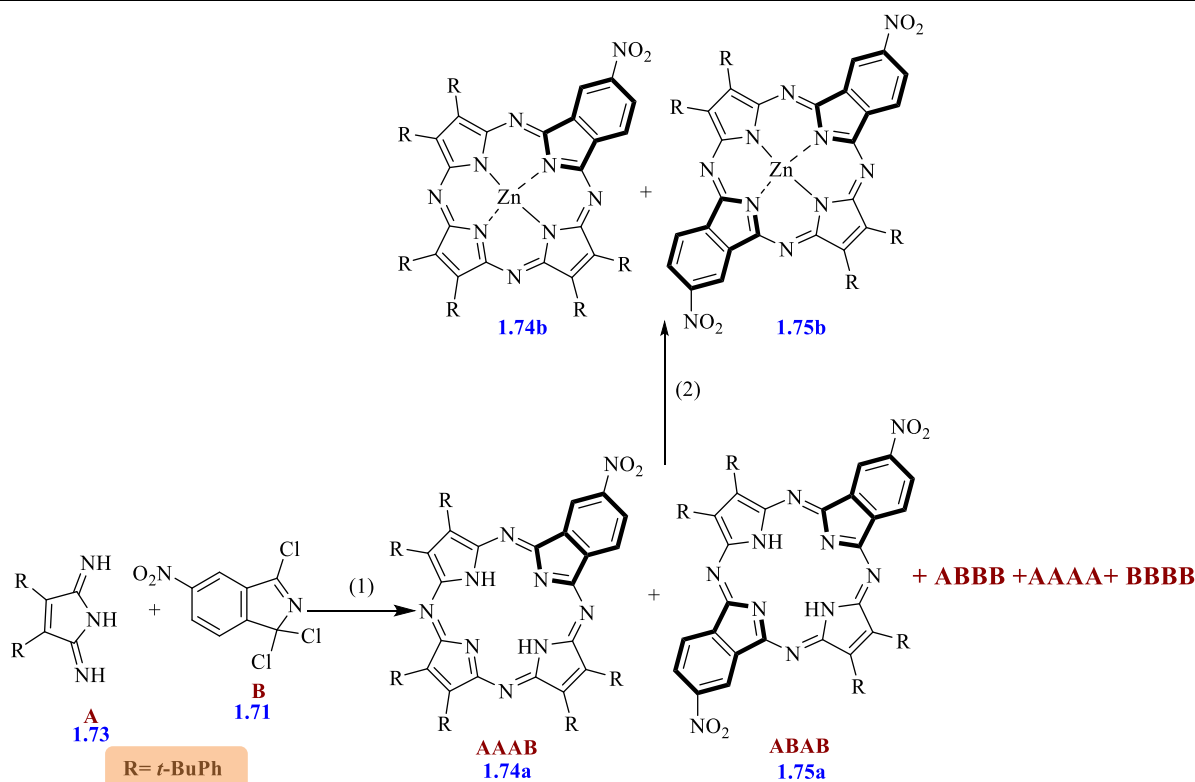
Scheme 1.30: The synthesis of porphyrazine molecules from diiminoisoindole derivative.

Furthermore, in Scheme 1.31, the synthesis of another Pz/Pc complex is shown as unsymmetrical dinitrobenzoporphyrazine ABAB **1.72a, b** from diiminopyrroline derivative was achieved by reacting the intermediate **1.70** with 5(6)-nitro-1,1,3-trichloro isoindoline **1.71** in the presence of triethylamine at 40 °C. The main compounds resulting are a mixture of free-base porphyrazines **1.72a** and the AAAB Pz. After that, the mixture was treated with zinc(II) acetate to metallate the porphyrazines **1.72b**. On the other hand, the low temperature used for the reaction almost prevented of the diiminopyrroline derivative **1.70** from self-condensing to afford symmetric porphyrazine AAAA.^{74,59}



Scheme 1.31: The synthesis of unsymmetrical Pzs from diiminopyrrole derivative.

In 2020, a direct condensation from diiminopyrrole derivatives was successfully used to synthesise metal-free and metal complexes of ABAB and AAAB Pz complexes **1.74a**, **1.75a**. This condensation involved the preparation of a solution from diiminopyrrole precursor **73** in THF followed by the slow addition to a solution of isoindole derivative **1.71** in THF and stirring for 3 h. Then, hydroquinone and sodium ethoxide were added to the reaction and refluxed for 10 h to obtain complexes ABAB and AAAB (Scheme 1.32). The undesired products are trace quantities of unsymmetrical AB BB and symmetric derivatives Pz AAAA and Pc BBBB. After the purification of the metal-free complexes, they were carried out with anhydrous Zn(OAc)₂ to be converted into metal porphyrin complexes **1.74 b**, **1.75 b**.⁵⁷



Scheme 1.32: The synthesis of Pz complexes (1) THF, TEA, hydroquinone, NaOEt, reflux
(2) Zn (CH₃COO)₂, 80-90 °C.

1.7 Properties of phthalocyanines/porphyrazines

1.7.1 Electronic absorption spectroscopy

Porphyrazines are synthetic aza-analogues of porphyrins, distinguished by the incorporation of nitrogen atoms into their macrocyclic structure, and they possess unique optical properties owing to their macrocyclic ring composed of four pyrrole units linked by azamethine bridges. When porphyrazines incorporate annulated benzo units, they form phthalocyanines. Both Pzs and Pcs exhibit notable properties, including electrochemical activity and strong absorption in the UV-Vis region, which are related to their electronic structures and the nature of their central metal ions.^{65, 75}

As we described earlier, a strong Soret band characterises porphyrins around λ 380-500 nm, and multiple *Q*-bands are observed between λ 500–700 nm in UV-Vis spectroscopy. These absorption features are linked to π - π^* electronic transitions within the macrocycle.^{75, 76} For phthalocyanines, the extended conjugation of the ring system results in lower energy π - π^* transitions which are observed in two main regions of the UV-Vis spectrum. Metallated phthalocyanines (M-Pcs) exhibit a distinct and strong absorption *Q*-band in the red/ near-infrared region between λ 670-720 nm, which gives phthalocyanines their characteristic

blue/green colour. In contrast, metal-free phthalocyanines (H_2Pcs) display a split Q -band due to reduced molecular symmetry in the structure. Both M - Pcs and H_2Pcs exhibit a weaker absorption band in the blue region of the spectrum, which is the Soret band located about 320–370 nm. TBTAPs exhibit lower symmetry due to the replacement of one nitrogen bridge with a methine in the *meso* position. The absorption spectra of Mg -TBTAPs and Mg - Pcs are quite similar. The main difference is that the Q -band of the Mg -TBTAPs is split into two distinct components.⁴¹ Similarly, porphyrazines display an intense Soret-band at wavelengths below 400 nm and a Q -band that has its principal absorption at λ greater than 600 nm, with the additional vibronic structure to shorter wavelength.⁶⁹ The Soret band corresponds to the π - π^* electronic transition and typically appears in the UV region, while the Q -bands, associated with the same transition, are in the visible region of the spectrum. The characteristic UV/Vis spectra of metal-free and metalated Pz offer a clear distinction between the two forms, making them helpful in monitoring de-metalation and metalation processes. Like porphyrins and phthalocyanines, metalated porphyrazines (M - Pzs) exhibit a higher degree of symmetry compared to their (H_2Pz) metal-free derivatives, leading to more pronounced Q -bands, usually centred around 670 nm. In contrast, metal-free Pzs exhibit split Q -bands, appearing between 690–710 nm due to their lower symmetry (Figure 1.11).⁷⁷ However, both metalated and metal-free Pzs feature a single Soret band at ~ 370 nm.^{78, 79}

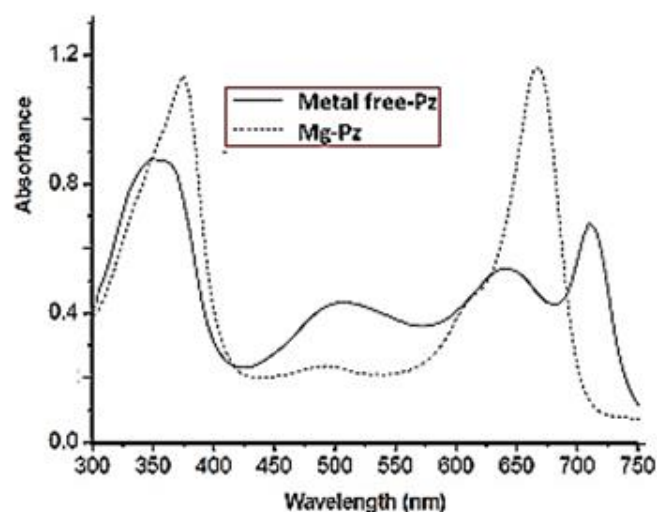


Figure 1.11: UV-Vis electronic spectra of metalated and demetallated porphyrazine in THF.⁷⁸

The electronic transitions in the UV-Vis region of porphyrins Pcs and Pzs can be explained using various theoretical models, the most widely accepted being Gouterman's four-orbital model.⁸⁰ Although beyond the scope of this thesis, the model is briefly described here.

Metalloporphyrins have D_{4h} symmetry and, according to this model, four orbitals (a_{2u} , a_{1u} and e_g) are responsible for the main transitions of these complexes that generate the Soret band and Q -band. In these complexes, the accidental degeneracy of the a_{1u} and a_{2u} orbitals lead to strong interaction between one electron excited state, resulting in a narrow energy difference between the Soret and Q -bands and a reduced intensity in the latter. However, with the substitution of *meso*-carbons with nitrogen atoms in Pzs and Pcs, the MO energies of the macrocycle are significantly affected. The a_{2u} orbital has a strong contribution to the *meso* positions of the ring and this removes the accidental degeneracy with the a_{1u} orbital, leading to the greater separation between the Soret and Q -bands and an increase in Q -band intensity.⁸¹

Figure 1.12 illustrates the UV-Vis absorption spectra of metalloporphyrin, metal phthalocyanines and metalloporphyrins. Both M-Pcs and M-Pzs exhibit a single sharp and intense Q -band with a weak vibronic Q shoulder at lower wavelengths. The Soret band is broader and less intense than the Q -band, particularly in M-Pcs compared to MPzs.⁸²

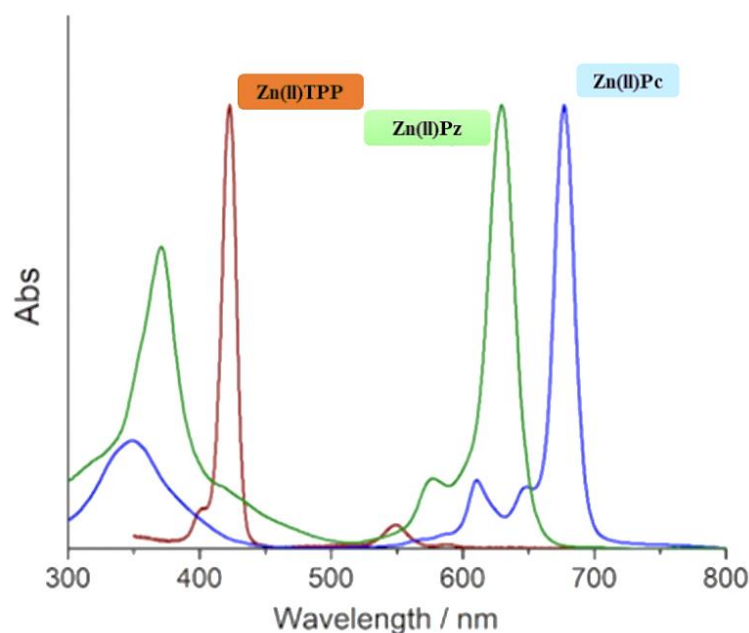


Figure 1.12: UV-Vis absorption spectra of the zinc(II) complexes of TPP (red), Pz (green) and Pc (blue).⁸²

The symmetry of the macrocyclic structure plays a key role in determining the electronic transitions observed in the UV-Vis spectra. Changes in the symmetry of the macrocycle structure of Pcs and Pzs provide different π -electronic arrangements, which results in the splitting of the Q -band and a shift toward longer wavelengths.⁸³

1.8 Applications

Porphyrazines and phthalocyanines belong to the classes of porphyrinoids, and they exhibit unique molecular structure that grants them exceptional physical and chemical properties. These properties enable their use in various applications as dyes, catalysts, optical sensors, solar energy converters and sensitisers for photodynamic and sonodynamic therapy.^{84, 85,86}

The advantageous properties of porphyrazines/phthalocyanine macrocycles were improved by replacing the metal ion in the macrocyclic core or incorporating different peripheral substituents. This metalation and functionalisation influence key properties such as electrochemical activity, light absorption in the UV-Vis range, and the ability to mediate singlet oxygen production, which is especially relevant in photodynamic therapy (PDT) applications.^{75, 82} Additionally, these macrocycles are used as electrocatalysts and in the preparation of green and blue dyes and pigments with significant resistance to photodegradation.⁸⁴

Unsubstituted porphyrazines and phthalocyanine rings are non-polar, and prone to aggregation due to π - π stacking interactions. This aggregation significantly impacts their solubility, limiting their use in scientific and technological applications where high solubility in water or organic solvents is necessary.⁶⁹ To address these issues, researchers have developed new aza-porphyrinoids derivatives with various peripheral substituents, which enhance solubility and reduce aggregation. For example, sulfanyl-based porphyrazine derivatives demonstrated significantly improved solubility, making them more suitable for practical applications.⁸⁴

1.8.1 Photodynamic therapy (PDT) applications

Photodynamic therapy is an emerging therapeutic technique primarily utilized for treating cancer and other diseases.^{87,88,89} PDT, a drug called a photosensitizer (PS) selectively accumulates in the tumour or damaged tissue. Upon exposure to UV, Visible, or near-infrared NIR light, the PS transitions to an excited state. In the presence of molecular oxygen, the activated PS generates reactive oxygen species (ROS), which oxidise biomolecules, leading to cell death and the loss of function of targeted cells. Porphyrazines and phthalocyanines, as second-generation photosensitizers,⁹⁰ exhibit strong absorption in the therapeutic wavelength region, making them more effective in PDT than porphyrins, which belong to the first-generation of PS but suffer from lower light absorption, limiting their use in deeper lesions.⁹¹ Porphyrinoids exhibit fluorescence that is highly beneficial for tracking the accumulation of photosensitizers within tissues, making them valuable for tumour imaging applications.^{92, 93}

Sulfanylporphyrazines, in particular, demonstrate significant potential as photosensitisers for PDT. Studies show that these complexes, especially those with dendrimeric moieties at the periphery, exhibit high photocytotoxicity against oral squamous cell carcinoma. For example, sulfanyl tribenzoporphyrazine with 4-[3,5-di(hydroxymethyl)phenoxy] butyl substituents have been identified as particularly effective against tongue-derived cancer cell lines (Figure 1.13).⁹⁴

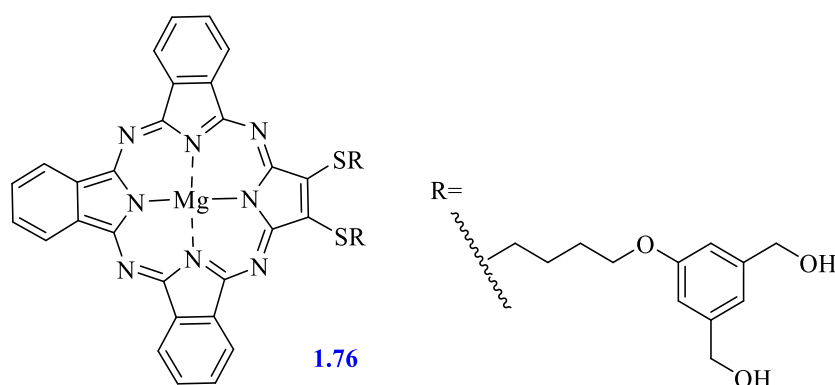


Figure 1.13: The structures of porphyrazine derivatives as photosensitisers for photodynamic treatment.

1.8.2 Antimicrobial applications in PDT

Photodynamic antimicrobial chemotherapy (PACT) offers a notable advantage over conventional antibiotic treatments, particularly in the face of increasing bacterial resistance to chemotherapeutic agents.⁹⁵ While typical antibiotic therapies rely on specific antibacterial drugs, PACT employs non-toxic photosensitisers PS that, upon activation by light, interact with microbial pathogens. This light-triggered interaction leads to the generation of reactive oxygen species (ROS), which damage the cellular components of the pathogens, ultimately resulting in their destruction.^{96,97} One promising class of photosensitisers used in PACT is magnesium (II) porphyrazines with dendrimeric groups such as 3,5-dimethoxybenzylthio related derivatives. These porphyrazine derivatives have demonstrated significant photodynamic activity, particularly against *Staphylococcus aureus*, a common pathogen found in wound infections (Figure 1.14).⁹⁸

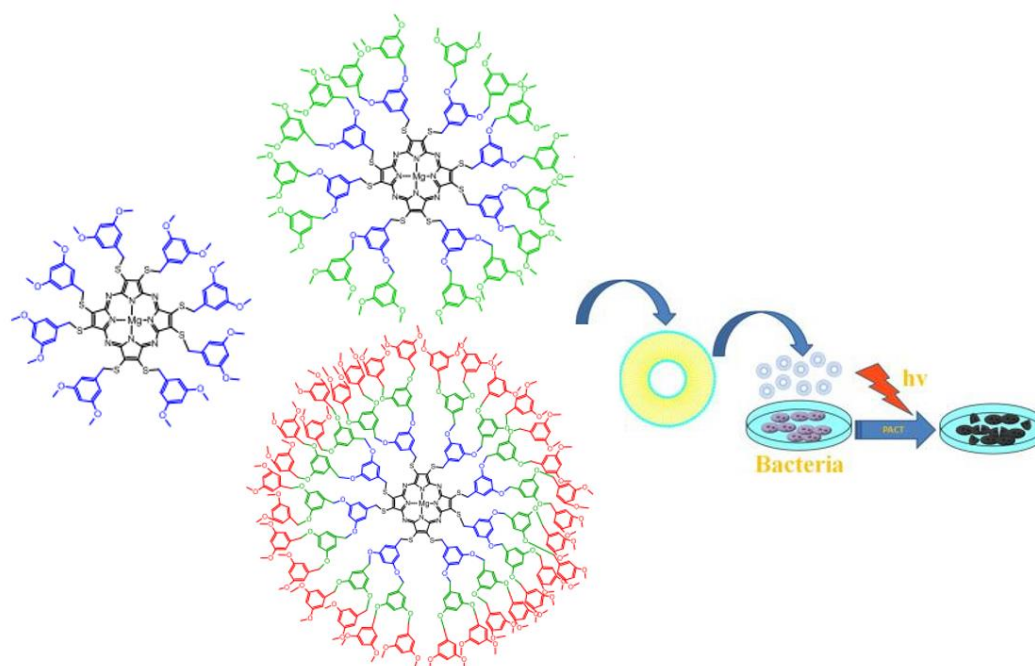


Figure 1.14: The structures of sulfanylporphyrazines with dendrimeric moieties as photosensitisers.

Peripherally substituted unsymmetrical porphyrazine and phthalocyanine complexes have recently garnered considerable attention due to their diverse range of potential applications.^{57,99} Even small structural modifications or shifts in the position of side groups on these compounds can result in significant changes to their optical, electrical, and catalytic properties. This tunability makes them highly valuable in fields such as photodynamic and sonodynamic therapies.^{100,101} For example, AAAB and AABB zinc(II)porphyrazine/phthalocyanine hybrid complexes **1.74b** and **1.75b** have been evaluated for their efficacy in treating bacterial infections and cancer (Figure 1.15). Both complexes demonstrated strong photodynamic antibacterial activity and showed promising results against squamous cell carcinoma and hypopharyngeal tumours.⁸³

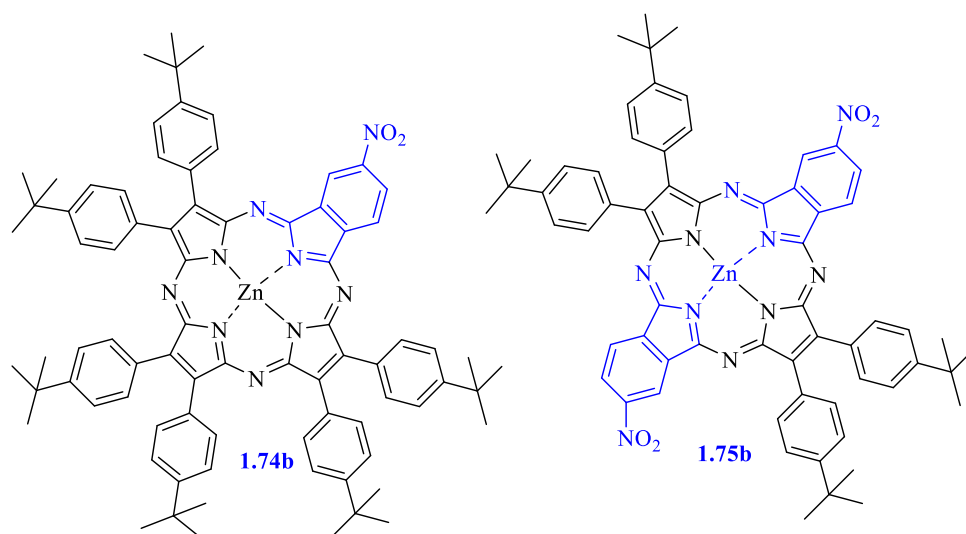


Figure 1.15: The structures of unsymmetrical porphyrazine and phthalocyanine complexes as antibacterial and anticancer agents.

1.8.3 Catalytic applications

The catalytic properties of porphyrazine/phthalocyanine complexes are influenced by the metal ions coordinated to the macrocyclic core, as well as the peripheral substituents attached to the structure. Iron (II/III) porphyrazine and phthalocyanine complexes, for instance, are highly selective catalysts that operate under mild, environmentally friendly conditions with low energy consumption. Studies have demonstrated that these complexes are effective in facilitating reactions such as the hydroxylation of aromatic and aliphatic molecules and the incorporation of amino substituents.^{102, 103} In addition, unsymmetrical iron (III) porphyrazines have been shown to catalyse the decomposition of organic pollutants from industrial wastes, making them valuable for industrial waste treatment. The most commonly used catalysts applied were symmetrical iron sulfanylporphyrazines **1.77**, **1.78** and **1.79**, as well as unsymmetrical **1.80** (Figure 1.16).¹⁰³

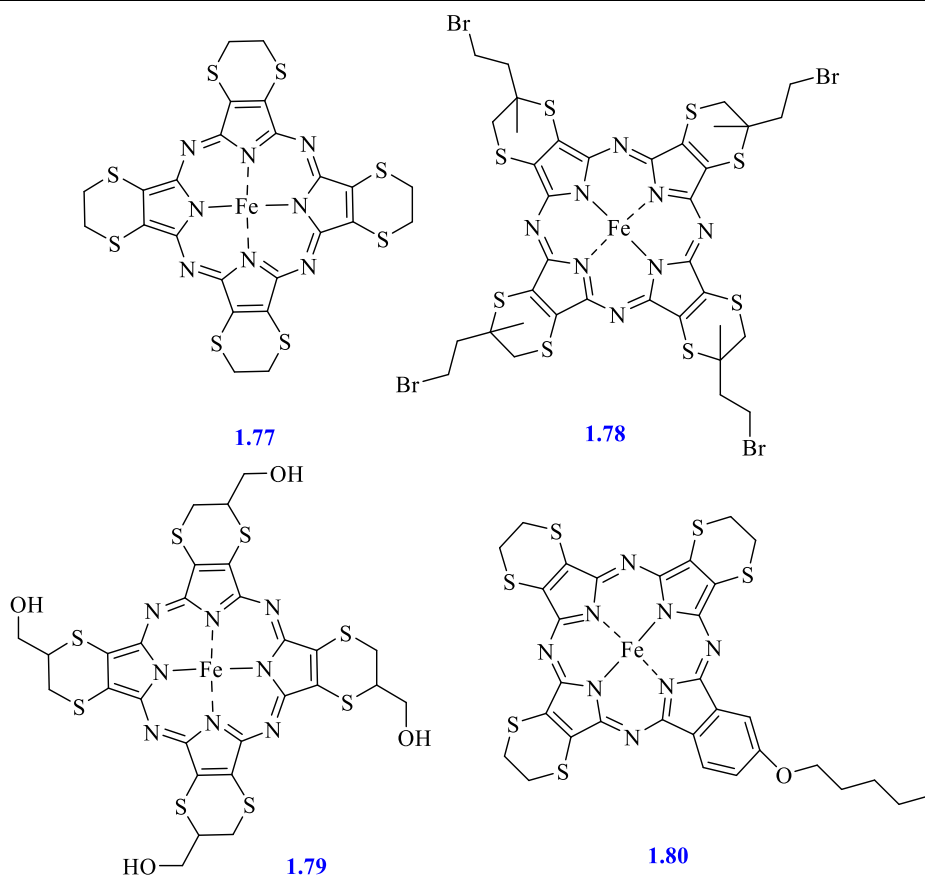


Figure 1.16: The structures of iron(II) sulfanylporphyrazines **1.77**, **1.78**, **1.79** and **1.80**.

1.8.4 Solar energy conversion and dye applications

Developing organic dyes and pigments is essential in current material chemical research. This includes applications such as dye-sensitised solar cells (DSSCs),¹⁰⁴ organic photovoltaics (OPVs),¹⁰⁵ photosynthesis mimics, and chemical sensors. Tuning Pzs/Pcs colour is a very important topic since the properties of functional groups of dyes affect the optical properties. For example, efficient DSSC requires organic photosensitiser dyes with broad and intense electronic absorption in UV and Visible regions (Soret and *Q*-bands). This excellent optical activity, which Pzs have, makes them favourable dyes for many such fields and applications. A notable example is the (tetraazaporphyrinato)phosphorous(V) complexes (Figure 1.17 shows an example, PPz **1.81**), which exhibit unique absorption. The phosphorus(V) ion contributes to a minor shift in both the *Q*-band and the Soret band positions. *Q*-band absorption was identified at 664 nm, and the Soret band at 342 nm. Furthermore, a broad intense absorption band was detected between the Soret and *Q* bands at 534 nm. Consequently, PPz **1.81** exhibits absorption across the entire UV-Vis region, making it an attractive choice for these applications.¹⁰⁶

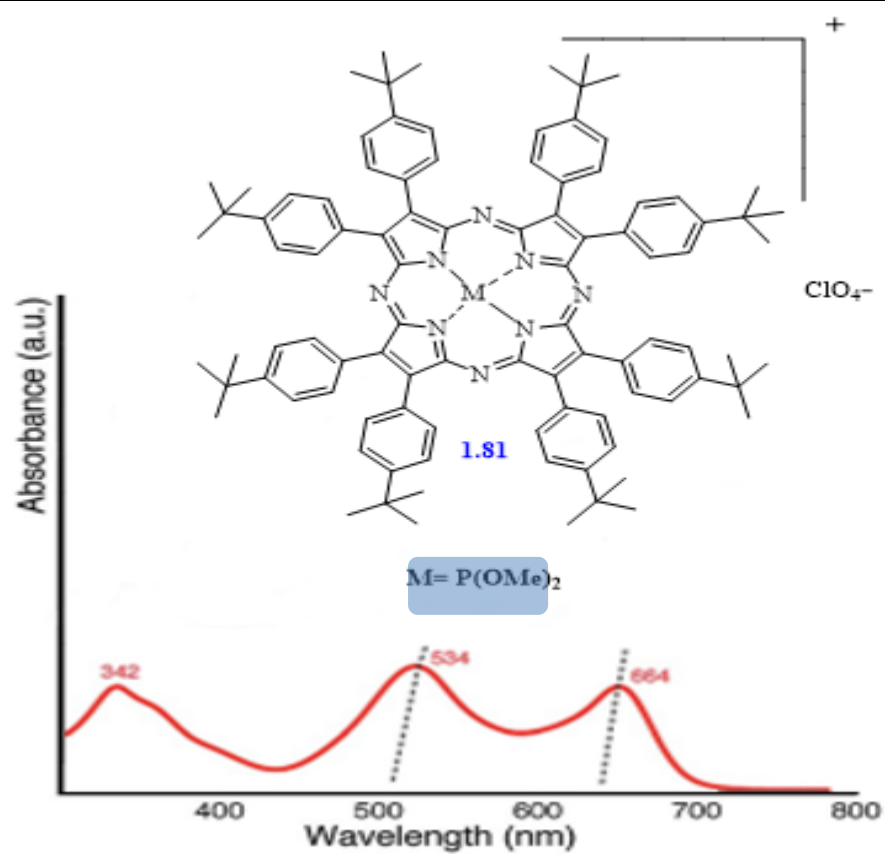
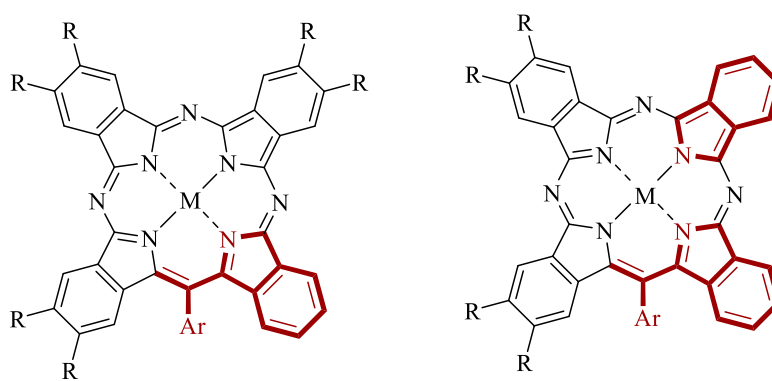


Figure 1.17: The structure of porphyrazine derivative (PPz **1.81**) as organic photosensitiser and its UV-vis absorption spectrum in DCM.¹⁰⁶

1.9 Aim of the project

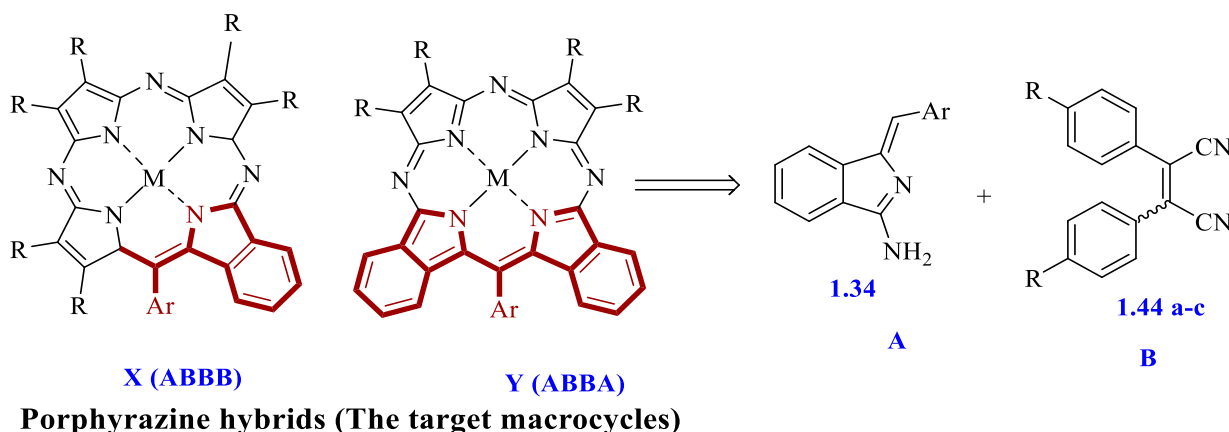
Porphyrazines are intermediate structures between the phthalocyanines and porphyrins. These compounds are tetraazaporphyrins and can be prepared by macrocyclisation of succinonitrile or fumaronitrile derivatives. It has also been discussed that hybrid structures between porphyrin and phthalocyanine can be produced through replacement of one or more *meso* carbons with nitrogen.



Tetrabenzotriazaporphyrin (TBTAP) hybrids

Figure 2.18: Molecular structures of 3:1 and 2:2 TBTAPs.

This project aims to investigate a new series of macrocyclic unsymmetrical mono- and disubstituted porphyrazine-phthalocyanine hybrids with both modifications—monobenzotriazaporphyrins **MBTAPs X** and **DBTAPs Y**. As described in the introduction, recent developments by the Cammidge group have demonstrated that aminoisindoline precursor **1.34** can be used to induce cyclisation with phthalonitrile and to access **TBTAPs**. Specifically, the project will investigate the reaction between our known aminoisindoline precursor and (substituted and unsubstituted) alkene dinitriles aiming to obtain the following derivatives (Scheme 1.33).⁷³



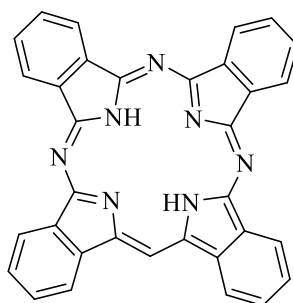
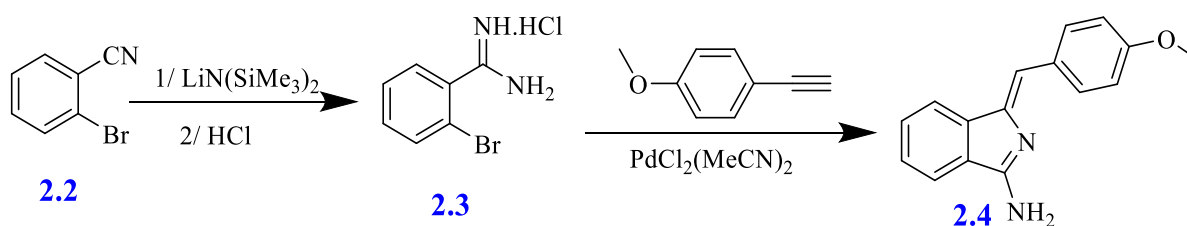
Scheme 1.33: Molecular structures of porphyrazines hybrids.

CHAPTER 2:

Results and Discussion

2.1 Introduction

The Cammidge research group has become increasingly interested in the synthesis of tetrabenzotriazaporphyrin (TBTAP) hybrids since they discovered their first example by chance during a typical phthalocyanine preparation.¹⁰⁷ Encouraged by their initial results, the research group has been dedicated to developing a modern synthetic method for creating TBTAPs **2.1**. With notable progress, the group successfully reported a straightforward, versatile, synthesis of *meso*-substituted TBTAPs in good yield.²⁹ The key to the new synthesis approach involved employing an aminoisoindoline as a precursor, which was easily accessible through the methodology shown in Scheme 2.1.³⁰ The starting point of this project was, therefore, to repeat this synthesis to become familiar with the chemistry and use the aminoisoindoline as a precursor for initiating TBTAP syntheses. In this reaction sequence, we found that reasonable yields were only achieved using carefully executed reaction conditions; the optimised sequence of reactions is therefore described in full.

**2.1****Figure 2.1:** The chemical structure of tetrabenzotriazaporphyrin (TBTAP) **2.1**.**Scheme 2.1:** Synthesis of the aminoisoindoline **2.4**.

2.2 Synthesis of [20-(4-methoxyphenyl)-tetrabenzob[*b, g, q, l*]-5, 10, 15-triaza-porphyrinato] magnesium “*meso*-(4-methoxyphenyl) TBTAP Mg” from aminoisoindoline

2.2.1 Synthesis of *o*-Bromobenzamidine 2.3

Briefly, *o*-bromobenzamidine salt **2.3** was prepared by treating a solution of 2-bromobenzonitrile **2.2** in THF with lithium bis(trimethylsilyl)amide (1.0 M in THF) at room temperature.¹⁰⁸ The reaction was quenched with a mixture of HCl-isopropanol (1:1) at 0 °C followed by stirring at room temperature overnight to give *o*-Br-benzamidine hydrochloride salt **2.3** as a white solid in good yield 89%. The *o*-Br-benzamidine salt **2.3** was confirmed by ¹H NMR spectroscopy, where the characteristic peak for protons of N-H is observed as a broad singlet at the chemical shift δ 9.42 ppm (Figure 2.2).

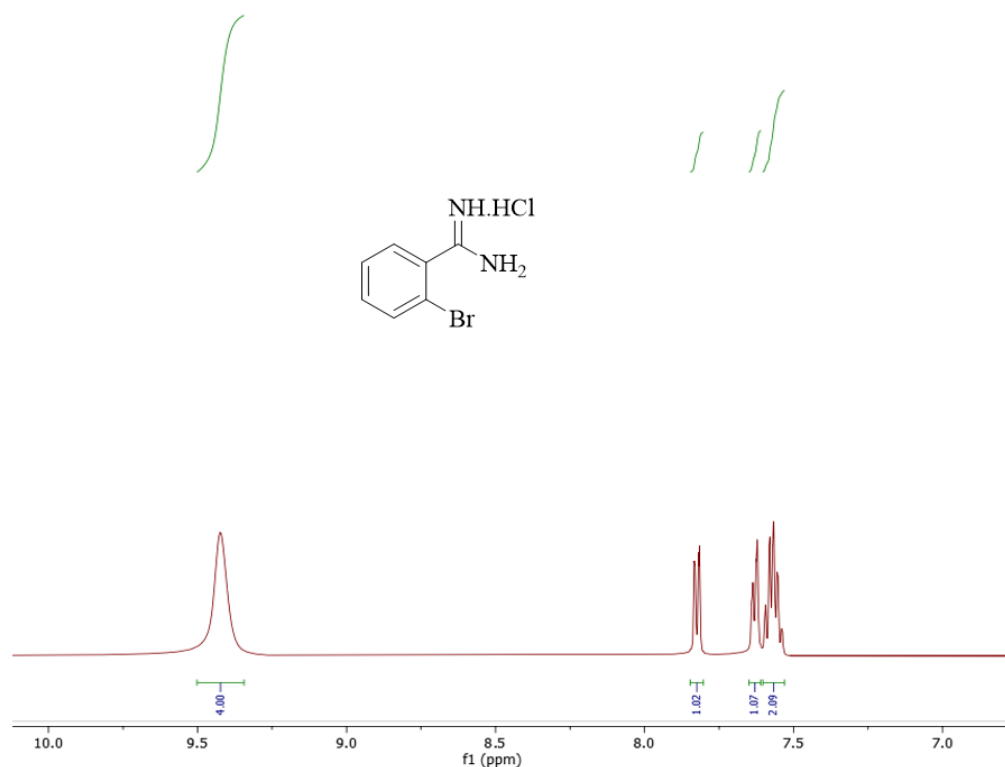
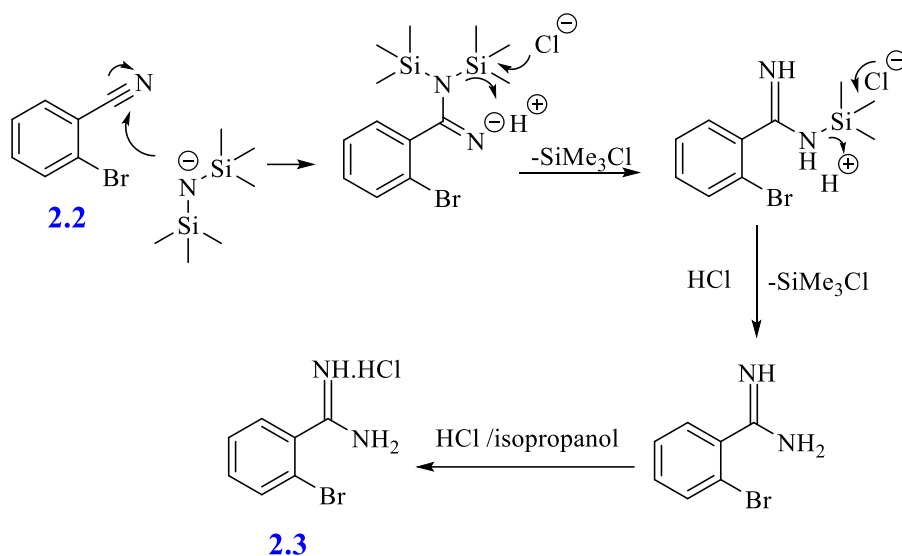


Figure 2.2: ¹H NMR spectrum of *o*-bromobenzamidine hydrochloride salt **2.3** in DMSO-*d*₆.

The formation of benzamidine salt **2.3** can be explained by the nucleophilic attack of the nitrogen atom in the bis-trimethylsilylamino anion at the partially positive carbon atom of the nitrile group, forming an imine anion. This is followed by acid hydrolysis of trimethylsilyl groups to give the corresponding salt **2.3** (Scheme 2.2).



Scheme 2.2: The mechanism for preparing *o*-bromobenzamidine hydrochloride salt **2.3**.

2.2.2 Synthesis of (*Z*)-1-(4-methoxyphenylmethylene)-1*H*-isoindol-3-amine **2.4**

The next step involved cross-coupling (copper free Sonogashira reaction) followed by cycloisomerization reaction of the amidine salt **2.3** with 4-methoxyphenylacetylene using palladium catalyst and BINAP as ligand, in the presence of DBU as a base in dry DMF solvent under nitrogen.⁴⁹ The reaction mixture was heated to 120 °C for 1 h under microwave irradiation and then worked up. The crude product was purified by column chromatography and crystallization to give pure isoindoline derivative **2.4** as yellow needles with 49% yield. The structure of the isoindoline derivative was confirmed by ¹H NMR spectroscopy, which showed the characteristic peaks for the OCH₃ and CH alkene group at 3.84 ppm and ~ 6.83 ppm, respectively (Figure 2.3).

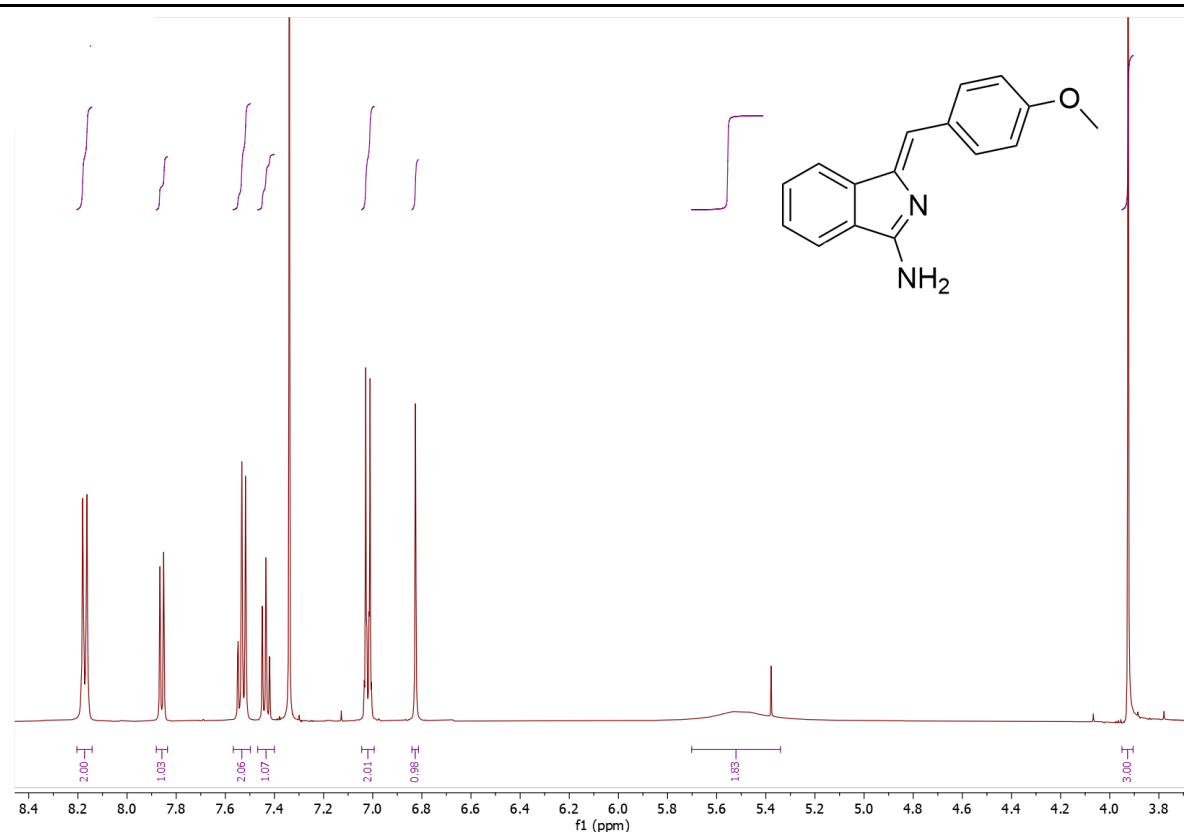
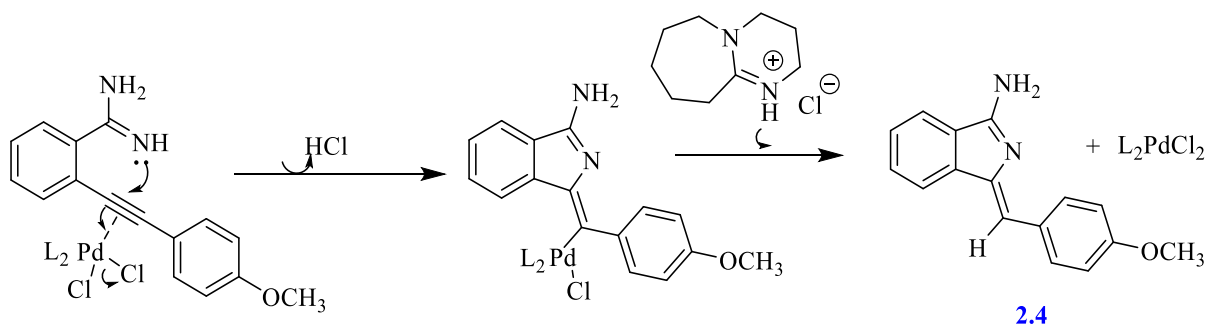


Figure 2.3: ^1H NMR spectrum of (*Z*)-1-(4-methoxyphenylmethylene)-1*H*-isoindol-3-amine **2.4** in CDCl_3 .

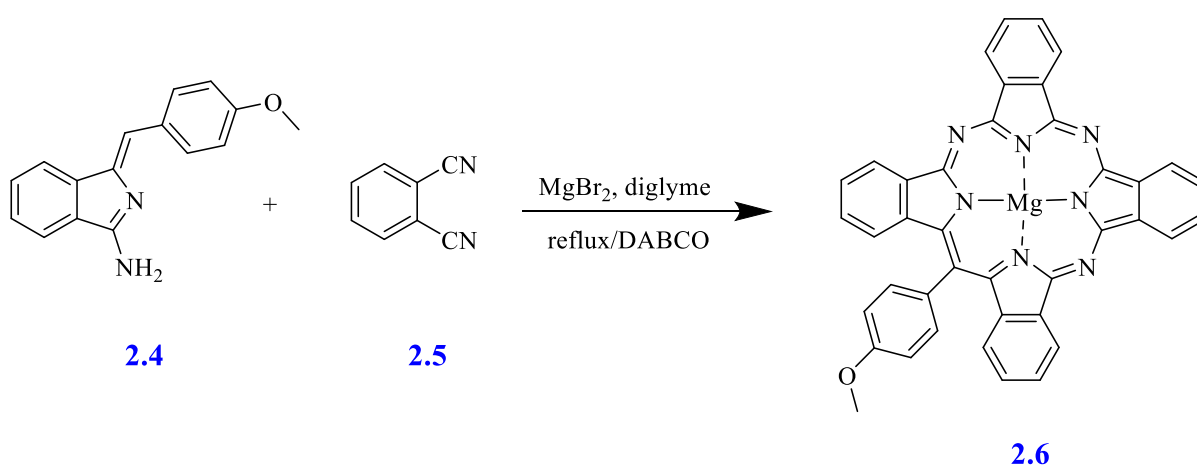
Copper-free Sonogashira cross-coupling mechanism is well known.¹⁰⁹ As shown in Scheme 2.4, this initial step is immediately followed by a regio-selective 5-*exo-dig* cycloisomerization domino reaction that yields aminoisoindoline **2.4**. NOSEY NMR during the original studies reveals that the reaction selectively produces the *Z*-alkene geometry.⁴⁹ The proposed mechanism, outlined in Scheme 2.3, involved three steps: initial coordination between the palladium catalyst and the alkyne, subsequent loss of HCl molecule, and final protonation with catalyst regeneration.¹⁰⁹



Scheme 2.3: Suggested mechanism to formation aminoisoindoline **2.4**.

2.2.3 Synthesis of [20-(4-methoxyphenyl)-tetrabenzo [*b, g, q, l*]-5,10,15-triazaporphyrinato] magnesium **2.6**

The final step is synthesising the target *meso*-substituted TBTAP derivative involves cyclising the intermediate aminoisindoline with phthalonitrile around a metal template (magnesium), as reported by Cammidge and coworkers.³⁰ Aminoisindoline **2.4** and phthalonitrile **2.5** were combined with MgBr₂ in diglyme in the presence of DABCO. The mixture was heated at 220 °C for 4 h under an argon atmosphere using an oil bath. After the reaction was completed, the crude product was purified via two successive column chromatography steps, followed by recrystallization from a mixture of acetone and EtOH (1:1) to give the desired (Mg TBTAP-OCH₃) **2.6** as green crystals with a 16% yield (Scheme 2.4).



Scheme 2.4: Synthesis of *meso*-(4-methoxyphenyl) TBTAP **2.6**.

Based on the ¹H NMR spectrum shown in (Figure 2.4), we can observe that the four protons corresponding to the aromatic ring on the *meso* position appeared as doublets at δ 8.07 and 7.60 ppm. Furthermore, the peak of the methoxy group is observed as a singlet peak at 4.24 ppm. These observed data are in good agreement with the values found in the reference reported compound.³⁰

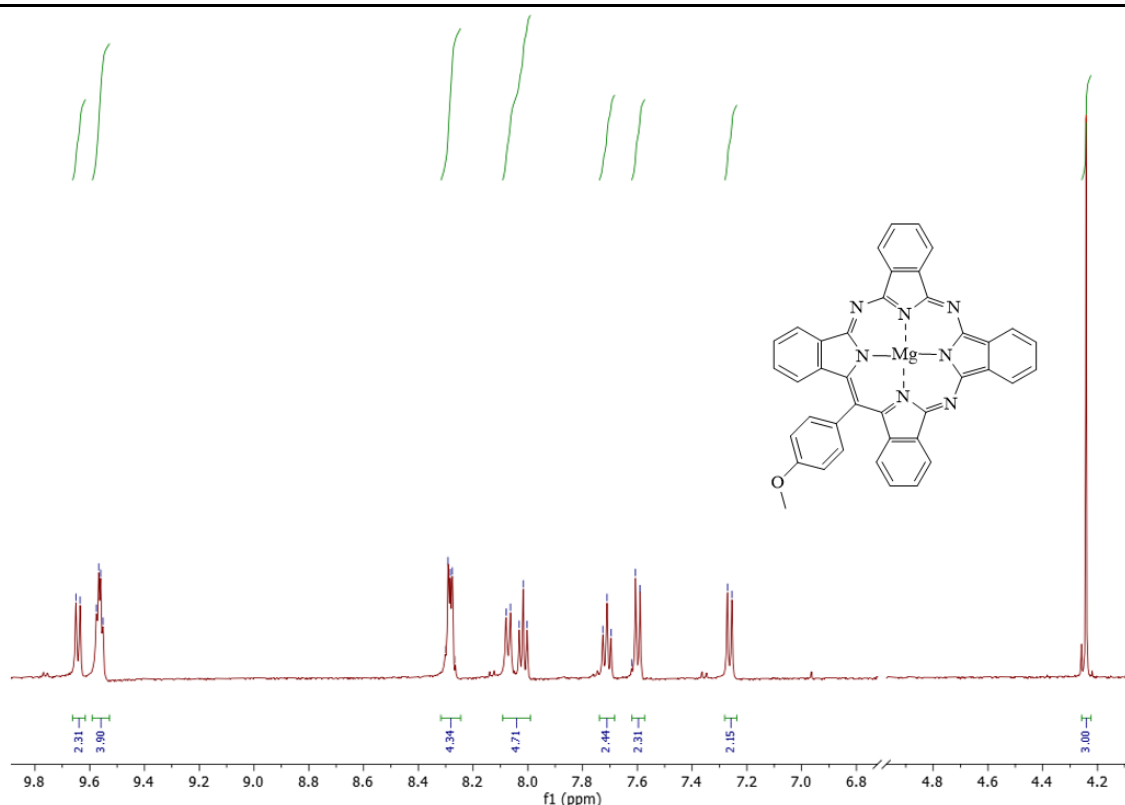


Figure 2.4: ^1H NMR spectrum of *meso*-(4-methoxyphenyl) TBTAP **2.6** in $\text{acetone-}d_6$.

The MALDI-TOF MS data are concordant with previously published data, and the UV-Vis spectra obtained agreed and confirmed the successful synthesis of Mg-TBTAP **2.6**. The spectrum exhibits the distinctive Soret and *Q*-bands typically observed in 18- π electron macrocycles, and the λ_{max} values are closely approaching the values reported in the literature for Mg-TBTAP **2.6**.¹¹⁰

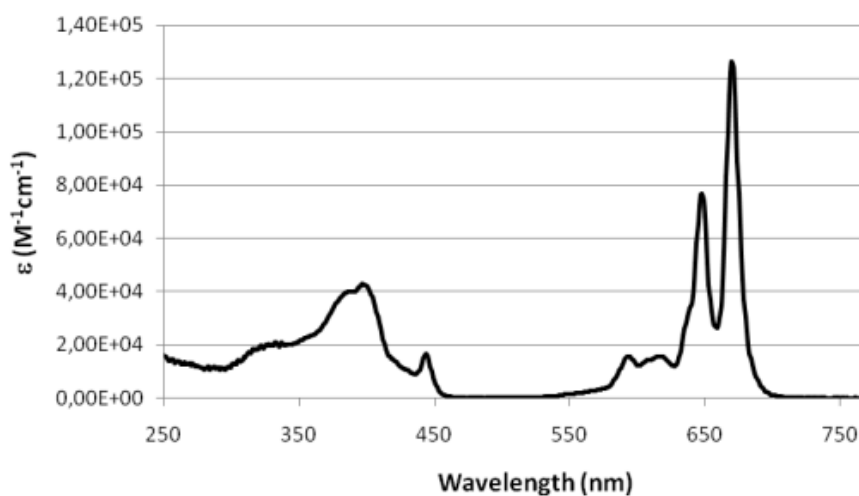


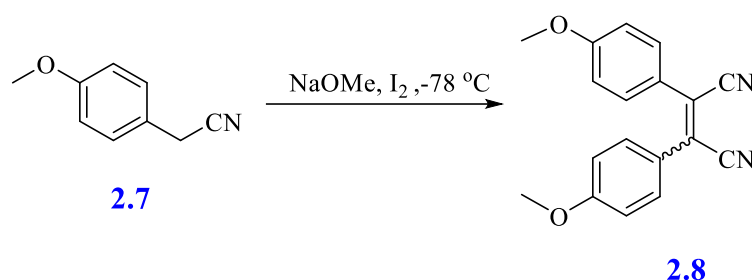
Figure 2.5: UV-Vis spectrum of TBTAP **2.6** in THF.

2.3 Synthesis of porphyrazine Mg hybrids from dinitrile derivatives

The most common synthetic protocol for the preparation of porphyrazine was developed by Linstead and Whalle,⁵³ based on the cyclisation of different maleic dinitriles derivatives to Pzs by reacting them with Mg propoxide in n-propyl alcohol to give magnesium tetraazaporphyrins.

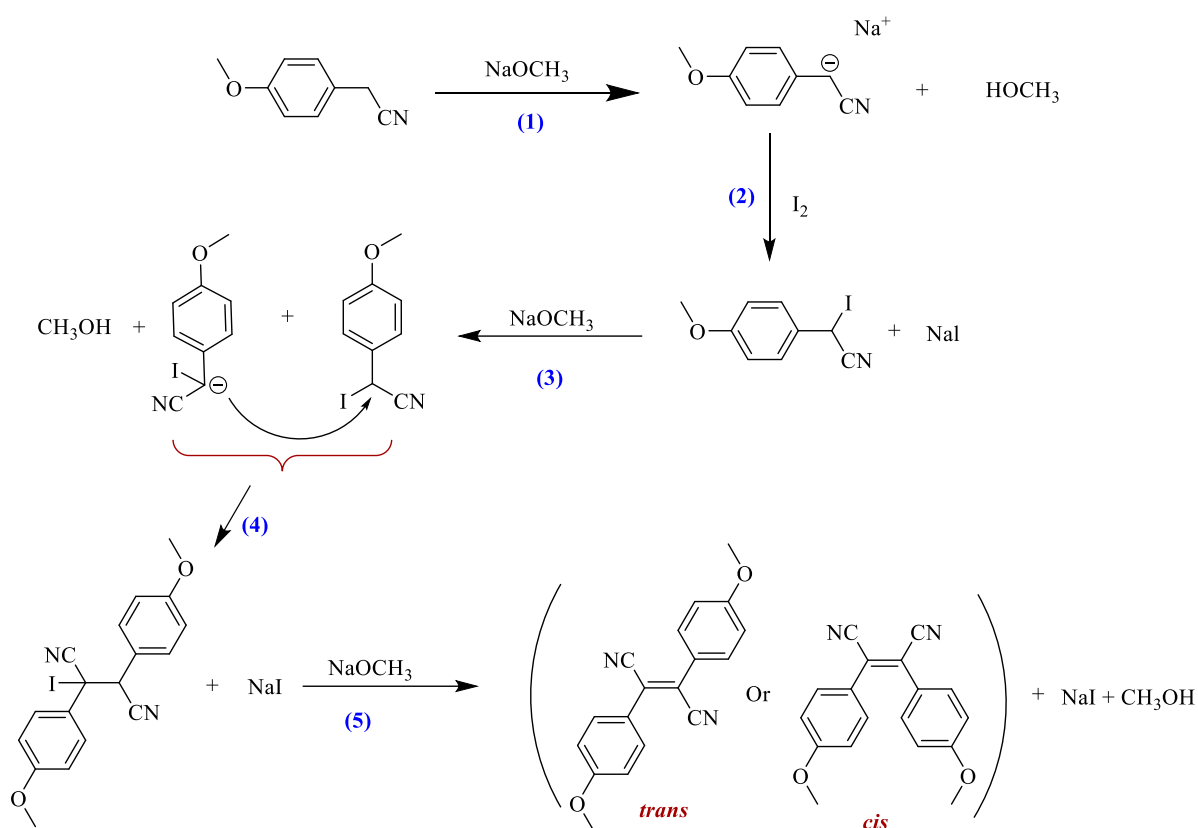
2.3.1 Synthesis of bis-(4-methoxyphenyl)-dicyanoethylene 2.8

Diphenyl-dicyanoethylene derivative **2.8** was prepared from 4-methoxyphenyl acetonitrile **2.7** via an oxidative coupling reaction in diethyl ether solvent using iodine in the presence of sodium methoxide (NaOCH₃) base. The reaction mixture was cooled to -78 °C under argon. Then, a solution of sodium methoxide was added dropwise. The reaction mixture was stirred at room temperature for 2 h. Work up of the reaction mixture gave a yellow powder of dicyanoethylene **2.8** with approximately 26% yield.⁶⁵



Scheme 2.5: Synthesis route of substituted dinitriles **2.8**.

This reaction was explained by the mechanism shown in (Scheme 2.6) in five consecutive steps. Three deprotonation steps, two of a benzylic carbon of 4-methoxyphenyl acetonitrile (steps 1, 3) and deprotonation of 2-iodo-2,3-bis(4-methoxyphenyl) succinonitrile (step 5). The halogenation of benzylic carbon (step 2) and nucleophilic substitution with subsequent elimination reaction (steps 4, 5) gave *trans* and *cis* isomers of bis-(4-methoxyphenyl)-dicyanoethylene due to the different geometric arrangement of the two cyanide (CN) groups around the C=C double bond.⁶³



Scheme 2.6: Suggested mechanism for synthesis of bis-(4-methoxyphenyl)-dicyanoethylene **2.8**.

In previous work, a combination of *cis* and *trans* isomers was separated.¹¹¹ However, in our work, we isolated a single isomer. Comparing the ^1H NMR spectra with the published data suggests that we specifically obtained the *trans* isomer (Figure 2.6).⁶³ Also, compound **2.8** was characterized by using MALDI-TOF mass spectrometry, which showed a peak around (291.20 m/z) corresponding to the required product (Figure 2.7). Furthermore, the FT-IR spectrum showed a characteristic vibrational band at wavenumber 2214 cm^{-1} for the cyanide CN group.

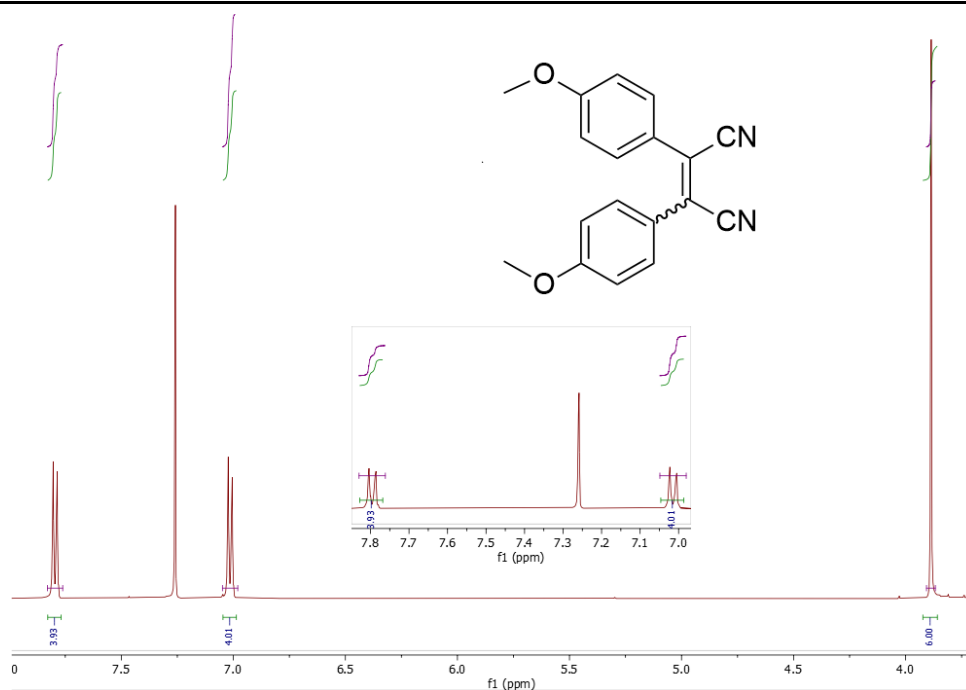


Figure 2.6: ¹H NMR spectrum of bis-(4-methoxyphenyl)-dicyanoethylene **2.8** in CDCl₃.

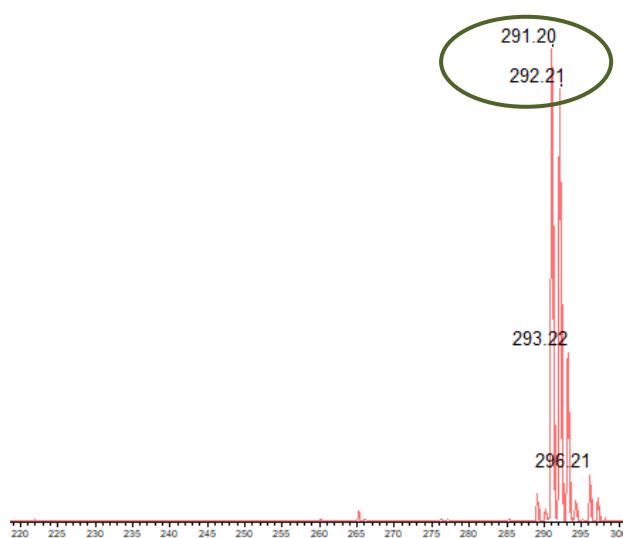
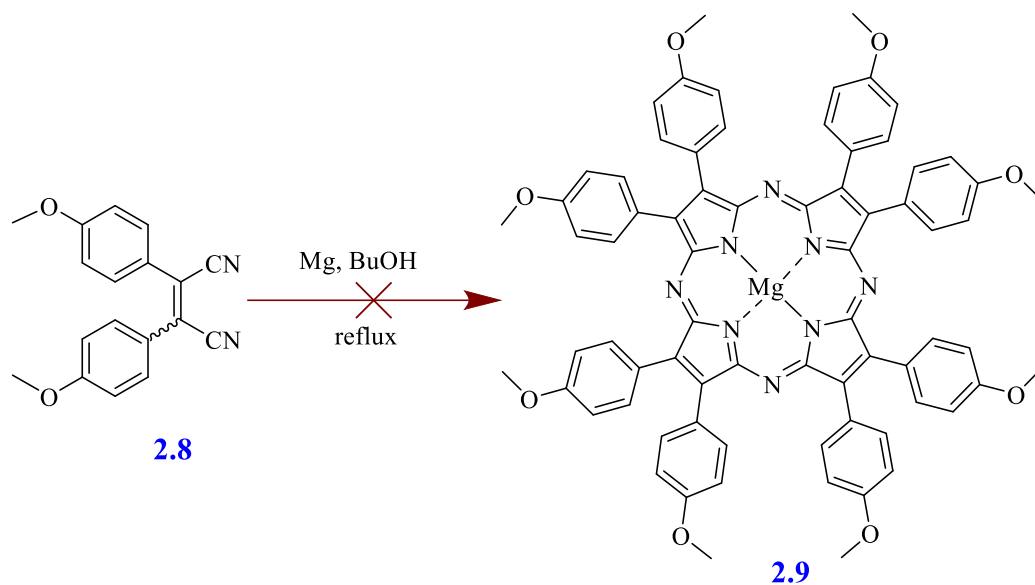


Figure 2.7: MALDI-TOF- MS spectrum of bis-(4-methoxyphenyl)-dicyanoethylene **2.8**.

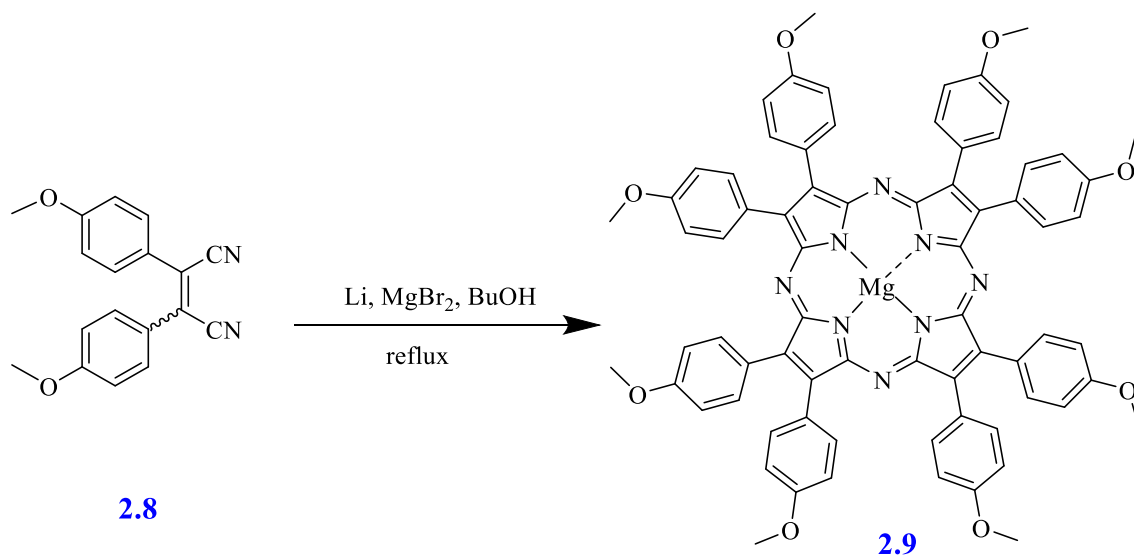
2.3.2 Synthesis of octa(4-methoxyphenyl) porphyrazine Mg (II) **2.9**

This initial attempt involved the synthesis of the target tetraazaporphyrin derivative with the Mg template by cyclisation reaction of bis-(4-methoxyphenyl)-dicyanoethylene **2.8**. We followed the procedure reported for the synthesis of tetraazaporphyrin by dissolving magnesium turnings in butanol under reflux conditions. The expectation was that all Mg would react with butanol to form magnesium butoxide Mg(OBu)₂, followed by the addition of the dinitrile **2.8**.¹¹¹ Unfortunately, this reaction was ineffective because the Mg was inert in butanol (Scheme 2.7).



Scheme 2.7: Suggested pathway to octa(4-methoxyphenyl) porphyrazine Mg (II) **2.9**.

From the above result, we modified the previous protocol by adding lithium metal first to react with butanol and forming lithium butoxide (LiOBu), then adding MgBr₂. After that, we added bis-(4-methoxyphenyl)-dicyanoethylene **2.8** to the reaction mixture and heated under reflux overnight (Scheme 2.8). The resulting precipitate was separated and washed with methanol, followed by recrystallization, producing a bluish-green solid material with a low yield.



Scheme 2.8: Synthesis of octa(4-methoxyphenyl)porphyrazine Mg (II) **2.9**.

MALDI-TOF mass spectrometry characterized the resulting compound **2.9**, which showed a peak cluster around (1186.61 m/z) corresponding to the molecular weight of the required compound (Figure 2.8). Furthermore, the UV-Vis spectrum showed Q and the Soret absorption bands at 650 nm and 382 nm, respectively (Figure 2.9). All analytical data were consistent with the molecular structure of the predicted product.¹¹¹

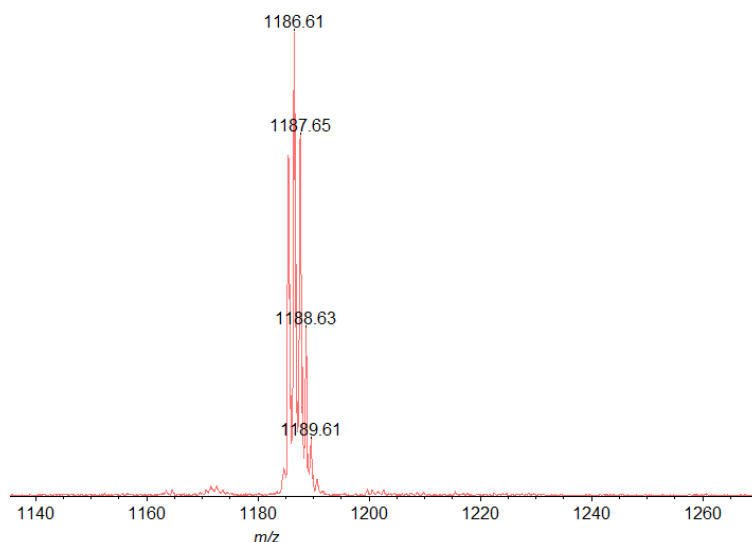


Figure 2.8: MALDI-TOF- MS spectrum of octa(4-methoxyphenyl) porphyrazine Mg (II) **2.9**.

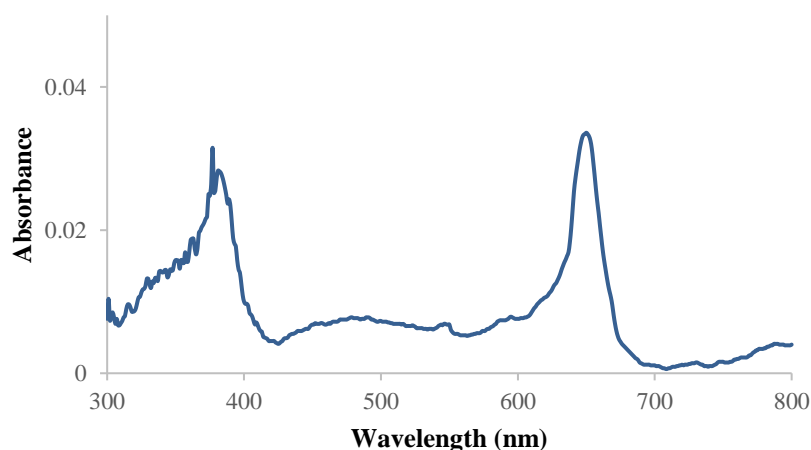
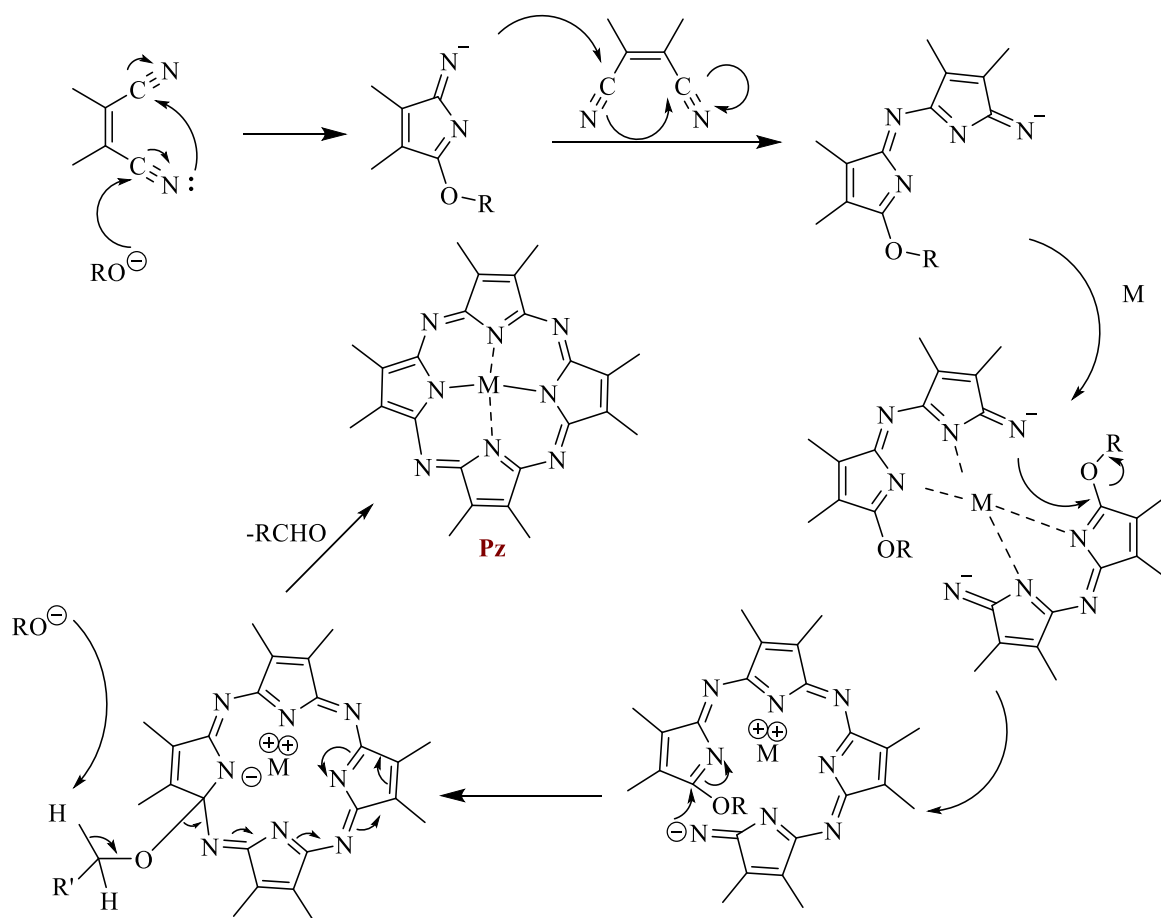


Figure 2.9: UV-Vis absorption spectrum of octa(4-methoxyphenyl) porphyrazine Mg (II) **2.9** in THF.

Linstead *et al.* have proposed the following mechanism for the formation of tetraazaporphyrin through cyclotetramerization of the substituted dinitriles in the presence of a template ion and alkoxide, as shown below (Scheme 2.9).^{60,112} Magnesium alkoxide, as a strong nucleophile, attacks the cyanide triple bond of dinitrile to obtain the intermediate with a negatively charged nitrogen atom (nucleophile). Subsequently, this intermediate attacks another

dinitrile to form a dimer. Two molecules of a dimer surround a metal-ion template to form the tetramer intermediate, which loses an aldehyde to form porphyrazine complex.



Scheme 2.9: The mechanism proposed for the formation of tetraazaporphyrin **2.9** (Aryl substituents not shown).

2.4 Synthesis of porphyrazine hybrids from aminoisoindoline (A) and dinitrile (B) derivatives

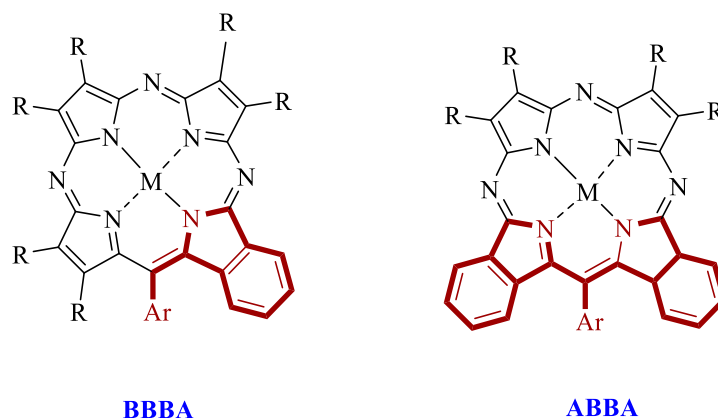
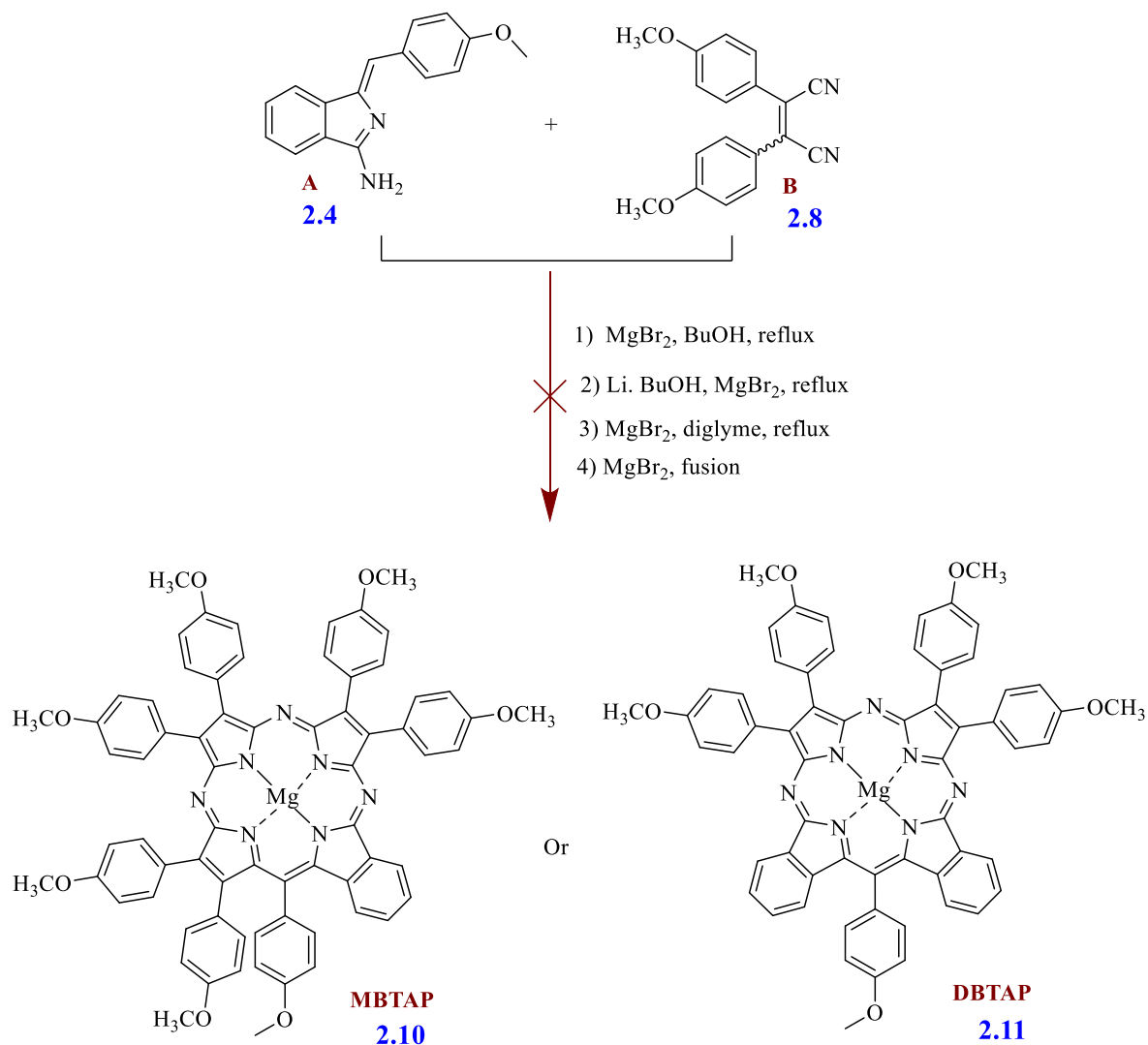


Figure 2.10: Molecular structures of target porphyrazine hybrids.

We synthesised a BBBB porphyrazine successfully as a standard for our target hybrids ABBA and ABBA Pz, as shown in Figure 2.10. Therefore, we started our challenge to prepare metalated Pzs hybrids by following a similar approach that was used in the synthesis of TBTAP through cyclisation of the key intermediate aminoisoindoline **2.4 (A)** with substituted dinitrile **2.8 (B)** around a metal template (Magnesium). We anticipated this process would not be straightforward or simple. These attempts are shown in the following Table 2.1 and the chemical reaction is presented in Scheme 2.10.

Table 2.1: Attempted conditions for preparing porphyrazine hybrids.

Salt	Solvent	Metal element	Conditions	Time	Results
MgBr₂	BuOH	-	Reflux	30 h	Only the starting materials + dimer of aminoisoindoline 4 + BBBB Pz
	PeOH	Li		overnight	
	diglyme	-		4 h	
	-	-	Fusion	10 min.	Several unknown products (no selectivity)



Scheme 2.10: Our attempts at synthesis of MBTAP 2.10, DBTAP 2.11.

We noticed that in all our attempts, we obtained a red product characterized as self-condensed aminoisindoline **2.4** to form dimer **2.12** (Figure 2.11). The MALDI TOF-MS data for the crude reaction identified the molecular ion peak at (480.75 m/z) for the aza-(dibenzo) dipyrromethene derivative **2.12** (Figure 2.12). However, BBBA hybrid **2.10** and ABBA hybrid **2.11** have not been observed.

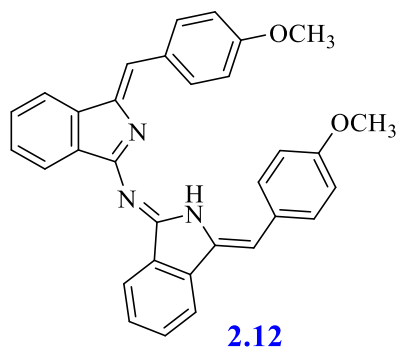


Figure 2.11: Aza-(dibenzo) dipyrromethene derivative **2.12**.

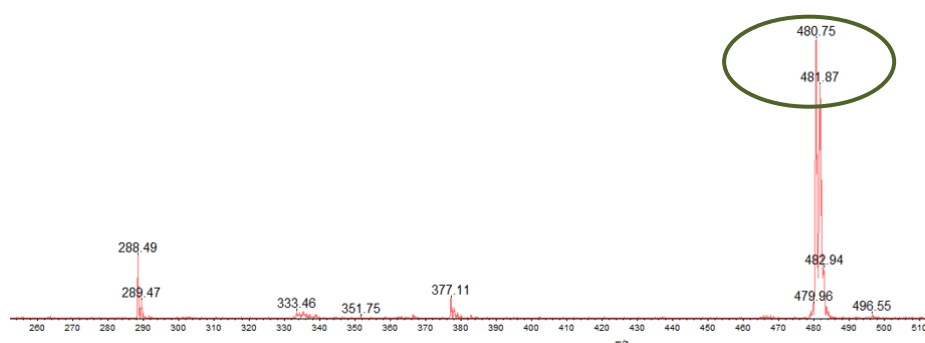
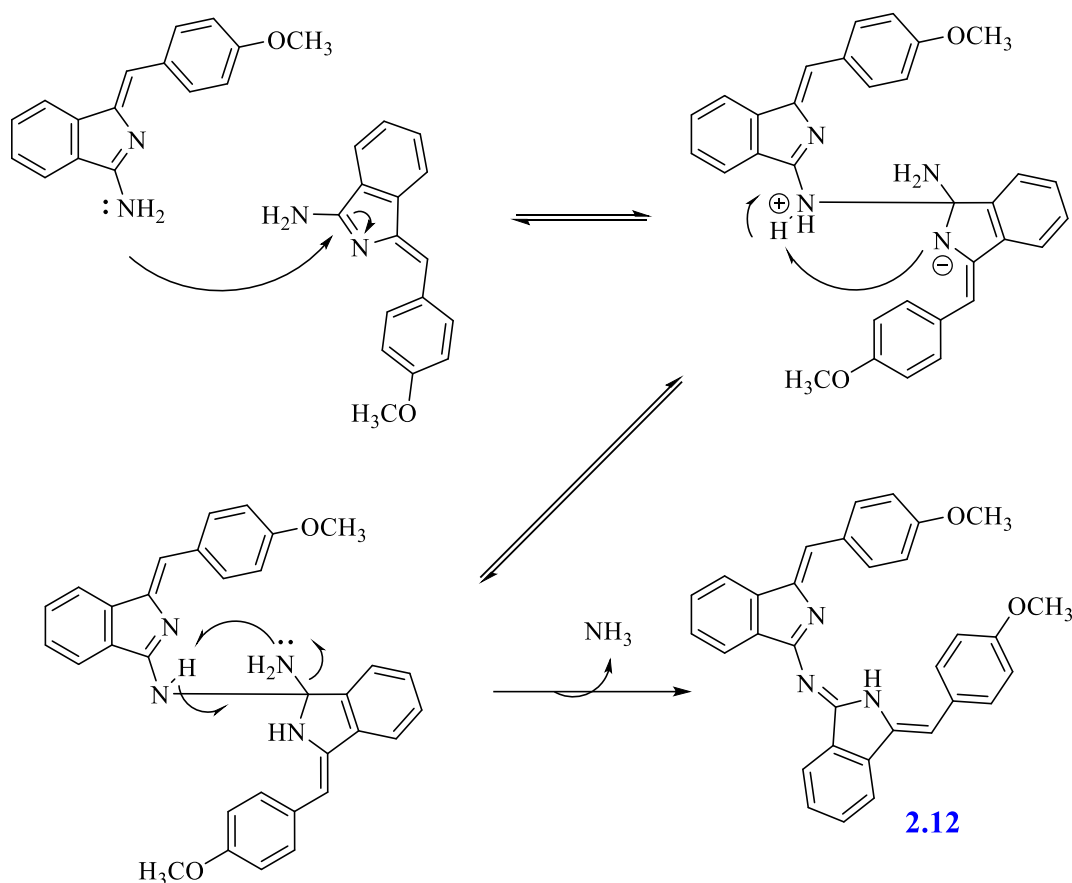


Figure 2.12: MALDI-TOF- MS spectrum of aza-(dibenzo) dipyrromethene derivative **2.12**.

2.4.1 Self-condensation mechanism for aminoindoline forming dimers

Scheme 2.11 illustrates the mechanism by which aminoindoline **2.4** undergoes self-condensation into a dimer. In addition to possessing a nucleophilic amine, the α C atom also acts as an electrophilic centre. This enables one molecule to undergo nucleophilic attack by another nucleophile, eliminating the ammonia (NH_3) molecule and forming the self-condensation product dimer **2.12**.¹¹²



Scheme 2.11: The hypothesized mechanism for the self-condensation of aminoisoindoline **2.4** forming azadipyrromethene derivative dimer **2.12**.

Based on the findings obtained earlier, we observed that the dimerization reaction of aminoisoindoline **2.4** proceeds much more rapidly than the cyclisation reaction of aminoisoindoline **2.4** with dinitrile **2.8**. Additionally, we believe that the dicyanoethylene derivatives **2.8** exist primarily in the *E* (*trans*) isomer configuration, which consequently impedes the cyclisation process required for the synthesis of porphyrazines **2.10** and **2.11**.

To further investigate the potential for *cis* isomer formation through the photoisomerization of *trans* isomers, we dissolved the *trans* isomer **2.8** in DCM solvent and subjected samples to two different conditions. In the first, the solution was stirred overnight at room temperature under normal visible light. In the second pathway, the solution was irradiated under short wavelength UV light (at 254 nm). Subsequent TLC analysis of both conditions revealed the presence of two distinct spots, indicating the formation of *cis* isomers in the reaction mixture.

The ^1H NMR spectrum of this mixture displayed two sets of peaks, the first pair at δ 7.05 and 7.83 ppm, corresponding to the aromatic protons of the *trans* isomer (diphenylfumaronitrile), and two relatively shielded peaks at δ 6.82 and 7.29 ppm, corresponding to the aromatic protons of the *cis* isomer (diphenyl malic nitrile). These findings agree with the previously published data for similar compounds (Figure 2.13).⁶³

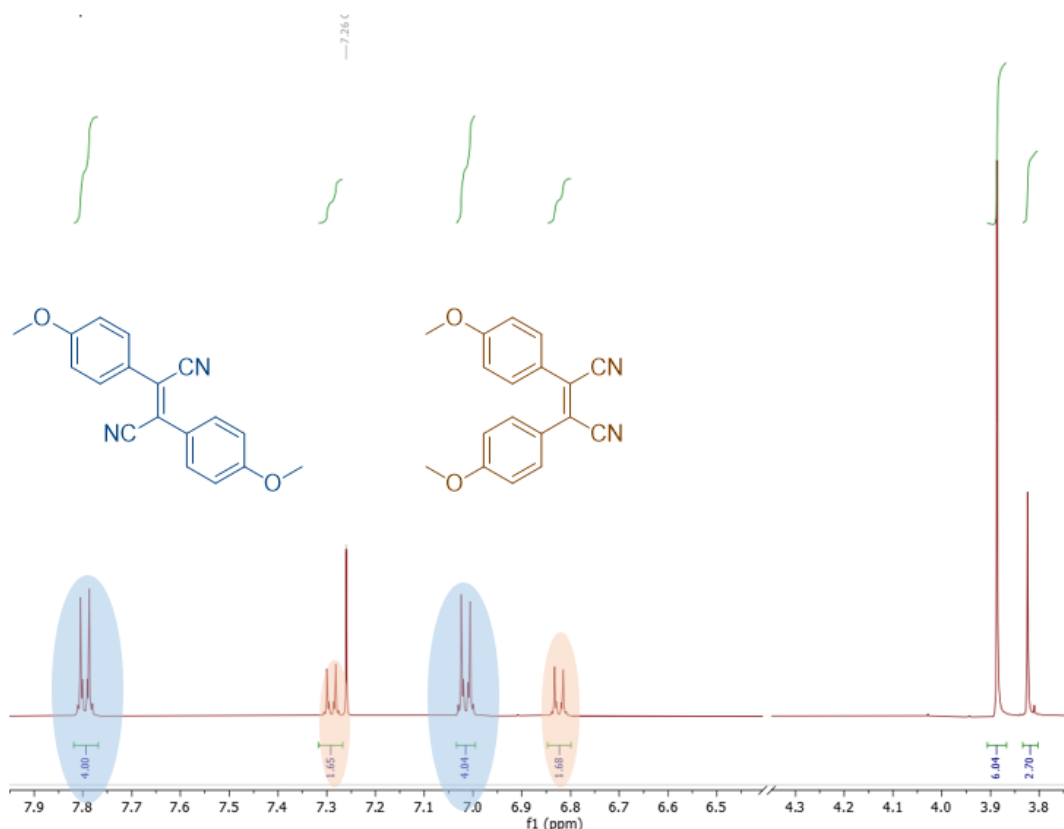


Figure 2.13: The ^1H NMR spectrum for the mixture of *cis/trans* dinitrile **2.8** in CDCl_3 .

The mixture of isomers was separated using column chromatography using petroleum ether: AcOEt (1:4) as an eluent, and the two yellow products were checked using the ^1H NMR spectra. Figure 2.14 compares the ^1H NMR spectrum for the first fraction, which matches the *trans* isomer discussed previously (Figure 2.6). However, the other ^1H NMR spectrum for the second fraction showed the upfield shift in the aromatic protons compared with the *trans* isomer, confirming the formation of the *cis* isomer in agreement with the previously reported study (Figure 2.14).⁶³

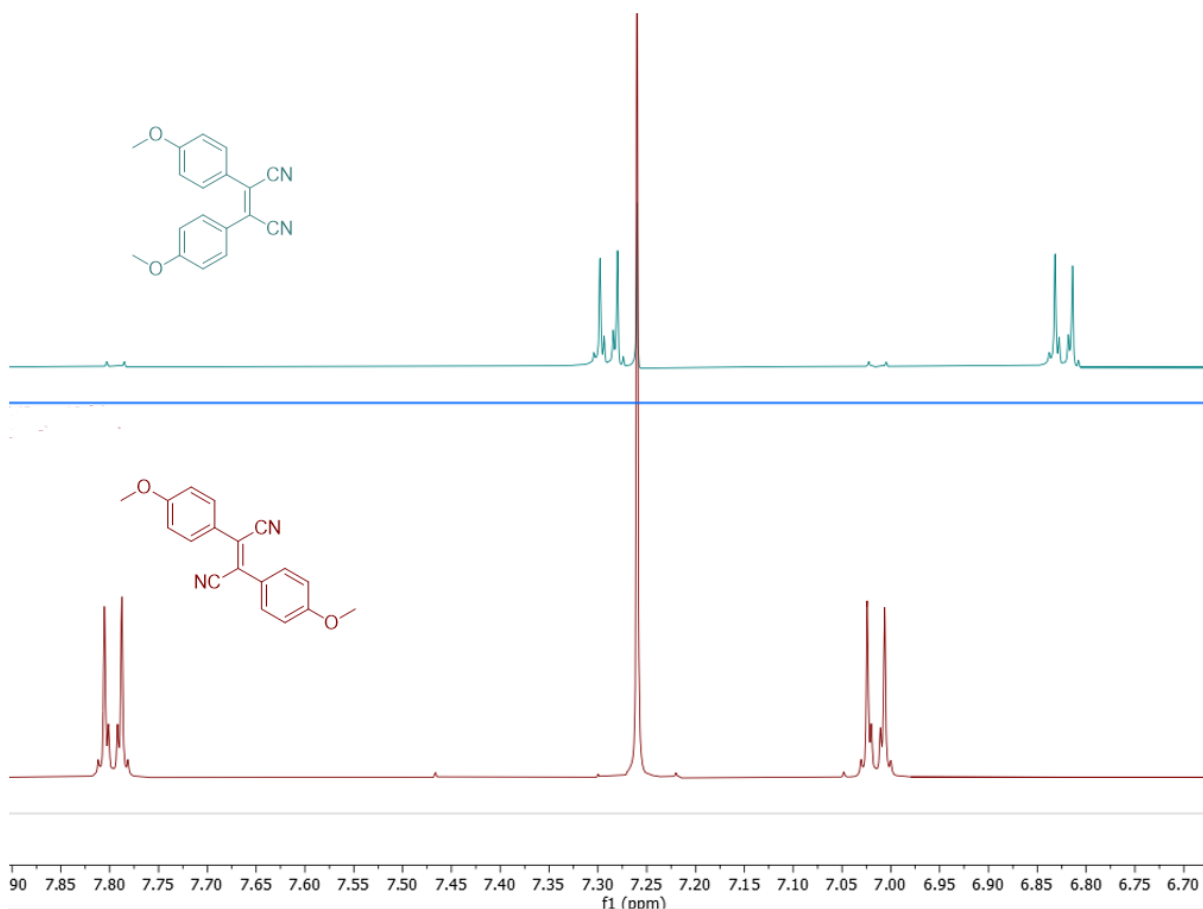


Figure 2.14: The ^1H NMR spectra of bis-(4-methoxyphenyl)fumaronitrile (top), bis-(4-methoxyphenyl)maleic dinitriles (bottom) in the aromatic region in CDCl_3 .

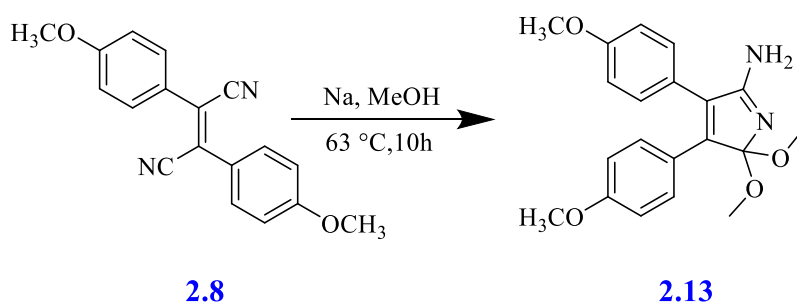
From the previous results, we inferred that the hindrance in synthesising our target porphyrazines was due to the dinitrile predominantly preferring a *trans* geometrical configuration. Furthermore, the conversion process of the *trans* isomer to the *cis* isomer configuration resulted in a low yield and was therefore not a viable alternative approach to improving the synthesis. Therefore, to avoid that and prevent the formation of the azadipyrromethene derivative **2.12**, we investigated trapping a reactive *cis* intermediate (from dinitrile analogues) anticipating their higher reactivity when combined with aminoisoindoline **2.4**.

2.5 Employing a reactive “*cis*” intermediate

2.5.1 Synthesis of dimethoxypyrrole intermediate derivative 2.13

Previously, in the introduction chapter, we discussed the use of pyrroline-2,5-dimine derivatives as effective reactive intermediates for the synthesis of unsymmetrical porphyrazines with different dinitriles.⁶² However, our group has recently had success employing with phthalonitrile analogues, specifically dimethoxyisoindoline intermediates, under various low temperature conditions in macrocycle synthesis.⁵⁰ As a continuation of this approach, we aimed to explore the simultaneous isomerisation and “activation” of our maleic dinitriles to prepare more reactive intermediates like **2.13** for hybrid porphyrazine synthesis.

In practice, intermediate **2.13** was synthesised in a relatively straightforward manner using modified versions of the protocols previously reported at UEA for phthalonitrile (where of course the nitriles are fixed in a *cis*-like configuration).^{50,113} Bis-(4-methoxyphenyl)-maleic dinitrile **2.8** was dissolved in methanol along with 1.2 equiv. of Na metal. The mixture was stirred at room temperature overnight. However, due to the insolubility of dinitrile **2.8** in methanol, the reaction temperature was elevated to 63 °C (Scheme 2.12).



Scheme 2.12: Synthesis of dimethoxypyrrole derivative **2.13**.

The MALDI-TOF mass spectrum for the crude product showed a peak at 352.89 *m/z* corresponding to the molecular weight for dimethoxypyrrole derivative **2.13** and several peaks for additional side products (Figure 2.15).

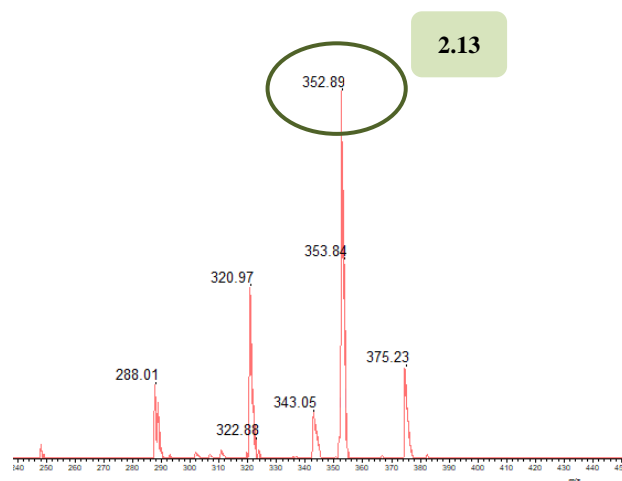
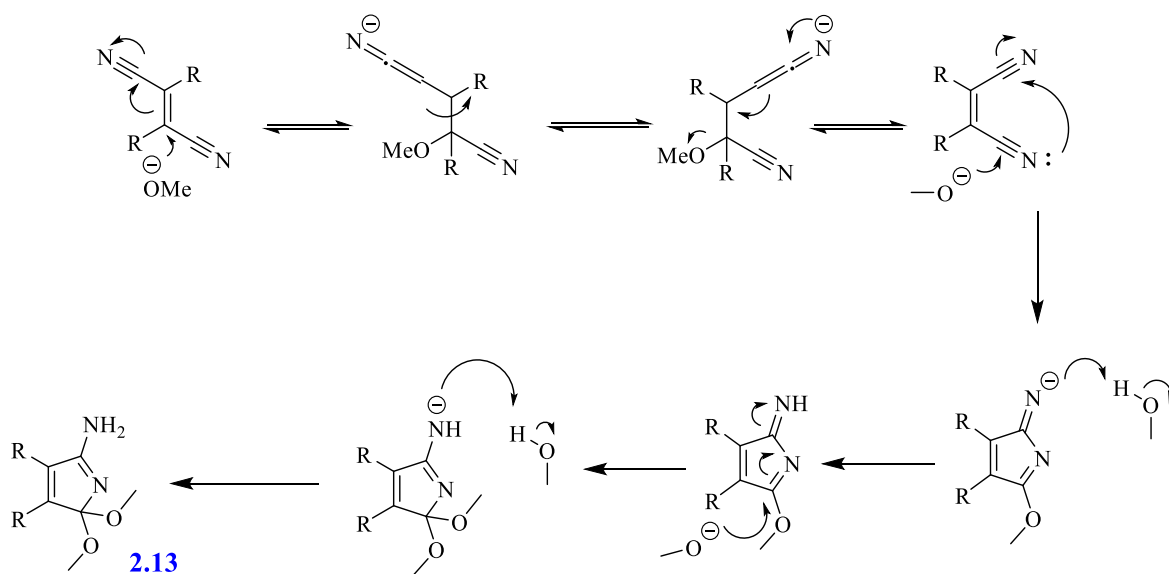


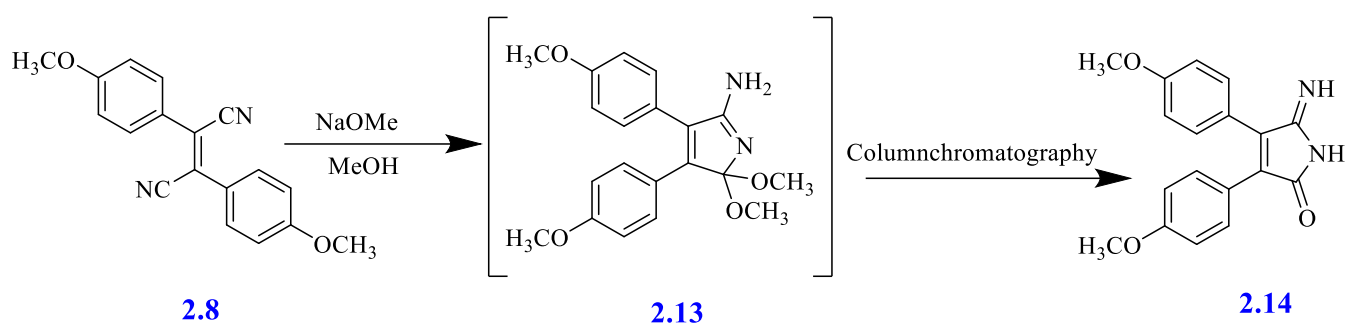
Figure 2.15: The MALDI-TOF mass spectrum for the crude product **2.13**.

Below is depicted the suggested formation mechanism (Scheme 2.13) for dimethoxypyrrole derivative **2.13**, including the potential initial isomerisation mechanism through reversible Michael addition of methoxide.



Scheme 2.13: A mechanism proposed for forming dimethoxypyrrole **2.13**.⁵⁰

Unfortunately, when trying to purify the crude product using column chromatography, the dimethoxypyrrole derivative **2.13** was hydrolyzed into pyrrolone derivative **2.14** (a lime yellow precipitate (Scheme 2.14).



Scheme 2.14: Hydrolysis of dimethoxypyrrole intermediate **2.13** to pyrralone derivative **2.14**.

NMR and MALDI-TOF mass spectra confirmed the structure of compound **2.14** and showed the molecular ion peak for the pyrralone derivative at 309.49 m/z (Figure 2.16).

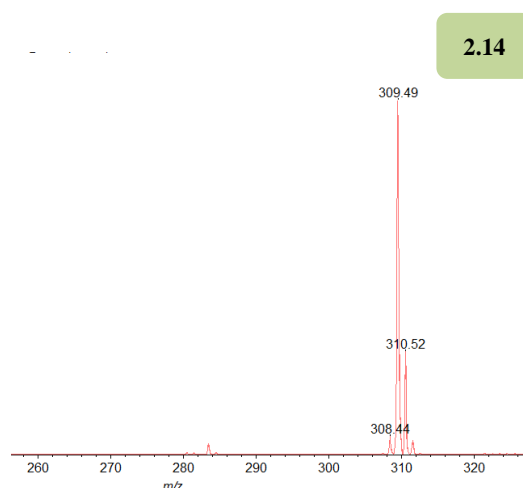


Figure 2.16: MALDI-TOF- MS spectrum compound **2.14**.

Furthermore, the ^{13}C NMR spectrum showed a peak of high δ 163.88 ppm corresponding to highly de-shielded C=O carbon. Also, ^1H NMR spectra showed only two methyl groups at δ = 3.73 and 3.79 ppm, respectively, corresponding to the presence of two methoxy groups (OCH_3) only on the aromatic benzene rings (Figure 2.17).

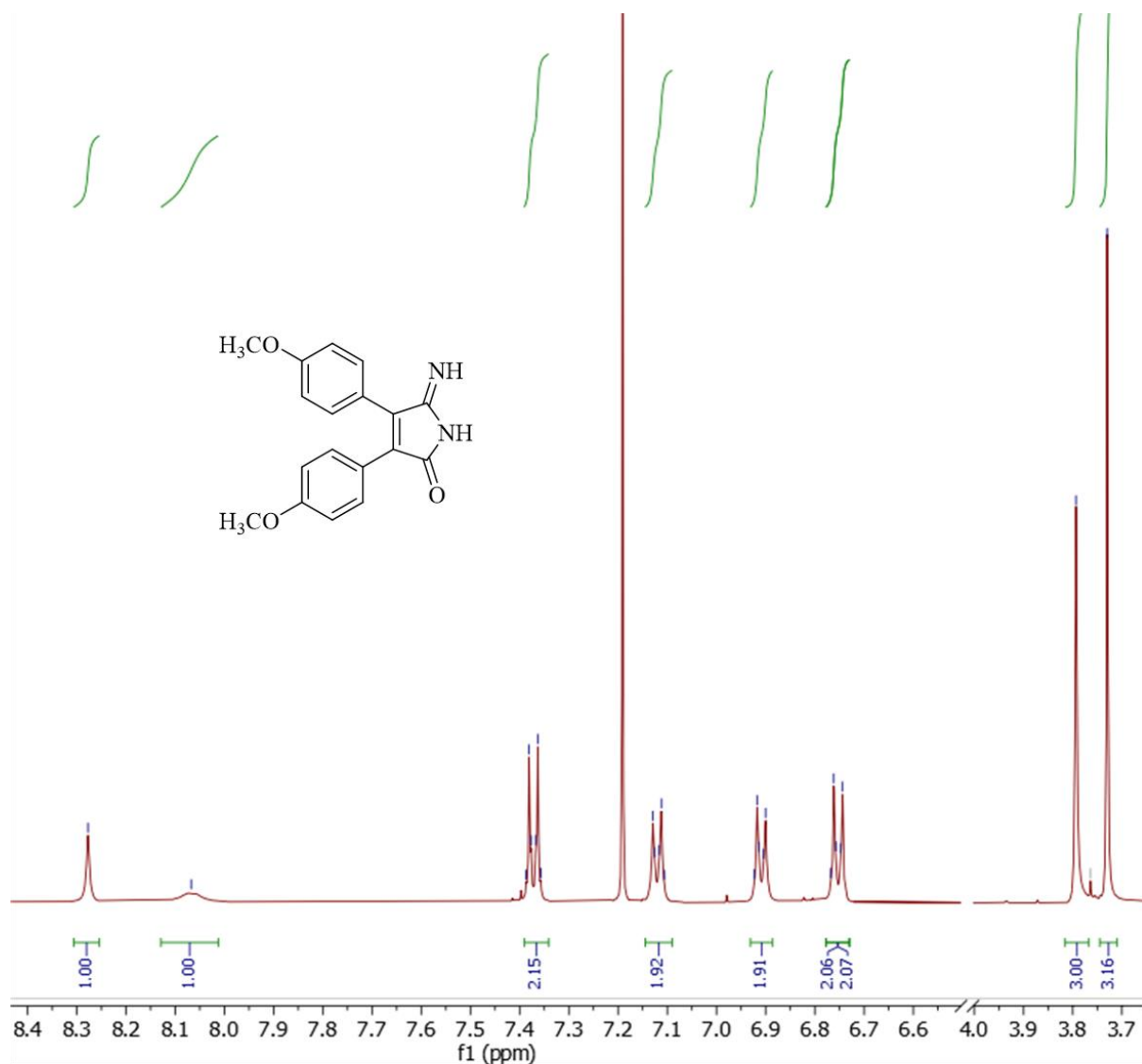


Figure 2.17: The ^1H NMR spectrum of compound **2.14** in CDCl_3 .

The compound gave suitable single crystals for X-ray diffraction analysis, which confirmed its molecular structure. This crystal was grown from a mixture of DCM/petroleum ether (1:1) (Figure 2.18). The X-ray crystal structure was solved by our collaborator, Dr David Hughes, and his comments on the detail of the structure can be found in the appendix.

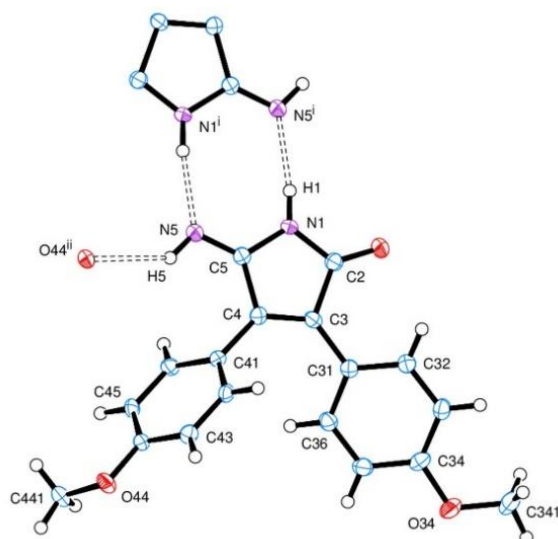


Figure 2.18: View of a molecule of (hydrolysed) intermediate **2.14**, showing the hydrogen-bonded neighbours and indicating the atom numbering scheme. Thermal ellipsoids are drawn at the 50% probability level.

To optimise conditions for the synthesis of the dimethoxypyrrrole derivative **2.13**, we conducted the reaction at various temperatures and the number of Na equiv. during 12 h in methanol. However, all trials led to the formation of multiple products, particularly at high temperatures. This caused the reaction mixture to change from a yellowish green to a reddish-brown colour, indicating the formation of a dimer, tentatively formulated as **2.15**. The MALDI-TOF MS data support these conclusions (Figure 2.19), and the peak was identified at 642.56 m/z .

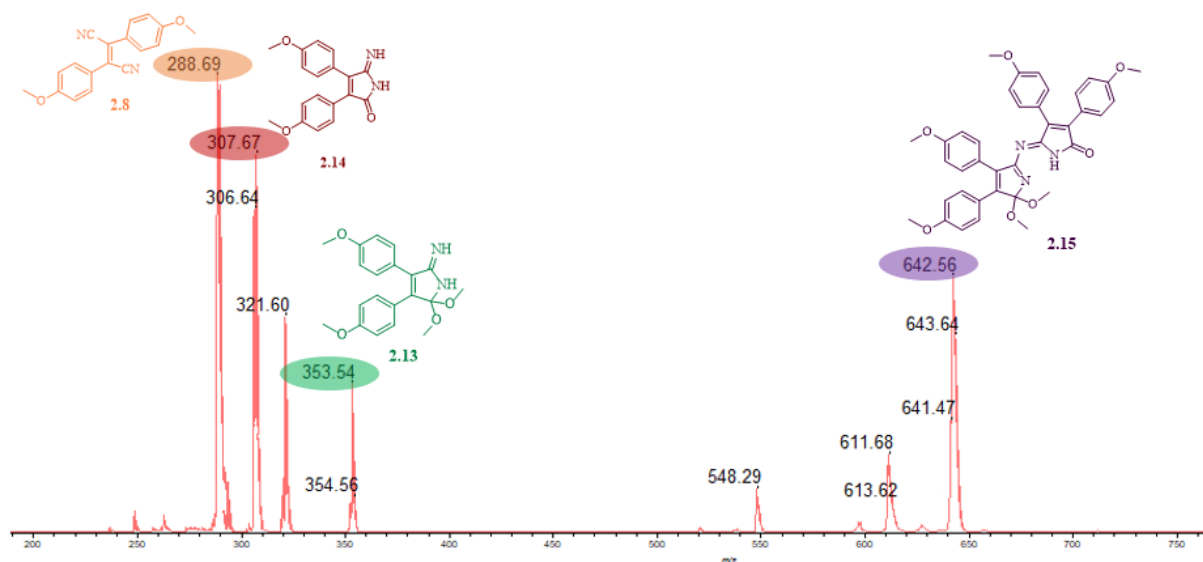


Figure 2.19: The MALDI-TOF- MS spectrum of the reaction mixture reveals the side products obtained during the attempt to synthesise precursor **2.13**.

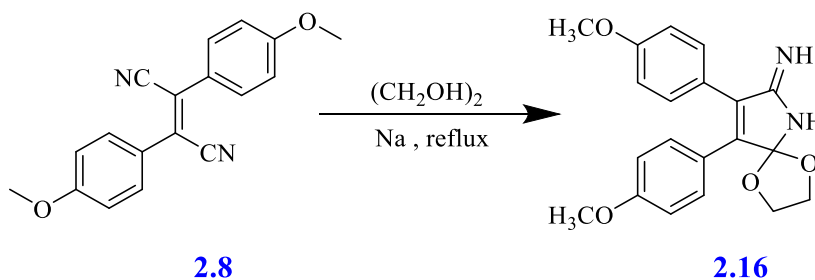
Our attempts are summarised in Table 2.2, recording the MALDI-TOF mass spectra for each reaction product.

Table 2.2: Effect of the heating temperature and Na equiv. on synthesis of compound **2.13**.

Entry	Na equiv.	Temp.	Observation
1	1.2	r.t	Only the starting material 2.8 observed at (290.87 <i>m/z</i>).
2	1.2	63 °C	A mixture of products 2.13 and 2.15 at (353.57 <i>m/z</i>), (642,97 <i>m/z</i>) respectively.
3	2.2		A mixture of unknown products with 2.13 and 2.15 was obtained.
4	0.1		A mixture of starting material 2.8 and products 2.14 , 2.13 , 2.15 .
5	1.2	vigorous reflux	Product 2.15 was the dominant product at (642.98 <i>m/z</i>).

2.5.2 Synthesis of ethylenedioxy pyrrole intermediate derivative **2.16**

Additionally, we attempted to prepare cycloalkyloxypyrrole precursors (cyclic acetals) **2.16** by using ethylene glycol as a solvent, instead of methanol, with 5 equiv. Na metal at room temperature (Scheme 2.15).¹¹⁴ Unfortunately, the starting material **2.8** did not dissolve, even on raising the temperature to 65 °C. By further increasing the temperature to 80 °C, the dinitrile was dissolved and stirred overnight, the reaction was followed by using TLC and the product was characterised using MALDI-TOF MS. We can observe the target product **2.16** at 351.79 *m/z* and other peaks (Figure 2.20). The crude product was purified by column chromatography with three mobile phase systems to remove the impurities starting from DCM then DCM/CHCl₃ (1:1), and finally with CHCl₃. The yield of intermediate derivative **2.16** was poor (7.5%). The mixture of the side reaction products included a likely pyrrolone derivative **2.14** and the dimer (plus hydrolysis products) from precursor **2.16**.



Scheme 2.15: Synthesis of the intermediate **2.16**.

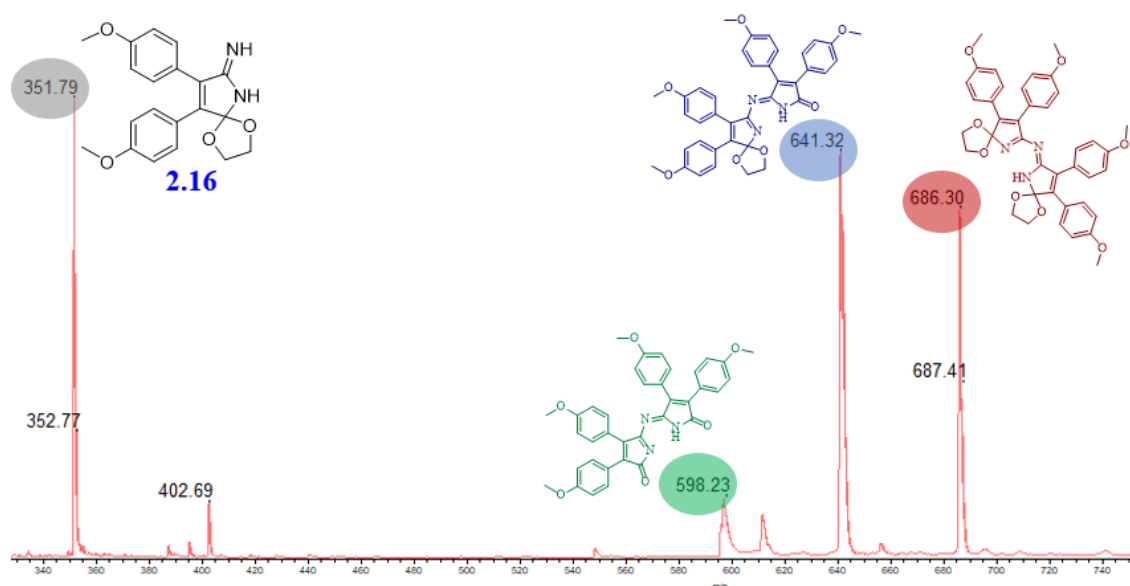
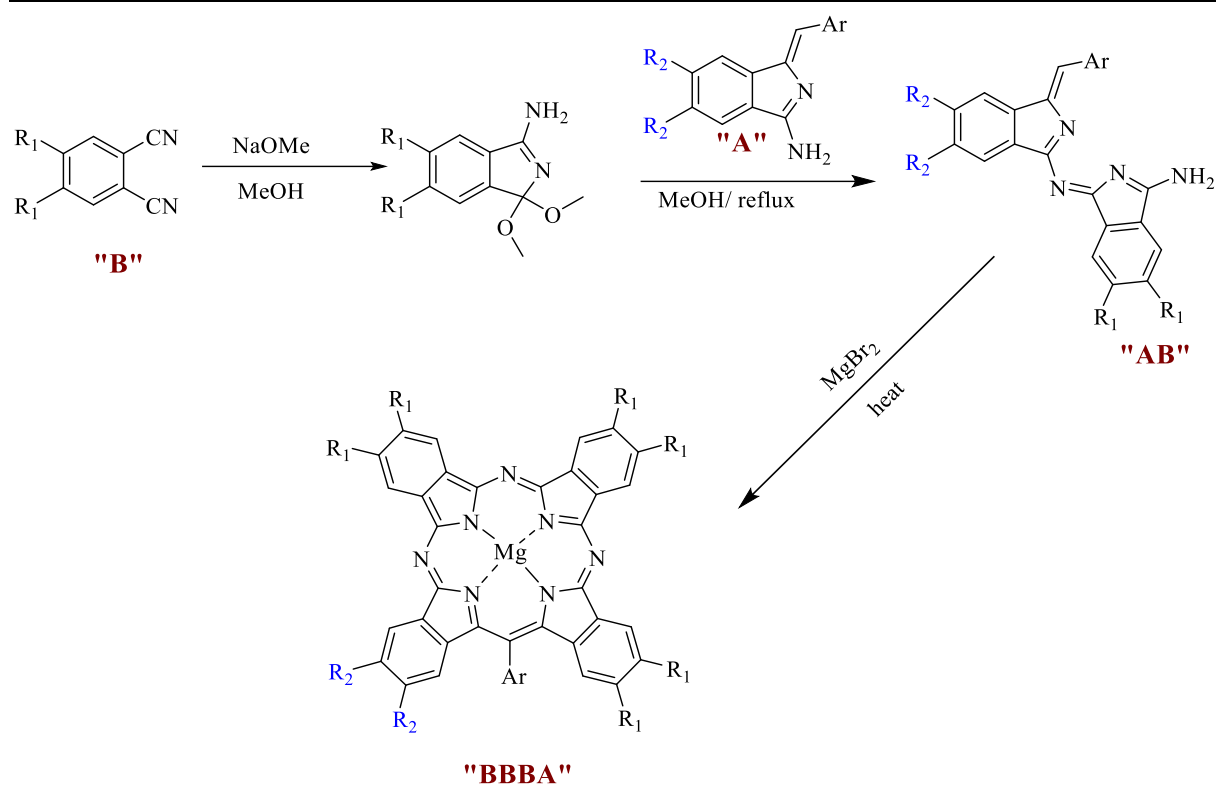


Figure 2.20: The MALDI-TOF mass spectrum for the crude reaction forming intermediate 2.16.

2.6 Syntheses of porphyrazine hybrids from (AB dimer) intermediate

The Cammidge group are attempting different synthesis methods to prepare substituted porphyrinoids. Recently, the group has made significant progress by expanding their previous work on TBTAP hybrids. They have obtained new and exciting precursors, conditions, and pathways that are suitable and selective for the synthesis of unsymmetrical ABBB-TBTAPs. This methodology uses the new intermediate material (AB dimer) to synthesise 3:1 Mg-TBTAPs under mild conditions and with improved yields. These dimers are formed through the reaction of aminoisoindoline (“A”) and activated dinitrile derivatives (“B”) (dimethoxypyrrole derivatives). Scheme 2.16 provides an overview of the new synthetic methodology for the selective synthesis of TBTAPs from AB dimers.⁵⁰



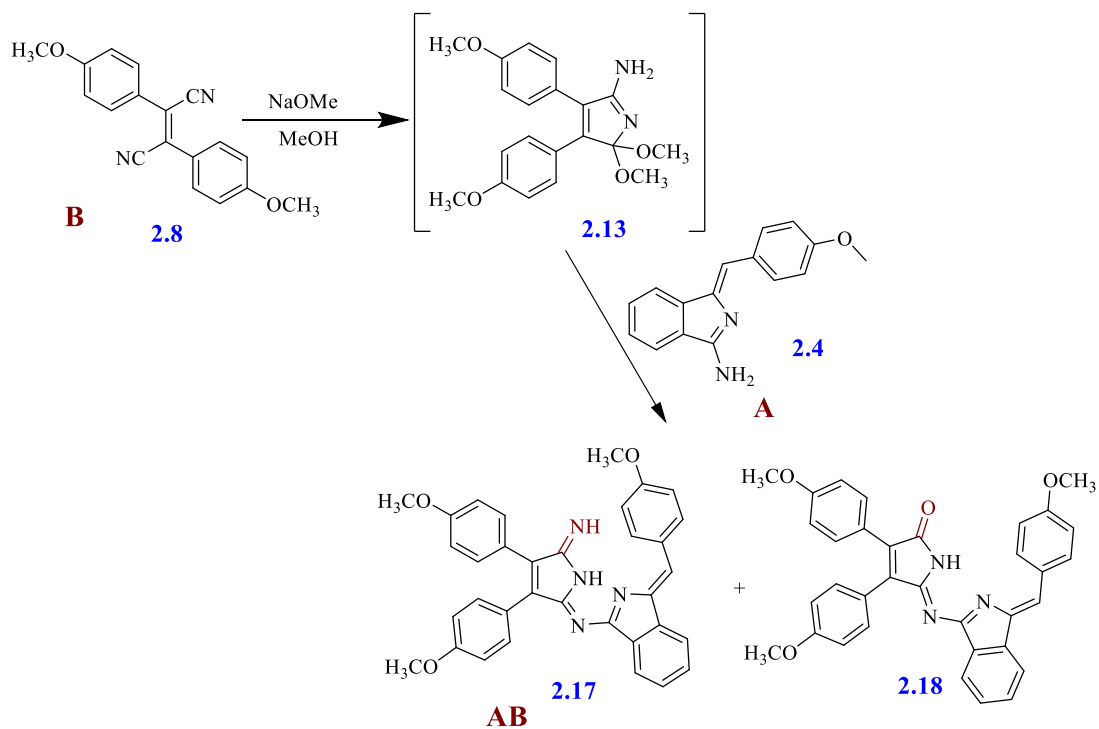
Scheme 2.16: Synthesis of 3:1 Mg-TBTAP systems from derivatives of (AB dimer) prepared by Cammidge *et al.*

Based on the above results, we investigated the same methodology for the synthesis of our target unsymmetrical porphyrazines hybrids MBTAP **2.10** and DBTAP **2.11**. The first step was preparing our AB dimer by reacting the aminoisoindole **2.4** with dinitrile derivative **2.8**.

2.6.1 Synthesis of 4-methoxyphenyl-substituted AB dimer intermediate **2.17**

To avoid the hydrolysis of dimethoxypyrrole derivatives **2.13** into pyrrolone derivatives, we modified the previous methodology for preparing AB dimers by directly reacting dinitrile derivative **2.8** (**B**) with aminoisoindole **2.4** (**A**) using an equimolar ratio directly in methanol in the presence of sodium methoxide at reflux without separating the dimethoxypyrrole derivatives (Scheme 2.17). This method has become widely adopted in the group. Initial TLC analysis showed two red spots, the second corresponding to our target AB dimer **2.17**, and the first, isolated using column chromatography, was a side product identified later as hydrolysed dimer **2.18**. The reaction continued for 18 h, and a dark red precipitate formed upon completion. The crude product was extracted and purified by column chromatography. It successfully separated the two compounds in a pure state. Recrystallization from DCM /MeOH yielded the desired dimer **17** in 42% and the side product dimer **2.18** in 22%. We noticed that by raising the temperature, the formation rate of C=O dimer **2.18** increased, indicating that the temperature

(and likely time) can control this reaction, and the observation is consistent with a pathway whereby AB intermediate **2.17** is initially formed and subsequently hydrolyses on prolonged heating. It is also likely that some further hydrolysis occurs during the silica gel chromatography, so care was taken to complete separations as quickly as possible.



Scheme 2.17: One step synthesis of AB dimer intermediate **2.17**.

^1H NMR, ^{13}C NMR, MALDI-TOF MS, and UV-Vis spectroscopy confirmed the structure of dimer **2.17**. The ^1H NMR spectrum is consistent with the proposed structure (Figure 2.21).

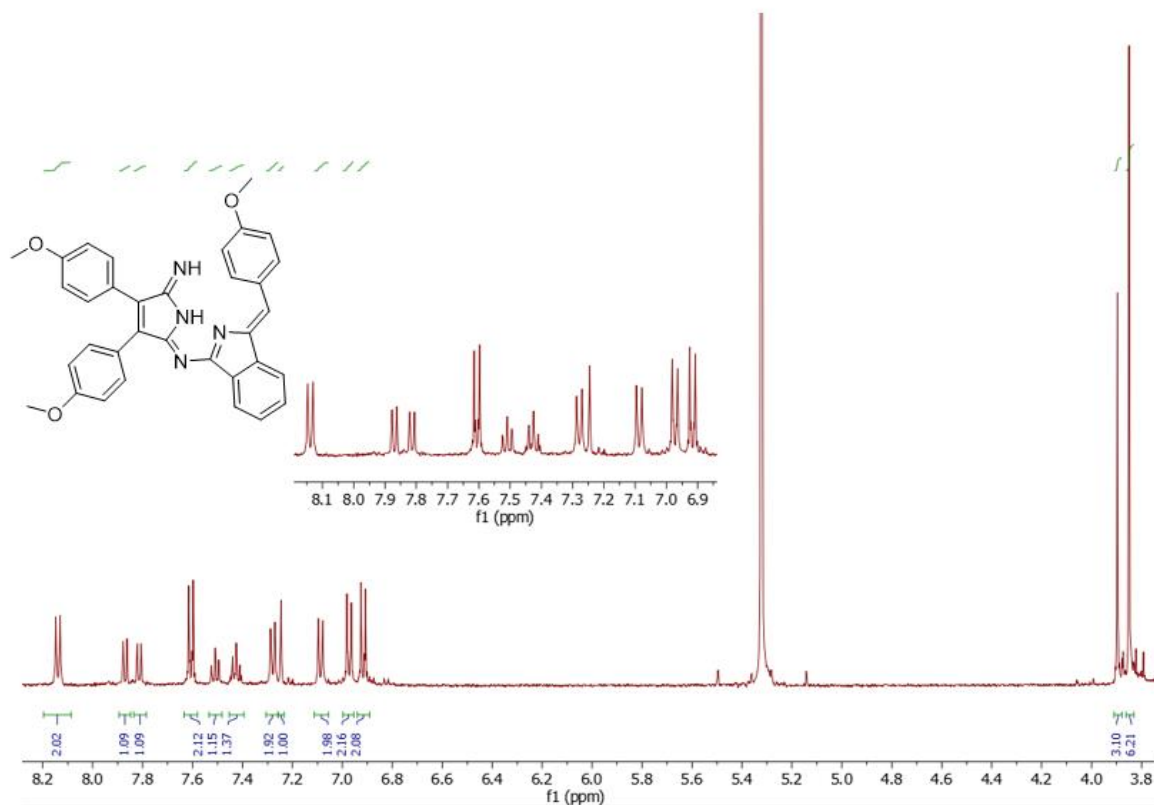


Figure 2.21: ^1H NMR spectrum of (AB dimer) **2.17** in $\text{DCM-}d_2$.

Initially, the first orange-red material was unidentified and confusing due to the MALDI-TOF mass spectra showing a peak around ($541.76\ m/z$) similar to the molecular ion peak on the MALDI-TOF MS to dimer **2.17** as shown in Figure 2.22.

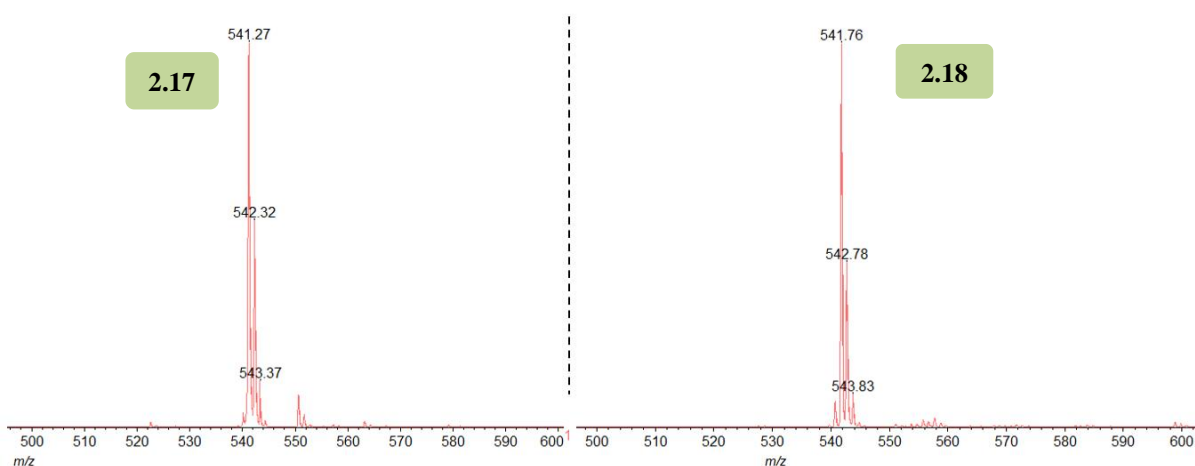


Figure 2.22: MALDI-TOF- MS spectrum for (AB dimers **2.17** and **2.18**).

The ^1H NMR spectra, Figure 2.23, show that both dimers exhibited similar sets of signals, but there is a significant difference observed in the chemical shifts of protons in the aromatic range and the peak (separation) of methoxy groups in the aliphatic region. These observations

are consistent with the proposed structures, exchanging only C=NH to C=O groups. Furthermore, ^{13}C NMR showed a peak at $\delta=161.46$ ppm for C=NH carbon of **2.17**, and the ^{13}C NMR spectra for **2.18** supported the above conclusions by showing that peak $\delta=170.60$ ppm due to a carbon in the C=O group.

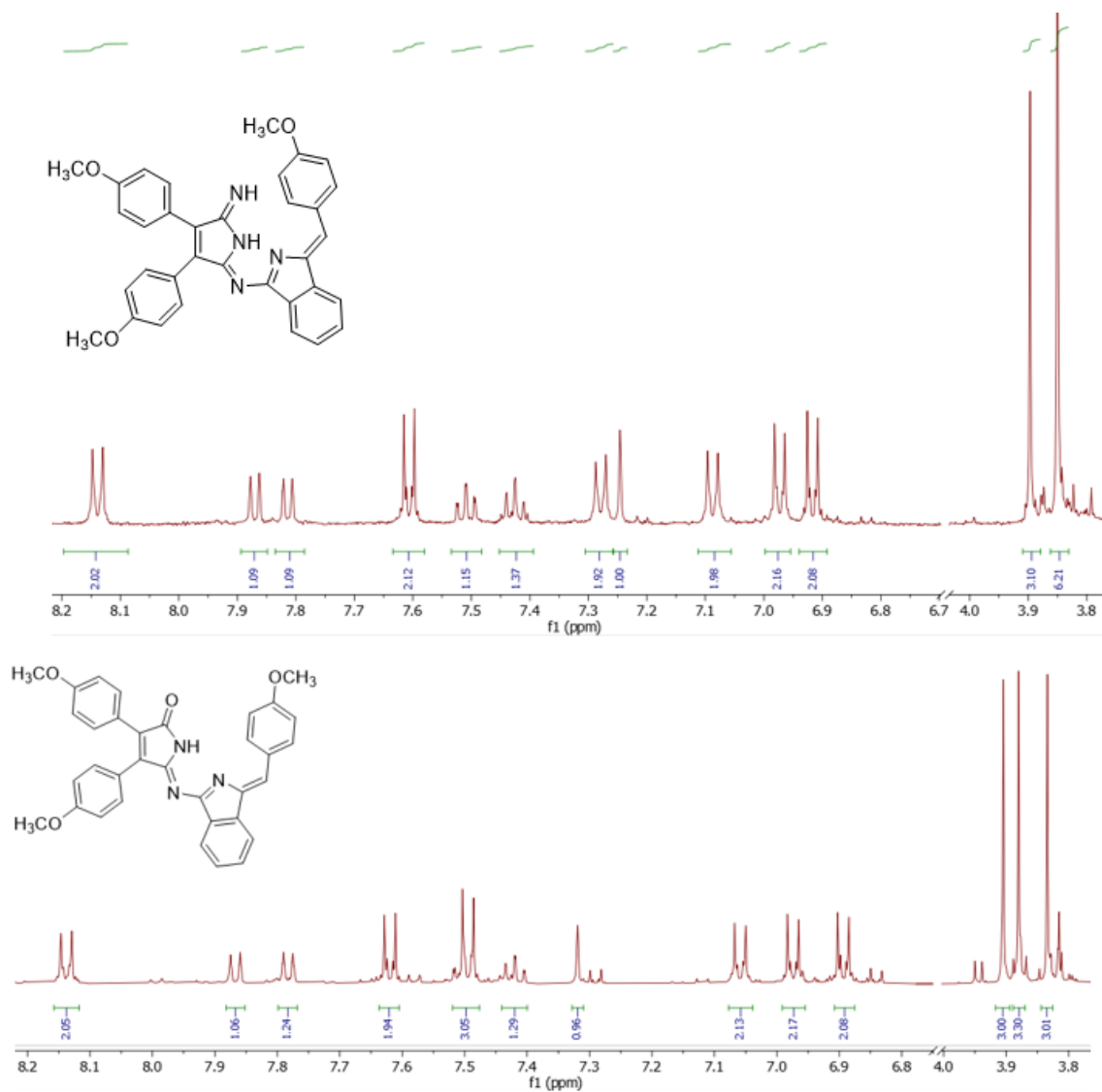


Figure 2.23: Comparison of ^1H NMR spectra between dimers **2.17** and **2.18** in DCM-d_2 .

Figure 2.24 displays UV-Vis absorption spectra for dimers C=NH **2.17** and C=O **2.18**, showing similar absorption characteristics.

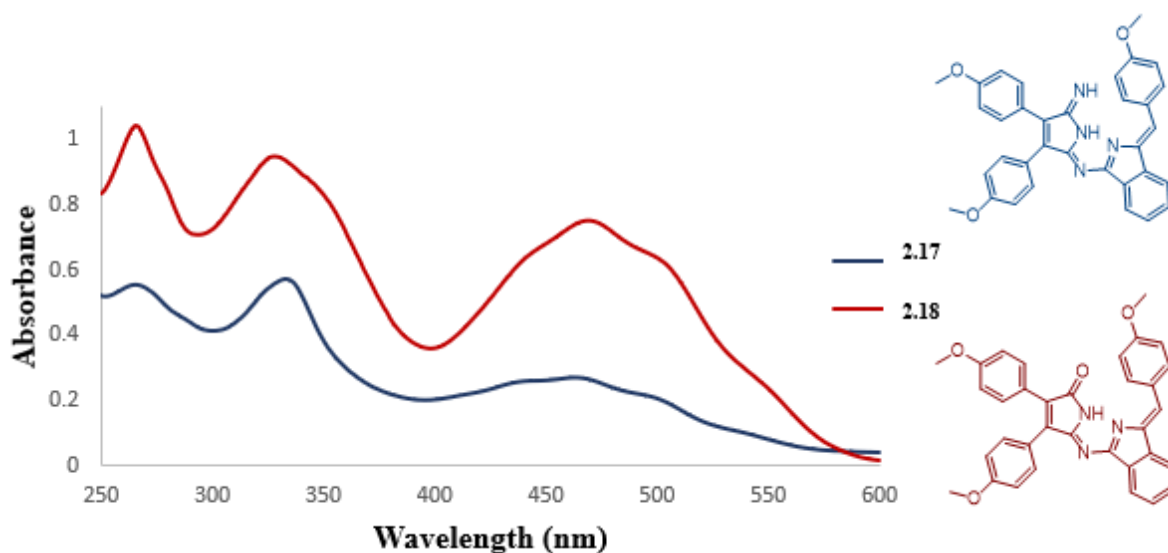


Figure 2.24: UV-Visible spectrum of dimers **2.17** and **2.18** in DCM.

Our doubts were resolved after obtaining the crystal structure of dimer **2.18**, as shown in Figure 2.25. The X-ray crystal structure was solved by our collaborator, Dr David Hughes, and his comments on the detail of the structure can be found in the appendix.

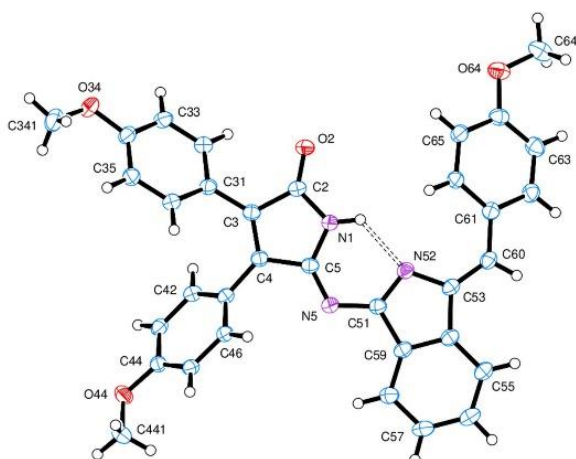
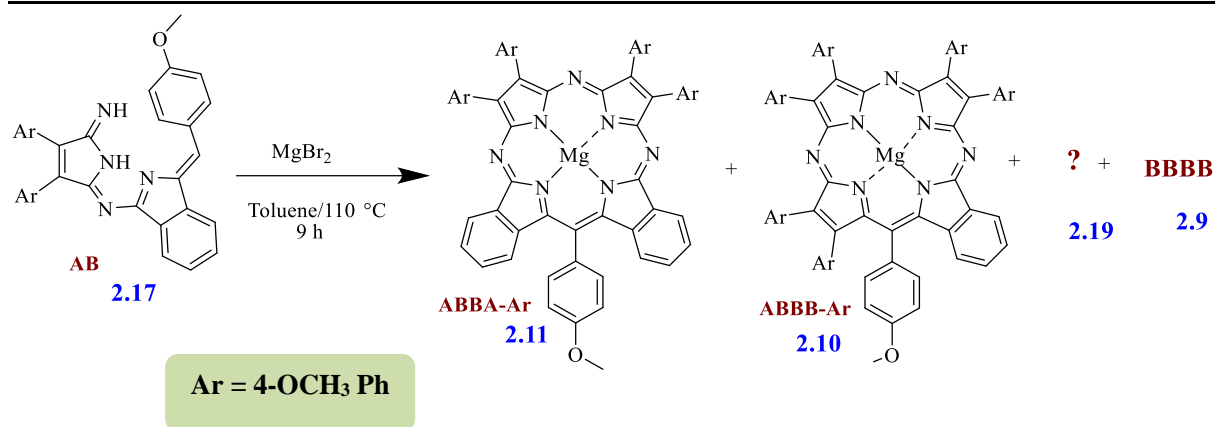


Figure 2.25: The X-ray structure view of a molecule of the C=O dimer **2.18**, indicating the atom numbering scheme. Thermal ellipsoids are drawn at the 50% probability level.

2.6.2 Synthesis of Mg-porphyrazine hybrids from novel AB intermediates

Following the successful synthesis of the (AB dimer) **2.17**, the next step in our challenge addressed synthesising the porphyrazine hybrids. We started by employing the protocol used recently in the group for the synthesis of the Mg-TBTAP hybrids from **AB** dimers with Mg template. 2 equiv. of AB dimer **2.17** was reacted with MgBr_2 in toluene and refluxed under a nitrogen atmosphere for 9 h (Scheme 2.18).



Scheme 2.18: Synthesised porphyrazines hybrids with Mg template from intermediate **2.17** (**AB** dimer).

The reaction mixture turned from red to dark green colour, which indicated the formation of macrocycle(s)/Pz hybrids. TLC monitoring showed multiple spots, which encouraged us to analyze the reaction mixture by MALDI-TOF MS spectra, which gave some indications for the identities of the green coloured products. Unlike what we expected from the group's results on the phthalocyanine hybrid series where ABBB hybrids are favoured, this reaction produces several hybrids. The first spot was easily identified as corresponding to the Mg-ABBA Pz/Pc derivative **2.11** at (964.91 m/z). This spot was the major macrocyclic product in the reaction mixture. An unknown blue fraction was then seen that exhibited a MALDI-TOF mass peak at (1021.65 m/z). Pleasingly, the next spot corresponded to our expected unsymmetrical macrocycle Mg-ABBB-Pz derivative **2.10** at (1126.90 m/z). Finally, the last spot was for the undesired symmetric Pz BBBB product **2.9**. The TLC and multiple ion peaks in MALDI-TOF mass confirmed the formation of more than one reaction product. The purification of these macrocycles was performed through several consecutive column chromatography. Separation was challenging because of the many side products, and the spots were near to each other. The initial column was employed to remove the main impurities and isolate the mixed green fraction. Subsequent columns were designed for purifying the (combined) green fraction, which consisted of the macrocycles. The main challenge in these columns was that the mono substituted Pz ABBB-Ar **2.10** and the unknown fraction **2.19** were hard to isolate due to their similar mobility. On the other hand, the *disubstituted* Pz/Pc ABBA hybrid was more accessible for isolation. However, we eventually successfully separated the compounds in a pure state (Figure 2.27). These fractions were obtained in relatively low yields, with 6% for hybrid **2.11**, 4% for Pz **2.19** and 1% for Pz **2.10**. Despite the relatively modest yields, it is worth emphasising

that the compounds correspond to the first reported examples of hybrid materials of this subclass.

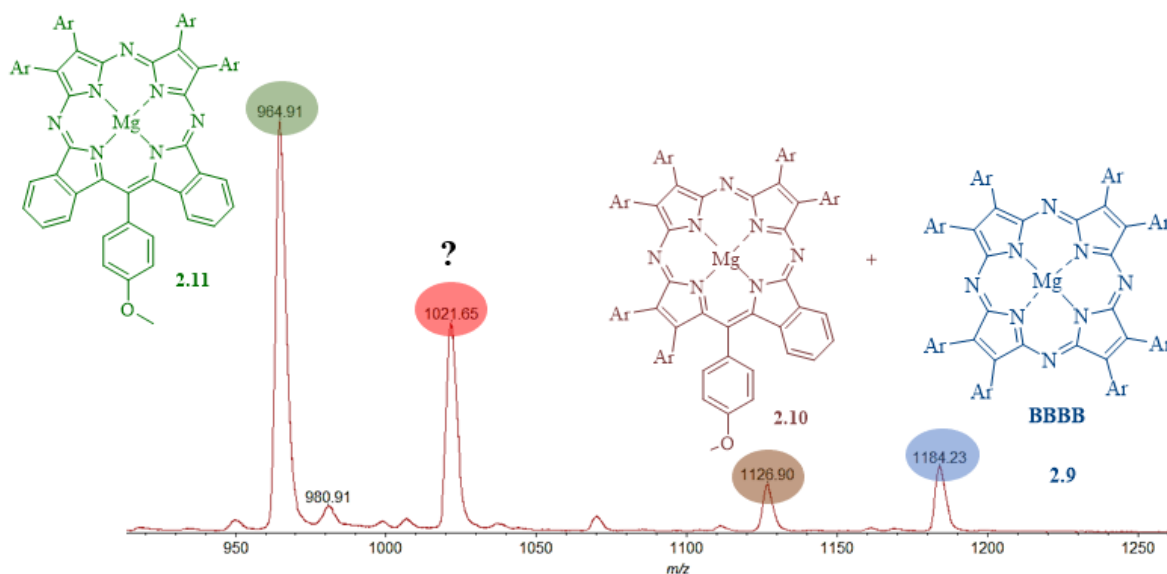


Figure 2.26: The MALDI-TOF- MS spectrum for the combined green fraction.

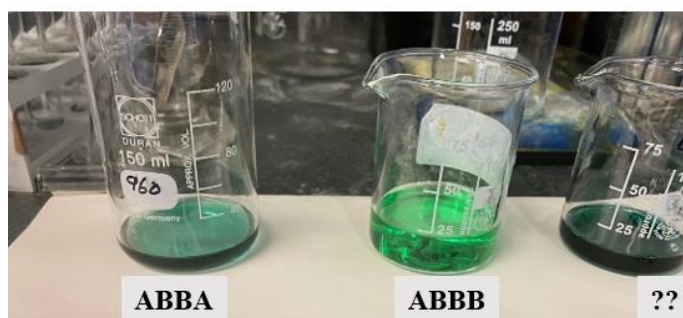


Figure 2.27: Visual inspection of the separation of the three pure Pz macrocycles in solution.

2.6.3 Characterization of the prepared target hybrids

Compound **2.11** (the ABBA-Ar hybrid) is a solid green material. ^1H NMR spectra in deuterated tetrahydrofuran confirmed the structure, which gave expected signals corresponding to all protons, as shown in (Figure 2.28). Two protons were found in the highly de-shielded range at 9.46 ppm from the non-peripheral sites of isoindoline rings of the macrocycle. The peaks in the range δ 8.08 -7.30 ppm confirmed the existence of ten protons from Ph groups at *meso*- and the peripheral position and another non-peripheral position which is labelled as (1) of the isoindoline rings. The protons of four Ph groups at a beta position appeared as pairs of AB doublets with the integration of 4 protons each at δ range from 8.54 - 8.45 and 7.29 - 7.19 ppm. The protons of OCH_3 at the *meso*-position resonate at δ 4.19 ppm. The other 12 protons of the 4 methoxy group appeared as 2 singlets at \sim 4.00 ppm.

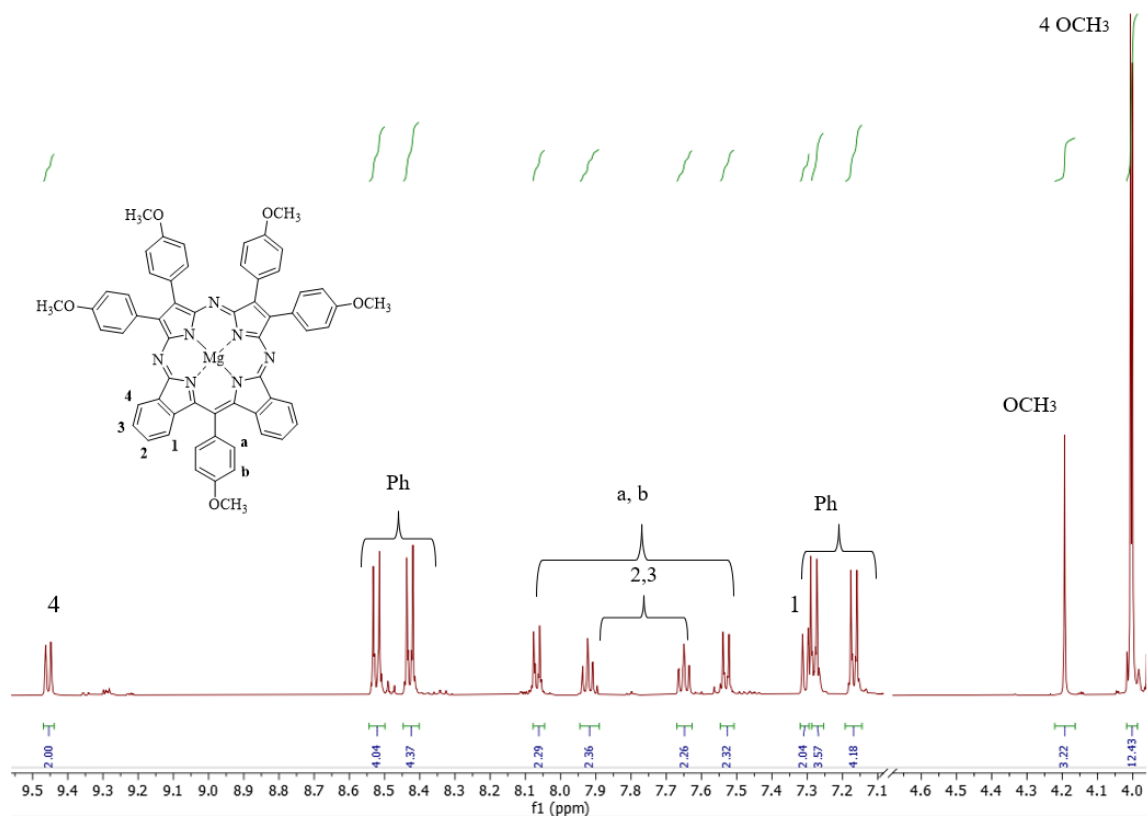


Figure 2.28: The ¹H NMR spectrum of compound **2.11** in THF-*d*₈.

UV-Vis analysed the Pz/Pc macrocycle **2.11**. The electronic absorption spectrum showed the split *Q*-band at λ_{max} 643 and 662 nm (Figure 2.29).

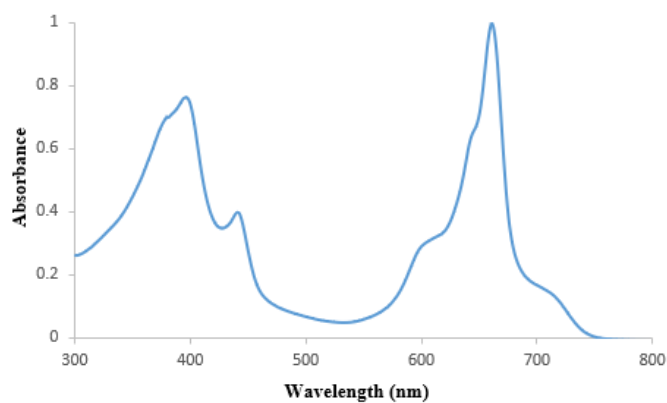


Figure 2.29: The UV-Vis spectrum of the Mg-ABBA Pz/Pc **2.11** in DCM.

MALDI-TOF MS indicated that we had isolated the novel hybrid ABBA-Ar **2.10**, and it was characterised by NMR and UV-Vis spectroscopy. The ¹H NMR spectra in deuterated tetrahydrofuran show all signals corresponding to aromatic and aliphatic regions of the molecule, as shown in Figure 2.30. The aromatic protons, totalling 32 protons, appear in the chemical shift range of 9.38 - 6.68 ppm, as expected. The most de-shielded signal occurs at 9.38 ppm, corresponding to a single proton from the non-peripheral site of this hybrid. This is

likely to be the proton labelled 4, based on the comparison with TBTAP.³⁰ The reduced symmetry of this hybrid was evident, and a good example is seen for the protons of the (7 methoxy) groups that were found as distinct singlets in the range from $\sim \delta$ 4.00- 3.86 ppm, corresponding to 21 protons, which confirmed the ABBB-Ar porphyrazine structure.

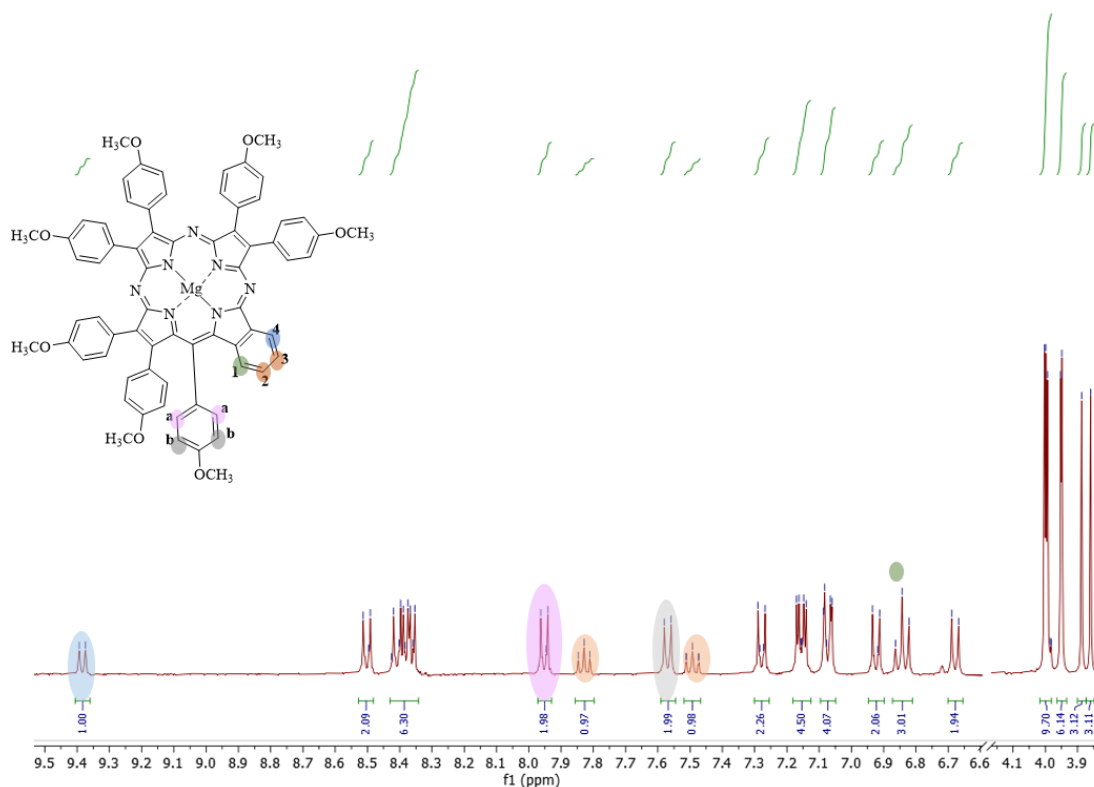


Figure 2.30: The ^1H NMR spectrum of compound **2.10** in $\text{THF-}d_8$.

We subsequently turned our attention to identifying the unknown blue fraction **2.19**, which presented a more challenging task in terms of identifying its structure. Through analysis of its ^1H NMR spectrum and MALDI-TOF MS, we initially deduced that the mass obtained *via* MALDI-TOF mass corresponds to an ABBB-Ar structure like Pz **2.10**, but with the loss of a methoxyphenyl unit. However, the precise identity of this compound remained uncertain.

Figure 2.31 provides a comparison of the ^1H NMR spectra for the unknown compound **2.19** and the previously characterised macrocycles **2.10** and **2.11**, which display similar spectra. These findings suggest that the unknown compound is likely a phthalocyanine / porphyrazine compound. The other observation was in the spectra of ABBB-Ar **2.10**, the chemical environments of the protons are influenced by the presence of the phenyl group at the *meso* position, which increases the electron density, thus resulting in significant differences in the chemical shifts and peak splitting patterns for both shielded and de-shielded protons. In contrast, the chemical shift in the Pz **2.11** was like the unknown compound **2.19**. One key observation emerged from comparing the aliphatic regions of ABBB-Ar **2.10** and the unknown

2.19, both spectra exhibit peaks corresponding to the protons of OCH₃ groups, appearing in the expected range of $\sim \delta$ 4.00 – 3.80 ppm, the difference is that hybrid **2.10** contains one additional methoxy group, confirming our earlier hypothesis. Based on this comparative analysis, we initially proposed that the unknown compound **2.19** is an ABBB derivative that has undergone the loss of a methoxy phenyl group at the *meso* position.

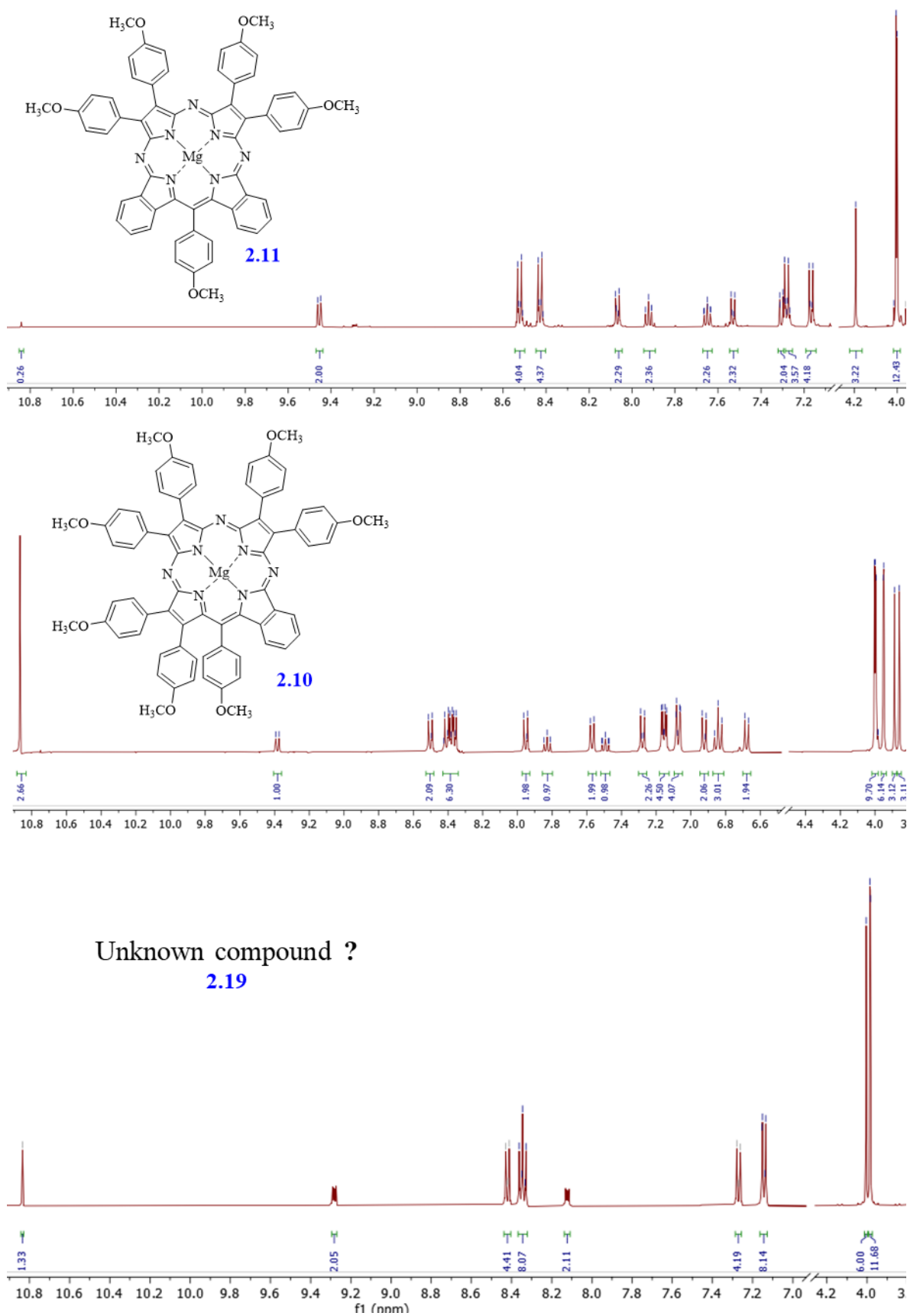
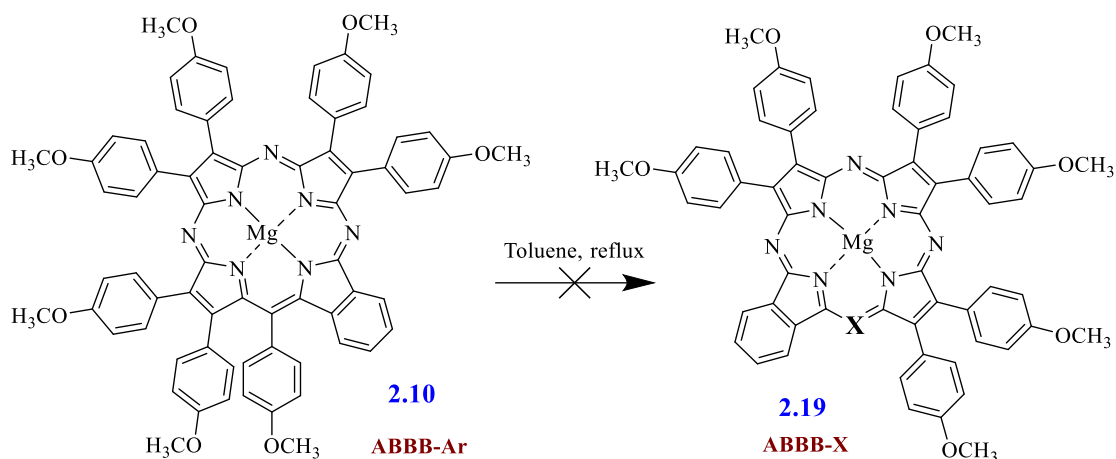


Figure 2.31: The ^1H NMR spectra of porphyrazine **2.10**, **2.11** and the unknown compound **2.19** in $\text{THF-}d_8$.

To better understand the formation of Pz **2.19**, we investigated the potential conversion of hybrid **2.10** to **2.19** in the experiment illustrated in Scheme 2.19. The ABBB-Ar hybrid **2.10** was subjected to identical reaction conditions (reflux in toluene). No reaction occurred, apart from some thermal decomposition after prolonged reaction. This observation means the formation of the ABBB-X hybrid **2.19** does not originate from hybrid **2.10**.



Scheme 2.19: Attempted to convert hybrid **2.10** to **2.19** Pz.

The initial assumption was that *meso* atom X (Figure 2.32) is a carbon atom (a C-H group) because previous studies have shown that *meso*-substituents can be lost in crowded hybrids.¹⁰⁷

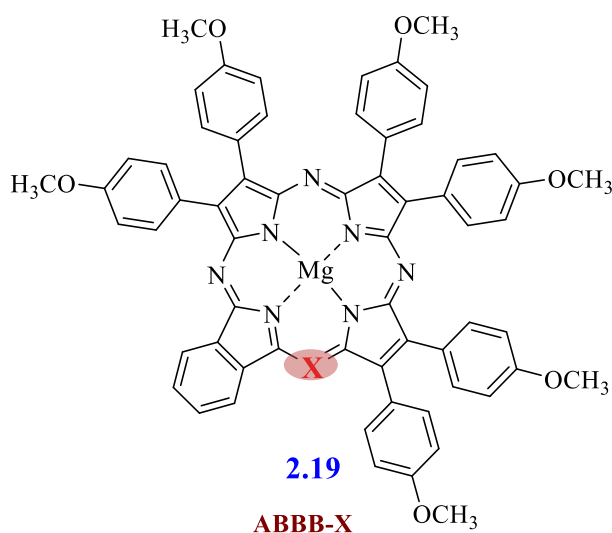


Figure 2.32: The chemical structures for Mg-ABBB-X **2.19**.

If this were the case, the proton at this position would be expected to appear in a highly de-shielded range. The ¹H NMR spectrum of **2.19** did indeed display a signal at δ 10.83 ppm

integrating for a single proton which supported our assumption. However, upon revisiting the ^1H NMR spectra of other related hybrids, which were also recorded in deuterated THF, we observed identical peaks in all the spectra (Figure 2.31). This led us to reconsider our interpretation and propose that these peaks are likely attributed to the THF solvent. This was simply verified by changing the concentration of the sample, and the coincidental matching integration was lost. Remarkably, the logical conclusion is that the *meso*-atom is nitrogen, and that the compound **2.19** is in fact a porphyrazine analogue.

Our ambiguities were finally resolved through the successfully solved X-ray crystal structure of hybrid **2.19**, which unequivocally confirmed the compound as the hybrid Mg ABBB-N, with the atom at the *meso*-position definitively identified as a nitrogen atom (Figure 2.33). This unexpected discovery highlights the formation of a rare 3:1 porphyrazine-phthalocyanine hybrid. The small number of related examples of such ABBB hybrids have been prepared from dinitrile and phthalonitrile derivatives in the literature,^{57, 71} but this is the first time that we have evidence of aminoisoindoline losing a benzyl fragment during macrocyclisation. It is possible that hybrids **2.10** and **2.19** originate from the same intermediate where the final macrocyclization step occurs with a loss of nitrogen to give **2.10** or a methoxybenzyl fragment to give **2.19**. The X-ray crystal structure was solved by our collaborator, Dr David Hughes, and his comments on the detail of the structure can be found in the appendix.

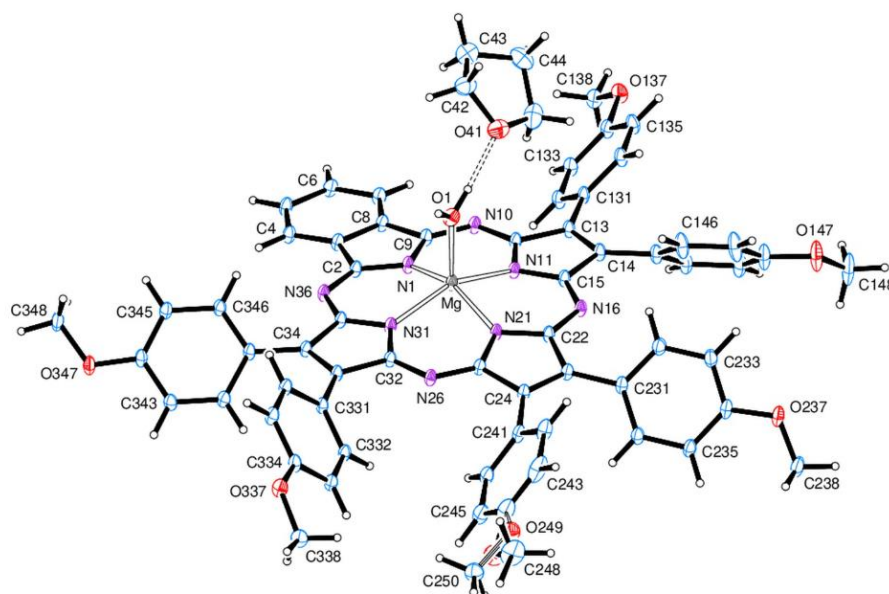


Figure 2.33: The X-ray crystal structure view of the porphyrazine **2.19**, with a hydrogen bonded THF molecule attached. The atom numbering scheme is indicated. Thermal ellipsoids are drawn at the 20% probability level.

The UV-Vis spectra of DCM solutions of porphyrazines **2.10** and **2.19**, in comparison to the parent Mg-BBBB-Pz **2.9**, are presented in Figure 2.34. Pz **2.10** exhibits intense *Q*-bands at λ_{max} 660 nm and 626 nm. In contrast, Pz **2.19** shows *Q*-bands at slightly higher wavelengths, λ_{max} 672 nm and 639 nm. This observed redshift is due to the structural differences introduced by the replacement of the phenyl-C group with a nitrogen atom at the *meso*-position. The parent porphyrazine **2.9** displays a single *Q*-band, intermediate between the other derivatives highlighting how the substitution of C/N and benzo-fusion effectively cancel each other out. These observations are consistent with the trends that seen in C/N hybrid structures.⁴⁷

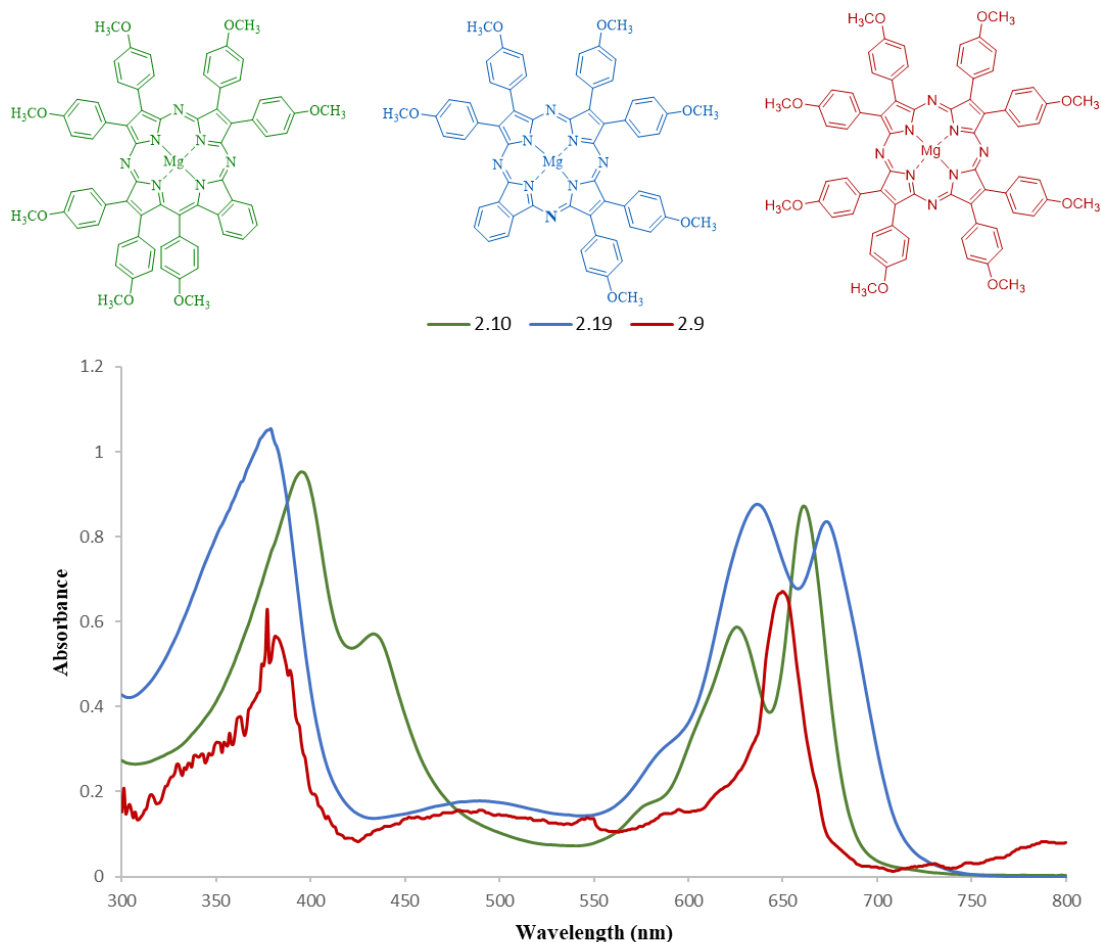


Figure 2.34: Comparison of the UV-Vis spectra of porphyrazines **2.10** and **2.19** with the parent porphyrazine Mg-Pz **2.9** in DCM.

2.6.4 Synthesis of Zn-porphyrazine hybrids from (AB dimer) intermediate

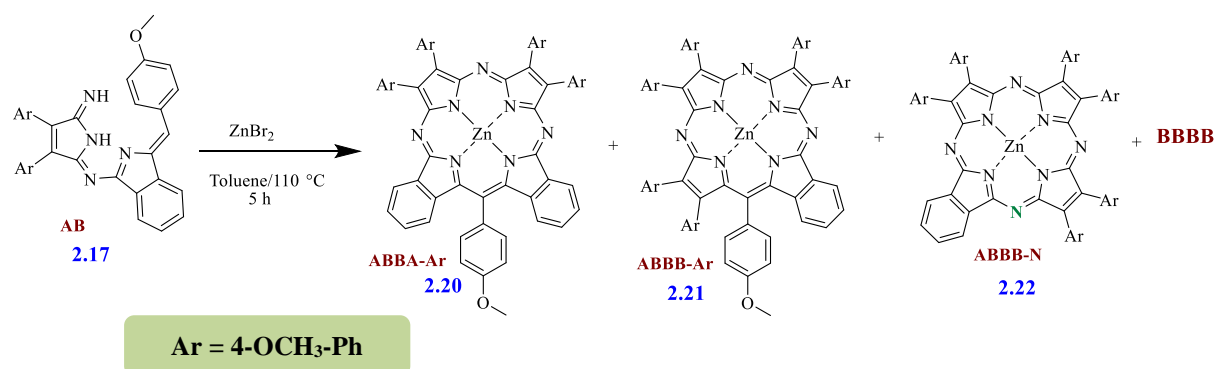
In our previous study, employing the magnesium template for macrocyclisation reaction presented significant challenges in separating the hybrid mixture by column chromatography, primarily due to variations in separation based on polarity. The template metal within the core of the macrocycle hybrid significantly influenced these separations. To mitigate this effect and the associated separation difficulties, we attempted to replace magnesium with a different metal

to enhance separation efficiency and perhaps influence reaction outcome and efficiency. Zinc was selected, used as the Zn(II) ion, from zinc bromide (ZnBr_2), which possessed a larger ionic radius and exhibits superior coordination ability compared to Mg (II).⁵⁰ Additionally, the Zn(II) ion acts as a stronger Lewis acid.

The next study will focus on investigating the effect of replacing the MgBr_2 with ZnBr_2 in the core of the macrocycle hybrids. The macrocyclisation reaction starts from our new intermediate (AB dimer). Specifically, this research aims to determine whether this replacement leads to the same formation of porphyrazine types, particularly N-ABBB Pz.

2.6.5 Synthesis of 4-methoxyphenyl-substituted Zn-Pz/Pc hybrids from dimer 2.17

To synthesise the Zn complexes, we followed the same methodology previously utilised for preparing Mg-porphyrazine hybrids. The (AB dimer) **2.17** was refluxed under an N_2 atmosphere with ZnBr_2 for 5 h (Scheme 2.20). The Zn complexes required shorter reaction times compared to the Mg complexes, and the reaction progress was monitored *via* TLC and MALDI-TOF MS (Figure 2.35). However, like the reactions involving Mg salts, the TLC analysis revealed multiple green spots, indicating the presence of various Zn-hybrids.



Scheme 2.20: Synthesised porphyrazine hybrids with Zn template from intermediate **2.17** (AB dimer).

Upon completion of the reaction, the purification process, which represented an obstacle, was slightly facilitated with Zn salts. However, it was still necessary to use several consecutive column chromatographies for purification. The first column utilised dichloromethane as the eluent to remove the main impurities. Subsequently, the polarity was adjusted with a mixture of DCM and tetrahydrofuran in a 5:3 ratio. The second column is used to isolate the green fraction, employing a gradient solvent system of petroleum ether and THF, starting from a less polar mixture and increasing the polarity. The green fraction was further purified using a

column that was eluted with EtOAc/DCM (5:100). This reaction yielded a similar mixture of Zn hybrids Zn ABBA, Zn ABBB-Ar, Zn BBBB and the unexpected hybrid ZnABBB-N, as shown in Figure 2.35. Isolating Zn ABBB-Ar **2.21** in a pure state was challenging due to the slight difference in R_f values between it and Zn ABBB-N **2.22**, which hindered the separation and analysis of Zn ABBB-Ar **2.21**. These outcomes are consistent with the results we obtained in the magnesium Pz reaction. In this reaction, the major product is expected to be Zn-ABBA **2.20**, similar to the previous reaction with the Mg. However, the most intriguing aspect of the results was the formation of hybrid **2.22**, which became the predominant product, with a yield of 13%, compared to an 8% yield for hybrid **2.20**. These interesting outcomes added a fascinating twist to our research, inviting further exploration.

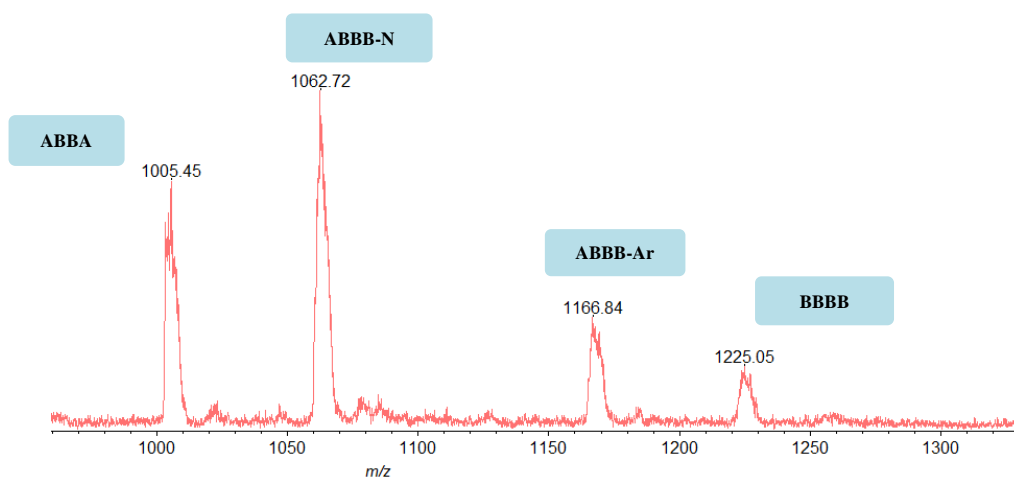


Figure 2.35: The MALDI-TOF- MS spectrum for the combined green fraction.

The identities of porphyrazine **2.20** and **2.22** were confirmed by ^1H NMR, MALDI-TOF MS, and UV-Vis spectra. The UV-Vis spectra for Zn-Pz **2.20** displayed an absorbance profile very similar to that of the identically substituted hybrid Mg-Pz **2.11**.

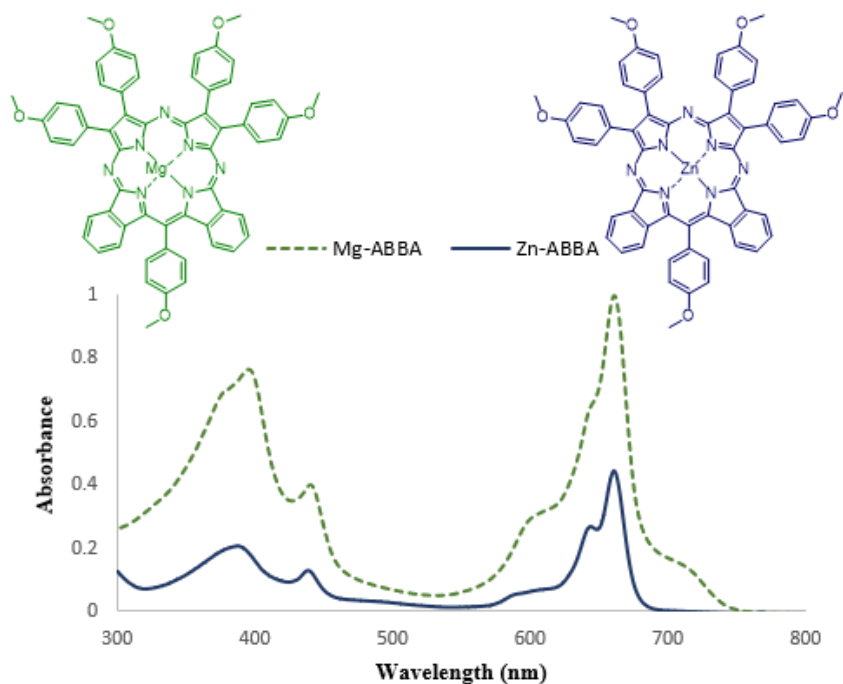


Figure 2.36: The UV-Vis spectrum of Mg, Zn ABBA-Pz **2.11** and **2.20** in DCM.

The ABBA-N **2.22** porphyrazine gave suitable single crystals for X-ray diffraction analysis (Figure 2.37). The X-ray crystal structure was solved by our collaborator, Dr David Hughes, and his comments on the detail of the structure can be found in the appendix.

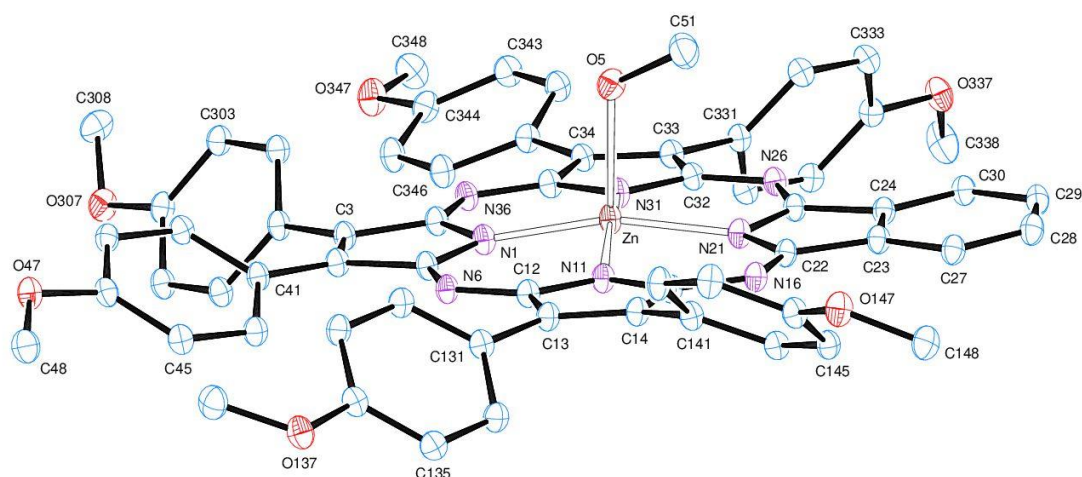


Figure 2.37: The X-ray crystal structure of the zinc complex molecule **2.22**, indicating the atom numbering scheme. Thermal ellipsoids are drawn at the 50% probability level.

2.6.6 Results and yields

Considering the previous reactions outlined in Schemes 2.18 and 2.20, we have demonstrated interesting reaction pathways that yield novel hybrids. The effect of the metal (Mg or Zn) in the hybrid is important; the main product of the magnesium reaction is ABBA Pz, while the zinc reaction predominantly yields ABBB-N. All the Pz hybrids demonstrate stability against photodegradation, in contrast to some TB TABs hybrids. The study was therefore extended to demonstrate reproducibility across different substituents.

2.7 Synthesis of (Zn)-porphyrazine/phthalocyanine hybrids – varying the β -aryl substituents

In this study we aimed to further investigate Pz hybrids by using various substituted dinitriles (**B**). Throughout, we consistently used the aminoisoindoline precursor **2.4** (**A**). The dinitrile derivatives were prepared and tested with *t*-butyl **2.23** and 4-isopropoxyphenyl **2.24** substitution. The precursors used are shown in Figure 2.38.

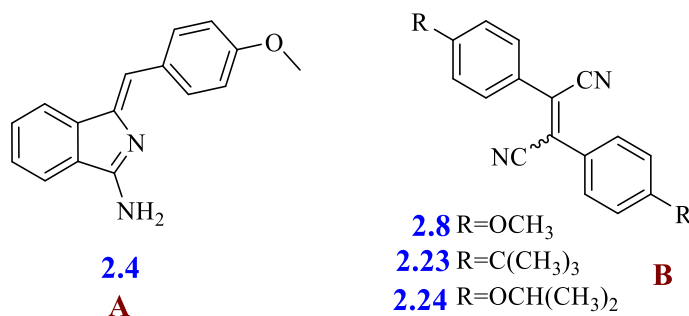
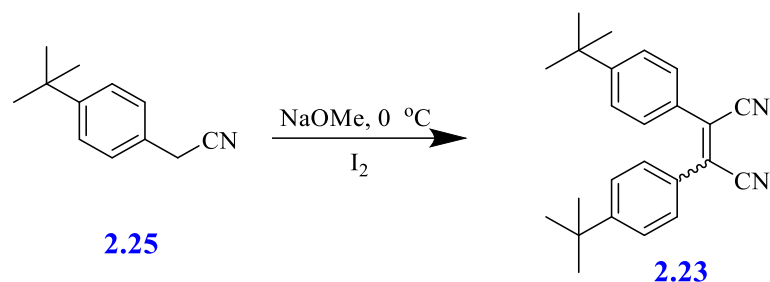


Figure 2.38: The aminoisoindoline and dinitrile derivatives used in the first type.

2.7.1 Synthesis of *t*-butyl-substituted dinitrile **2.23**.

The nature of the substituents affects the solubility of the dinitriles derivative in the reaction solvent (MeOH) and imparts good solubility to the final macrocycles. Consequently, we employed the *t*-butyl dinitrile instead of the methoxy dinitrile derivative. Our objective was to conduct the reaction at a lower temperature to prevent the formation of (AB C=O dimer), thus facilitating the formation and isolation of the (AB NH dimer). A method similar to that used for the preparation of methoxy dinitrile derivative **2.8** was utilized to synthesise the *t*-butyl dinitrile derivative **2.23** (Scheme 2.21).



Scheme 2.21 : Synthesis of *t*-butyl dinitrile derivative **2.23**.

The structure of *t*-butyl dinitrile **2.23** was verified through ^1H NMR spectroscopy and MALDI-TOF MS spectra. The ^1H NMR spectra exhibited a peak at δ 1.36 ppm, corresponding to 18 protons for 2 *t*-butyl groups. The MALDI-TOF MS analysis confirmed the targeted product **2.23** (Figure 2.39).

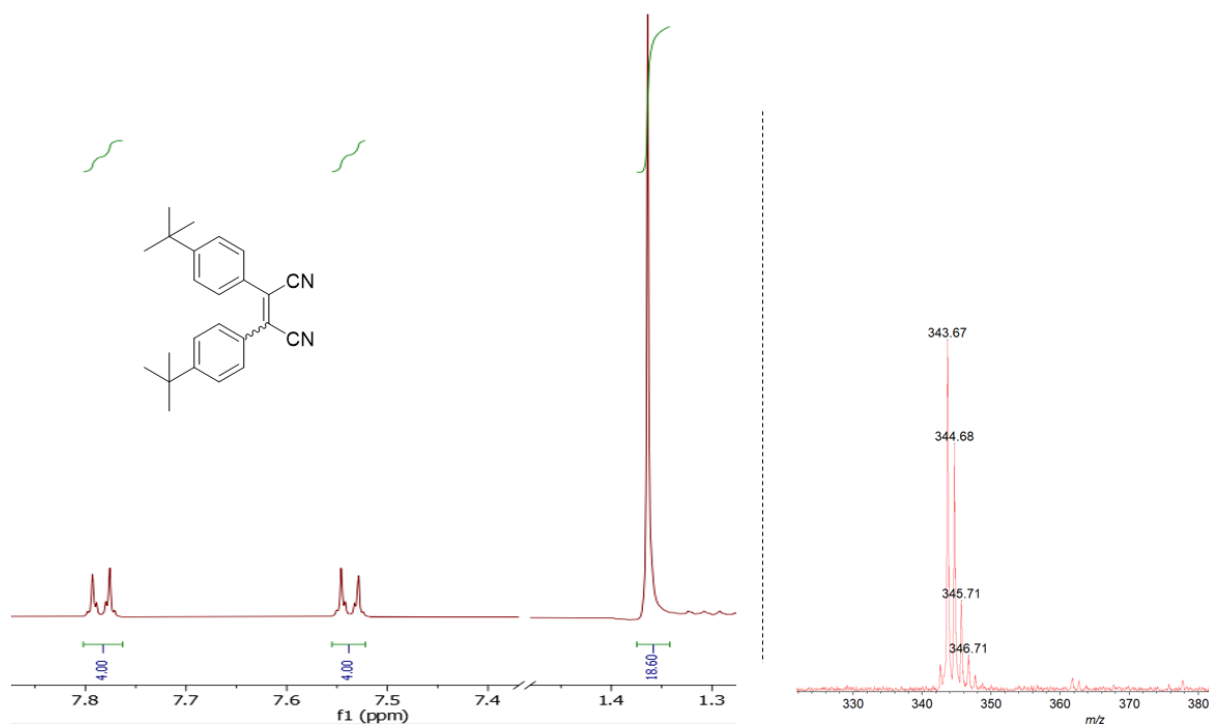
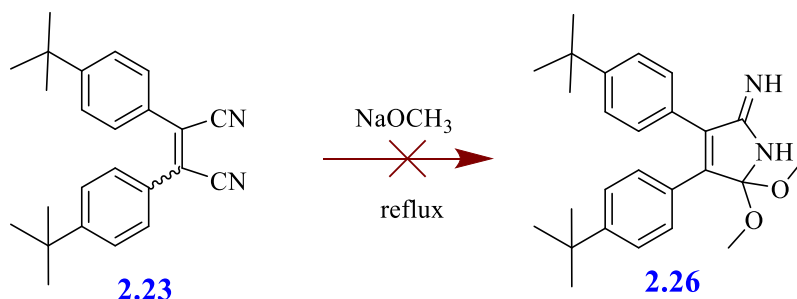


Figure 2.39: The partial ^1H NMR spectrum in CDCl_3 (left) and MALDI-TOF MS (right) for **2.23**.

2.7.2 Synthesis of *t*-butyl phenyl-substituted (AB dimer) **2.27**

Initially, we attempted to prepare dimethoxypyrrole derivative **2.26** using *t*-butyl dinitrile **2.23**, which is expected to be more soluble in the solvent (CH_3OH) than methoxy dinitrile derivative **2.8**, following the protocol outlined in Scheme 2.13. It was observed that **2.23** exhibited better solubility than compound **2.8** at 40°C . The MALDI-TOF mass analysis of the crude product indicated the presence of precursor **2.26**, with an ion peak at $407.54\ m/z$ (Figure

2.40). Unfortunately, during attempts at purification *via* column chromatography, the target material underwent hydrolysis, resulting in the formation of the pyrrolone derivative, analogous to the outcomes observed in previous experiments, with methoxy substitute dinitrile **2.8** (Scheme 2.22).



Scheme 2.22 : Synthesis of *t*-butyl-dimethoxypyrrole derivative **2.26**.

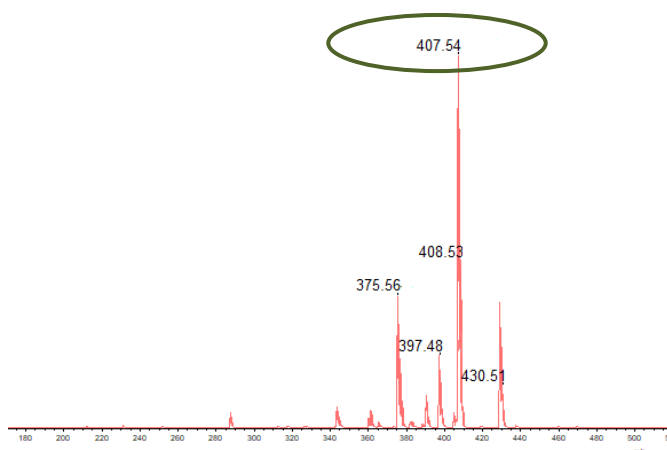
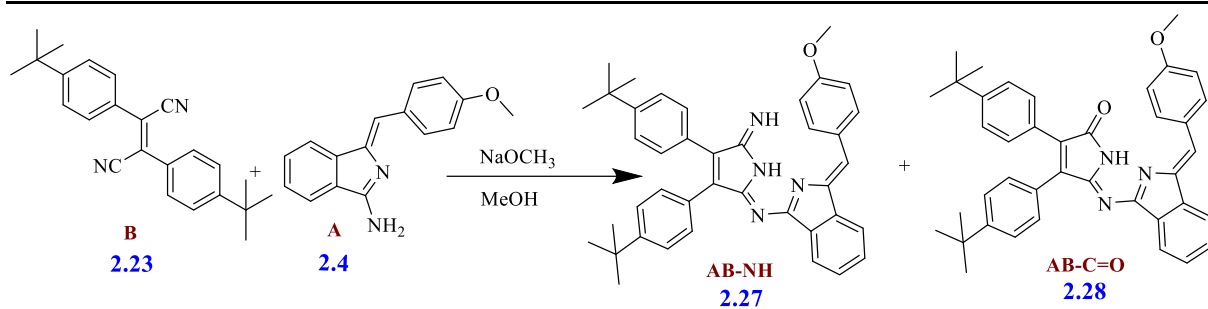


Figure 2.40: The MALDI-TOF MS spectrum for the crude product **2.26**.

However, the synthetic methodology to develop an intermediate (AB **2.17**) was successfully applied in the synthesis dimer **2.27**. The reaction mixture was refluxed for 10 h, and the crude product was purified by careful column chromatography using a gradient solvent from petroleum ether: DCM. Dimer **2.27** was successfully isolated as a red solid material (Scheme 2.23). The MALDI MS spectra confirmed the molecular weight of the target product **2.27** at (593.79 *m/z*) (Figure 2.41). Additionally, during this reaction, we observed the formation of a hydrolysed dimer (containing carbonyl (C=O) functional group) **2.28**, which was separated as a red-orange material. The yields were 38% for **2.27** and 18% for **2.28**; this finding aligns with our observation in the previous results.



Scheme 2.23: Synthesis of condensation product (AB dimer) **2.27** and hydrolysed **2.28**.

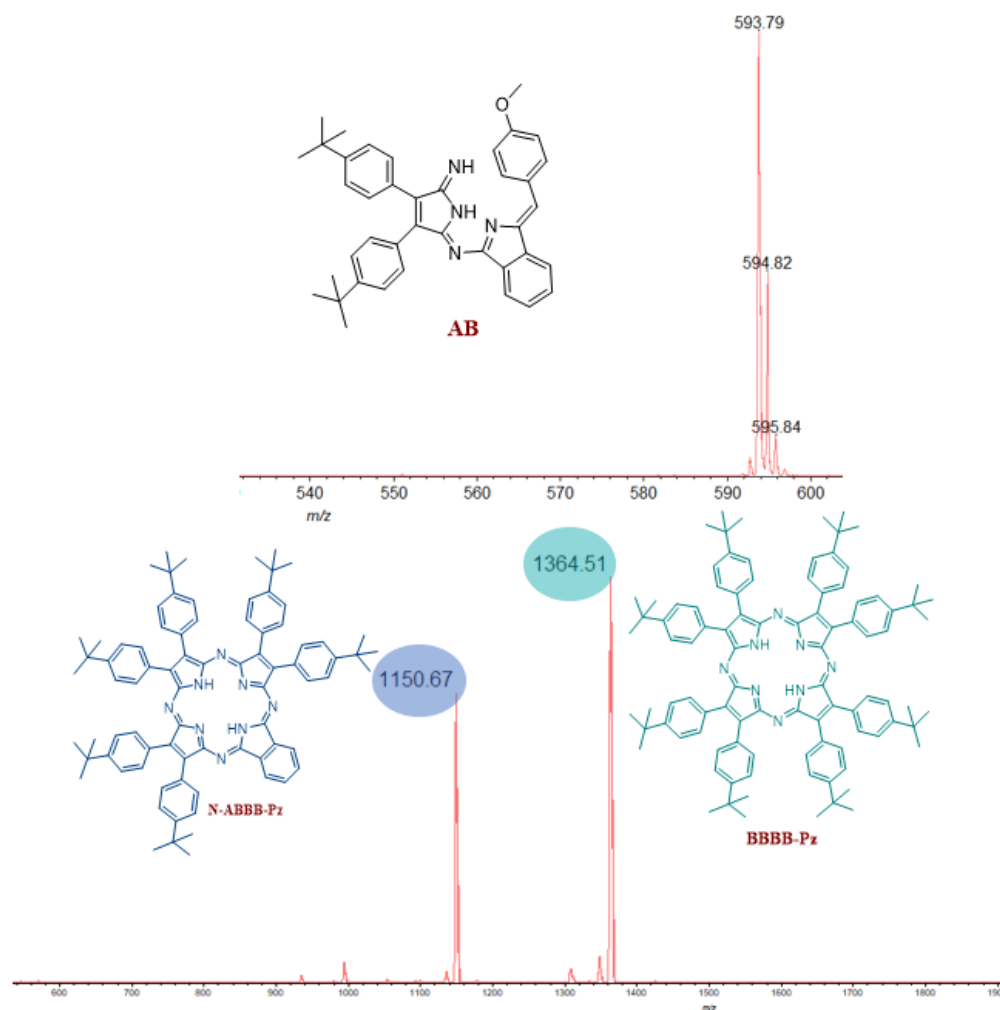


Figure 2.41: The MALDI-TOF MS spectrum of dimer **2.27** and the side products.

Figure 2.42 presents the ^1H NMR spectrum for dimer **27**, with key signals observed as follows: the aromatic protons of the isoindoline benzene rings, along with the phenyl-substituted pyrrole rings and the vinyl protons ($\text{C}=\text{C}-\text{H}$), were detected in the chemical shift range of δ 8.17 to 7.02 ppm. The methoxy group protons (OCH_3) exhibited a distinct singlet at δ 3.89 ppm, while the *tert*-butyl group protons presented as 2 singlets at δ \sim 1.36 ppm. In

contrast, the ^1H NMR spectrum for the C=O dimer **2.28**, as described earlier, showed a comparable pattern to the N-H dimer indicating structural similarities.

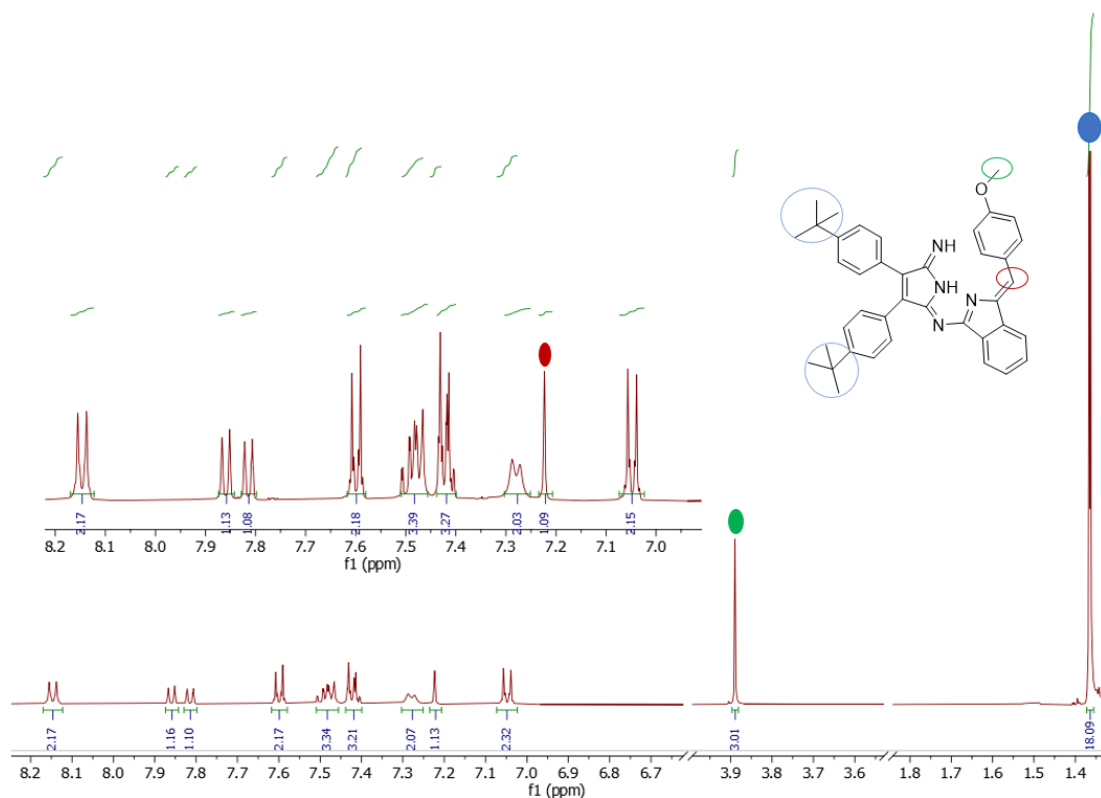


Figure 2.42: The ^1H NMR spectrum for dimer **2.27** in DCM-d_2 .

Furthermore, the crystal structure of the target N-H dimer **2.27** was conclusively determined by X-ray crystallography, as illustrated in Figure 2.43. The X-ray crystal structure was solved by our collaborator, Dr David Hughes, and his comments on the detail of the structure can be found in the appendix. Both dimers exhibited broad absorbance bands in their UV-Vis spectra (Figure 2.44).

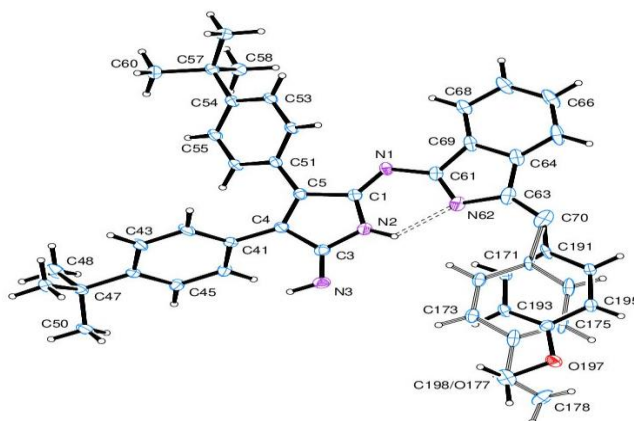


Figure 2.43: The X-ray structure view of dimer **2.27**, indicating the atom numbering scheme.

Thermal ellipsoids are drawn at the 20% probability level.

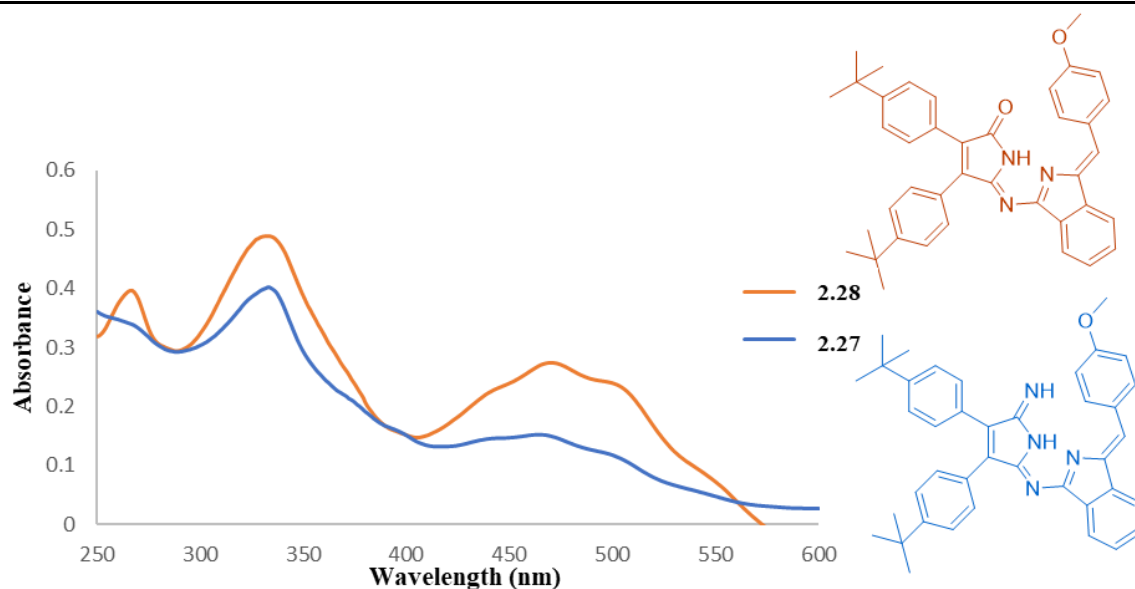
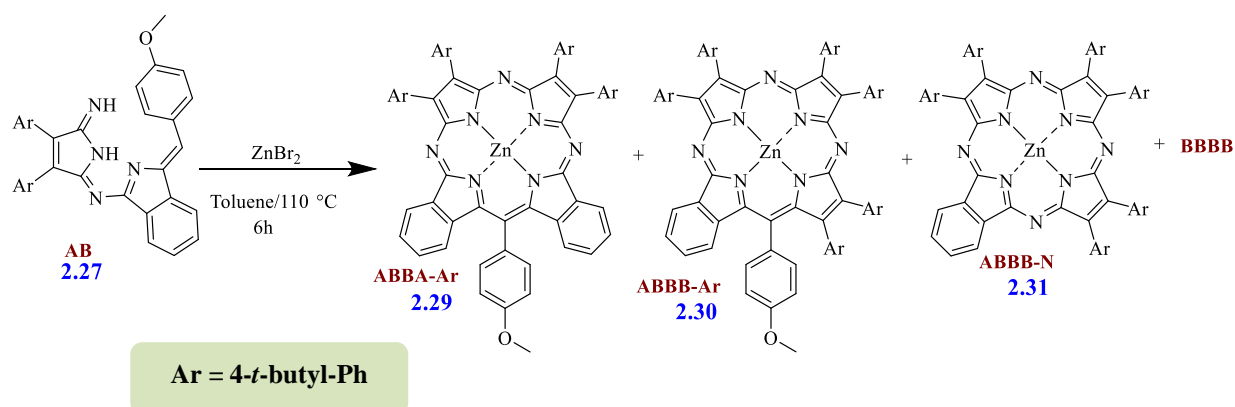


Figure 2.44: UV-Vis spectrum of condensation products **2.27** and **2.28** in DCM.

2.7.3 Synthesis of *t*-butyl phenyl Pz/Pc hybrids

The *t*-butyl phenyl substituted dimer **2.27** undergoes macrocyclisation in the presence of ZnBr₂ in toluene and reflux conditions under N₂ atmosphere. The reaction reaches completion after 6h, as shown in Scheme 2.24.



Scheme 2.24: Synthesis of *t*-butyl phenyl Zn-Pz/Pc hybrids.

The crude reaction mixture, when analysed by (TLC) exhibited multiple spots. This observation indicates the formation of various Pz hybrids, highlighting the complexity of the reaction mixture and underscoring the necessity for further purification steps to isolate the desired macrocyclic product, as we had previously with methoxyphenyl substituted hybrids. After workup, the pure compounds were separated by several consecutive column chromatography. The first column utilised two solvent systems to remove the impurities, starting with DCM /petroleum ether (1:1) → DCM to obtain the green fraction. The MALDI-TOF MS analysis of this fraction revealed the formation of hybrids similar to those observed in

the case of 4-methoxyphenyl porphyrazine/phthalocyanine. The molecular ion peaks were identified as corresponding to Zn-ABBA Pz/Pc **2.29** (1112.76 m/z), Zn-ABBB-Ar Pz **2.30** (1325.78 m/z), and Zn-ABBB-N Pz **2.31** (1220.81 m/z), and the BBBB Pz respectively (Figure 2.45).

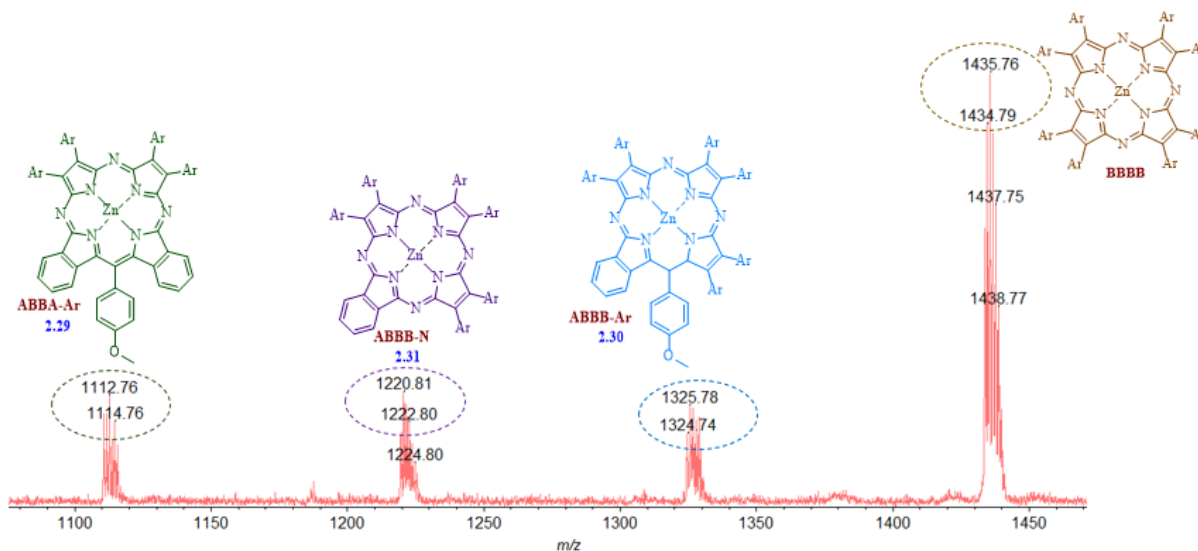


Figure 2.45: The MALDI-TOF MS spectrum for the combined green fraction.

The second column chromatography used a mixture of PE/ THF in a (6:1) ratio. The last column separation was achieved using petroleum ether/THF (20:1) to separate this mixture of hybrids. Similar to previous attempts, we encountered challenges in isolation (**2.30** and **2.31**). However, Porphyrazines **2.29** and **2.31** were successively separated and characterised by NMR spectroscopy. Figure 2.46 shows the ^1H NMR spectrum of compound **2.29**, all signals for 28 aromatic protons from the δ 9.46 -7.32 ppm range are observed. Moreover, a broad singlet peak at δ ~1.55 ppm corresponds to all *t*-butyl groups, and the other singlet peak at δ 4.20 ppm is characteristic of the methoxy group from the Ph ring at the *meso* position.

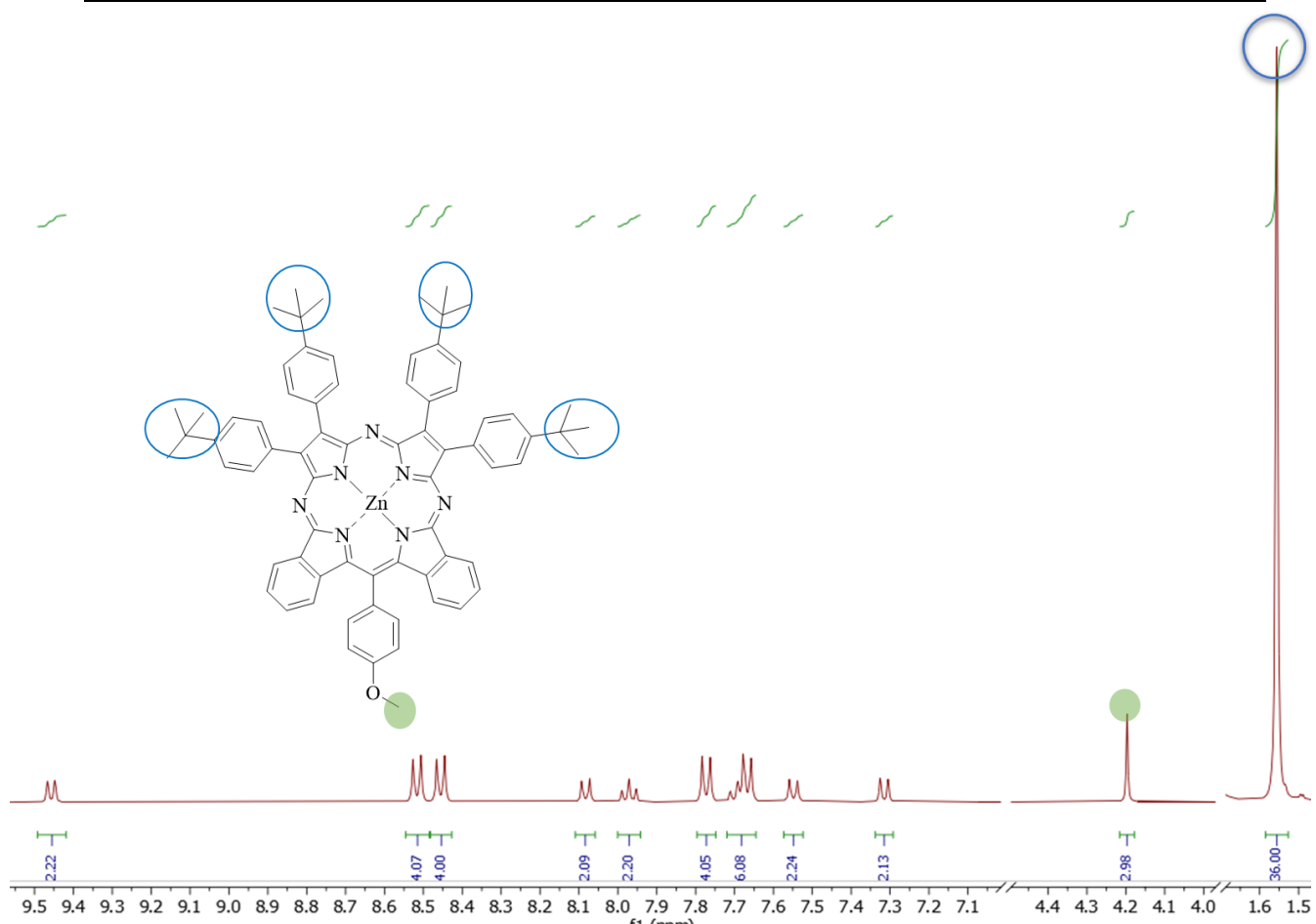


Figure 2.46: The ^1H NMR spectrum of compound **2.29** in $\text{THF-}d_8$.

The UV-Vis absorption spectrum for ABBA hybrid **2.29** exhibited the characteristic Q -band splitting at 657 and 640 nm. Figure 2.47 compares the ABBA hybrids spectra of the methoxy Mg-pz **2.11**, Zn-pz **2.20** and Zn-pz *t*-butyl **2.29** substituted derivatives. Unsurprisingly, the spectra are essentially identical.

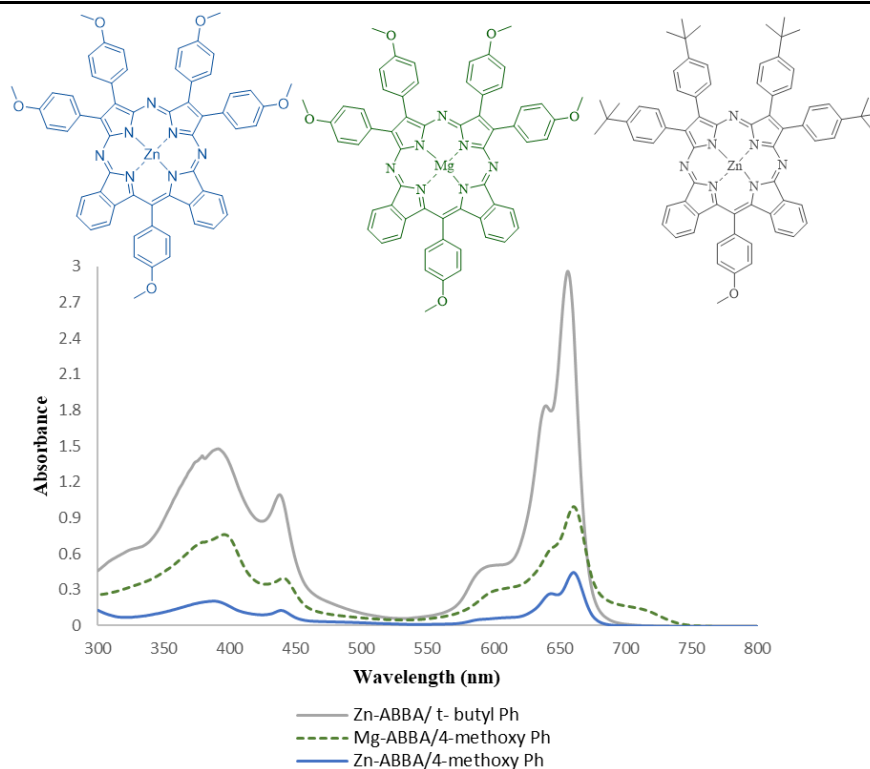


Figure 2.47: The UV-Vis absorption spectra comparing different ABBA hybrids: **2.11** (green line), **2.20** (blue line) and **2.29** (grey line) in DCM.

For the first time, the novel hybrid structure for Zn-ABBA **2.29** successfully formed a single crystal suitable for X-ray crystallographic analysis. This achievement confirms the structure of phthalocyanine/porphyrazine Zn-ABBA Pz (Figure 2.48). The preliminary X-ray crystal structure has been obtained by our collaborator, Dr David Hughes. He reports that the data is sufficient to confirm the molecular structure but not for detailed analysis.

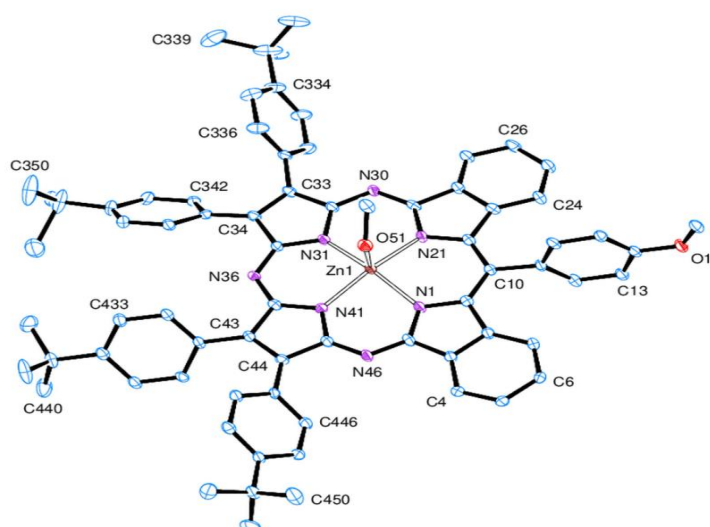


Figure 2.48: View of a molecule **2.29** indicating the atom numbering scheme. Thermal ellipsoids are drawn at the 50% probability level.

As for the other separated hybrid Pz ABBB-N **2.31**, the ^1H NMR spectra clearly displayed three singlet peaks in the $\sim \delta$ 1.56 – 1.53 ppm, corresponding to 54 protons, indicating the presence of six *t*-butyl groups. Additionally, two peaks at δ 9.25 and 8.15 ppm, corresponding to four protons, confirmed the presence of the fused benzene ring of the isoindole moiety (Figure 2.49). This finding confirms the molecular structure of the novel (3:1) Zn ABBB-N **2.31**.

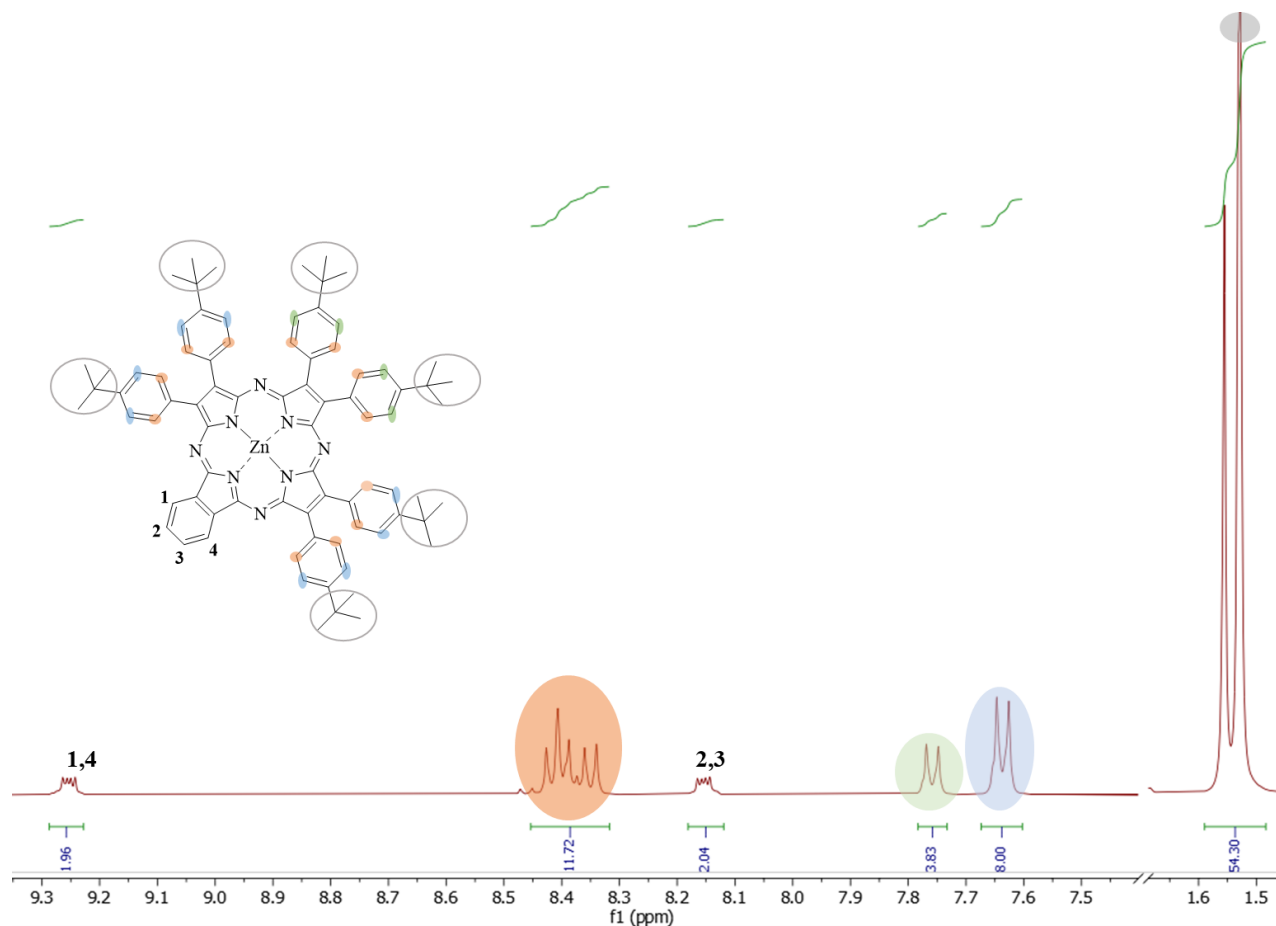
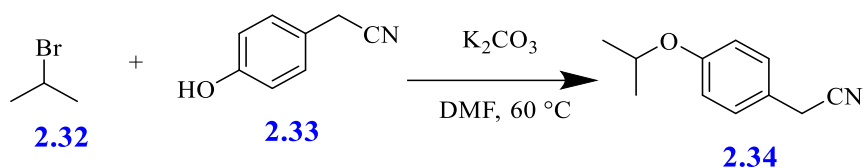


Figure 2.49: The ^1H NMR spectrum of porphyrazine **2.31** in $\text{THF-}d_8$.

2.7.4 Synthesis of isopropoxyphenyl substituted dinitrile **2.24**

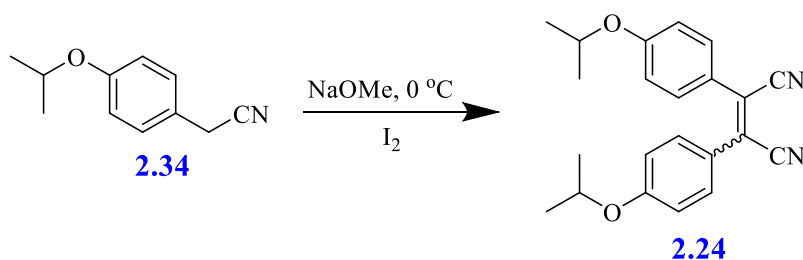
Isopropoxyphenyl dinitrile **2.24** was selected to be the final substituted dinitrile precursor in this series to investigate the outcomes for the Zn-Pz hybrids. This substituent is expected to exhibit moderate solubility in alcohols and other organic solvents. To synthesise **2.24**, we first prepared 2-(4-isopropoxyphenyl) acetonitrile **2.34** as an intermediate. This was achieved by reacting 2-bromopropane **2.32** with 4-hydroxyphenyl acetonitrile **2.33** in DMF in the presence of K_2CO_3 at 60°C for 21h. The crude reaction mixture was extracted with DCM, and the product was concentrated to yield the pure product as pale-yellow needles with a 62% yield (Scheme 2.25). The intermediate **2.34** was characterized using ^1H NMR and ^{13}C NMR

spectroscopy. The spectra obtained matched the previously reported reference, thereby confirming the chemical structure.¹¹⁵



Scheme 2.25: Synthesis of 2-(4-isopropoxyphenyl) acetonitrile **2.34**.

Subsequently, as shown in Scheme 2.26, compound **2.34** was dissolved in diethyl ether in the presence of iodine and stirred under an N_2 atmosphere. The reaction mixture was cooled in an ice bath to $0\text{ }^\circ\text{C}$, and a solution of sodium methoxide was added dropwise. The reaction mixture was then stirred at room temperature for 2h and quenched with cold water. The resulting precipitate was collected by vacuum filtration and washed with cold methanol to yield 50% of the new dinitrile precursor **2.24**.



Scheme 2.26: Synthesis of Isopropoxyphenyl substituted dinitrile **2.24**.

The structure of dinitrile **2.24** was confirmed using NMR spectroscopy (Figure 2.50), and the MALDI-TOF MS spectra exhibited a molecular ion peak at ($346.63\text{ }m/z$). Furthermore, single crystals suitable for X-ray diffraction analysis were obtained, which confirmed the molecular structure and the *trans* geometrical configuration around the $C=C$ double bond (Figure 2.51). The structure shown is a preliminary one that confirms the molecule **2.24**. The X-ray crystal structure was solved by our collaborator, Dr David Hughes, and his comments on the detail of the structure can be found in the appendix.

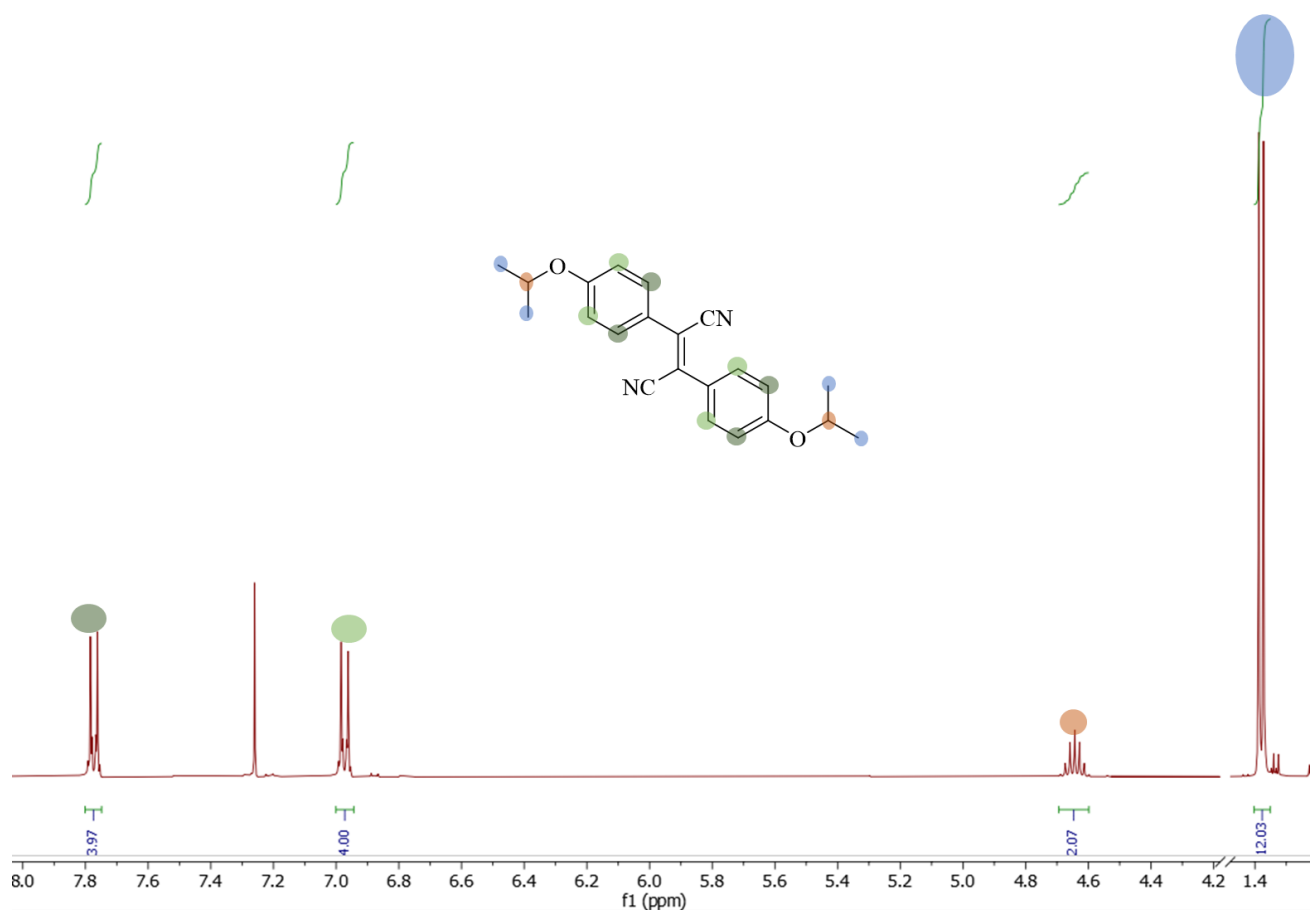


Figure 2.50: The ^1H NMR spectrum of compound **2.24** in CDCl_3 .

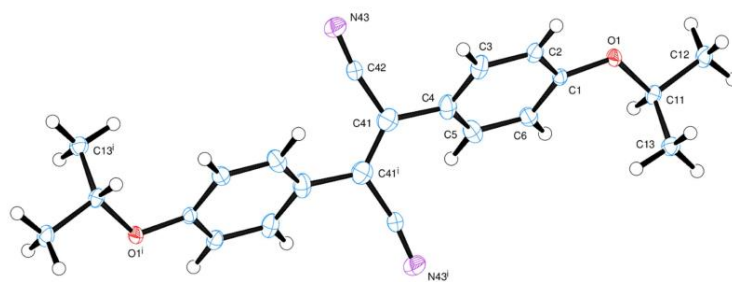
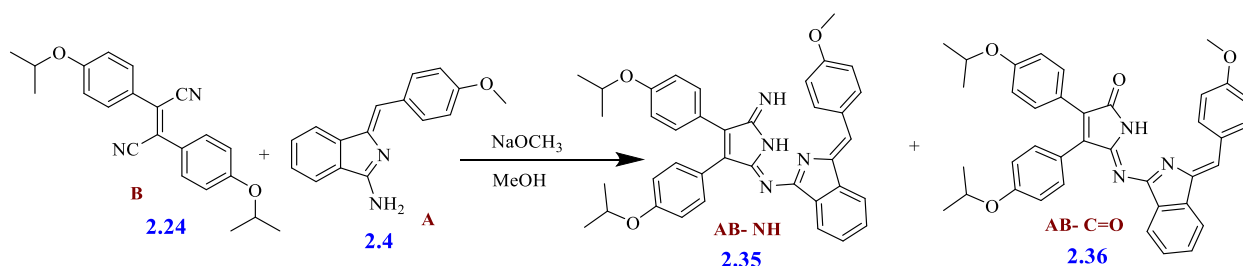


Figure 2.51: The X-ray structure view of dinitrile precursor **2.24**. The atom numbering scheme is indicated. Thermal ellipsoids are drawn at the 50% probability level.

2.7.5 Synthesis of isopropoxyphenyl substituted (AB dimer) 2.35

The synthesis of isopropoxyl dimer **2.35** was achieved following the same approach optimised earlier, involving the reaction between aminoisindoline and dinitrile precursor **2.24** (Scheme 2.27). A solution of sodium methoxide and isopropoxyphenyl substituted dinitrile **2.24** was added to aminoisindoline **2.4**, and the reaction mixture was refluxed for 18 h. In this reaction a small amount of dark black impurities adhered to the reaction flask and were insoluble in the reaction solvent (MeOH).

The crude product was extracted, the organic phases were washed and dried, then purified by column chromatography using petroleum ether: DCM (1:1), (1:2) and finally only DCM, resulting in a 35% yield of the desired dimer **2.35**. During this reaction, we also observed the formation of pyrrolone dimer **2.36** as a byproduct with a 13% yield.



Scheme 2.27: Synthesis of condensation products (AB dimer) **2.35** and **2.36**.

NMR spectroscopy and MALDI-TOF mass spectrometry confirmed the structures of dimers **2.35** and **2.36**. In the ¹H NMR spectra, both structures showed similarities. The primary differences were the separation of the isopropoxy group protons in the aliphatic region, as observed in Figure 2.52, and variations in chemical shifts in some cases.

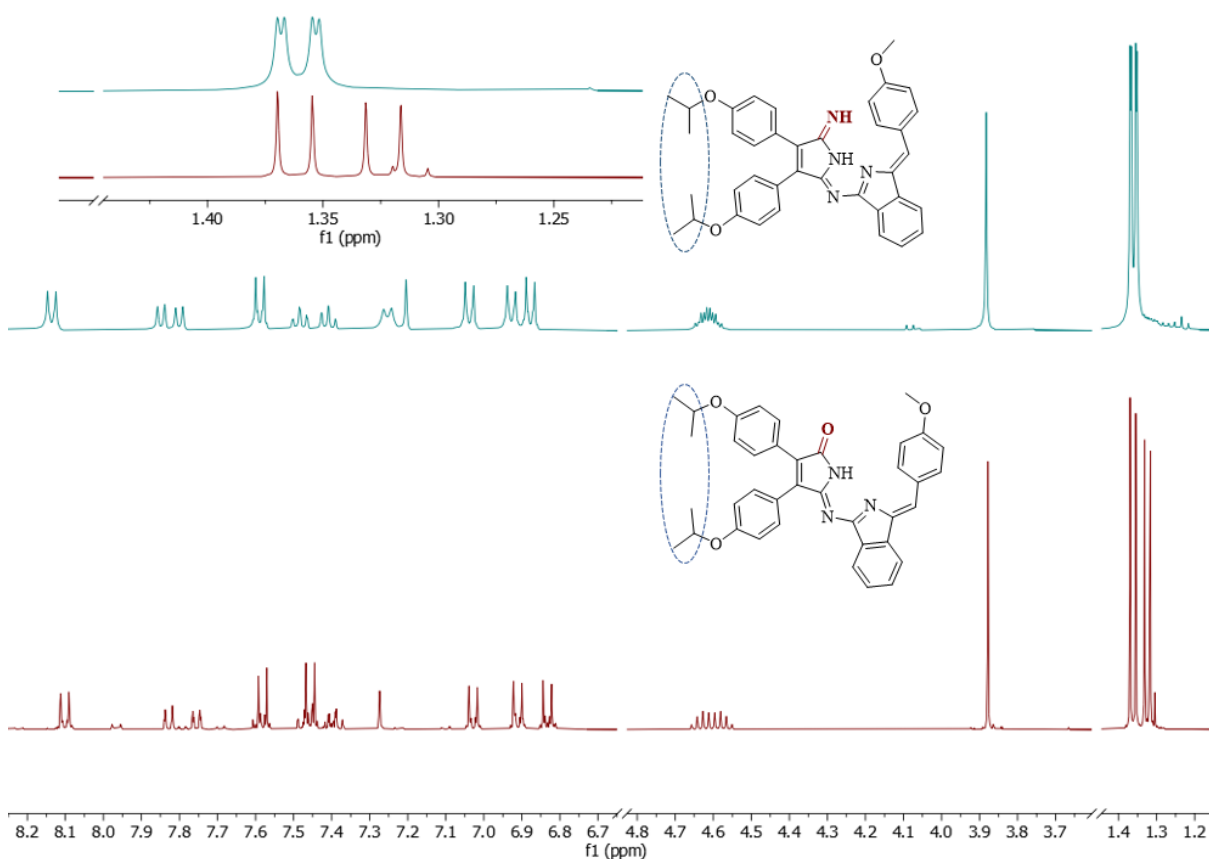


Figure 2.52: The ^1H NMR spectra for (AB) N-H/C=O dimers **2.35** and **2.36** in DCM-d_2 .

Drawing on the experience gained from our previous experiments in synthesising dimers and guided by MALDI-TOF MS analysis, we identified the products present in the dark impurities encountered during the synthesis of N-H dimer **2.35**. These impurities were identified as the metal-free ABBB-N hybrid **2.37**, which exhibited a peak at $1169.38\ m/z$, and the other was identified as the BBBB porphyrazine derivative, displaying a peak at $1388.42\ m/z$ (Figure 2.53).

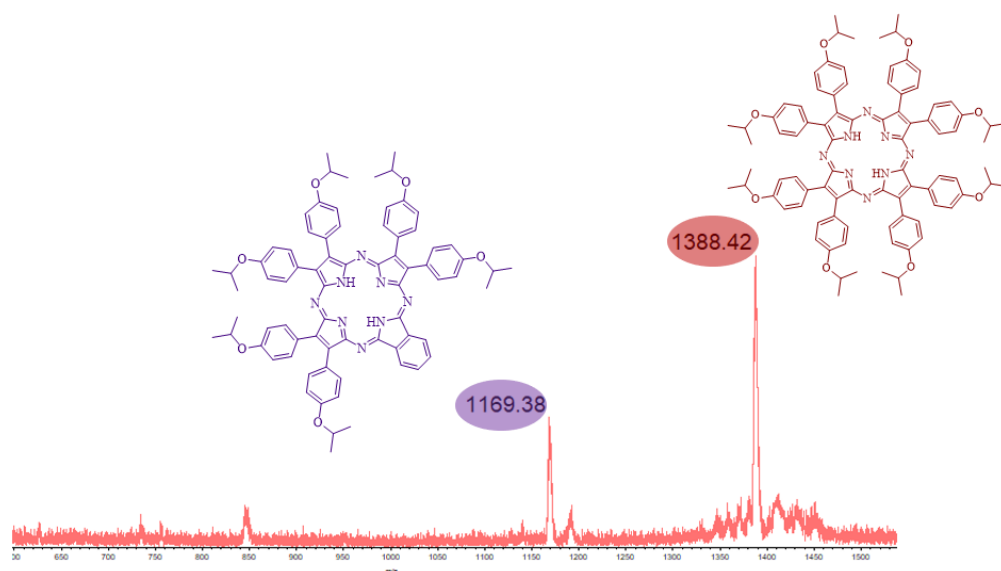


Figure 2.53: The MALDI-TOF mass spectrum of dark impurities (metal-free Pz ABBB-N and BBBB).

Using column chromatography with petroleum ether/ ethyl acetate as the eluent at volume ratios of (6:1) \rightarrow (3:1), we successfully isolated the metal-free porphyrazine H₂-ABBB-N Pz **2.37** in a pure state. The ¹H NMR spectrum of this hybrid recorded in deuterated dichloromethane, exhibited all the expected proton signals (Figure 2.54).

The spectrum displayed sharp peaks for 24 aromatic protons in the δ range of 8.18 -7.05 ppm for phenyl rings of the porphyrazine macrocycle, and the remaining four protons at δ 8.83 and 7.95 ppm corresponding to the protons of benzene unit fused to the pyrrole ring. The six protons appeared as multiple peaks at δ 4.79 ppm, corresponding to the CH group from the isopropoxyl group. In the aliphatic region, the protons for the methyl groups on the 6 phenyl rings were observed as multiple at δ ~ 1.57 ppm. Finally, the characteristic signal for 2H in the centre of the porphyrazine appeared at δ -2.34 ppm.

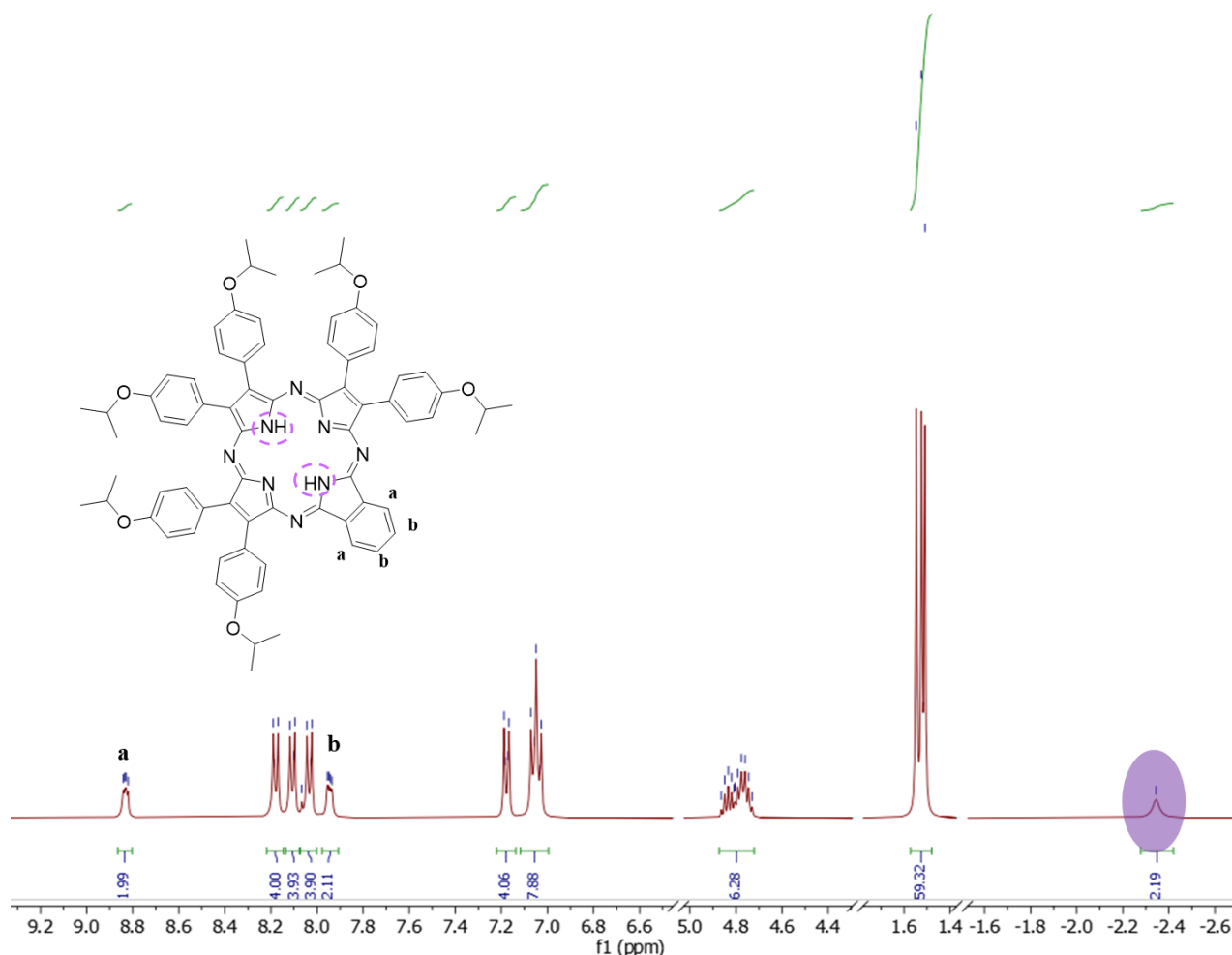


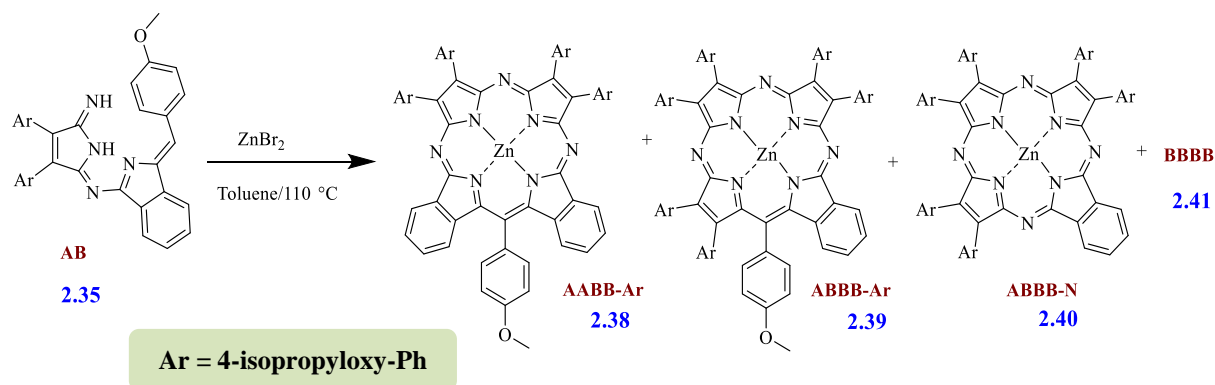
Figure 2.54: The ¹H NMR spectrum for metal-free porphyrazine **2.37** in DCM-d₂.

2.7.6 Synthesis of Zn-Pz/Pc hybrids (4-isopropoxyphenyl-substituted) from dimer **2.35**

To investigate the Zn hybrids produced by using isopropoxyl derivative dimer **35**, the dimer was reacted with ZnBr₂ (2 equiv.) in toluene under N₂ atmosphere for 6 h (Scheme 2.28). The reaction yielded a dark green solution, which was worked up and purified over silica gel using multiple consecutive column chromatography. The first column was employed to isolate the green fraction from other impurities using a DCM / PE (1:1) → DCM system. Analysis of the green fraction mixture by TLC revealed multiple spots corresponding to the four porphyrazine hybrids, similar to the observations made with the other substituted dinitrile dimers **2.17** and **2.27**.

To further purify the green fraction, a gradient solvent system of DCM/ EtOAc (100:1) → (3:5) was applied respectively, and more purification was performed using a third column with petroleum ether/THF (5:1) as the eluent. However, as previously encountered, the minimal

difference in (R_f) values between the ABBB-N **2.40** and ABBB-Ar **2.39** Pzs made their separation challenging. Consequently, isolating the ABBB-Ar **2.39** porphyrazine in a pure state proved difficult. The porphyrazine-Pc hybrid **2.40** emerged as the major product with a yield of 12%, while the ABBA Pz **2.38** was obtained with an 8% yield.



Scheme 2.28: Synthesis of Zn- Pz/Pc hybrids from dimer **2.35**.

Zn-ABBA **2.38** exhibited a light green colour. The MALDI-TOF mass spectrum showed a molecular ion peak at 1117.70 m/z , consistent with the expected structure. The ^1H NMR spectra displayed 24 protons as two doublet peaks with integration of twelve protons for each in the δ 1.55 and 1.53 ppm range, indicating the presence of eight methyl groups in a similar chemical environment, and a three protons singlet appeared at δ 4.25 ppm, confirming the presence of the OCH_3 group in the phenyl ring at the *meso* position. Additionally, the four protons associated with the CH groups of the isopropoxyl substituents appear as a multiple at δ \sim 4.95 ppm. Within the aromatic region, the spectrum shows all expected peaks ranging from δ 9.34 to 7.11 ppm, corresponding to the 28 aromatic protons associated with the phenyl rings of the porphyrazine macrocycle (Figure 2.55). The UV-Vis spectrum showed a split *Q*-band at 663 and 646 nm.

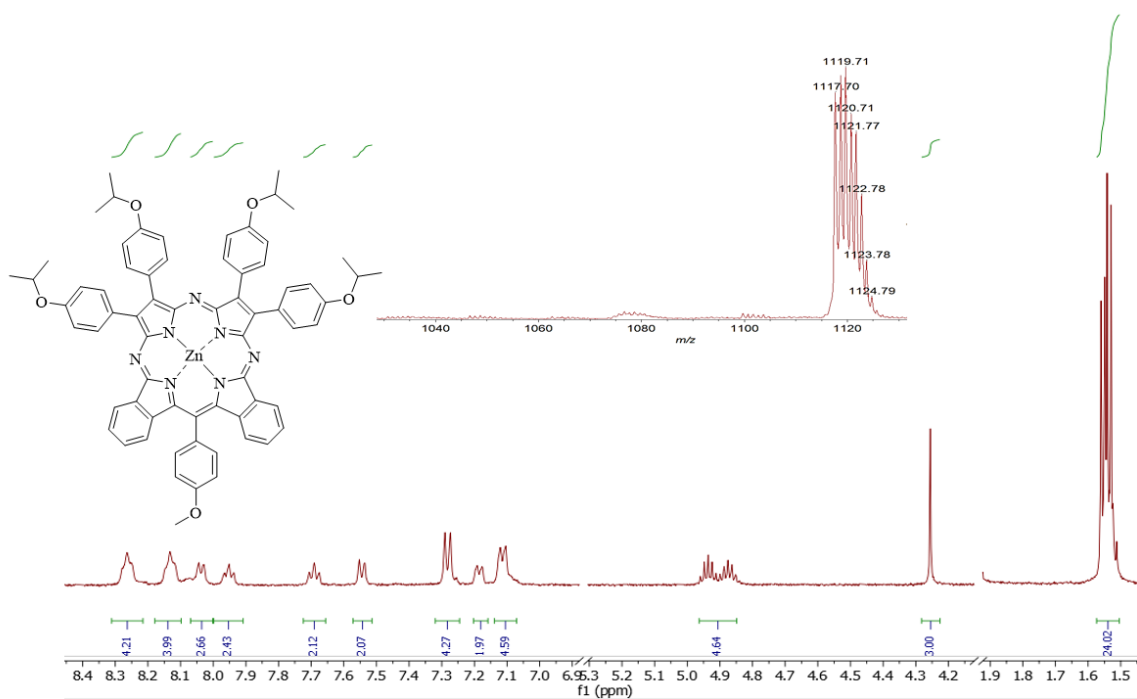


Figure 2.55: The ¹H NMR and MALDI-TOF MS spectrum of Zn-Pc/Pz hybrid **2.38** in acetone-*d*₆.

The second fraction, containing the Zn-ABBB-N **2.40**, was isolated as a dark blue compound with a molecular ion peak (1232.15 *m/z*). The ¹H NMR spectrum recorded in deuterated tetrahydrofuran exhibited all expected signals corresponding to the protons within the molecule, confirming the structure of the compound (Figure 2.56).

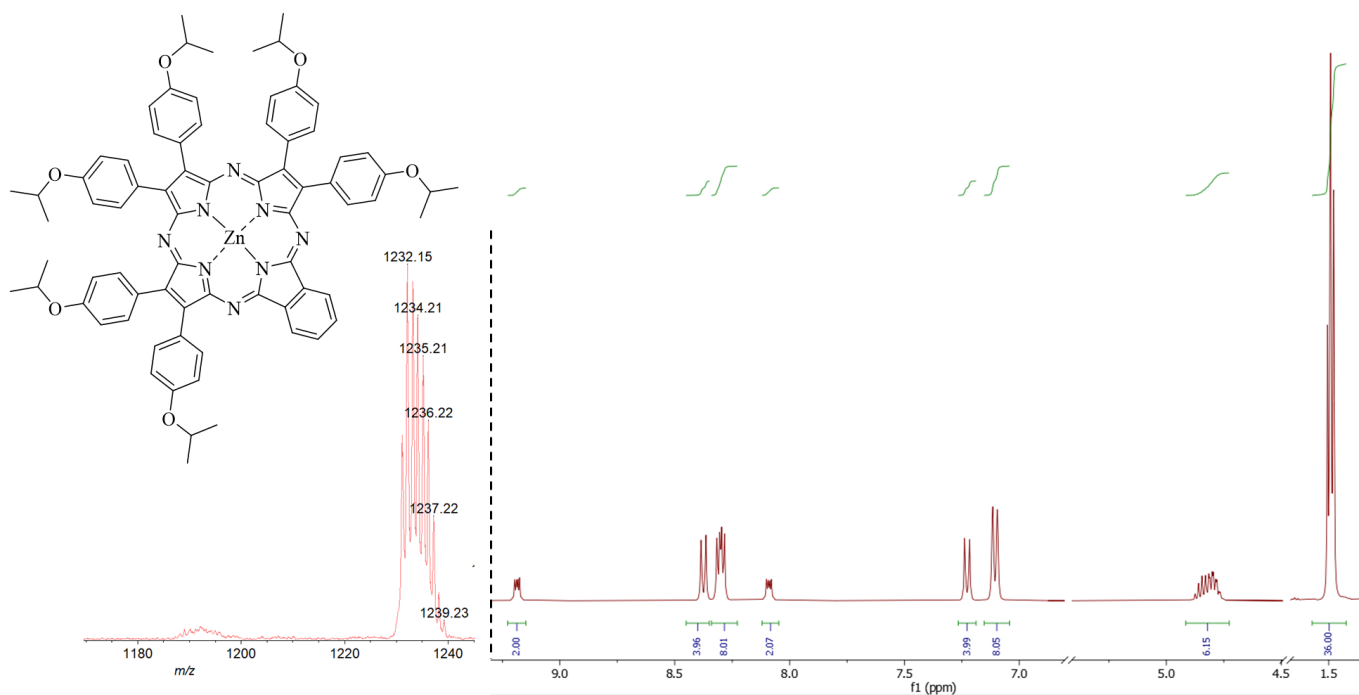


Figure 2.56: The MALDI-TOF MS (left) and ¹H NMR spectrum in THF-*d*₈ for hybrid **2.40**.

The electronic absorption spectrum of hybrid ABBB **2.40** exhibited the characteristic split *Q*-bands in metalated porphyrazine-Pc hybrids at 674 and 639 nm. In contrast, as shown in Figure 2.57, its metal-free counterpart, ABBB **2.37**, which possesses even lower symmetry than the metalated porphyrazines, exhibits greater splitting of the *Q*-band into peaks at 702 nm and 598 nm. This redshift to higher wavelengths, compared to other Zn complexes, is consistent with the UV-Vis electronic absorption spectra of non-metalated porphyrazines.^{57, 116} The differences in the absorption spectra underscore the significant impact of metal coordination on the electronic properties of the porphyrazine macrocycles.

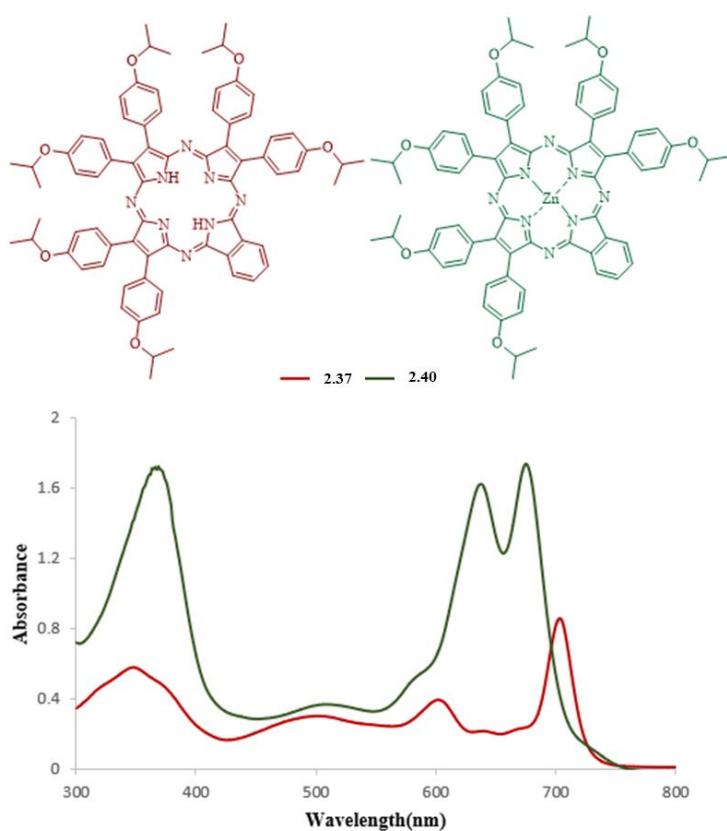


Figure 2.57: The UV-Vis absorption spectra comparing the ABBB-N hybrids in its metalated from (Zn) **2.40**, with metal-free **2.37** in DCM.

The remainder of the green fraction was subjected to additional column chromatography, using petroleum ether /THF (5:1) as the eluent to obtain porphyrazine BBBB **2.41** as a dark green compound, exhibiting a molecular ion peak at 1451.85 m/z (Figure 2.58). This peak indicates the formation of a new symmetrical hybrid **2.41**, resulting from the cyclisation of four units of the starting material, dinitrile **2.24**.

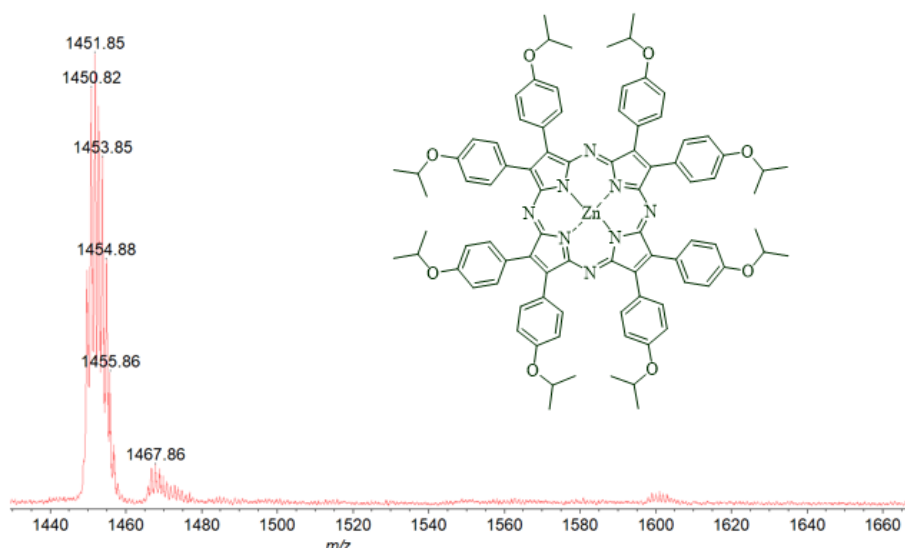


Figure 2.58: The chemical structure and MALDI-TOF MS spectrum of Zn-porphyrazine **2.41**.

NMR spectroscopy confirmed the high symmetry of this structure of porphyrazine **2.41**, and this is also reflected in its UV-Vis spectrum, which shows a sharp single *Q*-band absorption without splitting at 653 nm. Additionally, a broad Soret band absorption is observed at 379 nm, consistent with the typical spectral characteristics of metalated porphyrazines.¹¹¹ These observations confirm the formation of this BBBB hybrid as a byproduct (Figure 2.59).

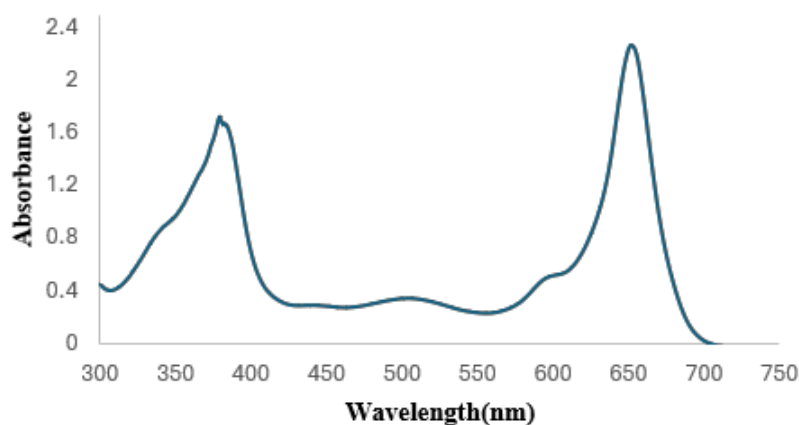


Figure 2.59: The UV-Vis absorption spectrum of Zn- BBBB porphyrazine **2.41** in THF.

2.8 Synthesis of Zn-Pz/Pc hybrids with different *meso*-aryl substituent

In our previous work, we developed *meso*-phenyl porphyrazine hybrids by incorporating various dinitriles onto the same aminoisoindoline **2.4**. In this subsequent approach, we introduced an alternatively substituted aminoisoindoline, aiming in part, for the reduction of a steric hindrance at the *meso* position of the Zn-porphyrazines. To achieve this, we employed

thiophene substituted aminoisoindoline **2.42** in combination with dinitrile **2.8** (Figure 2.60), thereby investigating the Zn-porphyrazine hybrids produced.

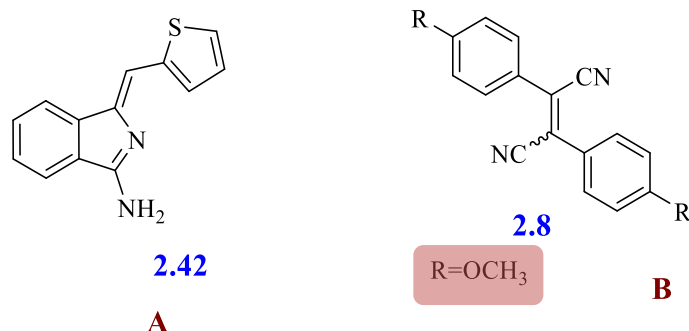
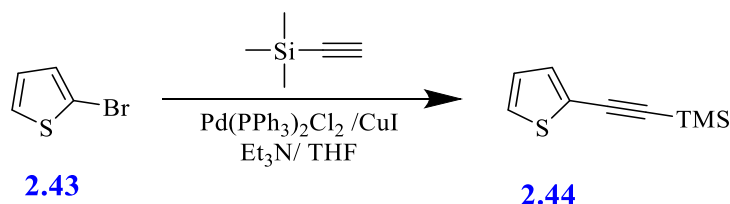


Figure 2.60: The aminoisoindoline and dinitrile derivatives were used in the second study.

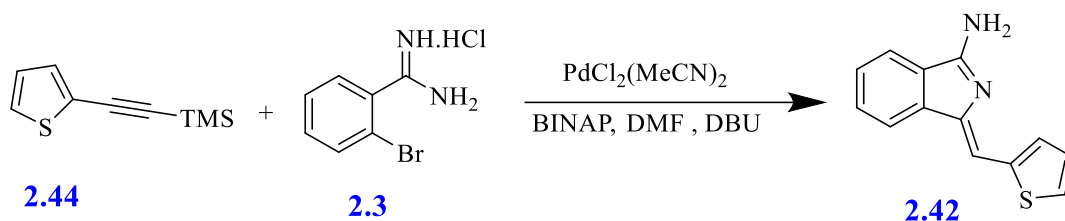
2.8.1 Synthesis of (Z)-1-(4-thiophenylmethylene)-1H-isoindol-3-amine **2.42**

To initiate the synthesis of a new class of porphyrazine hybrids, we first prepared 2-[(trimethylsilyl)ethynyl]thiophene **2.44** by reacting 2-bromothiophene **2.43** with (trimethylsilyl)acetylene under reflux at 60 °C for 10 h *via* Sonogashira coupling reaction (Scheme 2.29). Following the workup, the crude product was purified by column chromatography, yielding compound **2.44** as a brown oil with a 21% yield. The structure of the compound was confirmed by NMR spectroscopy.¹¹⁷



Scheme 2.29: Synthesis of compound **2.44**.

To synthesise the aminoisoindoline derivative **2.42**, the procedure published by Hellal *et al.* as explained previously was followed.⁴⁹ *o*-Br-benzamidine. HCl salt **2.3** was directly reacted with thiophene derivative **2.44**. The reaction was conducted in a sealed microwave vial in the presence of BINAP, PdCl₂(MeCN)₂ as the catalyst with DBU in DMF. The mixture was heated to 120 °C for 1 h under microwave irradiation. After the reaction was complete, the crude product was subjected to column chromatography for purification using a gradient of petroleum ether PE and ethyl acetate EtOAc (1:1), followed by pure EtOAc. The purified product was then recrystallized from a dichloromethane and PE mixture, yielding yellow needles with a 92% yield (Scheme 2.30).³⁰



Scheme 2.30: Synthesis of aminoisoindoline **2.42**.

Pure product **2.42** was fully characterized by NMR and MALDI-TOF mass spectroscopies, which proved the formation of the aminoisoindoline (Figure 2.61).

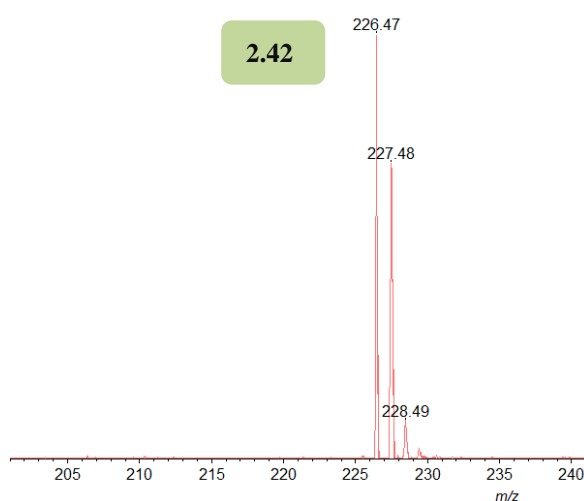


Figure 2.61: The MALDI-TOF MS spectrum for aminoisoindoline **2.42**.

The ^1H NMR spectrum (Figure 2.62) was recorded in deuterated acetone. Two doublets of triplets appeared at δ 7.82 and 7.79 ppm, corresponding to the protons at positions 1 and 4 on the benzene ring of the isoindoline structure. Additionally, a set of multiples at δ ~7.45 and 7.37 ppm represents four protons (labelled as 3, d, 2 and b), respectively. The alkene proton appeared as a sharp singlet at δ 7.07 ppm, consistent with its expected chemical shift. Finally, the doublet of doublets peak at δ 7.01 corresponds to the proton on the thiophene ring labelled as c, confirming the presence of the thiophene ring within the structure.

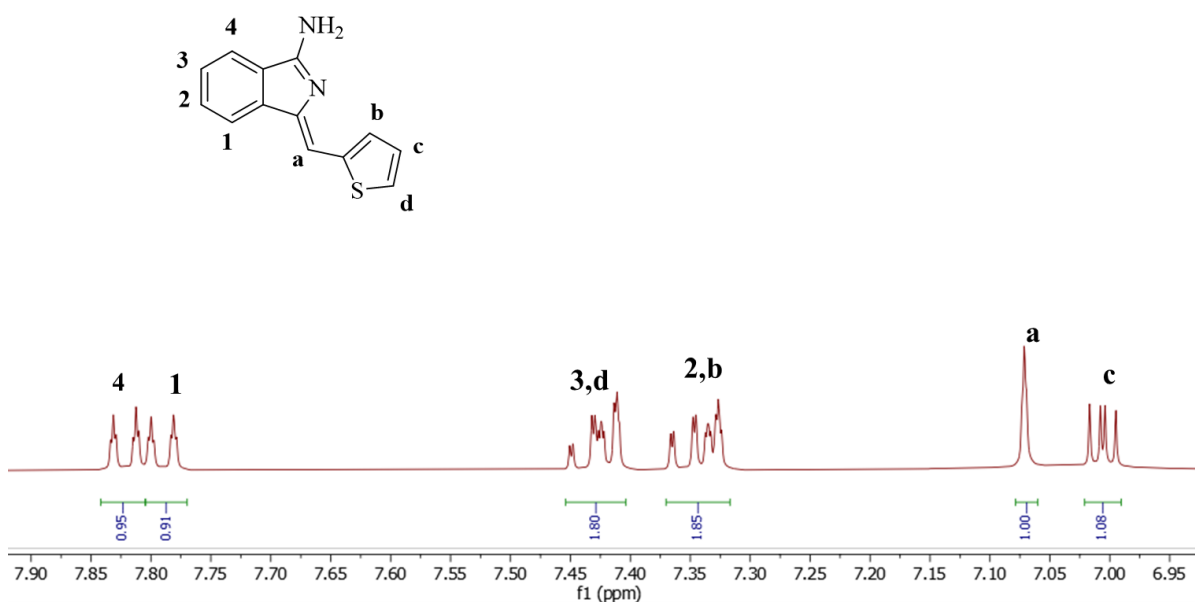
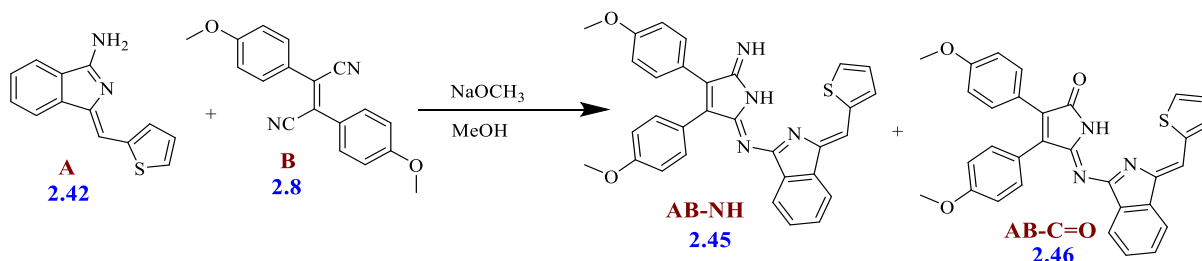


Figure 2.62: The ^1H NMR spectrum of aminoisindoline **2.42**.

2.8.2 Synthesis of 4-methoxyphenyl-substituted (AB dimer) with 4-thiophenylmethylene)-1*H*-isindol-3-amine **2.45**

After successfully synthesising the thiophene aminoisindoline derivative, we proceeded to prepare the new (AB dimer) by reacting it with dinitrile **2.8**. Following the previously described procedure, a mixture of the methoxy dinitrile derivative **2.8** and aminoisindoline **2.42** was refluxed in methanol (MeOH) in the presence of sodium methoxide (NaOMe) for 14 h (Scheme 2.31). Once the reaction was completed, the mixture was cooled, and the crude product was extracted and then dried. The crude product was subsequently purified by column chromatography, employing a gradient elution system of petroleum ether/DCM (2:1), (1:1), and pure DCM as the final eluent. The target dimer **2.45** was obtained as red crystals after recrystallization from a DCM/methanol (1:1), yielding 44%. Consistent with previous synthesis of other derivatives (AB dimers), a side product identified as the pyrrolone derivative **2.46** was also observed.



Scheme 2.31: Synthesis of new AB dimer **2.45**.

The MALDI-TOF MS spectral analysis revealed molecular ion peaks at approximately 517.28 and 518.44 m/z , corresponding to dimers **2.45** and **2.46**, respectively. The molecular structures of these dimers were further confirmed through single-crystal X-ray analysis, as shown in Figure 2.63. They were solved by our collaborator Dr David Hughes, and his comments on the detail of the structures can be found in the appendix.

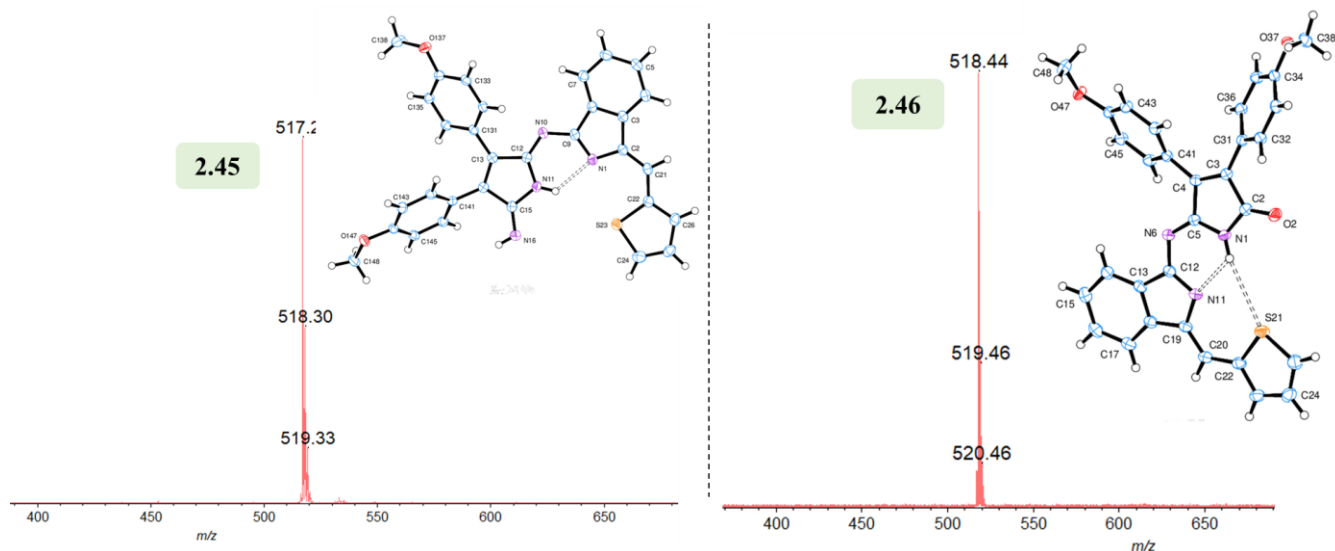


Figure 2.63: The MALDI-TOF MS spectrum and X-ray structure of compounds **2.45** (left), **2.46** (right) with views of the molecules with their intramolecular hydrogen bond and indicating the atom numbering scheme. Thermal ellipsoids are drawn at the 50% probability level.

The ^1H NMR spectra of dimers **2.45** and **2.46**, as illustrated in Figure 2.64, reveal notable differences in the chemical environments of the protons, particularly in the aromatic region. In dimer **45**, which contains a C=NH group, the aromatic protons exhibit signals with relatively sharper peaks. Dimer **2.46**, with the C=O group, shows a slight downfield shift for some aromatic protons, reflecting the electron-withdrawing effect of the carbonyl group. Additionally, in dimer **2.46**, the methoxy groups appear as two singlet peaks, each integrating to 3H, whereas in dimer **2.45**, the methoxy group is observed as a single peak with integration to 6H. The vinyl proton C=C-H appeared at δ 7.51 ppm for dimer **2.45** while at 7.90 ppm for **2.46**. Finally, in dimer **2.46**, we observed a broad singlet peak belonging to the NH proton at δ 11.38 ppm.

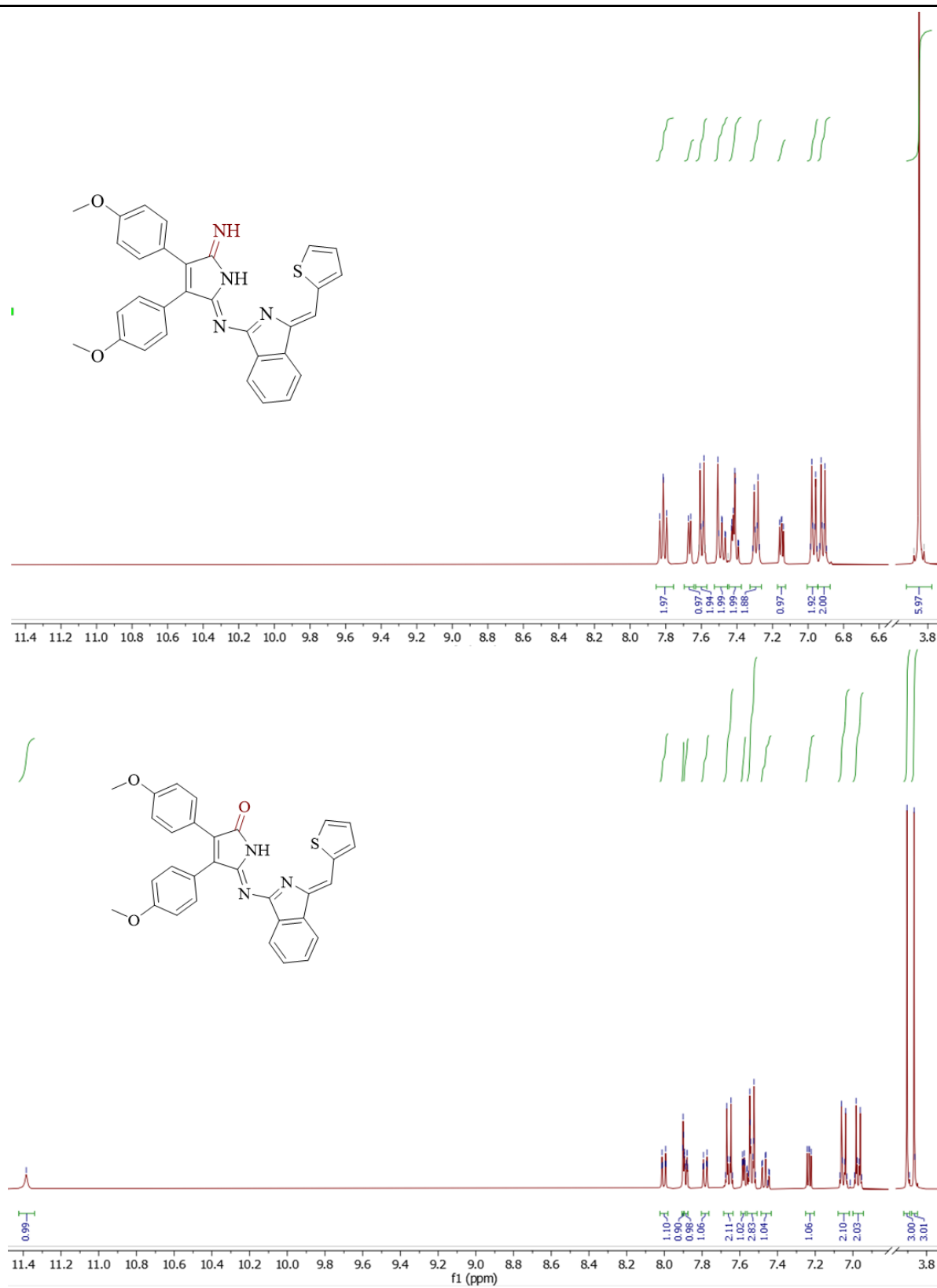
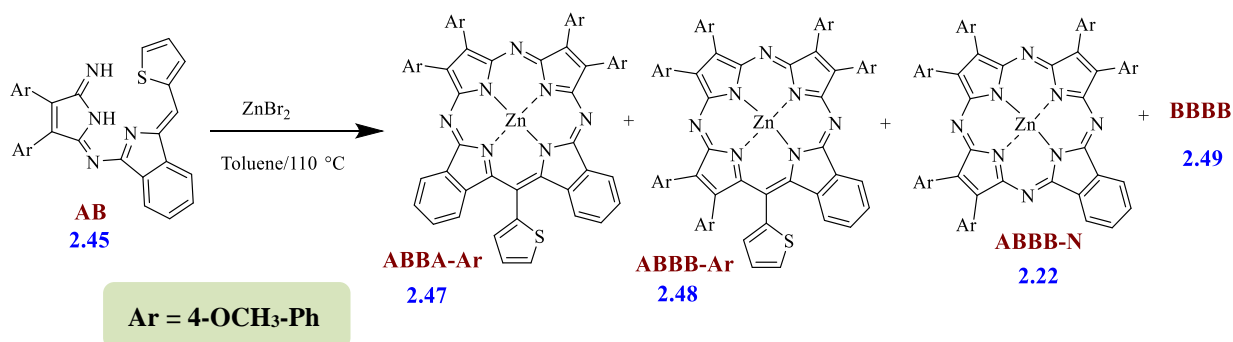


Figure 2.64: The ^1H NMR spectrum for both dimers **2.45** in $\text{DCM-}d_2$, **2.46** in $\text{acetone-}d_6$.

2.8.3 Synthesis of Zn-porphyrazine hybrids with *meso*-thiophene substitution from dimer 2.45

After successfully synthesising the new dimer **2.45**, we proceeded to conduct our experiments aimed at preparing porphyrazine hybrids using a zinc template. This approach will provide insights into the influence of the thiophene dimer structure (the *meso*-substituent) on the formation and properties of the porphyrazine hybrids.

We employed the established methodology, reacting dimer **2.45** with ZnBr₂ in toluene under heating for 12 h in an inert nitrogen atmosphere (Scheme 2.32).



Scheme 2.32: Synthesis of the *meso*-thiophene Zn-Pz/Pc hybrids.

Following the completion of the reaction, the product mixture was subjected to several purification processes using multi-column chromatography. The first column effectively removed the main impurities, while the green fraction was further purified through the next columns. The TLC analysis of the combined green fraction revealed the presence of multiple green spots, indicating the potential formation of various porphyrazine hybrids, which is consistent with our previous findings involving *meso*-phenyl substituents. Further analysis using MALDI-TOF MS identified four distinct molecular ion peaks: 981.40 *m/z* for Zn-ABBA **2.47**, 1063.50 *m/z* for Zn-ABBB-N for **2.22**, 1145.48 *m/z* for Zn-ABBB-Ar **2.48** and 1226.52 *m/z* for BBBB Pz **2.49**, respectively as depicted in Figure 2.65.

It is noteworthy that porphyrazines **2.22** and BBBB Pz were previously obtained in an earlier reaction involving dimer **2.17**, as illustrated in Scheme 2.33. Dimers **2.17** and **2.45** were both synthesised from the same dinitrile **2.8** but with different aminoisoindoline derivatives.

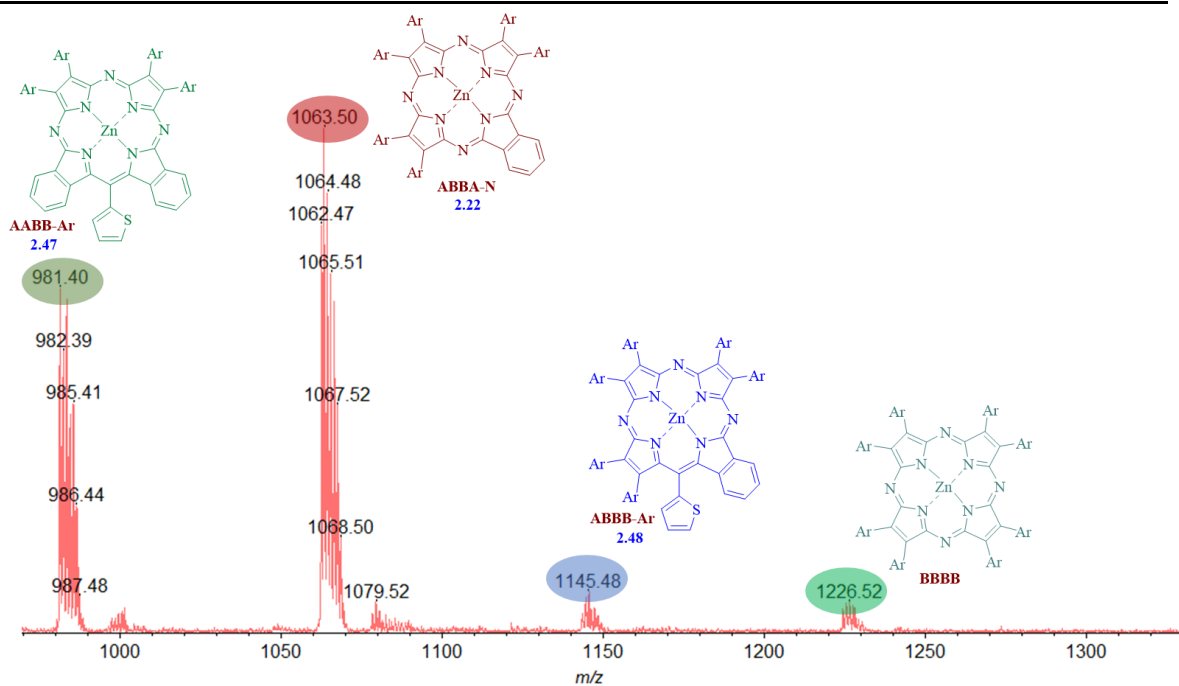
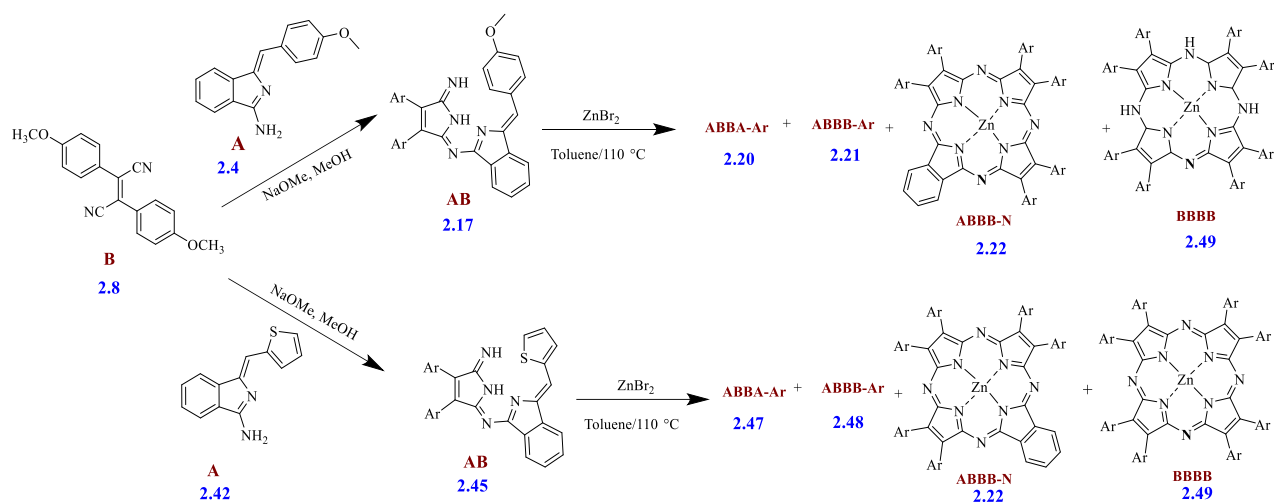


Figure 2.65: The MALDI-TOF MS spectrum of the combined green fraction.



Scheme 2.33: Similar porphyrazines (ABBB-N and BBBB Pz) were obtained from different reaction pathways.

These results for the porphyrazine hybrids are consistent with previous findings from other dimer reactions. This consistency supports the reliability of the synthetic method used, showing that the formation of multiple porphyrazine hybrids under these conditions is a common outcome across different dimer structures, particularly in the case of porphyrazine ABBA-N **2.22**, where the thiophene ring at the *meso* position was also lost, and a nitrogen atom was incorporated into the porphyrazine core.

The next separation was achieved using three more of column chromatographies. This process successfully isolated all the porphyrazine hybrids. The first isolated compound,

corresponding to **2.47**, was obtained as a dark green crystalline product with a 10% yield. The second compound, identified as Pz **2.22**, was the major product with a 15% yield. The third compound, corresponding to Pz **2.48**, was isolated with a 5% yield, while the final compound, identified as BBBB Pz **2.49**, was obtained with a 2% yield. Notably, the separation and analysis of these hybrids were more straightforward compared to similar hybrids with a *meso*-phenyl substituent, particularly in the case of separating hybrids **2.22** and **2.48**. This indicates that the substitution pattern significantly influences the ease of purification and characterisation of these porphyrazine derivatives.

The structures of the four Pz hybrids were confirmed using NMR spectroscopy and MALDI-TOF MS. The ^1H NMR spectrum of compound **2.47** exhibited multiple signal characteristics for the thiophene ring, appearing in the range of δ 7.80-7.72 ppm. The high symmetry and the proton count in the spectrum align with the proposed structure, thereby confirming the successful formation of the phthalocyanine/porphyrazine hybrid **2.47** (Figure 2.66).

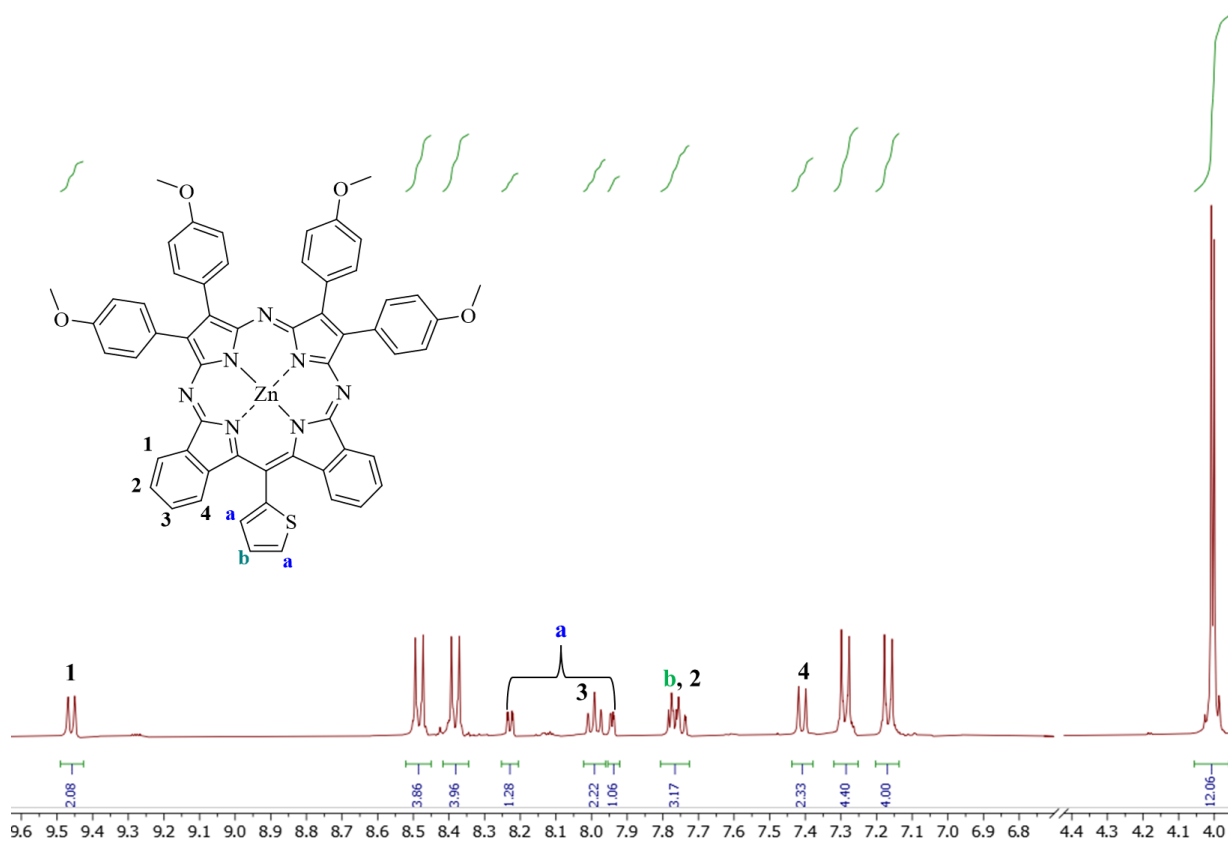


Figure 2.66: The ^1H NMR spectrum of hybrid **2.47** in $\text{THF-}d_8$.

Due to hybrid **2.47** being able to form high-quality crystals, X-ray crystallographic analysis was performed, which further confirmed the compound's structure (Figure 2.67). The

X-ray crystal structure was solved by our collaborator, Dr David Hughes, and his comments on the detail of the structure can be found in the appendix.

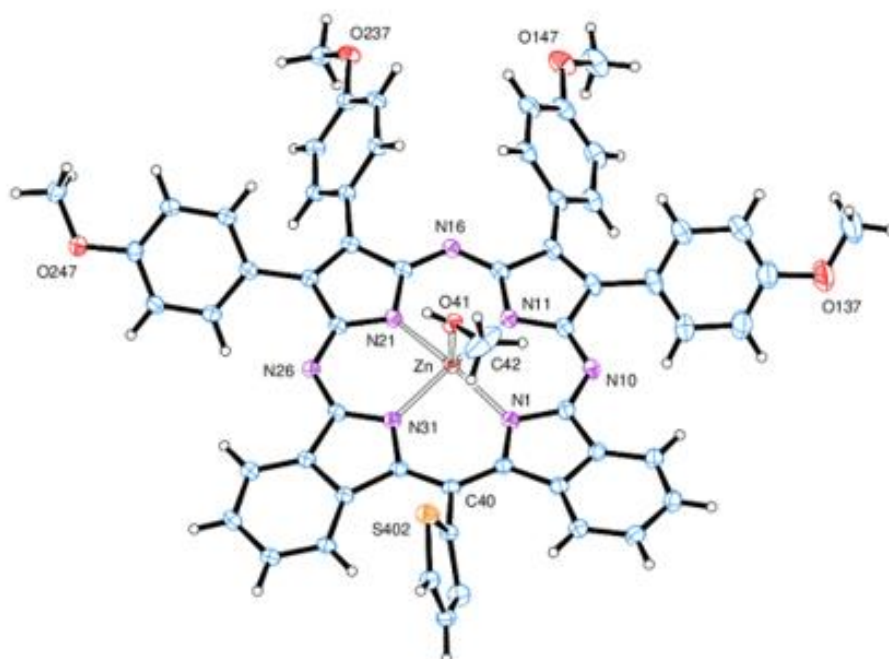


Figure 2.67: The X-ray structure view of the Zn-ABBA hybrid **2.47**, indicating the atom numbering scheme. Thermal ellipsoids are drawn at the 30% probability level.

We successfully obtained a clear ^1H NMR spectrum for the zinc ABBA-Ar **2.48**. The macrocyclic structure exhibited an upfield shift of aromatic protons within the aromatic region, which can be attributed to the distinct chemical environments of the aromatic rings when compared with hybrid ABBA **2.47**. Significantly, the signals corresponding to the thiophene ring were observed as expected, confirming the correct structure and the inclusion of the thiophene ring in the hybrid (Figure 2.68).

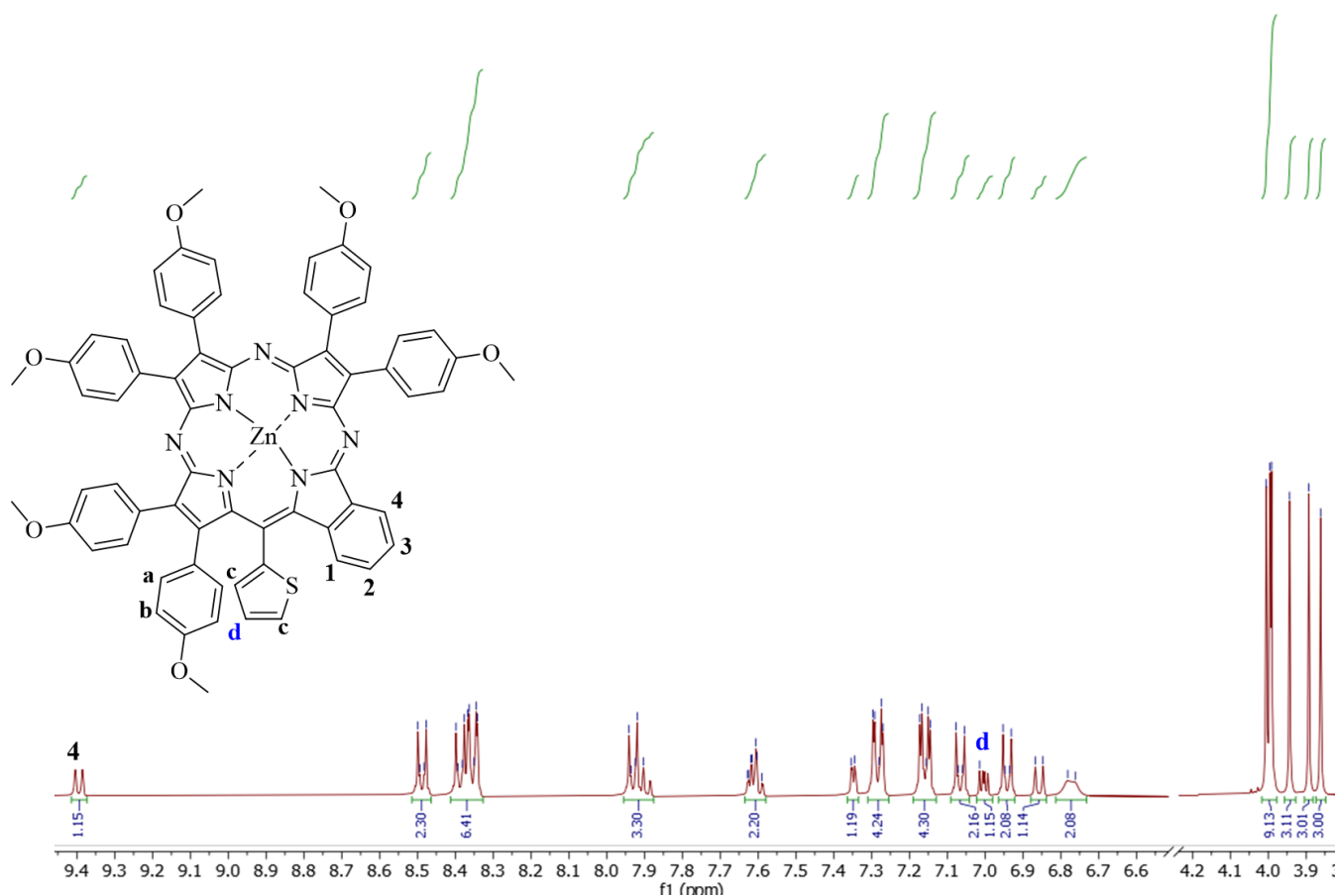


Figure 2.68: The ¹H NMR spectrum of Zn ABBB-Ar **2.48** in THF-*d*₈.

The UV-Vis absorption spectra of the ABBA Zn-porphyrin hybrids (**20** *meso*-phenyl substituents and **2.47** *meso*-thiophene substituent) are shown in Figure 2.70. It can be seen that the spectra are essentially identical, with maximum absorption for *Q*-bands at 661, 643 nm and 660, 645 nm, respectively.

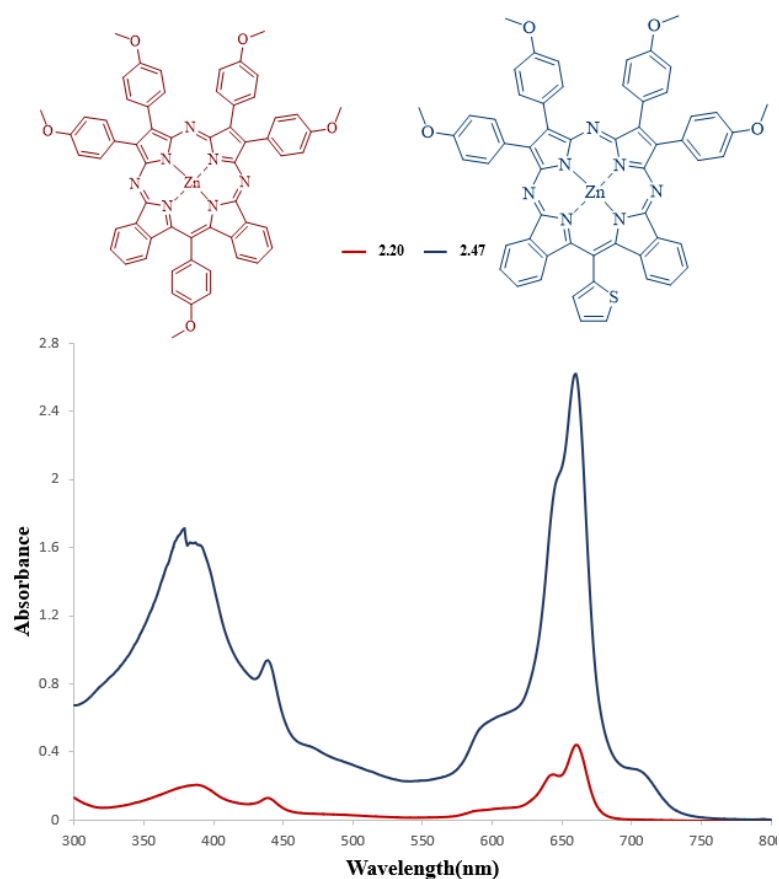


Figure 2.69: UV-Vis absorption spectrum comparing of ABBA Zn-porphyrazine hybrids with different *meso*-substituted in DCM.

Upon completion of our project, it was observed that the *meso*-thiophene derivative and its corresponding macrocyclic porphyrazines exhibited a higher yield and greater ease of separation compared to the initial *meso*-phenyl hybrids. The clarity and consistency of the results strongly suggest that the second type of porphyrazines, with the *meso*-thiophene substitution, is more effective for further study and analysis.

2.9 Electronic absorption spectra of porphyrazine hybrids

This part of the study summarises the influence of various substituents within the aromatic system of the macrocycle, the nature of the central metal ions, and the spatial structural arrangement of the optical properties of the synthesised porphyrazines.

The UV-Vis spectra of unsymmetrical Pz/ Pc hybrids share similar features with their parent phthalocyanines and porphyrazines. They have *Q*-bands at a wavelength > 600 nm that are affected by the central metal ion in the core, the structure of peripheral or non-peripheral substituents, and the length of π -electron conjugation.⁵⁷ The results, summarized in Table 2.3, present the optical parameters of the newly synthesised Pz/Pc macrocyclic complexes prepared

during this project. A key finding of our research is the redshifted absorption observed in the *Q*-bands. This shift indicates potential applications for these materials in optoelectronic devices, where such spectral shifts are often advantageous.

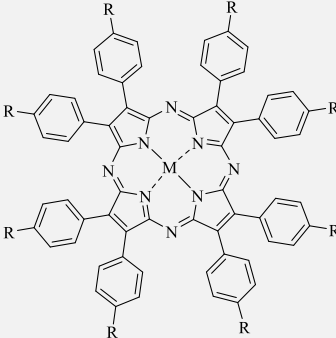
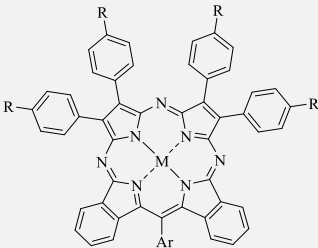
Our research encompasses the exploration of impact of different metals and various intermediate substituents, resulting in the formation of three distinct types of porphyrazine hybrids. Notably, when comparing the identical substituents (alkyloxy OCH₃) across different metals for hybrids ABBA **2.11**, ABBB-N **2.19** with Mg, and ABBA **2.20**, ABBB-N **2.22**, we observed small yet significant effects of metal coordination on the electronic properties of the porphyrazine macrocycle. Specifically, in the ABBB-N hybrids, the Zn-Pz hybrid **2.22** exhibits slight variations in wavelength compared to the Mg-Pz hybrid **2.19**, with shifts of up to 5 nm.

Secondly, the nature of the hybrids significantly influences their optical properties. ABBB-N porphyrazines exhibit a notable redshift of approximately 20 nm towards longer wavelengths in complexes **2.19**, **2.22**, and **2.40** when compared to their corresponding BBBB Pzs **2.9**, **2.49**, and **2.41** respectively. This observation clearly demonstrates the substantial impact of molecular structure on the electronic characteristics of these porphyrazine hybrids.

Moreover, examining the effect of various substituents on the beta position fused to the pyrrole ring within the porphyrazine core (with phenyl ring at the *meso* position), a comparison between Zn-ABBA and Zn-ABBB-N hybrids sheds additional light on their behaviour. Structures **2.20** ABBA and **2.22** ABBB-N with an -OCH₃ group, **2.29** ABBA and **2.31** ABBB-N with a -C(CH₃)₃ group, and **2.38** ABBA and **2.40** ABBB-N with an -OCH(CH₃)₃ group, reveals that the alkyloxy chain induces a slight shift of 4-8 nm toward longer wavelengths.

Lastly, the ABBB-Ar hybrids **2.10** and **2.48** exhibited a redshift in the λ_{\max} . by approximately 10 nm compared to parent BBBB Pzs **2.9** and **2.49**. This shift is attributed to the presence of an additional benzene ring fused to the core in the ABBB-Ar Pz structure, which enhances π -electron conjugation and delocalization across the molecule. This increased conjugation effectively lowers the energy gap between the highest occupied molecular orbital (HOMO) and the lowest unoccupied molecular orbital (LUMO), resulting in the observed redshift in the absorption spectrum.

In the parent Mg BBBB **2.9**, a series of increasing bathochromic redshifts in the λ_{\max} . of the *Q*-band is observed, from 650 nm for **2.9** to 662 nm for Mg ABBA **2.11**, 660 nm for Mg ABBB-Ar **2.10**, and 672 nm for Mg ABBB-N **2.19**. The most significant shift is noted in **2.19** Pz, which can be attributed to the introduction of the nitrogen atom at the aza-position in the ABBB-N Pz structure.

Pzs	Metal centre	Solvent	Q-bands λ_{\max}. nm(ϵ)
BBBB			
			
			2.9 M=Mg, R= OCH ₃ 2.49 M=Zn, R= OCH ₃ 2.40 M=Zn, R= OCH(CH ₃) ₂
2.9	Mg	THF	650 (3.58×10^4)
2.49	Zn	THF	651 (2.2×10^5)
2.41	Zn	THF	653 (2.04×10^5)
ABBA-Ar			
			
			2.11 M=Mg, R= OCH ₃ , Ar = OMe-Ph 2.20 M=Zn, R= OCH ₃ , Ar = OMe-Ph 2.29 M=Zn, R= C(CH ₃) ₃ , Ar = OMe-Ph 2.38 M=Zn, R= OCH(CH ₃) ₂ , Ar = OMe-Ph 2.47 M=Zn, R= OCH ₃ , Ar = Thiophene
2.11	Mg	DCM	662 (4.92×10^4), 643 (3.20×10^4)
2.20	Zn	THF	661 (1.11×10^5), 643 (6.72×10^4)
2.29	Zn	DCM	657 (1.03×10^5), 640 (6.46×10^4)
2.38	Zn	DCM	663 (4.03×10^4), 646 (3.04×10^4)
2.47	Zn	DCM	660 (3.9×10^4), 645 (2.9×10^4)

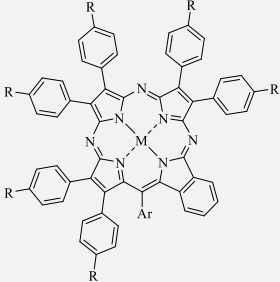
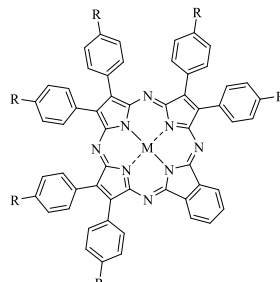
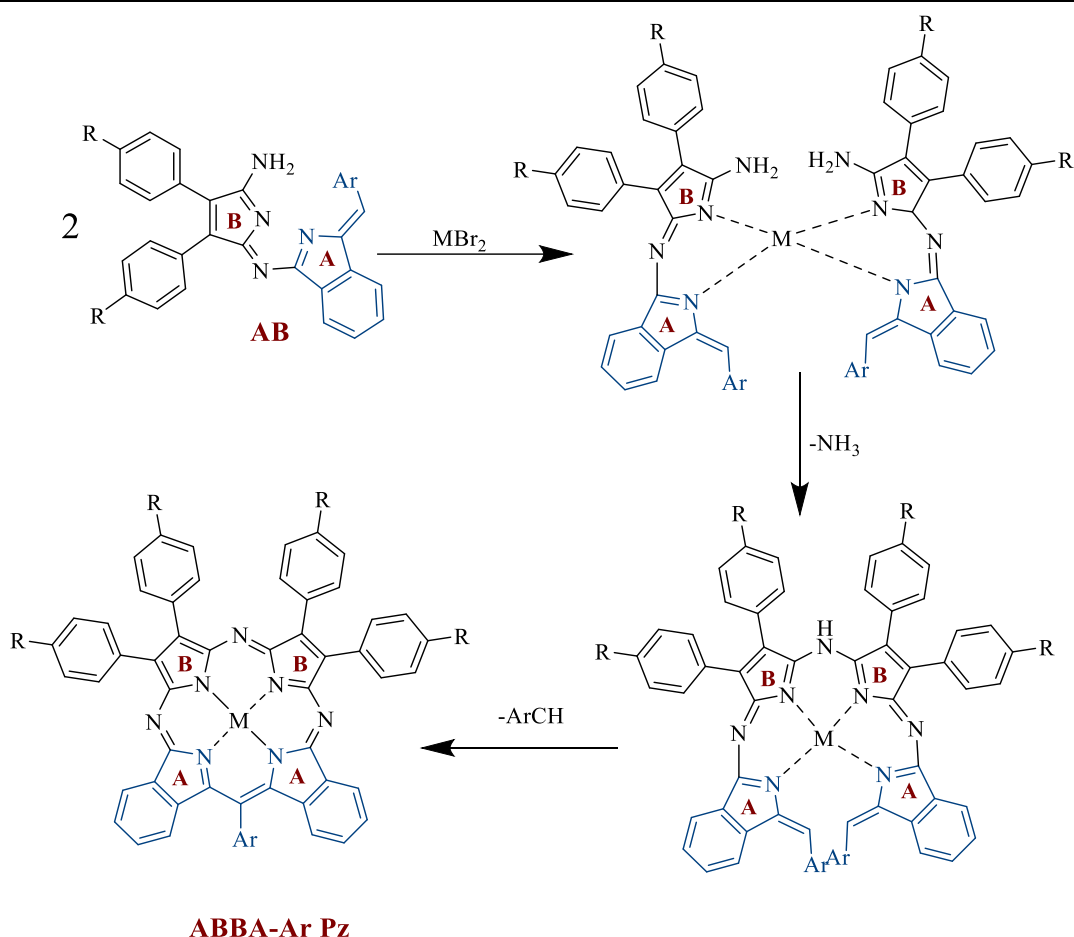
ABBB-Ar			
 <p> 2.10 M=Mg, R= OCH₃, Ar = OMe-Ph 2.48 M=Zn, R= OCH₃, Ar = Thiophene </p>			
2.10	Mg	DCM	660 (4.99×10^4), 626 (3.38×10^4)
2.48	Zn	DCM	662 (6.26×10^4), 625 (4.04×10^4)
ABBB-N			
 <p> 2.19 M=Mg, R= OCH₃ 2.22 M=Zn, R= OCH₃ 2.31 M=Zn, R= C(CH₃)₃ 2.40 M=Zn, R= OCH(CH₃)₂ </p>			
2.19	Mg	DCM	672 (2.54×10^4), 639 (6.22×10^4)
2.22	Zn	DCM	672 (6.66×10^4), 634 (6.22×10^4)
2.31	Zn	DCM	666 (7.75×10^4), 627 (7.9×10^4)
2.40	Zn	DCM	674 (1.07×10^5), 639 (9.99×10^4)

Table 2.3: UV-Vis absorption spectra of the porphyrazine and phthalocyanine hybrids.

2.10 Suggested mechanisms of formation of porphyrazine hybrids

The proposed mechanism for the formation of metal-porphyrazine hybrids from (AB dimer) intermediate involves a cyclotetramerization process under relatively mild reaction conditions. This approach has proven to be effective for synthesising ABBA Pz hybrids by promoting the cyclisation of the (AB dimer) to form the desired macrocyclic structure.

In this process, two units of (AB dimer) coordinate to a metal ion template (Mg or Zn) and subsequently undergo homocondensation. This step is accompanied by the elimination of an ammonia molecule (-NH₃) and is followed by the final elimination of an aromatic fragment (unknown mechanism) from the aminoisindoline moiety. The subsequent aromatization yields an ABBA porphyrazine/phthalocyanine hybrid, as illustrated in Schemes 2.34.



Scheme 2.34: Possible sequence involving the coordination of two (AB dimer) units to a metal ion template, condensation, macrocyclisation and aromatization to yield ABBA-Ar porphyrazine hybrid.

As previously discussed, when utilizing the (AB dimer) as the starting material for the synthesis of Pz hybrids, it was observed that this intermediate possessed three electrophilic sites susceptible to nucleophilic substitution reactions, which can proceed *via* either a dissociative (S_N1) or associative (S_N2) mechanism, as illustrated in Figure 2.70. Nucleophilic attack by the amine group of another (AB dimer) unit at position **C** results in the formation of the desired ABBA Pz/Pc hybrids. In contrast, nucleophilic attacks at positions **D** or **E** led to the formation of alternative Pz hybrid structures.⁵⁰

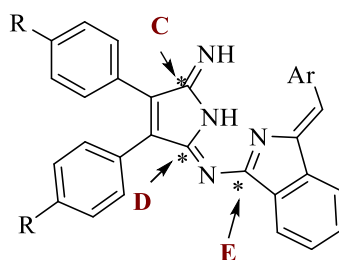
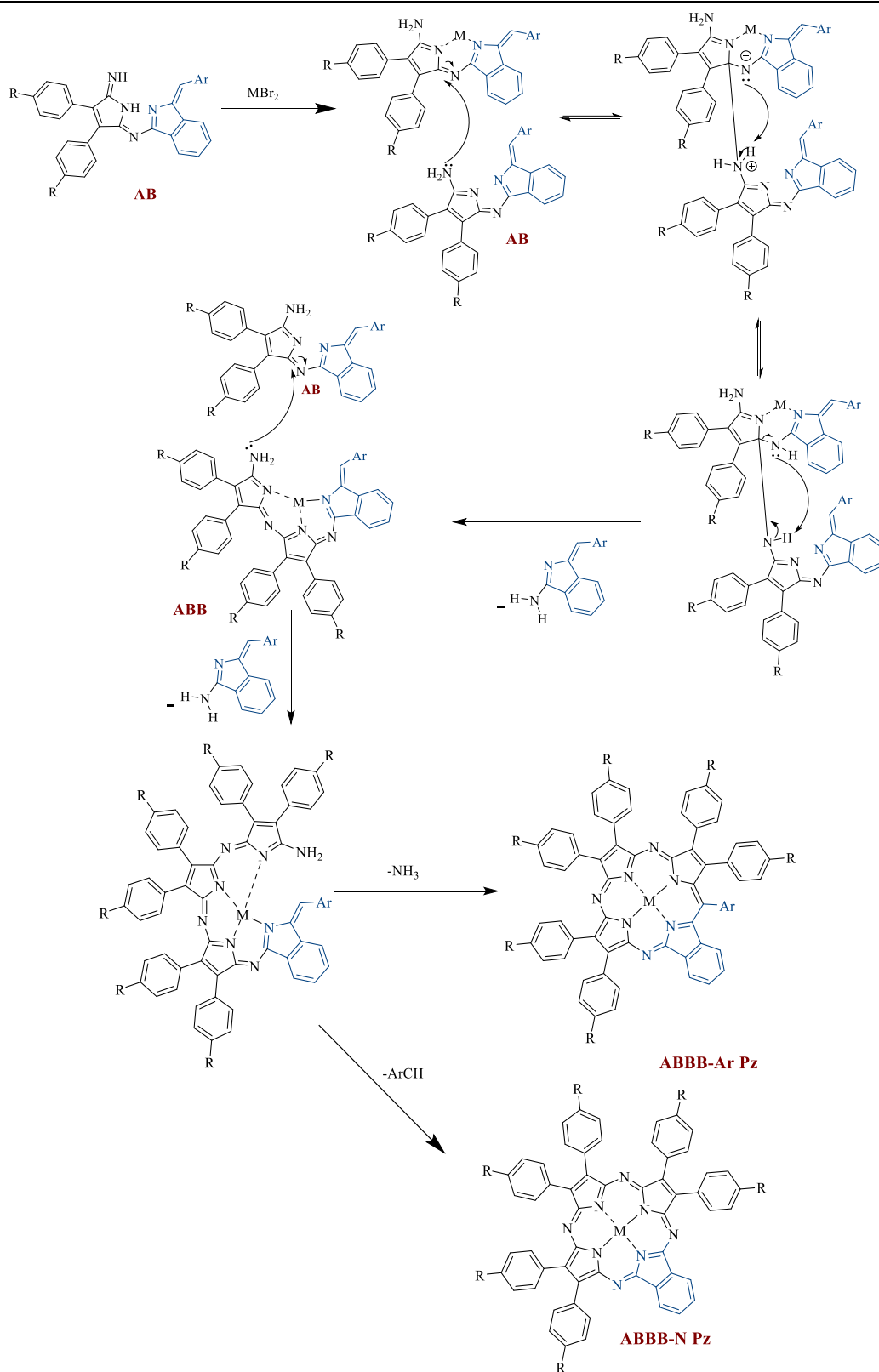


Figure 2.70: Positions susceptible to nucleophilic attack.

The formation of ABBB-Ar Pz hybrids from the (AB dimer) likely proceeds through a nucleophilic reaction involving aminoisindoline, which drives the assembly of a 1:3 porphyrazine hybrid. The mechanism initiates with the condensation of two (AB dimer) units, where nucleophilic attack occurs at distinct electrophilic sites, resulting in the elimination of aminoisindoline and the formation of an open-chain ABB intermediate. This intermediate undergoes further nucleophilic attack by another (AB dimer) unit, leading to the additional elimination of aminoisindoline. The final step involves macrocyclisation of the resulting 1:3 open-chain porphyrazine intermediate, with the concurrent elimination of an ammonia molecule, thereby forming the ABBB-Ar porphyrazine hybrid. Alternative loss of benzyl in this final step (mechanism unknown) can lead to the observed porphyrazine-Pc hybrids ABBB-N as depicted in Scheme 2.35.



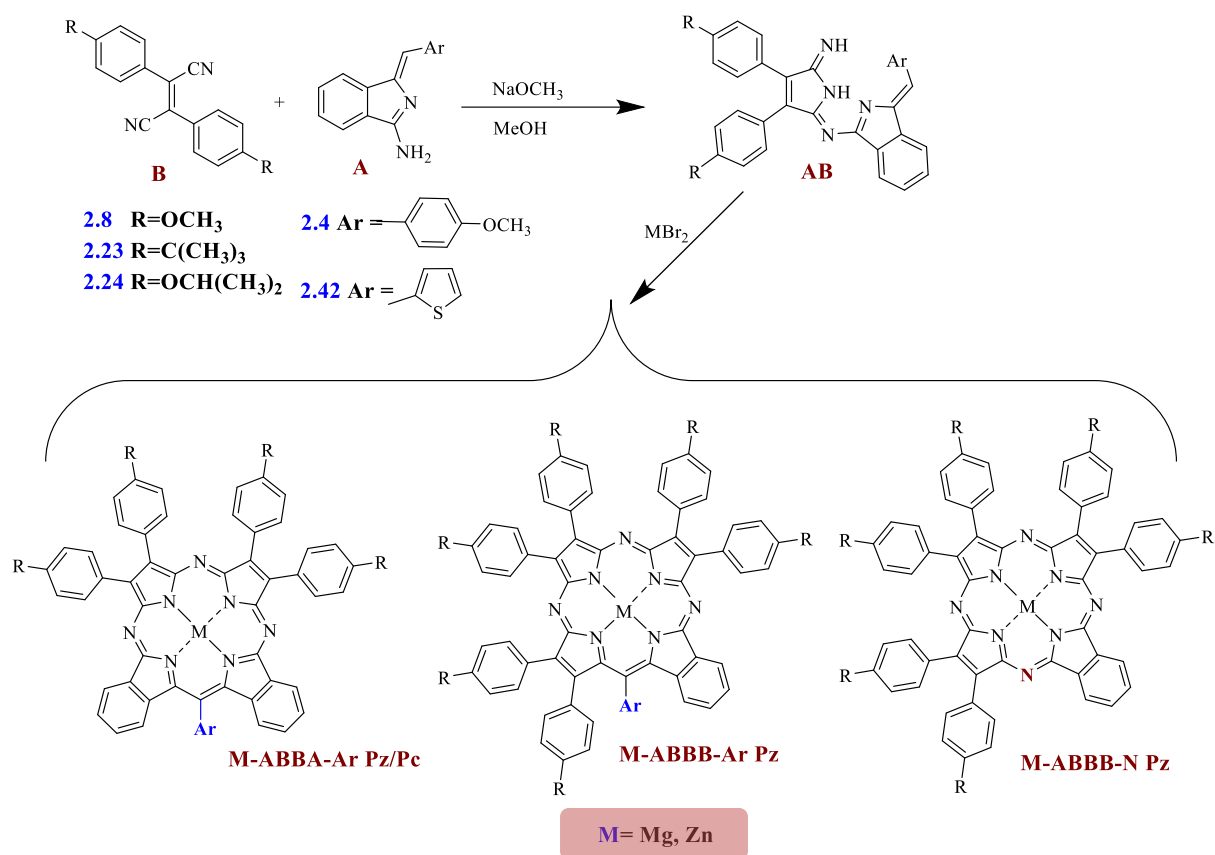
Scheme 2.35: Possible coordination of two units of dimer to metal, followed by condensation, macrocyclization and aromatisation to yield ABBB-Ar and ABBB-N.

2.11 Conclusion

Our project resulted in the development of novel precursors, reaction conditions, and synthetic pathways that are suitable for the synthesis of new porphyrazine hybrid derivatives. The utilization of the intermediate (AB dimer) enabled us to achieve new cores with various substitution patterns that are not easily accessible by conventional macrocyclisation methods. This innovative synthetic approach has significantly expanded the potential for creating novel and structurally diverse asymmetric porphyrazine hybrid macrocyclic systems.

Building upon the previous achievements of the Cambridge group in the field of porphyrin synthesis, the development of porphyrazine hybrids has been significantly enriched. The newly developed methodology, utilizing precursors derived from dimer **2.17** and its derivatives, has enabled the synthesis of novel metalated porphyrazine hybrids of the ABBA and ABBB structure under mild conditions without the need for catalysis. The carefully designed reaction conditions and selection of starting materials have facilitated the incorporation of substituents at both the *meso* and beta positions, as well as the effective metalation by employing Mg (II) and Zn (II) as core templates. A summary of these advancements is provided in Scheme 2.36.

The utilisation of reactive Mg metal has revealed that the predominant pathway results in the formation of novel ABBA-Ar hybrids, accompanied by the presence of key byproducts ABBB-Ar, ABBB-N and BBBB. In contrast, when Zn metal was employed, the dominant pathway favoured the formation of ABBB-N (porphyrazine-Pc) hybrids, accompanied by the presence of byproducts ABBA-Ar, ABBB-Ar and BBBB. The research successfully synthesised two series of porphyrazine complexes, incorporating either phenyl or thiophene at the *meso* position and different substitutions at the beta positions from various dinitrile derivatives. The use of AB dimer type starting materials has therefore been demonstrated to be useful in macrocycle synthesis, allowing hitherto unreported hybrids systems to be synthesised.



Scheme 2.36: Summary of the synthetic methodologies employed for the target hybrids 2:2,1:3 porphyrazine hybrids from (AB dimer).

CHAPTER 3:

Experimental

3.1 General methods

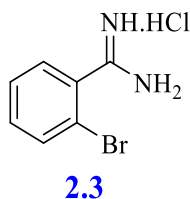
The chemical reagents and solvents were purchased from commercial sources and used without further purification unless otherwise specified. Reactions sensitive to water and air were conducted under an inert (nitrogen or argon) atmosphere. The term “brine” refers to a saturated aqueous solution of sodium chloride. Organic layers were dried using anhydrous magnesium sulphate, and solvents were evaporated using a Buchi rotary evaporator under reduced pressure.

The ^1H NMR spectra were recorded at either 400 MHz on an Ultrashield Plus TM 400 spectrometer or 500 MHz on a Bruker Ascend TM 500 spectrometer, using 5 mm diameter tubes. Chemical shifts (δ) were reported in parts per million (ppm), the residual solvent peak was used as reference, and coupling constants (J) were recorded in Hertz (Hz). The ^{13}C spectra were recorded at 101 MHz or 126 MHz. The low solubility of materials prevented acquisition of spectra in some cases. NMR analyses were performed in solution using deuterated as specified solvents at room temperature. UV-Vis absorption spectra were recorded on a Hitachi U-3310 spectrophotometer in the specified solvent (DCM or THF). MALDI-TOF-MS mass spectra were obtained with a Shimadzu Biotech Axima instrument. Infrared (IR) spectra were recorded on a Perkin-Elmer Spectrum BX FT-IR spectrometer.

Column chromatography was carried out using silica gel 60 Å mesh 70 - 230, with elution carried out using the specified solvent system at ambient temperature, occasionally applying moderate pressure using a hand pump. Solvent ratios are provided as volume/ volume (v:v). Thin-layer chromatography (TLC) was performed using aluminium sheets coated with Alugram® Sil G/UV254 (Macherey Nagel). The compounds were visualised under a short wavelength of UV light at 245 nm or 366 nm.

Melting points were determined using a Reichert Thermovar microscope equipped with thermoelectric temperature control. Reactions involving microwave irradiation were conducted using a Biotage initiator Microwave system.

3.2 Synthesis of 2-bromobenzamidine hydrochloride **2.3**



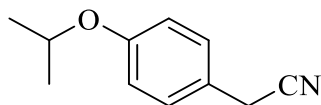
Following the method reported by Dalai,¹⁰⁸ 2-bromobenzonitrile **2.2** (4.18 g, 22.7 mmol) was dissolved in dry THF (3.4 mL) and then added to a solution of lithium bis(trimethylsilyl) amide (1.0 M in THF, 25 mL, 25 mmol). The reaction mixture was stirred at room temperature for 4 h. Following this, the reaction mixture was cooled on an ice bath, and a quenching mixture (15 mL) of 5N HCl and isopropanol (1:1 volume) was added dropwise with continuous stirring at room temperature continued overnight. The resulting precipitate was filtered off and washed with diethyl ether (20 mL) under vacuum, yielding white crystals (4.5 g, 89%).

m.p. > 300 °C. (lit. > 250 °C).¹⁰⁸

¹H NMR (500 MHz, DMSO-*d*₆) δ (ppm): 9.42 (br s, 4H), 7.82 (dd, *J* = 7.4, 1.8 Hz, 1H), 7.63 (dd, *J* = 7.2, 2.2 Hz, 1H), 7.60 – 7.52 (m, 2H).

¹³C NMR (126 MHz, DMSO-*d*₆) δ (ppm): 166.15, 133.53, 133.43, 132.18, 130.25, 128.38, 119.90.

3.3 Synthesis of 2-(4-isopropoxyphenyl) acetonitrile **2.34**



2.34

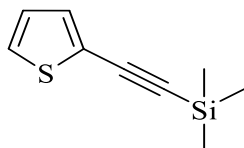
Following the method reported in the literature,¹¹⁵ to a solution of 4-hydroxyphenyl acetonitrile **2.33** (13.3 g, 0.1 mol, 1.0 equiv.) in DMF (50 mL) in the presence of K₂CO₃ (28 g, 0.2 mol, 2.0 equiv.), was added 2-bromopropane **2.32** (14 mL, 0.15 mol, 1.5 equiv.). The reaction mixture was stirred at 60°C for 21 h. After cooling to room temperature, water (100 mL) was added to the mixture. The aqueous layer was extracted with DCM (4 × 80 mL), and the organic layer was collected and washed with brine and dried over anhydrous MgSO₄. After filtration, the filtrate was concentrated under reduced pressure, yielding compound **2.34** as a pale-yellow oil that solidified on standing (10.82 g, 62%).

m.p. 25-30 °C. (lit 26-28°C).¹¹⁵

¹H NMR (400 MHz, chloroform-*d*) δ (ppm): 7.24 – 7.14 (m, 2H), 6.89 – 6.83 (m, 2H), 4.53 (hept, *J* = 6.1 Hz, 1H), 3.64 (s, 2H), 1.32 (d, *J* = 6.1 Hz, 6H).

¹³C NMR (101 MHz, chloroform-*d*) δ (ppm): 157.24, 128.72, 121.24, 117.97, 115.99, 69.60, 22.32, 21.56.

3.4 Synthesis of 2-[(trimethylsilyl)ethynyl] thiophene **2.44**¹¹⁷

**2.44**

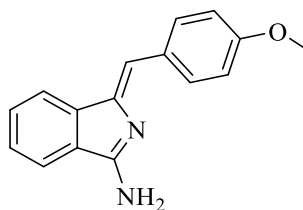
2-Bromothiophene **2.43** (0.6 g, 2.5 mmol) was dissolved in THF (15 mL), followed by the addition of copper iodide CuI (0.095g, 0.5mmol) as a cocatalyst and [Pd (PPh₃)₂Cl₂] (0.18 g, 0.25mmol) as a catalyst, along with triethylamine (5mL). To this stirred solution, (trimethylsilyl) acetylene (1.23g, 12.5mmol) was added under a nitrogen atmosphere. The reaction mixture was then heated at 60°C for 10 h. After cooling to room temperature, the mixture was filtered through a bed of Celite, and the filtrate was evaporated under reduced pressure. The resulting residue was purified *via* column chromatography using petroleum ether/DCM (5:1) as the eluent to yield compound **2.44** as a brown gel (0.47 g, 21%).

¹H NMR (400 MHz, chloroform-*d*) δ (ppm): 7.27 – 7.21 (m, 2H), 6.95 (dd, *J* = 5.1, 3.6 Hz, 1H), 0.29 (s, 9H).

¹³C NMR (101 MHz, chloroform-*d*) δ (ppm): 132.66, 127.35, 126.93, 123.33, 98.77, 97.75, 0.00.

3.5 Synthesis of aminoindoline derivatives

3.5.1 Synthesis of (Z)-1-(4-methoxybenzylidene)-1H-indol-3-amine **2.4**⁴⁹



2.4

A mixture of *o*-bromobenzamidinium hydrochloride salt **2.3** (1 g, 4.24 mmol), BINAP (0.14 g, 0.2 mmol) and PdCl₂ (MeCN)₂ (0.05 g, 0.21 mmol) were added in a sealed microwave vial with a magnetic bar and then purged and refilled with N₂ for 5 mins. 4-ethynylanisole (0.5 mL, 5 mmol) and DBU (1.6 g, 10.5 mmol) in dry DMF (12 ml) were added. The reaction mixture was irradiated in a microwave reactor at 120°C for 1 h. After the reaction was complete, the mixture was quenched with AcOEt (50mL) and a saturated solution of NaHCO₃ (75mL). The organic layer was extracted and dried with anhydrous MgSO₄, and the solvent was evaporated under a reduced pressure. The crude product was then purified by column chromatography using petroleum ether: AcOEt (1:1) as the eluent to yield a yellow solid and recrystallized from DCM/petroleum ether (1:1) to afford yellow needles (0.52 g, 49%).

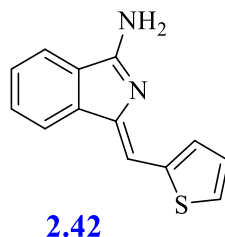
m.p 155-160 °C. (lit. 156- 157 °C).¹¹⁸

¹H NMR (500 MHz, CDCl₃-*d*) δ (ppm): 8.17 (d, *J* = 8.8 Hz, 2H), 7.86 (d, *J* = 9.5 Hz, 1H), 7.57 – 7.50 (m, 2H), 7.47 – 7.40 (m, 1H), 7.05 – 6.99 (m, 2H), 6.83 (s, 1H.), 5.55 (br s, 2H.), 3.93 (s, 3H).

¹³C NMR (126 MHz, CDCl₃-*d*) δ (ppm): 164.64, 158.92, 145.62, 142.95, 131.82, 130.61, 129.46, 128.82, 126.66, 119.41, 118.70, 115.16, 113.85, 55.16.

MS (MALDI-TOF): *m/z* = 250.42 [M]⁺, Chemical formula and calcd for C₁₆H₁₄N₂O:
250.11.

3.5.2 Synthesis of (Z)-1-(4-thiophenylmethylene)-1H-isoindol-3-amine 2.42⁴⁹



2-Bromobenzamidinium hydrochloride **2.3** (1g, 4.3 mmol), BINAP (0.13g, 0.2 mmol) and $\text{PdCl}_2(\text{MeCN})_2$ (0.06g, 0.2 mmol) were suspended in DMF (12 mL) in a microwave vial. The reaction mixture was degassed by nitrogen for 5 min., followed by the addition of DBU (1.62g, 10.6 mmol) and 2-[2-(trimethylsilyl) ethynyl]-thiophene (1.0 g, 5.55 mmol). The reaction mixture was heated to 120°C for 1 h using microwave irradiation. After cooling to room temperature, ethyl acetate (50 mL) was added. The organic layer was washed with a saturated solution of sodium bicarbonate (NaHCO_3) (3×75 mL), dried with anhydrous MgSO_4 , and the solvent was removed under reduced pressure. The crude product was purified *via* column chromatography using petroleum ether/EtOAc (1:1) as the eluent, followed by ethyl acetate. The resulting product was separated as a semi-solid yellow material, which was recrystallized from petroleum ether/DCM (1:1) to yield yellow needles (0.9 g, 92%).

m.p. 133-136 °C. (lit. 132.5-135 °C).¹¹⁹

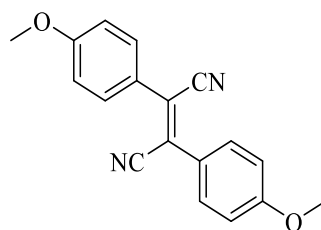
¹H NMR (500 MHz, acetone- d_6) δ (ppm): 7.82 (dt, $J = 7.6, 1.0$ Hz, 1H), 7.79 (dt, $J = 7.5, 1.0$ Hz, 1H), 7.45 – 7.40 (m, 2H), 7.37 – 7.32 (m, 2H), 7.07 (s, 1H), 7.01 (dd, $J = 5.1, 3.6$ Hz, 1H), the (NH_2) protons were not observed.

¹³C NMR (101 MHz, acetone- d_6) δ (ppm): 165.42, 147.64, 143.05, 141.68, 133.41, 129.35, 128.87, 128.78, 127.50, 127.05, 120.55, 119.98, 108.51.

MS (MALDI-TOF): $m/z = 226.47$ $[\text{M}]^+$, Chemical formula and calcd for $\text{C}_{13}\text{H}_{10}\text{N}_2\text{S}$: 226.06.

3.6 Synthesis of substituted dinitriles

3.6.1 Synthesis of 4-methoxyphenyl substituted dinitrile **2.8**



2.8

Following the method reported in the literature,⁶³ 4-methoxyphenyl acetonitrile **2.7** (1.0 g, 6.79 mmol) and I₂ (1.7 g, 6.79 mmol) were dissolved in distilled diethyl ether (20 mL) with stirring under a nitrogen atmosphere. The reaction mixture was cooled to -78 °C using a dry ice and acetone bath, and a solution of sodium methoxide (Na: 0.34g, 14.9 mmol in methanol (5 mL)) was added dropwise over 15 min. The reaction temperature was then allowed to rise to 0 °C, and stirring was continued for 2 h. Following this, the reaction mixture was quenched with cold water, and the resulting precipitate was collected by filtration and washed with cold methanol to afford the target compound **2.8** as a yellow solid (0.5 g, 51% yield).

m.p. 180- 185 °C. (lit. 198 °C).¹²⁰

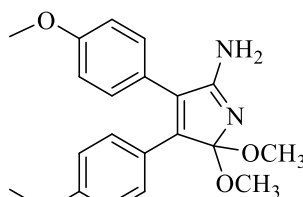
¹H NMR (500 MHz, CDCl₃-*d*) δ (ppm): 7.83-7.76 (m, 4H), 7.05-6.98 (m, 4H), 3.89 (s, 6H).

¹³C NMR (126 MHz, CDCl₃-*d*) δ (ppm): 161.90, 130.33, 124.51, 122.59, 117.20, 114.47, 55.43.

MS (MALDI-TOF): *m/z* = 291.20 [M+H]⁺, Chemical formula and calcd for C₁₈H₁₄N₂O₂: 290.11.

FT-IR *v* (cm⁻¹): 2214 (C≡N).

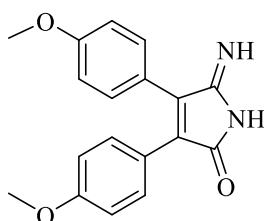
3.6.2 Synthesis of 2,2-dimethoxy-3,4-bis(4-dimethoxyphenyl)-5-amino-2H-pyrrole 2.13¹²¹

**2.13**

A solution of bis(4-methoxyphenyl)-dicyanoethylene **2.8** (0.5g, 1.72 mmol) was prepared in methanol (20 mL) containing sodium methoxide (Na: 0.1g, 5 mmol). The reaction mixture was heated to 63 °C for 10h. During the reaction, the solution colour changed from yellow to bright green, indicating the formation of compound **2.13**.

MS (MALDI-TOF): $m/z = 354.92 [M]^+$, Chemical formula and calcd for C₂₀H₂₂N₂O₄: 354.16.

3.6.3 Synthesis of 5-imino-3,4-bis(4-methoxyphenyl)-1H-pyrrol-2-one 2.14

**2.14**

This compound was obtained after trying to purify compound **2.13** by column chromatography using a petroleum ether: AcOEt (1:1) eluent system, which isolated a yellow solid. Subsequently, the product was recrystallized from DCM/ petroleum ether (1:1), affording yellow needles (350mg, 70% yield).

m.p. 195- 200 °C.

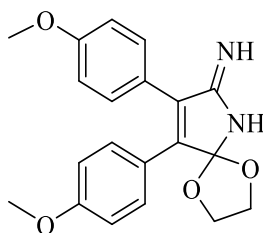
¹H NMR (500 MHz, CDCl₃-*d*) δ (ppm): 8.28 (s, 1H), 8.07 (br-s, 1H), 7.39 – 7.34 (m, 2H), 7.14 – 7.09 (m, 2H), 6.93 – 6.89 (m, 2H), 6.78 – 6.73 (m, 2H), 3.79 (s, 3H), 3.73 (s, 3H).

¹³C NMR (126 MHz, CDCl₃-*d*) δ (ppm): 163.88, 160.56, 160.41, 133.98, 131.34, 130.64, 121.55, 114.96, 113.91, 55.37, 55.26.

FT-IR ν (cm⁻¹): 3280 (NH), 1725 (C=O).

MS (MALDI-TOF): m/z = 309.49 [M+H]⁺, Chemical formula and calcd for C₁₈H₁₆N₂O₃: 308.12.

3.6.4 Synthesis of 5-imino-3,4-bis(4-methoxyphenyl)-1*H*-pyrrol-2-dioxolane **2.16**¹¹⁴



2.16

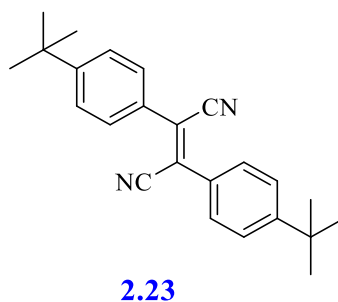
A solution of bis(4-methoxyphenyl)-dicyanoethylene **2.8** (0.1 g, 0.34 mmol) was added to Na (5 equiv.) in ethyl glycol (10 mL). The reaction mixture was heated to 80 °C under N₂ overnight. During the reaction, the solution colour changed from yellow to bright green. The reaction was then extracted with chloroform and a saturated NaHCO₃ solution. The organic layer was dried with MgSO₄, followed by solvent removal under reduced pressure. The crude product was purified by column chromatography using three solvent systems, starting from DCM, then DCM/CHCl₃ (1:1), and finally pure CHCl₃, yielding a luminescent green powder (9 mg, 7.5% yield).

m.p. 250 °C.

¹H NMR (500 MHz, chloroform-*d*) δ (ppm): 7.36 – 7.30 (m, 2H), 7.22 – 7.15 (m, 2H), 6.94 – 6.88 (m, 2H), 6.79 – 6.73 (m, 2H), 4.38 – 4.29 (m, 2H), 4.21 – 4.12 (m, 2H), 3.83 (s, 3H), 3.76 (s, 3H), the (NH₂) protons were not observed.

MS (MALDI-TOF): m/z = 351.79 [M]⁺, Chemical formula and calcd for C₂₀H₂₀N₂O₄: 352.14.

3.6.5 Synthesis of *t*-butylphenyl substituted dinitrile **2.23**⁶³



A solution of 4-*tert*-butylphenyl acetonitrile **2.25** (1.0 g, 5 mmol), and iodine (I₂) (1.46 g, 5 mmol) were dissolved in distilled diethyl ether (20 mL) with stirring under a nitrogen atmosphere. The reaction mixture was cooled to 10 °C using ice bath, and a solution of sodium methoxide (Na: 0.29g, 12.6 mmol in methanol (5 mL)) was added dropwise over 15 min. The reaction temperature was allowed to warm to room temperature and stirring continued for an additional 2 h. The reaction mixture was quenched with cold water, and the resulting precipitate was collected by filtration and washed with cold methanol to give a white solid (0.26 g, 39% yield).

m.p. 190-195 °C. (lit. 235 °C).¹²⁰

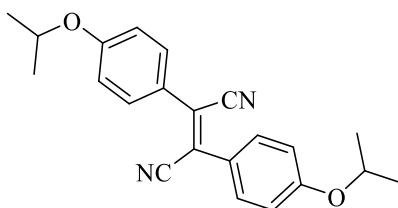
¹H NMR (500 MHz, CDCl₃-*d*) δ (ppm): 7.82 – 7.75 (m, 4H), 7.57 – 7.51 (m, 4H), 1.36 (s, 18H).

¹³C NMR (126 MHz, CDCl₃-*d*) δ (ppm): 155.22, 129.20, 128.40, 126.11, 124.29, 116.96, 34.99, 30.97.

MS (MALDI-TOF): $m/z = 343.67$ [M+H]⁺, Chemical formula and calcd for C₂₄H₂₆N₂: 342.21.

FT-IR ν (cm⁻¹): 2222 (C≡N).

3.6.6 Synthesis of isopropoxyphenyl substituted dinitrile 2.24⁶³

**2.24**

2-(4-isopropoxyphenyl) acetonitrile **2.32** (1.0 g, 5 mmol), and I₂ (1.46 g, 5 mmol) were dissolved in distilled diethyl ether (20 mL) with stirring under nitrogen atmosphere. The reaction mixture was cooled to 10 °C with ice and a solution of sodium methoxide (Na: 0.29g, 12.6 mmol in methanol (5 ml)) was added dropwise during 15 min. The reaction temperature was increased to r.t and the stirring continued for 2 h. The reaction mixture was quenched with cold water and the precipitate was collected by filtration and washed with cold methanol to give a white solid. Recrystallization from DCM and methanol gave white crystals (0.49 g, 50% yield).

m.p. 140-142 °C.

¹H NMR (400 MHz, chloroform-*d*) δ (ppm): 7.81 – 7.74 (m, 4H), 7.00 – 6.94 (m, 4H), 4.65 (hept, *J* = 12.1, 6.0 Hz, 2H), 1.38 (d, *J* = 6.0 Hz, 12H).

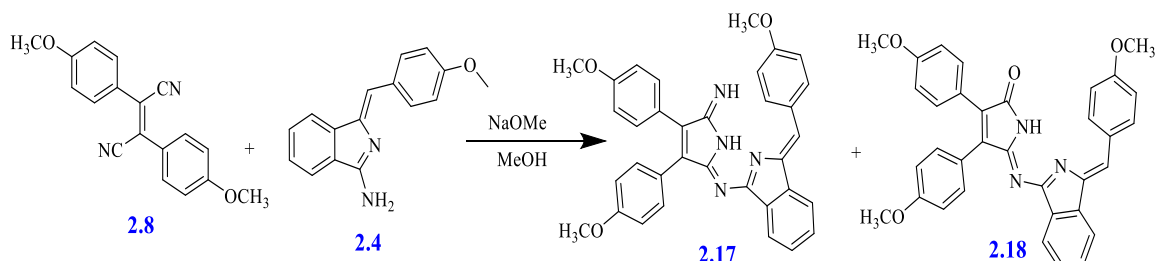
¹³C NMR (101 MHz, chloroform-*d*) δ (ppm): 160.32, 130.29, 124.05, 122.24, 117.25, 115.75, 70.11, 21.76.

MS (MALDI-TOF): *m/z* = 346.63 [M]⁺, Chemical formula and calcd for C₂₂H₂₂N₂O₂: 346.17.

FT-IR *ν* (cm⁻¹): 2218 (C≡N).

3.7 Dimeric condensation products of aminoisindoline derivatives with substituted dinitriles

3.7.1 Condensation products of aminoisindoline **4** with 4-methoxyphenyl dinitrile **2.8**



A solution of (4-methoxyphenyl)-dicyanoethylene **2.8** (0.2 g, 0.688 mmol) and sodium methoxide (Na metal: 0.02g, 0.82 mmol in methanol (15 mL)) was prepared under a nitrogen atmosphere. To this solution, aminoisindoline **2.4** (0.17g, 0.688 mmol) was added, the reaction mixture was refluxed for 18 h. After completion, the solvent was evaporated under vacuo, and the resulting product was dissolved in DCM and then washed with water, and the washings extracted with DCM several times. The organic layer was dried over anhydrous MgSO_4 , filtered, and the solvent was removed under reduced pressure. The crude product was purified by column chromatography using petroleum ether: AcOEt as the eluent in different volume ratios (5:1), (3:1), and (1:1). The first fraction yielded an orange-red solid corresponding to compound **2.18**, while the second fraction contained a red solid corresponding to compound **2.17**. Recrystallization from DCM and MeOH afforded orange-red crystals of dimer **2.18** (0.08 g, 22%), and red crystals of the target dimer **2.17** (0.155g, 42%).

3.7.1.1 Dimer **2.17**

m.p. 120- 125 °C.

$^1\text{H NMR}$ (500 MHz, methylene chloride- d_2) δ (ppm): 8.14 (d, $J = 8.7$ Hz, 2H), 7.87 (dt, $J = 7.7, 1.0$ Hz, 1H), 7.81 (dt, $J = 7.5, 1.0$ Hz, 1H), 7.63 – 7.58 (m, 2H), 7.51 (td, $J = 7.4, 1.1$ Hz, 1H), 7.43 (td, $J = 7.4, 0.9$ Hz, 1H), 7.28 (d, $J = 8.6$ Hz, 2H), 7.25 (s, 1H), 7.09 (d, $J = 8.8$ Hz, 2H), 7.00 – 6.95 (m, 2H), 6.94 – 6.89 (m, 2H), 3.90 (s, 3H), 3.85 (s, 6H), the 2 NH protons were not observed.

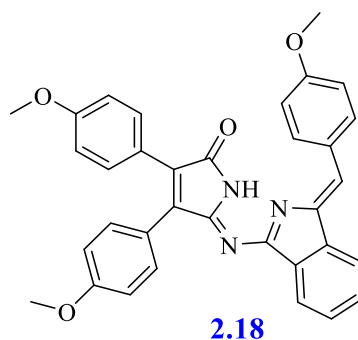
$^{13}\text{C NMR}$ (126 MHz, methylene chloride- d_2) δ (ppm): 161.46, 161.17, 160.02, 133.83, 132.96, 132.00, 129.78, 129.65, 128.15, 122.07, 115.32, 115.22, 114.29, 56.31, 56.18, 56.12.

MS (MALDI-TOF): $m/z = 541.27$ $[M+H]^+$, Chemical formula and calcd for $C_{34}H_{28}N_4O_3$: 540.22.

UV-Vis (CH_2Cl_2): λ_{max} . (nm) (ϵ ($M^{-1}.cm^{-1}$)) = 464 (1.8×10^4), 332 (3.8×10^4), 267 (3.7×10^5).

FT-IR ν (cm^{-1}): 3288 (NH).

3.7.1.2 Dimer 2.18



m.p. 90-95 °C.

1H NMR (500 MHz, methylene chloride- d_2) δ (ppm): 11.02 (br-s, 1H), 8.15 – 8.11 (m, 2H), 7.86 (dt, $J = 7.7, 0.9$ Hz, 1H), 7.78 (dt, $J = 7.5, 1.1$ Hz, 1H), 7.63 – 7.60 (m, 2H), 7.52 – 7.47 (m, 3H), 7.41 (td, $J = 7.4, 1.0$ Hz, 1H), 7.31 (s, 1H), 7.07 – 7.03 (m, 2H), 6.99 – 6.95 (m, 2H), 6.90 – 6.87 (m, 2H), 3.90 (s, 3H), 3.87 (s, 3H), 3.83 (s, 3H).

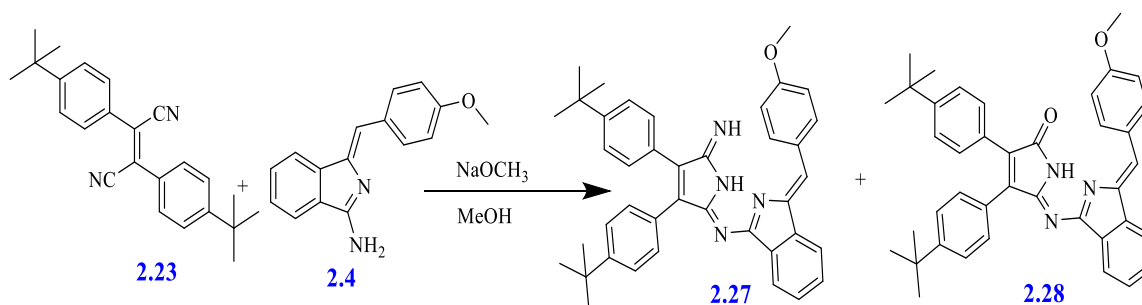
^{13}C NMR (126 MHz, methylene chloride- d_2) δ (ppm): 170.60, 161.02, 160.74, 160.59, 156.43, 146.32, 142.04, 139.95, 139.55, 136.65, 133.40, 132.52, 131.81, 131.57, 129.31, 127.72, 123.86, 123.01, 123.00, 121.63, 119.49, 114.88, 114.78, 114.38, 113.85, 55.85, 55.73, 55.66.

MS (MALDI-TOF): $m/z = 541.76$ $[M]^+$, Chemical formula and calcd for $C_{34}H_{27}N_3O_4$: 541.20.

UV-Vis (CH_2Cl_2): λ_{max} (nm) (ϵ ($M^{-1}.cm^{-1}$)) = 473 (3.40×10^4), 331 (4.28×10^4), 265 (6.42×10^4).

FT-IR ν (cm^{-1}): 1722 (C=O).

3.7.2 Condensation products of aminoisoindoline 4 with *t*-butylphenyl substituted dinitrile 2.23



A solution of sodium methoxide (Na : 0.02 g, 0.7 mmol in methanol (15 mL)) was prepared, and to this 4-*tert*-butylphenyl-dicyanoethylene **2.23** (0.2g, 0.58mmol) and aminoisoindoline **2.4** (0.14 g, 0.58 mmol) were added. The reaction mixture was then heated at 55 °C for 10 h under a nitrogen atmosphere. After cooling, the solvent was evaporated under reduced pressure, the crude product was dissolved in DCM and washed with water, and the washings were extracted with DCM several times. The organic layer was dried over anhydrous MgSO_4 , filtered and the solvent was removed under reduced pressure. The crude product was purified by column chromatography using petroleum ether: DCM system with different ratios (2:1), (1:1), and (1:2). Two fractions were obtained: an orange-red by-product solid identified as compound **2.28**, and a red solid identified as compound **2.27**. Both fractions recrystallized from DCM and MeOH, yielding orange-red crystals of **2.28** (0.062g, 18%), and red crystals of dimer **27** (133mg, 38%).

3.7.2.1 Dimer 2.27

m.p. 120-125 °C.

^1H NMR (500 MHz, methylene chloride- d_2) δ (ppm): 8.17 – 8.12 (m, 2H), 7.86 (dt, $J = 7.7, 0.9$ Hz, 1H), 7.81 (dt, $J = 7.5, 1.0$ Hz, 1H), 7.62 – 7.58 (m, 2H), 7.51 – 7.46 (m, 3H), 7.44 – 7.40 (m, 3H), 7.28 (d, $J = 7.9$ Hz, 2H), 7.22 (s, 1H), 7.07 – 7.02 (m, 2H), 3.89 (s, 3H), 1.366 (s, 9H), 1.363 (s, 9H), the 2NH protons were not observed.

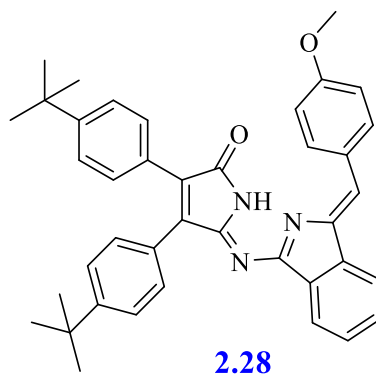
^{13}C NMR (126 MHz, methylene chloride- d_2) δ (ppm): 170.19, 161.39, 160.60, 152.39, 152.13, 145.85, 141.60, 136.18, 135.23, 134.23, 132.97, 130.33, 129.40, 128.87, 127.46, 127.29, 127.26, 125.91, 124.90, 123.49, 121.25, 119.05, 114.35, 55.41, 34.68, 34.65, 30.97, 30.94, 30.90, 30.84.

MS (MALDI-TOF): $m/z = 593.79 [M+H]^+$, Chemical formula and calcd for $C_{40}H_{40}N_4O$: 592.32.

UV-Vis (CH_2Cl_2) : $\lambda_{max.}(nm)$ ($\epsilon (M^{-1}.cm^{-1})$) = 463 (1.39×10^3), 335 (3.65×10^3), 261 (3.17×10^3).

FT-IR ν (cm^{-1}): 3300 (NH).

3.7.2.2 Dimer 2.28



m.p. 160-165 °C.

1H NMR (500 MHz, methylene chloride- d_2) δ (ppm): 11.08 (br-s, 1H), 8.17 – 8.11 (m, 2H), 7.87 (dd, $J = 7.1, 3.7$ Hz, 1H), 7.80 (dd, $J = 7.1, 3.6$ Hz, 1H), 7.61 (d, $J = 7.3$ Hz, 2H), 7.53 – 7.37 (m, 8H), 7.33 (s, 1H), 7.06 (d, $J = 7.9$ Hz, 2H), 3.90 (s, 3H), 1.36 (s, 9H), 1.33 (s, 9H).

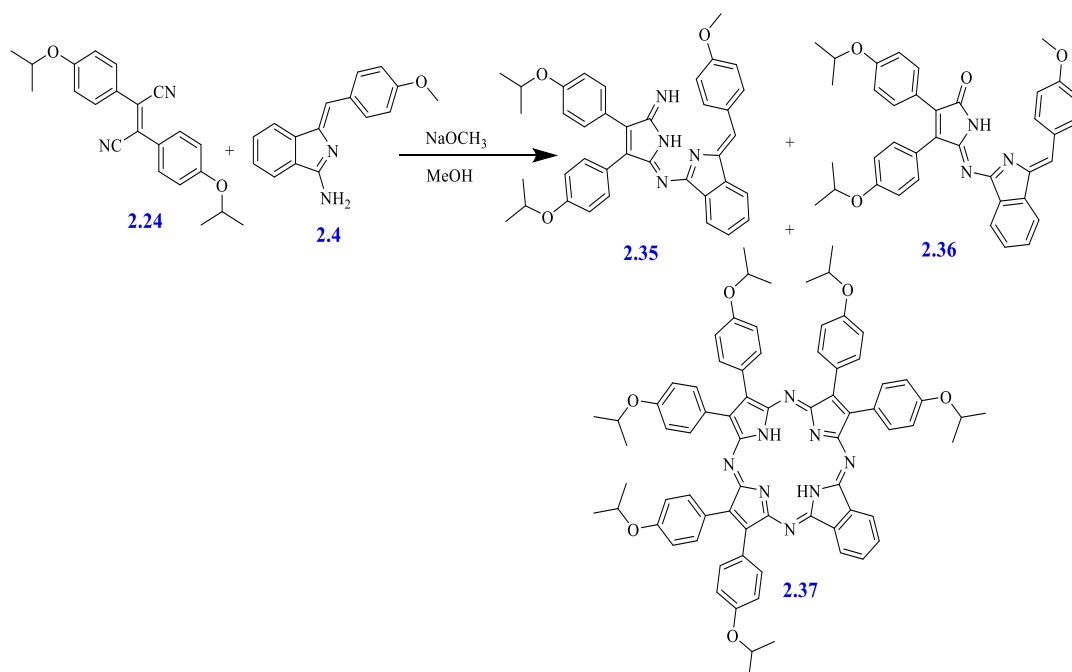
^{13}C NMR (126 MHz, methylene chloride- d_2) δ (ppm): 169.39, 161.07, 158.98, 152.68, 152.61, 145.79, 141.69, 135.78, 134.27, 133.39, 130.24, 129.67, 129.34, 128.68, 127.39, 127.01, 126.13, 125.31, 125.28, 125.15, 121.24, 119.13, 114.48, 55.47, 34.74, 34.69, 30.98, 30.95, 30.89, 30.82.

MS (MALDI-TOF): $m/z = 593.86 [M]^+$, Chemical formula and calcd for $C_{40}H_{39}N_3O_2$: 593.30.

UV-Vis (CH_2Cl_2) : $\lambda_{max.}(nm)$ ($\epsilon (M^{-1}.cm^{-1})$) = 470 (1.48×10^4), 330 (2.63×10^4), 265 (2.13×10^4).

FT-IR ν (cm^{-1}): 1714 (C=O).

3.7.3 Condensation products of aminoisoindoline **2.4** with isopropoxyphenyl substituted dinitrile **2.24**



Isopropoxyphenyl substituted dinitrile **2.24** (0.2 g, 0.57 mmol) was added to a solution of sodium methoxide (Na : 0.02g, 0.96 mmol in methanol (15 ml)). Aminoisoindoline **2.4** (0.144 g, 0.75 mmol) was subsequently added, and the reaction mixture was refluxed for 18 h under a nitrogen atmosphere. Upon completion, the reaction mixture was filtered to remove black impurities as a precipitate. The filtrate was concentrated under reduced pressure, and the resulting product was dissolved in DCM and then washed with water and the washings were extracted multiple times with DCM. The organic layer was dried over anhydrous MgSO_4 , filtered, and the solvent was removed under reduced pressure. The crude product was purified by column chromatography using a petroleum ether/DCM system as the eluent with different ratios, starting from (1:1), (1:2), and only DCM. This process afforded compound **2.36** as a side product, yielding red-orange crystals (0.043 mg, 13%) and the target dimer **2.35** as a red solid (0.12 g, 35%). The black impurities from the reaction mixture were further subjected to column chromatography by using a petroleum ether/ethyl acetate system (6:1) \rightarrow (3:1) as the eluent resulting in the isolation of ligand **2.37** as a solid purple macrocycle (20 mg, 2%).

3.7.3.1 Dimer 2.35

m.p. 105- 110 °C.

¹H NMR (400 MHz, methylene chloride-*d*₂) δ (ppm): 8.18 – 8.10 (m, 2H), 7.85 (dt, *J* = 7.6, 1.0 Hz, 1H), 7.80 (dt, *J* = 7.4, 1.0 Hz, 1H), 7.62 – 7.56 (m, 2H), 7.48 (td, *J* = 7.4, 1.2 Hz, 1H), 7.41 (td, *J* = 7.3, 1.0 Hz, 1H), 7.25 (d, *J* = 8.3 Hz, 2H), 7.20 (s, 1H), 7.07 – 7.00 (m, 2H), 6.96 – 6.90 (m, 2H), 6.90 – 6.84 (m, 2H), 4.68 – 4.53 (m, 2H), 3.88 (s, 3H), 1.36 (d, *J* = 6.0 Hz, 6H), 1.35 (d, *J* = 6.0 Hz, 6H), the 2NH protons were not observed.

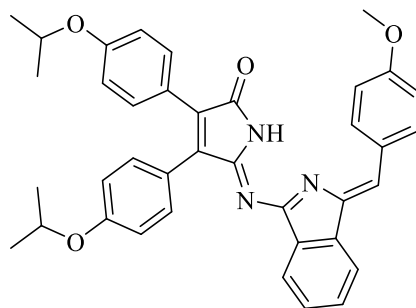
¹³C NMR (101 MHz, methylene chloride-*d*₂) δ (ppm): 170.64, 161.94, 161.00, 159.11, 158.98, 146.34, 142.05, 139.36, 136.68, 133.38, 132.55, 131.58, 129.33, 129.28, 127.70, 124.48, 123.77, 122.77, 122.65, 121.64, 119.48, 116.45, 115.36, 114.76, 108.86, 70.39, 70.24, 55.84, 22.23, 22.17.

MS (MALDI-TOF): *m/z* = 597.78 [M+H]⁺, Chemical formula and calcd for C₃₈H₃₆N₄O₃: 596.28.

UV-Vis (CH₂Cl₂): λ_{max}(nm)(ε (M⁻¹.cm⁻¹)) = 465 (2.90×10⁴), 331 (6.11×10⁴), 263 (5.32×10⁵).

FT-IR ν (cm⁻¹): 3275 (NH).

3.7.3.2 Dimer 2.36



2.36

m.p. 190- 195 °C.

¹H NMR (400 MHz, CD₂Cl₂-*d*₂) δ (ppm): 8.15 – 8.09 (m, 2H), 7.85 (dt, *J* = 7.6, 0.9 Hz, 1H), 7.77 (dt, *J* = 7.4, 1.0 Hz, 1H), 7.63 – 7.58 (m, 2H), 7.51 – 7.45 (m, 3H), 7.43 – 7.38 (m, 1H), 7.29 (s, 1H), 7.07 – 7.02 (m, 2H), 6.96 – 6.90 (m, 2H), 6.87 – 6.82 (m, 2H), 4.66 – 5.54 (m, 2H), 3.90 (s, 3H), 1.38 (d, *J* = 6.0 Hz, 6H), 1.34 (d, *J* = 6.1 Hz, 6H), the NH proton was not observed.

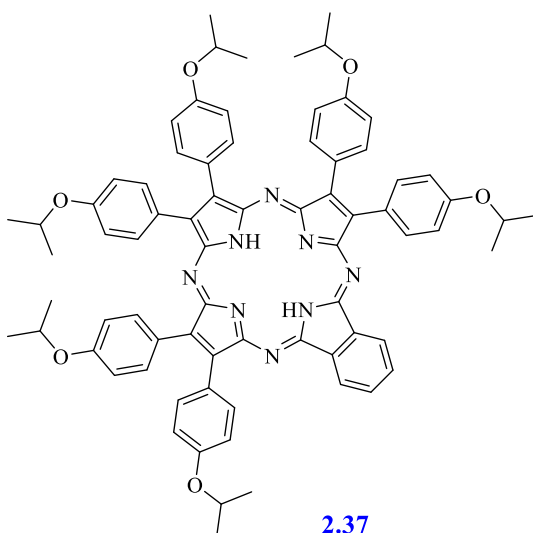
^{13}C NMR (101 MHz, $\text{CD}_2\text{Cl}_2-d_2$) δ (ppm): 170.49, 161.25, 159.17, 133.36, 132.09, 131.53, 129.04, 128.90, 127.83, 127.49, 126.01, 125.89, 122.44, 121.97, 121.88, 119.55, 119.24, 116.51, 115.35, 115.17, 114.46, 69.90, 55.47, 21.81, 21.75.

MS (MALDI-TOF): $m/z = 598.34$ $[\text{M}+\text{H}]^+$, Chemical formula and calcd for $\text{C}_{38}\text{H}_{35}\text{N}_3\text{O}_4$: 597.26.

FT-IR ν (cm^{-1}): 1714 (C=O).

UV-Vis (CH_2Cl_2): $\lambda_{\text{max.}}$ (nm)(ϵ ($\text{M}^{-1}\cdot\text{cm}^{-1}$)) = 469 (3.75×10^4), 328 (4.49×10^4), 267 (5.02×10^4).

3.7.3.3 Free-metal porphyrazine hybrid (H_2 -ABBB-N) 2.37



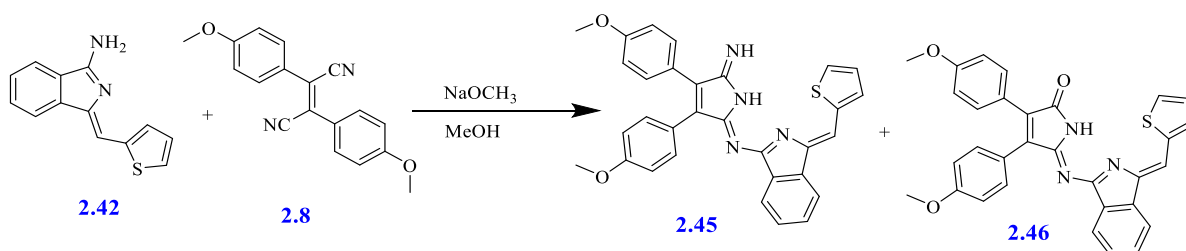
m.p. > 350 °C.

^1H NMR (400 MHz, methylene chloride- d_2) δ (ppm): 8.83 (dd, $J = 5.3, 3.0$ Hz, 2H), 8.18 (d, $J = 8.3$ Hz, 4H), 8.14 – 8.08 (m, 4H), 8.07 – 8.00 (m, 4H), 7.95 (dd, $J = 5.7, 2.7$ Hz, 2H), 7.22 – 7.14 (m, 4H), 7.05 (t, $J = 8.9$ Hz, 8H), 4.87– 4.72 (m, 6H), 1.57 – 1.48 (m, overlapping with water signal), -2.34 (s, 2H).

MS (MALDI-TOF): $m/z = 1169.96$ $[\text{M}^+\text{H}]^+$, Chemical formula and calcd for $\text{C}_{74}\text{H}_{72}\text{N}_8\text{O}_6$: 1168.56.

UV-Vis (CH_2Cl_2): $\lambda_{\text{max.}}$ (nm) (ϵ ($\text{M}^{-1}\cdot\text{cm}^{-1}$)) = 702 (6.59×10^4), 598 (2.98×10^4), 496(2.32×10^4), 349 (4.46×10^4).

3.7.4 Condensation products of aminoisoindoline **2.42** with 4-methoxyphenyl substituted dinitrile **2.8**



To a solution of sodium methoxide (Na: 0.19g, 0.82 mmol in methanol (15 ml)) and (4-methoxyphenyl)-dicyanoethylene **2.8** (0.2 g, 0.68 mmol), 1-(4-thiophenylmethylene)-1*H*-isoindol-3-amine **2.42** (0.15 g, 0.68 mmol) was added. The reaction mixture was refluxed for 14 h under a nitrogen atmosphere. Upon completion, the mixture was allowed to cool, and the solvent was evaporated under reduced pressure. The resulting product was dissolved in DCM and then washed with water, and the washings were extracted with DCM several times. The organic layer was dried over anhydrous MgSO₄, filtered, and the solvent was removed under reduced pressure. The crude product was purified by column chromatography using petroleum ether/DCM (2:1), (1:1), and only DCM systems as the eluent. The target compound was recrystallized from DCM/methanol (1:1) to give a red crystal of dimer **2.45** (0.16 g, 44%). Additionally, the side product, dimer **2.46** was also recrystallized from DCM/methanol (1:1) to produce orange-red crystals (0.05 g, 14%).

3.7.4.1 Dimer **2.45**

m.p. 185- 195 °C.

¹H NMR (400 MHz, methylene chloride-*d*₂) δ (ppm): 7.85 – 7.76 (m, 2H), 7.67 (d, *J* = 5.1 Hz, 1H), 7.63 – 7.57 (m, 2H), 7.51 (s, 1H), 7.47 (dd, *J* = 7.4, 1.2 Hz, 1H), 7.44 – 7.38 (m, 2H), 7.33 – 7.26 (m, 2H), 7.15 (dd, *J* = 5.1, 3.7 Hz, 1H), 7.01 – 6.95 (m, 2H), 6.95 – 6.88 (m, 2H), 3.85 (s, 6H), the 2 NH protons were not observed.

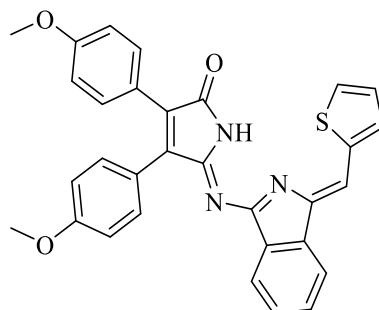
¹³C NMR (101 MHz, methylene chloride-*d*₂) δ (ppm): 162.55, 162.54, 162.04, 151.62, 140.50, 140.46, 139.92, 139.88, 134.37, 132.55, 132.42, 131.62, 129.67, 129.52, 129.23, 127.93, 126.84, 123.96, 122.42, 120.20, 119.27, 118.24, 117.38, 115.31, 113.87, 55.74, 55.67.

MS (MALDI-TOF): *m/z* = 517.28 [M⁺H]⁺, Chemical formula and calcd for C₃₁H₂₄N₄O₂S: 516.16.

UV-Vis (CH₂Cl₂) : λ_{\max} .(nm) (ϵ (M⁻¹.cm⁻¹)) = 472 (6.34×10³), 335 (1.30×10⁴), 271 (9.45×10³).

FT-IR ν (cm⁻¹): 3248 (NH).

3.7.4.2 Dimer 2.46



2.46

m.p. 170-175 °C.

¹H NMR (400 MHz, acetone-*d*₆) δ (ppm): 11.38 (br-s, 1H), 8.00 (dt, $J = 7.5, 0.9$ Hz, 1H), 7.90 (s, 1H), 7.89 (dt, $J = 5.2, 1.0$ Hz, 1H), 7.78 (dt, $J = 7.5, 1.0$ Hz, 1H), 7.69 – 7.64 (m, 2H), 7.58 (dt, $J = 3.7, 1.0$ Hz, 1H), 7.56 – 7.51 (m, 3H), 7.46 (td, $J = 7.4, 1.0$ Hz, 1H), 7.23 (dd, $J = 5.1, 3.7$ Hz, 1H), 7.08 – 7.02 (m, 2H), 7.00 – 6.95 (m, 2H), 3.90 (s, 3H), 3.87 (s, 3H).

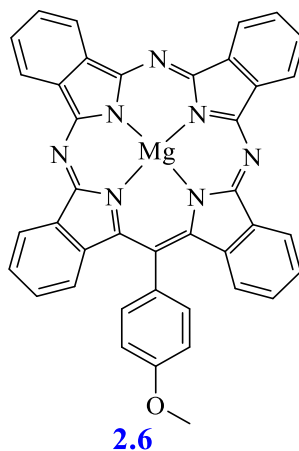
¹³C NMR (101 MHz, acetone-*d*₆) δ (ppm): 160.31, 159.83, 159.60, 149.73, 148.10, 133.54, 133.07, 132.08, 131.57, 121.27, 120.26, 113.85, 113.65, 55.43, 55.25.

MS (MALDI-TOF): $m/z = 518.44$ [M+H]⁺, Chemical formula and calcd for C₃₁H₂₃N₃O₃S: 517.15

UV-Vis (CH₂Cl₂) : λ_{\max} .(nm) (ϵ (M⁻¹.cm⁻¹)) = 473 (5.07×10⁴), 331 (6.40×10⁴), 265 (7.06×10⁴).

FT-IR ν (cm⁻¹): 1725 (C=O).

3.8 Synthesis of [20-(4-methoxyphenyl)-tetrabenzob[*b, g, q, l*]-5,10,15-triazaporphyrinato] magnesium **2.6**¹²²



Aminoisoindoline **2.4** (200 mg, 0.8 mmol), MgBr₂ (110.0 mg, 0.59 mmol), phthalonitrile **2.5** (102 mg, 0.8 mmol), and DABCO (67.0 mg, 0.59 mmol) were dissolved in diglyme (3 mL) and refluxed at 220 °C in an oil bath under an argon atmosphere for 4 h. Following the reaction, the solvent was evaporated by passing a stream of argon gas through the flask at high temperatures. After cooling the reaction mixture to room temperature, a mixture of DCM: MeOH 20 mL (1:1) was added, and the solvent was removed under reduced pressure. The product was purified through two consecutive column chromatography. The first column was eluted with three systems to remove yellow impurities, beginning with DCM, followed by DCM/Et₃N (20:1) and finally, DCM/THF/Et₃N (10:4:1). The second column was eluted with a petroleum ether/THF/MeOH (10:3:1) mixture to isolate the green fraction, which was recrystallized from an acetone/ethanol mixture (1:1) to afford green crystals (8 mg, 16%).

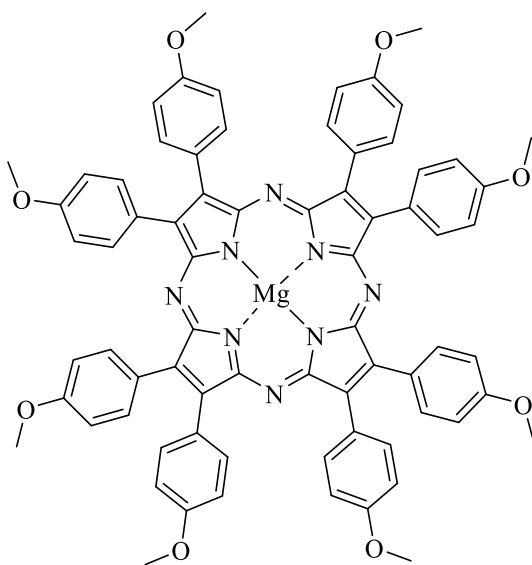
m.p. > 300 °C. (lit. > 300°C).¹¹⁸

¹H NMR (500 MHz, acetone-*d*₆) δ (ppm): 9.64 (d, *J* = 7.6 Hz, 2H), 9.56 (q, *J* = 4.4 Hz, 4H), 8.32 – 8.25 (m, 4H), 8.07 (d, *J* = 7.9 Hz, 2H), 8.02 (t, *J* = 7.2 Hz, 2H), 7.71 (t, *J* = 7.4 Hz, 2H), 7.60 (d, *J* = 8.3 Hz, 2H), 7.26 (d, *J* = 8.0 Hz, 2H), 4.24 (s, 3H).

MS (MALDI-TOF): *m/z* = 641.72 [M]⁺, Chemical formula and calcd for C₄₀H₂₃MgN₇O: 641.18.

UV-Vis (THF): λ_{max}.(nm) (ε (M⁻¹.cm⁻¹)) = 671 (1.57×10⁵), 648 (1.23 ×10⁵), 595 (2.59×10⁴), 446 (2.66×10⁴), 396 (7.07×10⁴).

3.9 Synthesis of octa(4-methoxyphenyl) porphyrazine Mg (II) complex 2.9

**2.9**

Lithium metal (0.002 g) was dissolved in butanol (3 mL) under a nitrogen atmosphere. To this solution, MgBr_2 (0.005g, 0.027 mmol) was added, followed by the addition of (4-methoxyphenyl)-dicyanoethylene **2.8** (0.015g, 0.054 mmol). The reaction mixture was refluxed overnight, resulting in the formation of a green precipitate. The precipitate was collected by filtration, washed with methanol (MeOH), and subsequently recrystallized from a THF/methanol mixture (1:1) to yield a bluish-green powder (1.3 mg, 2%).

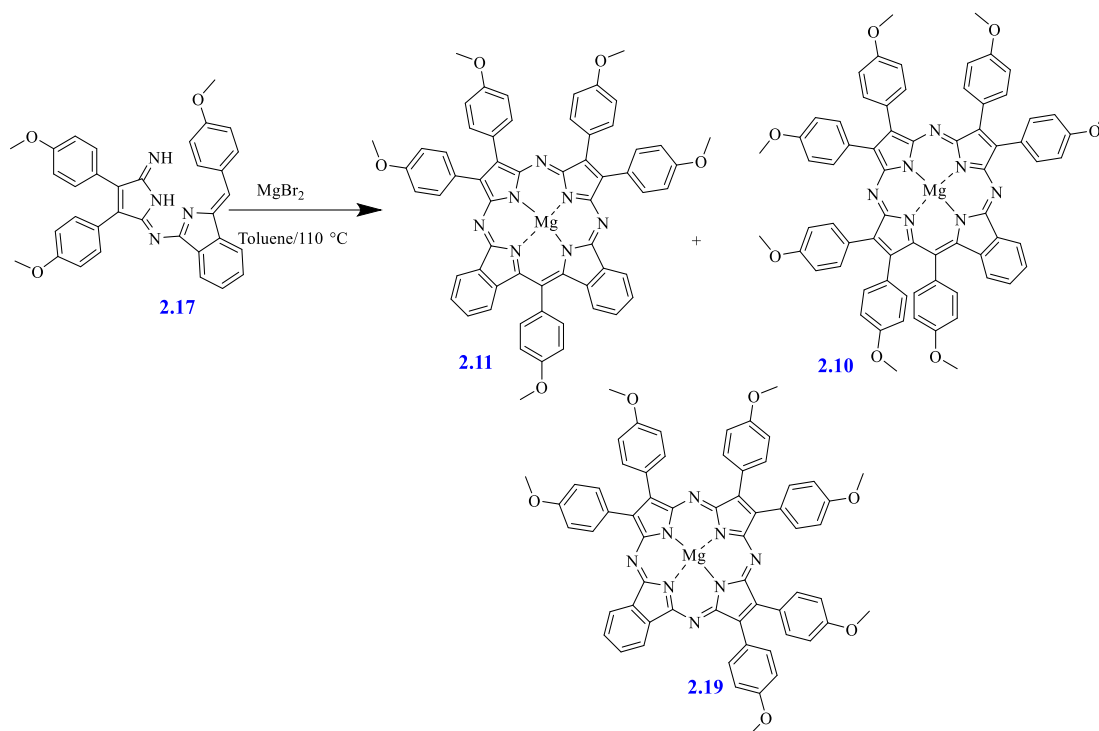
m.p. > 300 °C.

MS (MALDI-TOF): $m/z = 1185.58$ $[\text{M}+\text{H}]^+$, Chemical formula and calcd for $\text{C}_{72}\text{H}_{56}\text{MgN}_8\text{O}_8$: 1184.41.

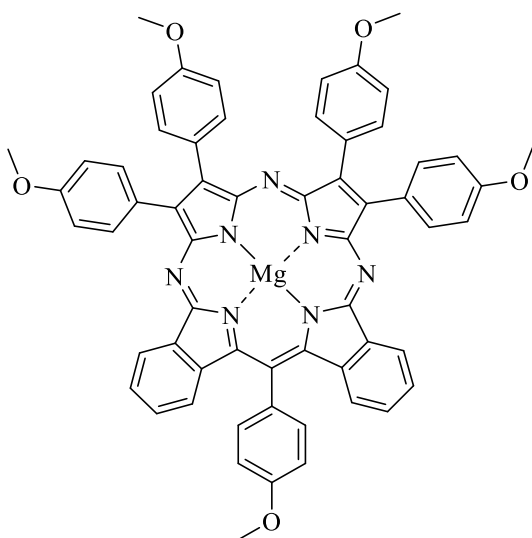
UV-Vis (THF): λ_{max} . (nm) (ϵ ($\text{M}^{-1}\cdot\text{cm}^{-1}$)) = 650 (3.58×10^4), 382 (2.47×10^4).

3.10 Synthesis of porphyrazine hybrids from dimer 2.17

3.10.1 Synthesis of Mg-porphyrazine hybrids from dimer 2.17



Dimer **17** (0.5 g, 0.92 mmol, 2 equiv.) and MgBr_2 (127.7mg, 0.69 mmol) were dissolved in toluene (15 mL) and refluxed under N_2 atmosphere for 9 h. After completion, the solvent was evaporated by passing a stream of nitrogen gas through the reaction flask at high temperatures. The crude product was subjected to several consecutive column chromatography for purification. The first column was eluted with two systems, starting with DCM and then DCM/THF (10:2), to remove impurities and isolate the green fraction. The second column was eluted with petroleum ether / DCM/ THF (10:5:2) to separate hybrid **2.11** from other porphyrizes in the green fraction. The solid product was precipitated by adding methanol and recrystallization from DCM and methanol, yielding compound **2.11** as dark green crystals (53 mg, 6%). Further purification of the green fraction was carried out using a third column eluted with EtOAc/DCM (5:100) as an eluent, resulting in the isolation of a blue fraction. This fraction was precipitated with methanol and recrystallized from DCM/methanol, yielding compound **2.19** as azure blue crystals (38mg, 4%). Finally, the remaining green fraction was purified through a final column chromatography step using EtOAc/DCM (5:100), and the light green fraction was collected. This fraction was also precipitated with methanol and recrystallized from DCM / methanol to afford porphyrazine **2.10** as green crystals (10 mg, 1%).

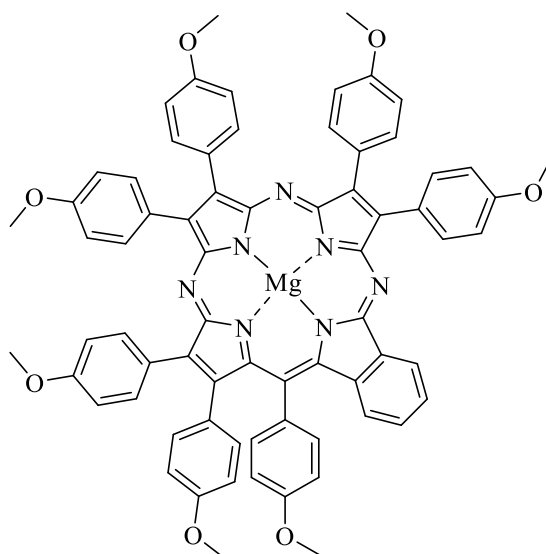
3.10.1.1 Mg-*meso*-(4-methoxyphenyl) ABBA Pz/Pc hybrid 2.11**2.11**

m.p. 275-280 °C.

¹H NMR (500 MHz, THF-*d*₈) δ (ppm) : 9.46 (dt, $J = 7.5, 1.0$ Hz, 2H), 8.54 – 8.50 (m, 4H), 8.45 – 8.40 (m, 4H), 8.08 – 8.05 (m, 2H), 7.95 – 7.89 (m, 2H), 7.67 – 7.63 (m, 2H), 7.55 – 7.51 (m, 2H), 7.30 (dd, $J = 8.0, 0.9$ Hz, 2H), 7.29 – 7.25 (m, 4H), 7.19 – 7.14 (m, 4H), 4.19 (s, 3H), 4.01 (s, 6H), 4.00 (s, 6H).

MS (MALDI-TOF): $m/z = 966.22$ [M+H]⁺, Chemical formula and calcd for C₆₀H₄₃MgN₇O₅ : 965.32.

UV-Vis (CH₂Cl₂) : $\lambda_{\max.}$ (nm) (ϵ (M⁻¹.cm⁻¹) = 662 (4.92×10⁴), 643 (3.20×10⁴), 438 (1.95×10⁴), 395 (3.81×10⁴).

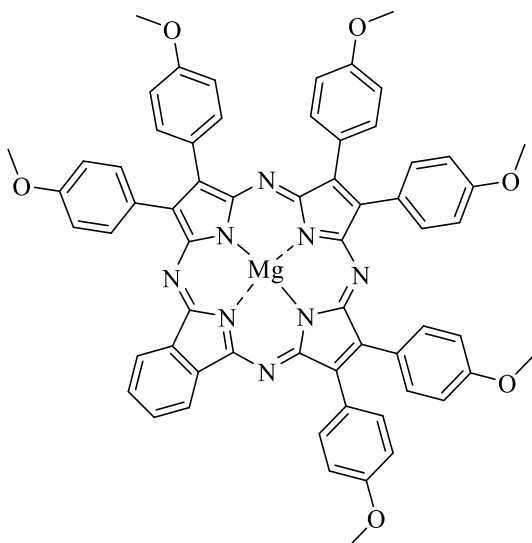
3.10.1.2 Mg-*meso*-(4-methoxyphenyl) ABBB-Ar Pz/Pc hybrid 2.10**2.10**

m.p. 205-209 °C.

¹H NMR (400 MHz, THF-*d*₈) δ (ppm): 9.38 (d, *J* = 7.5 Hz, 1H), 8.50 (d, *J* = 8.7 Hz, 2H), 8.44 – 8.33 (m, 6H), 7.95 (d, *J* = 8.8 Hz, 2H), 7.83 (t, *J* = 7.3 Hz, 1H), 7.57 (d, *J* = 8.4 Hz, 2H), 7.52 – 7.46 (m, 1H), 7.31 – 7.25 (m, 2H), 7.19 – 7.12 (m, 4H), 7.11 – 7.04 (m, 4H), 6.92 (d, *J* = 8.8 Hz, 2H), 6.84 (t, *J* = 8.4 Hz, 3H), 6.68 (d, *J* = 8.5 Hz, 2H), 4.00 (s, 3H), 3.997 (s, 3H), 3.993 (s, 3H), 3.94(s, 3H), 3.95(s, 3H), 3.89 (s, 3H), 3.86 (s, 3H).

MS (MALDI-TOF): *m/z* =1128.72 [M+H]⁺, Chemical formula and calcd for C₇₀H₅₃MgN₇O₇: 1127.39.

UV-Vis (CH₂Cl₂): λ_{max.}(nm) (ε (M⁻¹.cm⁻¹)) = 660 (4.99×10⁴), 626 (3.38×10⁴), 433 (3.29×10⁴), 394 (5.48×10⁴).

3.10.1.3 Mg-ABBB-N Pz/Pc complex 2.19**2.19**

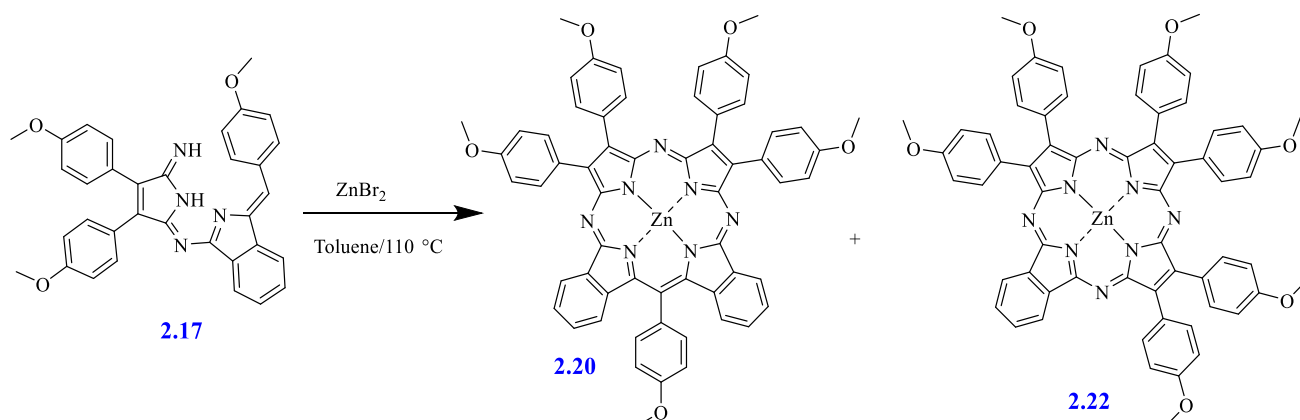
m.p. 185-190 °C.

¹H NMR (500 MHz, THF-*d*₈) δ (ppm): 9.29-9.26 (m, 2H), 8.42 (d, *J* = 8.8 Hz, 4H), 8.37 – 8.32 (m, 8H), 8.13-8.10 (m, 2H), 7.31 – 7.24 (m, 4H), 7.16 – 7.13 (m, 8H), 4.00 (s, 6H), 3.985 (s, 6H), 3.983 (s, 6H).

MS (MALDI-TOF): *m/z* = 1023.54 [M+H]⁺, Chemical formula and calcd for C₆₂H₄₆MgN₈O₆: 1022.34.

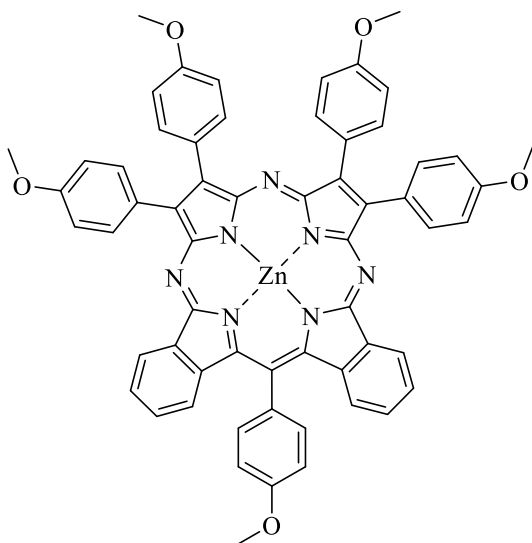
UV-Vis (CH₂Cl₂): λ_{max.}(nm) (ε (M⁻¹.cm⁻¹)) = 672 (2.54 × 10⁴), 639 (6.22 × 10⁴), 378 (3.21 × 10⁴).

3.10.2 Synthesis of Zn-porphyrazine hybrids from dimer **2.17**



A solution of dimer **2.17** (500 mg, 0.92 mmol, 2 equiv.) and ZnBr_2 (156 mg, 0.69 mmol) in toluene (15 mL) was refluxed under a nitrogen atmosphere for 5 h. After the reaction was complete, the solvent was evaporated by passing a stream of an N_2 gas through the reaction flask at high temperatures. The crude product underwent several consecutive column chromatography steps for purification, with fractions separated based on their colours. The first column chromatography was used to remove the impurities, utilizing DCM followed by DCM/THF (5:3) as the eluent. Only the green fraction was subjected to a second column, which was eluted using the THF/petroleum ether system, starting from (2:5) to (3:5), respectively. The first fraction obtained from the green fraction was precipitated by adding methanol and was recrystallized from DCM and methanol, yielding the dark green crystals hybrid **2.20** (75mg, 8%). Further purification of the green fraction was performed using a third column eluted with EtOAc/DCM (5:100). The blue fraction was collected, precipitated with methanol and recrystallized from a DCM / methanol to give Pz **2.22** as azure blue crystals (125mg, 13%).

3.10.2.1 Zn-*meso*-(4-methoxyphenyl) ABBA Pz/Pc hybrid 2.20



2.20

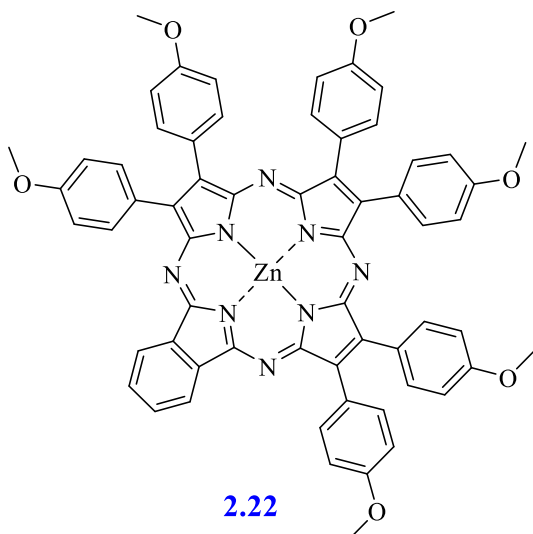
m.p. > 360 °C.

¹H NMR (400 MHz, THF-*d*₈) δ (ppm): 9.46 (dt, *J* = 7.5, 1.0 Hz, 2H), 8.52 – 8.47 (m, 4H), 8.41 – 8.37 (m, 4H), 8.09 – 8.05 (m, 2H), 7.95 (ddd, *J* = 7.8, 7.0, 0.9 Hz, 2H), 7.68 (ddd, *J* = 8.2, 7.0, 1.2 Hz, 2H), 7.57 – 7.51 (m, 2H), 7.32 – 7.26 (m, 6H), 7.19 – 7.14 (m, 4H), 4.20 (s, 3H), 4.01 (s, 6H), 4.00 (s, 6H).

¹³C NMR (101 MHz, THF-*d*₈) δ (ppm): 160.17, 160.00, 156.25, 153.90, 147.84, 140.48, 140.33, 140.02, 138.41, 134.64, 134.56, 133.89, 133.81, 128.56, 128.55, 128.01, 125.88, 123.67, 115.14, 114.10, 114.01, 66.78, 66.56, 55.12.

MS (MALDI-TOF): *m/z* = 1005.83 [M]⁺, Chemical formula and calcd for C₆₀H₄₃ZnN₇O₅: 1005.26.

UV-Vis (CH₂Cl₂): λ_{max}(nm) (ε (dm³·mol⁻¹·cm⁻¹)) = 661 (1.11×10⁵), 643 (6.72×10⁴), 438 (3.21×10⁴), 386 (5.11×10⁴).

3.10.2.2 Zn-ABBB-N Pz/Pc complex 2.22

m.p. > 350 °C.

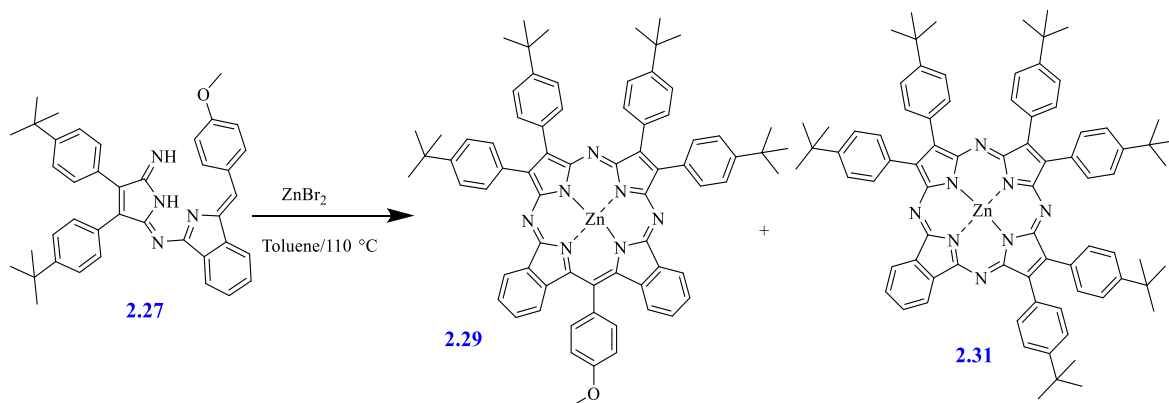
¹H NMR (400 MHz, THF-*d*₈) δ (ppm): 9.21 (dd, *J* = 5.5, 3.0 Hz, 2H), 8.42 – 8.35 (m, 4H), 8.35 – 8.28 (m, 8H), 8.10 (dd, *J* = 5.6, 2.9 Hz, 2H), 7.29 – 7.22 (m, 4H), 7.17 – 7.10 (m, 8H), 4.00 (s, 6H), 3.984 (s, 6H), 3.982 (s, 6H).

¹³C NMR (101 MHz, THF-*d*₈) δ (ppm): 160.21, 160.08, 158.66, 157.17, 156.30, 141.56, 140.36, 140.05, 134.54, 134.49, 134.39, 130.51, 129.92, 127.78, 127.36, 114.18, 114.07, 66.78, 66.56, 55.13.

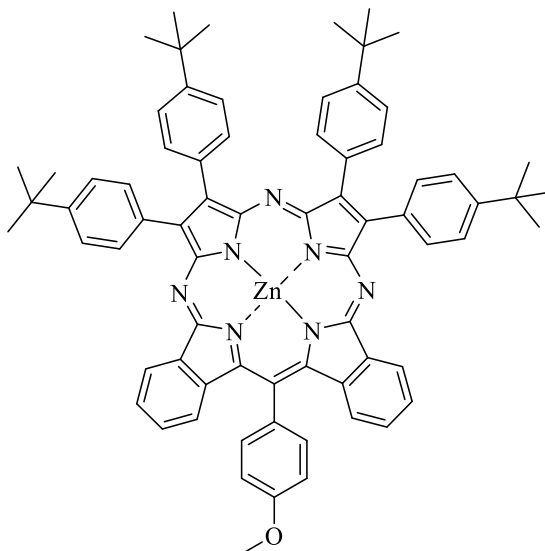
MS (MALDI-TOF): *m/z* = 1062.86 [M]⁺, Chemical formula and calcd for C₆₂H₄₆ZnN₈O₆ 1062.28.

UV-Vis (CH₂Cl₂) : λ_{max}.(nm) (ε (M⁻¹.cm⁻¹)) = 672 (6.66×10⁴), 634 (6.22×10⁴), 366 (6.47×10⁴).

3.11 Synthesis of Zn-porphyrazine hybrids from dimer 2.27



Compound **2.27** (500 mg, 0.8 mmol, 2 eq) and ZnBr₂ (142 mg, 0.6 mmol) were refluxed in toluene (15 mL) under a nitrogen atmosphere for 6 h. After the reaction was complete, the solvent was evaporated by passing a stream of N₂ gas through the reaction flask at a high temperature. Several consecutive column chromatographs purified the crude product. The first column employed a solvent system starting with petroleum ether/DCM (1:1) to pure DCM to remove impurities and isolate the green fraction. The second column, eluted with petroleum ether/THF (6:1), was used to separate the porphyrazine **2.29** from other porphyrizes complexes in the green fraction. The collected product was precipitated with methanol and recrystallized from DCM and methanol to afford dark green crystals of hybrid **2.29** (56 mg, 6%). Further purification of the green fraction was achieved using a third column eluted with petroleum ether/THF (20:1). The blue fraction was collected, precipitated with methanol, and recrystallized from DCM / methanol, yielding azure blue crystals of compound **2.31** (98 mg, 10%).

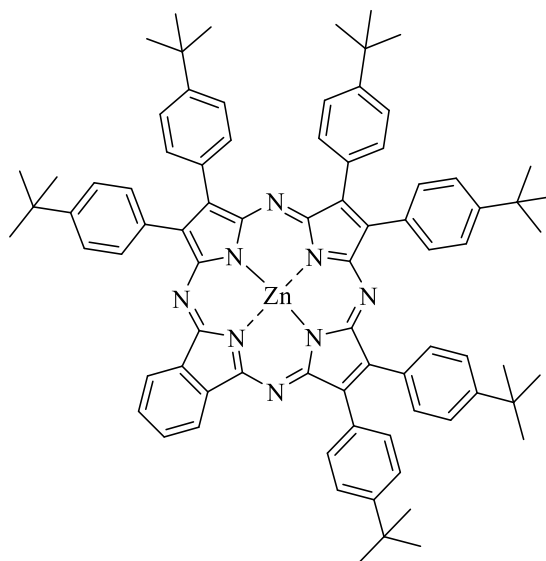
3.11.1 Zn-meso-(4-methoxyphenyl) ABBA Pz/Pc hybrid 2.29**2.29**

m.p. >350 °C.

¹H NMR (400 MHz, THF-*d*₈) δ (ppm): 9.46 (d, *J* = 7.5 Hz, 2H), 8.55 – 8.48 (m, 4H), 8.48 – 8.43 (m, 4H), 8.11 – 8.04 (m, 2H), 7.97 (t, *J* = 7.3 Hz, 2H), 7.80 – 7.75 (m, 4H), 7.67 (dd, *J* = 7.9, 5.9 Hz, 6H), 7.58 – 7.52 (m, 2H), 7.32 (d, *J* = 8.0 Hz, 2H), 4.20 (s, 3H), 1.55 (br-s, 36H).

MS (MALDI-TOF): *m/z* = 1109.98 [M]⁺, Chemical formula and calcd for C₇₂H₆₇N₇OZn: 1109.47.

UV-Vis (CH₂Cl₂): λ_{max.} (nm) (ε (M⁻¹.cm⁻¹)) = 657 (1.03×10⁵), 640 (6.46×10⁴), 436 (3.79×10⁴), 389 (5.18×10⁴).

3.11.2 Zn-ABBB-N Pz/Pc complex 2.31**2.31**

m.p. >350 °C.

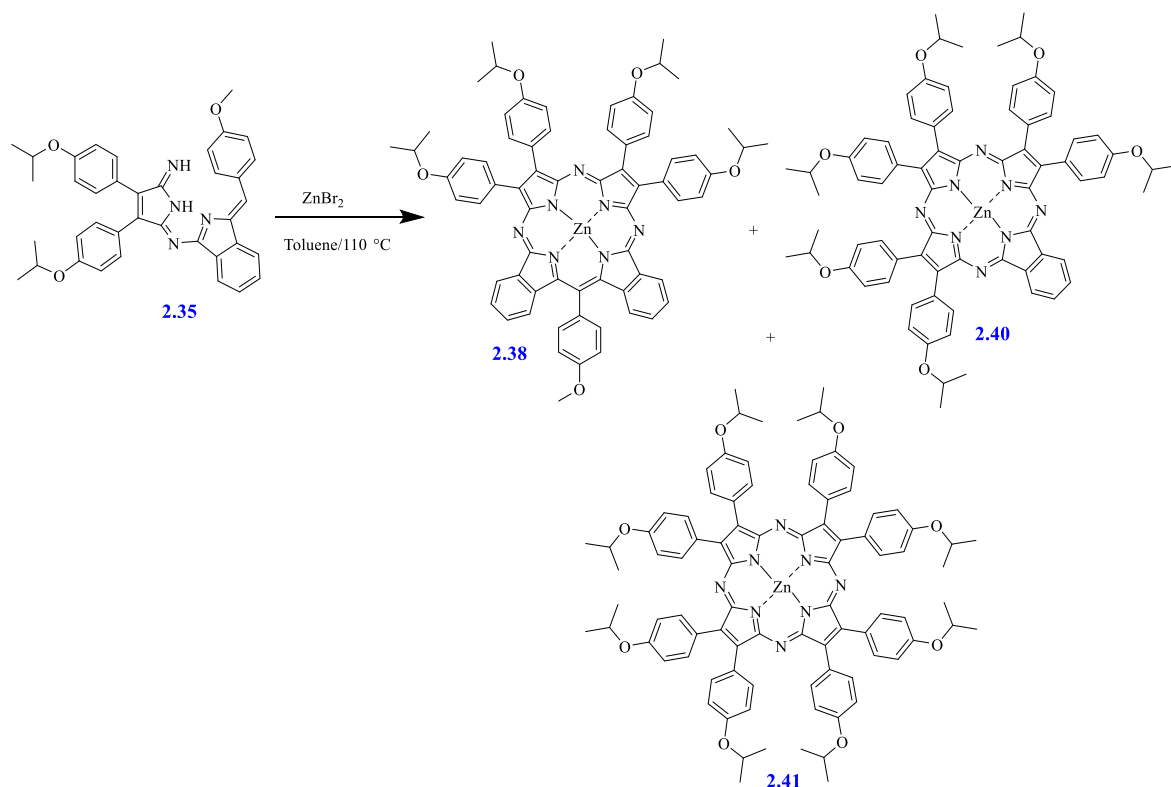
¹H NMR (400 MHz, THF-*d*₈) δ (ppm): 9.25 (dd, *J* = 5.5, 3.0 Hz, 2H), 8.45 – 8.32 (m, 12H), 8.15 (dd, *J* = 5.6, 2.9 Hz, 2H), 7.78 – 7.73 (m, 4H), 7.64 (dd, *J* = 8.5, 2.7 Hz, 8H), 1.56 (s, 18H), 1.53 (s, 18H), 1.53 (s, 18H).

¹³C NMR (101 MHz, THF-*d*₈) δ (ppm): 175.68, 175.57, 171.37, 158.90, 158.88, 157.76, 157.31, 156.72, 156.43, 155.23, 154.57, 150.92, 150.85, 149.98, 149.06, 142.62, 141.70, 140.65, 133.30, 133.26, 133.21, 132.74, 130.50, 125.51, 125.47, 125.43, 123.65, 66.91, 66.69, 35.21, 31.79, 31.76, 31.67, 30.38, 24.84, 24.65.

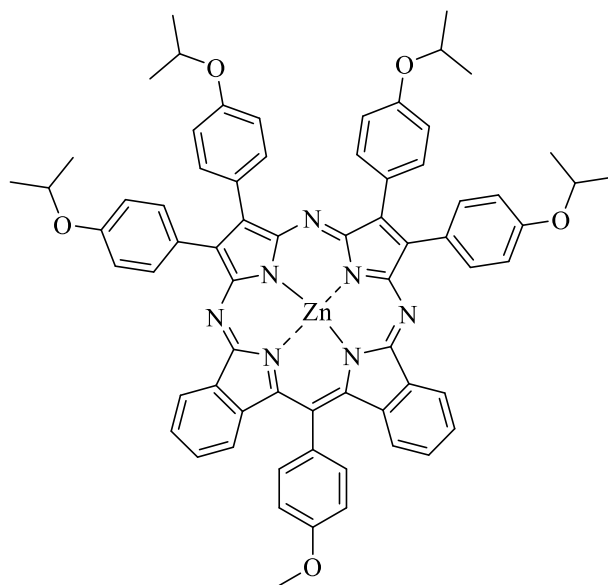
MS (MALDI-TOF): *m/z* = 1218.59[M]⁺, Chemical formula and calcd for C₈₀H₈₂N₈Zn: 1218.60.

UV-Vis (CH₂Cl₂) : λ_{max}(nm) (ε (M⁻¹.cm⁻¹)) = 666 (7.75×10⁴), 627 (7.9×10⁴), 367 (9.45×10⁴).

3.12 Synthesis of Zn-porphyrazine hybrids from dimer 2.35



Dimer **2.35** (500 mg, 0.84 mmol, 2 equiv.) and ZnBr₂ (141.5 mg, 0.6mmol) were dissolved in toluene (15 mL) and refluxed under a nitrogen atmosphere for 6 h. After the reaction was complete, the solvent was evaporated by passing a stream of N₂ gas through the reaction flask at a high temperature. The crude product was purified through multiple consecutive column chromatographs. The first column chromatography employed a petroleum ether/DCM (1:1) elution system, transitioning to pure DCM to remove impurities and isolate the green fraction. This green fraction was loaded onto a second column, and the target compound **2.38** was separated using DCM/EtOAc (100:1) → (3:5), respectively. The collected product was precipitated with methanol and recrystallized from a DCM / methanol to give light green crystals (75 mg, 8%). Further purification of the green fraction was performed using a third column with petroleum ether/THF (5:1) as the eluent. The blue fraction was collected and precipitated with methanol, followed by recrystallization from DCM and methanol to afford compound **2.40** as azure blue crystals (120 mg, 12%). The remainder green fraction was subjected to additional column chromatography, again using petroleum ether /THF (5:1) as the eluent. The final green fraction was collected, precipitated with methanol, and recrystallized from DCM and methanol, yielding pz **2.41** as dark green crystals (25 mg, 2%).

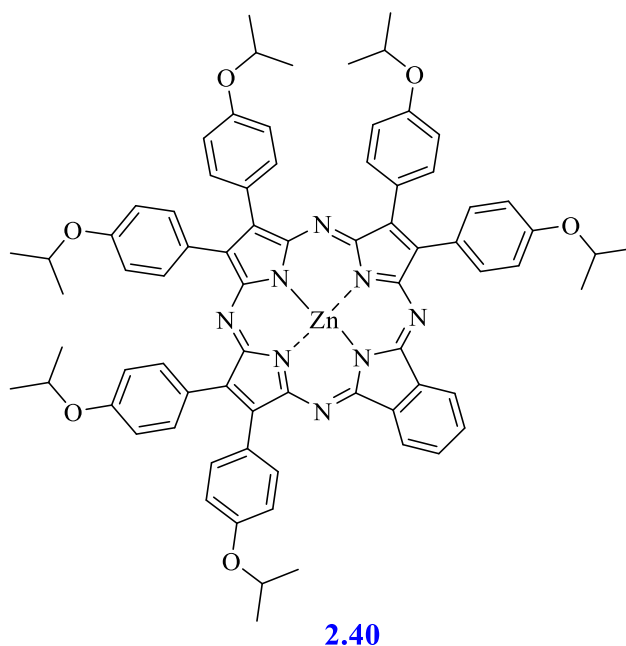
3.12.1 Zn-*meso*-(4-methoxyphenyl) ABBA Pz/Pc hybrid 2.38**2.38**

m.p. > 350 °C.

¹H NMR (500 MHz, acetone-*d*₆) δ (ppm): 9.34 (d, *J* = 7.3 Hz, 2H), 8.26 (m, 4H), 8.13 (m, 4H), 8.03 (d, *J* = 7.8 Hz, 2H), 7.95 (t, *J* = 7.4 Hz, 2H), 7.69 (t, *J* = 7.5 Hz, 2H), 7.54 (d, *J* = 7.8 Hz, 2H), 7.28 (d, *J* = 8.2 Hz, 4H), 7.18 (d, *J* = 8.0 Hz, 2H), 7.11 (d, *J* = 8.1 Hz, 4H), 4.95 – 4.83 (m, 4H), 4.25 (s, 3H), 1.55 (d, *J* = 6.0 Hz, 12H), 1.53(d, 6.0 Hz, 12 H).

MS (MALDI-TOF): *m/z* = 1117.70 [M]⁺, Chemical formula and calcd for C₆₈H₅₉N₇O₅Zn: 1117.39.

UV-Vis (CH₂Cl₂) : λ_{max}(nm) (ε (M⁻¹.cm⁻¹)) = 663 (4.03×10⁴), 646 (3.04×10⁴), 439 (1.31×10⁴), 376 (2.70×10⁴).

3.12.2 Zn-ABBB-N Pz/Pc complex 2.40

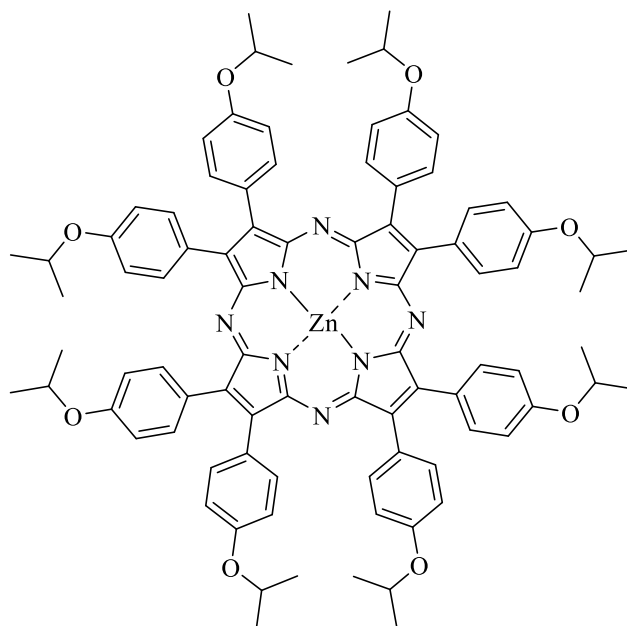
m.p. > 350 °C.

¹H NMR (400 MHz, THF-*d*₈) δ (ppm): 9.19 (dd, *J* = 5.5, 3.0 Hz, 2H), 8.41 – 8.34 (m, 4H), 8.34 – 8.25 (m, 8H), 8.09 (dd, *J* = 5.6, 2.9 Hz, 2H), 7.26 – 7.19 (m, 4H), 7.14 – 7.05 (m, 8H), 4.88 – 4.76 (m, 6H), 1.57-1.42(m, 36H).

¹³C NMR (101 MHz, THF-*d*₈) δ (ppm):159.59, 159.51, 159.45, 159.30, 157.67, 157.42, 157.03, 142.44, 141.35, 140.89, 135.62, 135.57, 135.49, 128.57, 128.48, 128.33, 124.39, 116.72, 70.87, 68.58, 68.45, 68.23, 26.46, 26.33, 26.25, 26.13, 23.29, 23.21.

MS (MALDI-TOF): *m/z* = 1230.57[M]⁺, Chemical formula and calcd for C₇₄H₇₀N₈O₆Zn: 1230.47.

UV-Vis (CH₂Cl₂) : λ_{max.} (nm)(ε (M⁻¹.cm⁻¹)) = 674 (1.07×10⁵), 639 (9.99×10⁴), 367 (1.05×10⁴).

3.12.3 Porphyrazine complex Zn-BBBB 2.41**2.41**

m.p. > 350 °C.

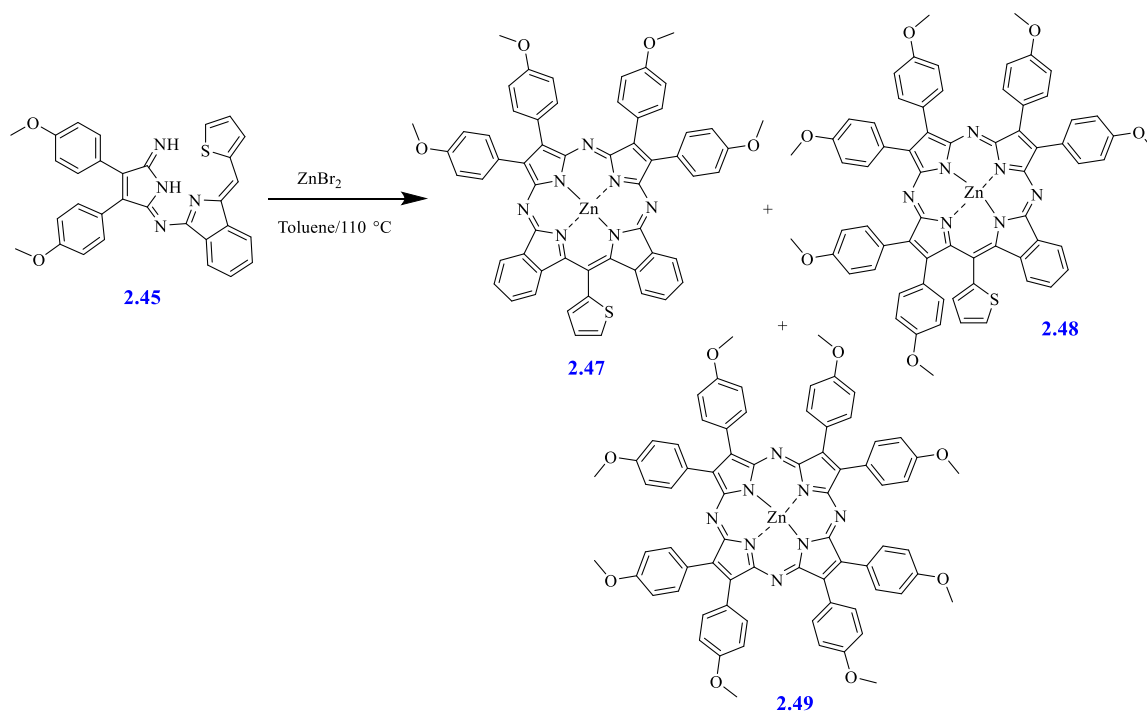
¹H NMR (400 MHz, THF-*d*₈) δ (ppm): 8.36 – 8.27 (m, 16H), 7.14 – 7.07 (m, 16H), 4.80 (hept, *J* = 5.7 Hz, 8H), 1.48 (d, *J* = 6.1 Hz, 48H).

¹³C NMR (101 MHz, THF-*d*₈) δ (ppm): 158.97, 158.29, 141.50, 135.19, 127.95, 116.30, 70.44, 68.15, 68.01, 26.02, 25.89, 22.85.

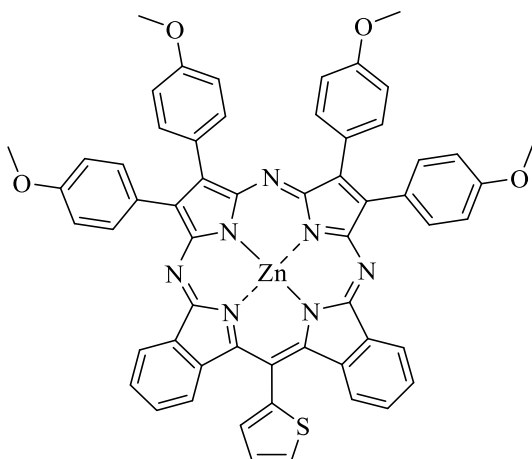
MS (MALDI-TOF): *m/z* = 1448.70[M]⁺, Chemical formula and calcd for C₈₈H₈₈N₈O₈Zn: 1448.60.

UV-Vis (THF) :λ_{max.}(nm) (ε (M⁻¹.cm⁻¹)) = 653 (2.04×10⁵), 379 (1.56×10⁵).

3.13 Synthesis of Zn-porphyrazine hybrids from dimer 2.45



Dimer **2.45** (500 mg, 0.96 mmol, 2 equiv.) and ZnBr_2 (0.16 mg, 0.72 mmol) were dissolved in toluene (25 mL) and refluxed under a nitrogen atmosphere for 12 h. Upon completion, the solvent was removed by passing a stream of N_2 gas through the reaction flask at a high temperature. The crude product underwent purification through several consecutive column chromatographs. The first column was used to remove the impurities, employing DCM followed by DCM/THF (10:1) systems as the eluent. Only the green fraction was submitted to the second column, using gradient elution from DCM/EtOAc (100:3) to (3:4). The first fraction obtained was hybrid **2.47**, which was precipitated with methanol and recrystallized from DCM and methanol to give dark green crystals (94 mg, 10%). Further purification of the green fraction was performed using a third column eluted with EtOAc/DCM. The next green fraction was collected and precipitated with methanol to yield Pz **2.48** as a green solid (55 mg, 5%). The final fraction was purified by silica gel chromatography with EtOAc/DCM as the eluent, the target product was collected, precipitated with methanol, to afford porphyrazine **2.49** as a dark green solid (22 mg, 2%).

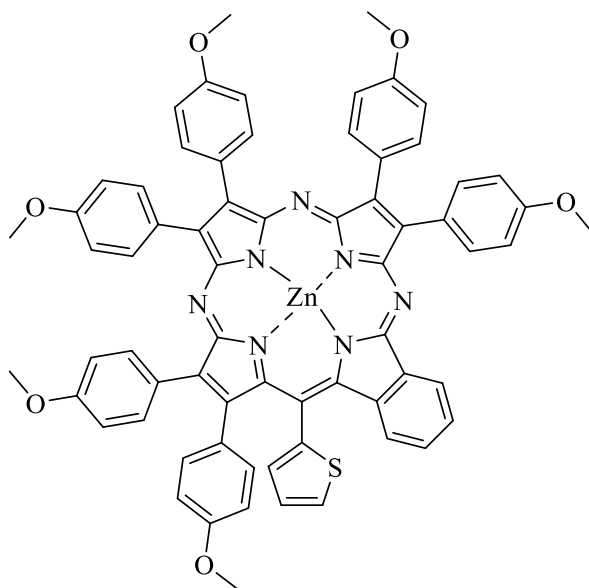
3.13.1 Zn-meso-(4-thiophene) ABBA Pz/Pc hybrid 2.47**2.47**

m.p. > 350 °C.

¹H NMR (400 MHz, THF-*d*₈) δ(ppm): 9.46 (dd, *J* = 7.5, 1.0 Hz, 2H), 8.53 – 8.45 (m, 4H), 8.42 – 8.35 (m, 4H), 8.23 (dd, *J* = 5.3, 1.2 Hz, 1H), 8.03 – 7.96 (m, 2H), 7.94 (dd, *J* = 3.4, 1.3 Hz, 1H), 7.80 – 7.72 (m, 3H), 7.41 (dd, *J* = 8.0, 0.9 Hz, 2H), 7.32 – 7.25 (m, 4H), 7.19 – 7.13 (m, 4H), 4.00 (s, 6H), 3.99 (s, 6H).

MS (MALDI-TOF): *m/z* = 982.06 [M+H]⁺, Chemical formula and calcd for C₅₇H₃₉N₇O₄SZn: 981.21.

UV-Vis (CH₂Cl₂): λ_{max}(nm) (ε(M⁻¹.cm⁻¹)) = 660(3.9×10⁴), 645 (2.9×10⁴), 437 (1.4×10⁴), 377 (2.5×10⁴).

3.13.2 Zn-meso-(4-thiophene) ABBB-Ar Pz/Pc hybrid 2.48**2.48**

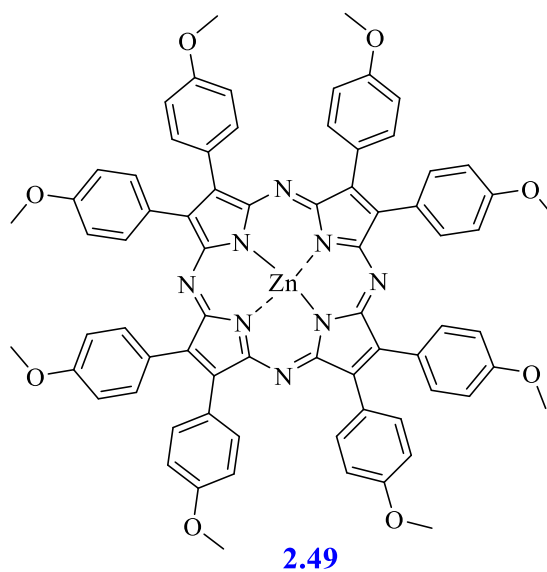
m.p. > 350 °C.

¹H NMR (400 MHz, THF-*d*₈) δ (ppm): 9.39 (dt, *J* = 7.6, 1.0 Hz, 1H), 8.51 – 8.46 (m, 2H), 8.41 – 8.33 (m, 6H), 7.96 – 7.88 (m, 3H), 7.63 – 7.58 (m, 2H), 7.35 (dd, *J* = 3.5, 1.2 Hz, 1H), 7.31 – 7.25 (m, 4H), 7.19 – 7.13 (m, 4H), 7.09 – 7.04 (m, 2H), 7.00 (dd, *J* = 5.3, 3.4 Hz, 1H), 6.96 – 6.92 (m, 2H), 6.86 (d, *J* = 8.0 Hz, 1H), 6.77 (d, *J* = 8.0 Hz, 2H), 4.0 (s, 3H), 3.995 (s, 3H), 3.991 (s, 3H), 3.94 (s, 3H), 3.89 (s, 3H), 3.86 (s, 3H).

MS (MALDI-TOF): *m/z* = 1143.81 [M]⁺, Chemical formula and calcd for C₆₇H₄₉N₇O₆SZn: 1143.28.

UV-Vis (CH₂Cl₂): λ_{max.}(nm) (ε (M⁻¹.cm⁻¹)) = 662 (6.26×10⁴), 625 (4.04×10⁴), 426 (3.23×10⁴), 389 (5.15×10⁴).

3.13.3 Porphyrazine complex Zn-BBBB 2.49



m.p. > 350 °C.

¹H NMR, ¹³C NMR: The pure compound is poorly soluble, even in THF solvent.

MS (MALDI-TOF): $m/z = 1225.68$ $[M^+H]^+$, Chemical formula and calcd for $C_{72}H_{56}N_8O_8Zn$: 1224.35

UV-Vis (THF): λ_{max} . (nm) (ϵ ($M^{-1}\cdot cm^{-1}$)) = 651 (2.2×10^5), 381 (1.6×10^5).

References

- (1) Milgrom, L. R. *The Colours of Life: An introduction to the Chemistry of Porphyrins and Related Compounds*; Oxford university press, **1997**.
- (2) Shimizu, S. Recent advances in subporphyrins and triphyrin analogues: Contracted porphyrins comprising three pyrrole rings. *Chem. Rev.* **2017**, *117* (4), 2730-2784.
- (3) McEvoy, J. P.; Brudvig, G. W. Water-splitting chemistry of photosystem II. *Chem. Rev.* **2006**, *106* (11), 4455-4483.
- (4) Shimizu, D.; Osuka, A. Porphyrinoids as a platform of stable radicals. *Chemical Science* **2018**, *9* (6), 1408-1423.
- (5) Willstätter, R.; Stoll, A. *Untersuchungen über Chlorophyll Methoden und Ergebnisse*; Verlag von Julius Springer, Berlin, **1913**.
- (6) Lightner, D. A.; Lightner, D. A. The Status of Bilirubin in 1930. *Bilirubin: Jekyll and Hyde Pigment of Life: Pursuit of Its Structure Through Two World Wars to the New Millennium* **2013**, 357-431.
- (7) Senge, M. O.; Sergeeva, N. N.; Hale, K. J. Classic highlights in porphyrin and porphyrinoid total synthesis and biosynthesis. *Chem. Soc. Rev.* **2021**, *50* (7), 4730-4789.
- (8) Moss, G. P. Nomenclature of tetrapyrroles: recommendations 1986. *European journal of biochemistry* **1988**, *178* (2), 277-328.
- (9) Almutairi, T. Synthetic studies towards multichromophore arrays. University of East Anglia, 2015.
- (10) Rothmund, P. A new porphyrin synthesis. The synthesis of porphin. *J. Am. Chem. Soc.* **1936**, *58* (4), 625-627.
- (11) Semeikin, A.; Koifman, O.; Berezin, B. Synthesis of tetraphenylporphins with active groups in the phenyl rings. 1. Preparation of tetrakis (4-aminophenyl) porphin. *Chemistry of heterocyclic compounds* **1982**, *18* (10), 1046-1047.
- (12) Adler, A. D.; Longo, F. R.; Finarelli, J. D.; Goldmacher, J.; Assour, J.; Korsakoff, L. A simplified synthesis for meso-tetraphenylporphine. *J. Org. Chem.* **1967**, *32* (2), 476-476.
- (13) Lindsey, J. S.; Hsu, H. C.; Schreiman, I. C. Synthesis of tetraphenylporphyrins under very mild conditions. *Tetrahedron lett* **1986**, *27* (41), 4969-4970.

-
- (14) Lindsey, J. S.; Schreiman, I. C.; Hsu, H. C.; Kearney, P. C.; Marguerettaz, A. M. Rothmund and Adler-Longo reactions revisited: synthesis of tetraphenylporphyrins under equilibrium conditions. *J. Org. Chem.* **1987**, *52* (5), 827-836.
- (15) Sessler, J. L.; Mozaffari, A.; Johnson, M. R. 3, 4-Diethylpyrrole and 2, 3, 7, 8, 12, 13, 17, 18-Octaethylporphyrin: Pyrrole, 3, 4-diethyl and 21H, 23H-Porphine, 2, 3, 7, 8, 12, 13, 17, 18-octaethyl-. *Organic Syntheses* **2003**, *70*, 68-68.
- (16) Eisner, U.; Lichtarowicz, A.; Linstead, R. P. 142. Chlorophyll and related compounds. Part VI. The synthesis of octaethylchlorin. *J. Chem. Soc. (Resumed)* **1957**, 733-739.
- (17) Aoyagi, K.; Haga, T.; Toi, H.; Aoyama, Y.; Mizutani, T.; Ogoshi, H. Electron Deficient Porphyrins III. Facile Syntheses of Perfluoroalkylporphyrins Including Water Soluble Porphyrin. *Bulletin of the Chemical Society of Japan* **1997**, *70* (4), 937-943.
- (18) Bohandy, J. SPECTROSCOPY OF PORPHYRINS. *APL Tech.Dig* **1981**, *2*, 153-163.
- (19) Nasri, H. Porphyrins and metalloporphyrins: an overview. *2020 IEEE International Conference on Design & Test of Integrated Micro & Nano-Systems (DTS)* **2020**, 1-6. DOI: 10.1109/DTS48731.2020.9196129.
- (20) Giovannetti, R. The use of spectrophotometry UV-Vis for the study of porphyrins. *Macro to nano spectroscopy* **2012**, 87-108.
- (21) Caughey, W. S.; Koski, W. Nuclear magnetic resonance spectra of porphyrins. *Biochemistry* **1962**, *1* (5), 923-931.
- (22) Al Neyadi, S. S.; Alzamly, A.; Al-Hemyari, A.; Tahir, I. M.; Al-Meqbali, S.; Ali Ahmad, M.; Bufaroosha, M. An undergraduate experiment using microwave-assisted synthesis of metalloporphyrins: Characterization and spectroscopic investigations. *World J. Chem.wo* **2019**, *7* (1), 26-32.
- (23) Braun, A. v.; Tcherniac, J. Über die produkte der einwirkung von acetanhydrid auf phthalamid. *Berichte der deutschen chemischen Gesellschaft* **1907**, *40* (2), 2709-2714.
- (24) De Diesbach, H.; Von Der Weid, E. Some salt complexes of o-dinitriles with copper and pyridine. *Helv. Chim. Acta* **1927**, *10*, 886-888.
- (25) Dandridge, A.; Drescher, H.; Thomas, J. British Patent 322, 169. *Scottish Dyes, Ltd.) May* **1929**, *16*.
- (26) Linstead, R. P. 212. Phthalocyanines. Part I. A new type of synthetic colouring matters. *J. Chem. Soc. (Resumed)* **1934**, 1016-1017.
- (27) Robertson, J.; An, X. ray study of the structure of the phthalocyanines: the metal- free, nickel, copper and platinum complexes. **1935**, *615* 621.
-

-
- (28) Nexelson, F. Novel oligomeric phthalocyanines and a new synthesis of tetrabenzotriazaporphyrin. University of East Anglia, Norwich, University of East Anglia, Norwich, 2005.
- (29) Alharbi, N.; Tizzard, G. J.; Coles, S. J.; Cook, M. J.; Cammidge, A. N. First examples of functionalisation of meso-aryl tetrabenzotriazaporphyrins (TBTAPs) through cross-coupling reactions. *Tetrahedron* **2015**, *71* (39), 7227-7232.
- (30) Díaz-Moscoso, A.; Tizzard, G. J.; Coles, S. J.; Cammidge, A. N. Synthesis of meso-Substituted Tetrabenzotriazaporphyrins: Easy Access to Hybrid Macrocycles. *Angewandte Chemie* **2013**, *125* (41), 10984-10987.
- (31) Booth, G. The Chemistry of Synthetic Dyes. by K. Venkataraman, Academic Press, New York and London **1971**, 5. Lux, F. In Kevane, CJ; Moeller, T. In Proc. Rare Earth Res. Conf. 10th, 1973.
- (32) Erka, P.; Hengelsberg, H. Phthalocyanine Dyes and 119 Pigments. *The Porphyrin Handbook: Applications of Phthalocyanines* **2003**, *19*, 106.
- (33) Mack, J.; Kobayashi, N. Low symmetry phthalocyanines and their analogues. *Chem. Rev.* **2011**, *111* (2), 281-321.
- (34) Leznoff, C.; Lever, A. phthalocyanines Properties and Applications. *VCH, New York* **1989**, *4*.
- (35) Baumann, F.; Bienert, B.; Rösch, G.; Vollmann, H.; Wolf, W. Isoindolenine als Zwischenprodukte der Phthalocyanin-Synthese. *Angewandte Chemie* **1956**, *68* (4), 133-150.
- (36) Max, W. Process for producing coloring matters of the phthalocyanine series. *U.S. Patent* **1940**, *2,197,458*.
- (37) Elvidge, J. A.; Linstead, R. P. Conjugated macrocycles. Part XXVII. The formation of tetrazaporphins from imidines. Tribenzotetrazaporphin. *J. Chem. Soc. (Resumed)* **1955**, 3536-3544.
- (38) Pawlowski, G.; Hanack, M. A convenient synthesis of trifluoromethyl substituted phthalocyanines. *Synthetic Communications* **1981**, *11* (5), 351-363.
- (39) Sakamoto, K.; Ohno-Okumura, E. Syntheses and functional properties of phthalocyanines. *Materials* **2009**, *2* (3), 1127-1179.
- (40) Barrett, P. A.; Dent, C. E.; Linstead, R. P. 382. Phthalocyanines. Part VII. Phthalocyanine as a co-ordinating group. A general investigation of the metallic derivatives. *J. Chem. Soc. (Resumed)* **1936**, 1719-1736.
- (41) Cammidge, A. N.; Chambrier, I.; Cook, M. J.; Sosa-Vargas, L. 75 Synthesis and Properties of the Hybrid Phthalocyanine-Tetrabenzoporphyrin Macrocycles. In *Handbook of*
-

Porphyrin Science: With Applications to Chemistry, Physics, Materials Science, Engineering, Biology and Medicine—Volume 16: Synthetic Developments (Part I), World Scientific, **2012**; pp 331-404.

(42) Helberger, J. H. *Lie. Ann* **1937**, 529, 205-218.

(43) Linstead, R. P.; Rowe, G. A. 195. Phthalocyanines and related compounds. Part XVII. Intermediates for the preparation of tetrabenzporphyrins: acids derived from phthalimidine. *J. Chem. Soc. (Resumed)* **1940**, 1070-1076.

(44) B. Kalleta, M. R., W. Wolf, and D. R. Terrell. *German Patent* **1991**, 39 37 716 A711.

(45) Barrett, P. A.; Linstead, R. P.; Tuey, G.; Robertson, J. 371. Phthalocyanines and related compounds. Part XV. Tetrabenztriazaporphin: its preparation from phthalonitrile and a proof of its structure. With a note on a preliminary X-ray investigation. *J. Chem. Soc.(Resumed)* **1939**, 1809-1820.

(46) Leznoff, C. C.; McKeown, N. B. Preparation of substituted tetrabenzotriazaporphyrins and a tetranaphthotriazaporphyrin: a route to mono-meso-substituted phthalocyanine analogs. *J. Org. Chem.* **1990**, 55 (7), 2186-2190.

(47) Cammidge, A. N.; Chambrier, I.; Cook, M. J.; Hughes, D. L.; Rahman, M.; Sosa-Vargas, L. Phthalocyanine Analogues: Unexpectedly Facile Access to Non-Peripherally Substituted Octaalkyl Tetrabenzotriazaporphyrins, Tetrabenzodiazaporphyrins, Tetrabenzomonoazaporphyrins and Tetrabenzoporphyrins. *Chem.-Eur. J.* **2011**, 17 (11), 3136-3146.

(48) Alharbi, N.; Díaz-Moscoso, A.; Tizzard, G. J.; Coles, S. J.; Cook, M. J.; Cammidge, A. N. Improved syntheses of meso-aryl tetrabenzotriazaporphyrins (TBTAPs). *Tetrahedron* **2014**, 70 (40), 7370-7379.

(49) Hellal, M.; Cuny, G. D. Microwave assisted copper-free Sonogashira coupling/5-exo-dig cycloisomerization domino reaction: access to 3-(phenylmethylene) isoindolin-1-ones and related heterocycles. *Tetrahedron lett* **2011**, 52 (42), 5508-5511.

(50) Gretton, J. Phthalocyanine and Subphthalocyanine hybrid macrocycles: improved accessibility and synthetic control via new intermediates. University of East Anglia, **2022**.

(51) Cong, L. Electrochemical and Chemical Investigations of Various Substituted Porphyrins, Chlorins and Porphyrazines. University of Houston, **2019**.

(52) Mori, G. D. Novel classes of porphyrazine macrocycles: effect of-delocalization, exocyclic coordination and quaternization processes. University of Rome Sapienza Italy, University of Rome Sapienza Italy, **2012**.

- (53) Linstead, R. P.; Whalley, M. 944. Conjugated macrocycles. Part XXII. Tetrazaporphin and its metallic derivatives. *Journal of the Chemical Society (Resumed)* **1952**, 4839-4846.
- (54) Luk'yanets, E. A. *Zh. Org. Khim* **1971**, 7, 369.
- (55) Renjie, L.; Dongdong, Q.; Jianzhuang, J.; Yongzhong, B. Benzo-fused low symmetry metal-free tetraazaporphyrin and phthalocyanine analogs: synthesis, spectroscopy, electrochemistry, and density functional theory calculations. *Journal of Porphyrins and Phthalocyanines* **2010**, 14 (05), 421-437.
- (56) Michel, S. L.; Hoffman, B. M.; Baum, S. M.; Barrett, A. G. Peripherally functionalized porphyrazines: novel metallomacrocycles with broad, untapped potential. *Progress in inorganic chemistry* **2001**, 50, 473-590.
- (57) Güzel, E.; Yarasir, M. N.; Özkaya, A. R. Low symmetry solitaire-and trans-functional porphyrazine/phthalocyanine hybrid complexes: Synthesis, isolation, characterization, and electrochemical and in-situ spectroelectrochemical properties. *Synthetic Metals* **2020**, 262, 116331.
- (58) Rodríguez-Morgade, M.; Torres, T. 17.9. 24 Phthalocyanines and Related Compounds. *Science of Synthesis Knowledge Updates* **2017**, 2, 146-149.
- (59) Güzel, E.; Medina, D.-P.; Medel, M.; Kandaz, M.; Torres, T.; Rodríguez-Morgade, M. S. A versatile, divergent route for the synthesis of ABAC tetraazaporphyrins: molecularly engineered, push-pull phthalocyanine-type dyes. *J. Mater. Chem. C* **2021**, 9 (33), 10802-10810.
- (60) Cook, A. H.; Linstead, R. P. 189. Phthalocyanines. Part XI. The preparation of octaphenylporphyrazines from diphenylmaleinitrile. *J. Chem. Soc. (Resumed)* **1937**, 929-933.
- (61) L. S. Beall, N. S. M., A. J. P. White, D. J. Williams, A. G. M. Barrett, and Hoffman, B.M. J. . *Org. Chem* **1998**, 63, 5806 - 5818. Steyn, A. M. Rand Afrikaans University South Africa, Rand Afrikaans University South Africa, 2000.
- (62) Baumann, T. F.; Barrett, A. G.; Hoffman, B. M. Porphyrazine binaries: synthesis, characterization, and spectroscopy of a metal-linked trinuclear porphyrazine dimer. *Inorganic Chemistry* **1997**, 36 (24), 5661-5665.
- (63) Yeh, H. C.; Wu, W. C.; Wen, Y. S.; Dai, D. C.; Wang, J. K.; Chen, C. T. Derivative of α , β -dicyanostilbene: Convenient precursor for the synthesis of diphenylmaleimide compounds, E-Z isomerization, crystal structure, and solid-State fluorescence. *J. Org. Chem.* **2004**, 69 (19), 6455-6462.
- (64) Joslin, E. E.; Zaragoza, J. P. T.; Baglia, R. A.; Siegler, M. A.; Goldberg, D. P. The influence of peripheral substituent modification on PV, MnIII, and MnV (O) corrolazines: X-

-
- ray crystallography, electrochemical and spectroscopic properties, and HAT and OAT reactivities. *Inorganic chemistry* **2016**, *55* (17), 8646-8660.
- (65) Rodríguez-Morgade, M. S.; Stuzhin, P. A. The chemistry of porphyrazines: an overview. *Journal of Porphyrins and Phthalocyanines* **2004**, *8* (09), 1129-1165.
- (66) Dmitrieva, O.; Ivanova, Y. B.; Semeikin, A.; Mamardashvili, N. Fluorescence properties and quantum-chemical modeling of tert-butyl-substituted porphyrazines: Structural and ionization effect. *Spectrochimica Acta Part A: Molecular and Biomolecular Spectroscopy* **2020**, *240*, 118601.
- (67) Malyasova, A.; Potekhina, O.; Aleksandriiskii, V.; Khelevina, O. Synthesis of Mg (II) Complexes of Phenyltetraazaporphyrins. *Russ. J. Gen. Chem.* **2017**, *87*, 3059-3062.
- (68) Montalban, A. G.; Jarrell, W.; Riguet, E.; McCubbin, Q. J.; Anderson, M. E.; White, A. J.; Williams, D. J.; Barrett, A. G.; Hoffman, B. M. Bis (dimethylamino) porphyrazines: Synthetic, structural, and spectroscopic investigations. *J. Org. Chem.* **2000**, *65* (8), 2472-2478.
- (69) Sibert, J. W.; Baumann, T. F.; Williams, D. J.; White, A. J.; Barrett, A.; Hoffman, B. M. Gemini-porphyrazines: the synthesis and characterization of metal-capped cis-and trans-porphyrazine tetrathiolates. *J. Am. Chem. Soc.* **1996**, *118* (43), 10487-10493.
- (70) Cheng, K. F. *Synthesis and characterization of supramolecular porphyrin and porphyrazine photonic materials and synthesis of a covalent base pair of DNA*; City University of New York, **2004**.
- (71) Vagin, S. I.; Hanack, M. Synthesis and Spectroscopic Properties of Non-Symmetrical Benzo-Annulated Porphyrazines and Their Metal Complexes. *Eur. J. Org. Chem.* **2002**, (16), 2859-2865.
- (72) Nie, H.; Barrett, A. G.; Hoffman, B. M. Porphyrazinehexamines and dinitroporphyrazines: synthesis, characterization, and complementary electrochemistry. *J. Org. Chem.* **1999**, *64* (18), 6791-6796.
- (73) Lee, S.; White, A. J.; Williams, D. J.; Barrett, A. G.; Hoffman, B. M. Synthesis of near-IR absorbing/emitting porphyrazine derivatives with tunable solubility. *J. Org. Chem.* **2001**, *66* (2), 461-465.
- (74) Stihler, P.; Hauschel, B.; Hanack, M. Synthesis of a bisdienophilic phthalocyanine and of precursors for repetitive Diels-Alder reactions based on hemiporphyrazines and phthalocyanines. *Chemische Berichte* **1997**, *130* (6), 801-806.
- (75) Mlynarczyk, D. T.; Ziental, D.; Kolasinski, E.; Sobotta, L.; Koczorowski, T.; Mielcarek, J.; Goslinski, T. Nipagin-Functionalized Porphyrazine and Phthalocyanine—Synthesis,
-

-
- Physicochemical Characterization and Toxicity Study after Deposition on Titanium Dioxide Nanoparticles P25. *Molecules* **2021**, *26* (9), 2657.
- (76) Giovannetti, R. *The use of spectrophotometry UV-Vis for the study of porphyrins*; InTech, **2012**.
- (77) Arabei, S.; Kuzmitsky, V.; Solovyov, K. Manifestation of the vibronic analogue of the Fermi resonance in quasi-line spectra of porphyrins: Experiment and theoretical analysis. *Optics and Spectroscopy* **2007**, *102*, 692-704.
- (78) Dufour, S. R. *Synthesis of polyionic tetraazaporphyrins and their Langmuir-Blodgett properties*; Library and Archives Canada= Bibliothèque et Archives Canada, Ottawa, **2007**.
- (79) Abdulhamied, E. First Synthesis of Amphiphilic Octa-Alkylthio Substituted Tetraazaporphyrin Derivatives with Four Terminal Carboxylic Acid Groups. University of Windsor (Canada), **2016**.
- (80) Gouterman, M. Study of the effects of substitution on the absorption spectra of porphyrin. *J. Chem. Phys.* **1959**, *30* (5), 1139-1161.
- (81) Fukuda, D.; Smith, A. E.; Kendall, K. L.; Graef, J. L.; Moon, J. R.; Stout, J. R. Acute Effects Of A Pre-Exercise Supplement On Critical Velocity And Anaerobic Running Capacity In College-Aged Men And Women. *The Journal of Strength & Conditioning Research* **2010**, *24*, 1.
- (82) Pereira, G. F.; Tasso, T. T. From cuvette to cells: How the central metal ion modulates the properties of phthalocyanines and porphyrazines as photosensitizers. *Inorganica Chimica Acta* **2021**, *519*, 120271.
- (83) Wysocki, M.; Ziental, D.; Jozkowiak, M.; Dlugaszewska, J.; Piotrowska-Kempisty, H.; Güzel, E.; Sobotta, L. Porphyrazine/phthalocyanine hybrid complexes—Antibacterial and anticancer photodynamic and sonodynamic activity. *Synthetic Metals* **2023**, *299*, 117474.
- (84) Rahman, M.; Asiri, A. M. *Recent Progress in Organometallic Chemistry*; **2017**.
- (85) Wysocki, M.; Czarczynska-Goslinska, B.; Ziental, D.; Michalak, M.; Güzel, E.; Sobotta, L. Excited state and reactive oxygen species against cancer and pathogens: a review on sonodynamic and sono-photodynamic therapy. *ChemMedChem* **2022**, *17* (13), e202200185.
- (86) Koczorowski, T.; Szczolko, W.; Bakun, P.; Wicher, B.; Sobotta, L.; Gdaniec, M.; Teubert, A.; Mielcarek, J.; Tykarska, E.; Korecki, J. The valence and spin state tuning of iron (II/III) porphyrazines with bulky pyrrolyl periphery in solution and solid state. *Molecules* **2022**, *27* (22), 7820.
- (87) Dougherty, T. J.; Gomer, C. J.; Henderson, B. W.; Jori, G.; Kessel, D.; Korbelik, M.; Moan, J.; Peng, Q. Photodynamic therapy. *J. Natl. Cancer Inst.*, **1998**, *90* (12), 889-905.
-

-
- (88) Correia, J. H.; Rodrigues, J. A.; Pimenta, S.; Dong, T.; Yang, Z. Photodynamic therapy review: principles, photosensitizers, applications, and future directions. *Pharmaceutics*. **2021**, *13* (9), 1332.
- (89) Felsher, D. W. Oncogenes as therapeutic targets. *Semin Cancer Biol.* **2004**, *14* (1), 1.
- (90) Abrahamse, H.; Hamblin, M. R. New photosensitizers for photodynamic therapy. *Biochem. J.* **2016**, *473* (4), 347-364.
- (91) Dąbrowski, J. M.; Pucelik, B.; Regiel-Futyra, A.; Brindell, M.; Mazuryk, O.; Kyzioł, A.; Stochel, G.; Macyk, W.; Arnaut, L. G. Engineering of relevant photodynamic processes through structural modifications of metallotetrapyrrolic photosensitizers. *Coord. Chem. Rev.* **2016**, *325*, 67-101.
- (92) Jeelani, S.; Reddy, R. J.; Maheswaran, T.; Asokan, G.; Dany, A.; Anand, B. Theranostics: A treasured tailor for tomorrow. *J. Pharm. Bioallied Sci.* **2014**, *6* (Suppl 1), S6-S8.
- (93) Lovell, J. F.; Lo, P.-C. Porphyrins and phthalocyanines for theranostics. *Theranostics* **2012**, *2* (9), 815.
- (94) Młynarczyk, D. T.; Lijewski, S.; Falkowski, M.; Piskorz, J.; Szczolko, W.; Sobotta, L.; Stolarska, M.; Popenda, L.; Jurga, S.; Konopka, K. Dendrimeric sulfanyl porphyrazines: synthesis, physico-chemical characterization, and biological activity for potential applications in photodynamic therapy. *ChemPlusChem* **2016**, *81* (5), 460-470.
- (95) Ventola, C. L. The antibiotic resistance crisis: part 1: causes and threats. *Pharmacy and therapeutics* **2015**, *40* (4), 277.
- (96) Pucelik, B.; Paczyński, R.; Dubin, G.; Pereira, M. M.; Arnaut, L. G.; Dąbrowski, J. M. Correction: Properties of halogenated and sulfonated porphyrins relevant for the selection of photosensitizers in anticancer and antimicrobial therapies. *Plos one* **2018**, *13* (1), e0191777.
- (97) İpek, Ö.; Meltem, G.; Vesselin, K.; Vanya, M.; Mahmut, D. Novel water-soluble silicon (IV) phthalocyanine for photodynamic therapy and antimicrobial inactivations. *Макрогетероциклы* **2019**, *12* (3), 255-263.
- (98) Stolarska, M.; Glowacka-Sobotta, A.; Ziental, D.; Długaszewska, J.; Falkowski, M.; Goslinski, T.; Sobotta, L. Photochemical properties and promising activity against staphylococci of sulfanyl porphyrazines with dendrimeric moieties. *Inorganica Chimica Acta* **2021**, *521*, 120321.
- (99) Urbani, M.; Ragoussi, M.-E.; Nazeeruddin, M. K.; Torres, T. Phthalocyanines for dye-sensitized solar cells. *Coord. Chem. Rev.* **2019**, *381*, 1-64.
-

- (100) Donzello, M. P.; Ercolani, C.; Stuzhin, P. A. Novel families of phthalocyanine-like macrocycles—Porphyrazines with annulated strongly electron-withdrawing 1, 2, 5-thia/selenodiazole rings. *Coord. Chem. Rev.* **2006**, *250* (11-12), 1530-1561.
- (101) Lange, S. J.; Sibert, J. W.; Barrett, A. G.; Hoffman, B. M. Synthesis and coordination chemistry of unsymmetrical tetraazaporphyrins containing single oxathia-and thiacycrown substituents. *Tetrahedron* **2000**, *56* (38), 7371-7377.
- (102) Paradine, S. M.; White, M. C. Iron-catalyzed intramolecular allylic C–H amination. *J. Am. Chem. Soc.* **2012**, *134* (4), 2036-2039.
- (103) Bolm, C.; Legros, J.; Le Paih, J.; Zani, L. Iron-catalyzed reactions in organic synthesis. *Chem. Rev.* **2004**, *104* (12), 6217-6254. Koczorowski, T.; Szczolko, W.; Goslinski, T. Physicochemical properties and catalytic applications of iron porphyrazines and phthalocyanines. In *Recent Progress in Organometallic Chemistry*, IntechOpen, 2017; pp 101-121.
- (104) Kanaparthi, R. K.; Kandhadi, J.; Giribabu, L. Metal-free organic dyes for dye-sensitized solar cells: recent advances. *Tetrahedron* **2012**, *68* (40), 8383-8393.
- (105) Leliege, A.; Blanchard, P.; Rousseau, T.; Roncali, J. Triphenylamine/tetracyanobutadiene-based DAD π -conjugated systems as molecular donors for organic solar cells. *Organic Letters* **2011**, *13* (12), 3098-3101.
- (106) Furuyama, T.; Yoshida, T.; Hashizume, D.; Kobayashi, N. Phosphorus (v) tetraazaporphyrins: porphyrinoids showing an exceptionally strong CT band between the Soret and Q bands. *Chemical Science* **2014**, *5* (6), 2466-2474.
- (107) Cammidge, A. N.; Cook, M. J.; Hughes, D. L.; Nekelson, F.; Rahman, M. A remarkable side-product from the synthesis of an octaalkylphthalocyanine: formation of a tetrabenzotriazaporphyrin. *Chemical communications* **2005**, (7), 930-932.
- (108) Dalai, S.; Belov, V. N.; Nizamov, S.; Rauch, K.; Finsinger, D.; de Meijere, A. Access to Variously Substituted 5, 6, 7, 8-Tetrahydro-3H-quinazolin-4-ones via Diels–Alder Adducts of Phenyl Vinyl Sulfone to Cyclobutene-Annulated Pyrimidinones. *Eur. J. Org. Chem* **2006**, 2753-2765.
- (109) Chinchilla, R.; Nájera, C. Recent advances in Sonogashira reactions. *Chem. Soc. Rev.* **2011**, *40* (10), 5084-5121.
- (110) Van As, A.; Joubert, C. C.; Buitendach, B. E.; Erasmus, E.; Conradie, J.; Cammidge, A. N.; Chambrier, I.; Cook, M. J.; Swarts, J. C. Tetrabenzoporphyrin and-mono-, -cis-di-and Tetrabenzotriazaporphyrin Derivatives: Electrochemical and Spectroscopic Implications of meso CH Group Replacement with Nitrogen. *Inorganic Chemistry* **2015**, *54* (11), 5329-5341.

-
- (111) Tasso, T. T.; Schlothauer, J. C.; Junqueira, H. C.; Matias, T. A.; Araki, K.; Liandra-Salvador, E.; Antonio, F. C.; Homem-de-Mello, P.; Baptista, M. S. Photobleaching efficiency parallels the enhancement of membrane damage for porphyrazine photosensitizers. *J. Am. Chem. Soc.* **2019**, *141* (39), 15547-15556.
- (112) Díaz-Moscoso, A.; Emond, E.; Hughes, D. L.; Tizzard, G. J.; Coles, S. J.; Cammidge, A. N. Synthesis of a class of core-modified aza-BODIPY derivatives. *J. Org. Chem.* **2014**, *79* (18), 8932-8936.
- (113) Melenchuk, T.; Danilova, E.; Islyaikin, M. Synthesis of N-alkylthiadiazole-containing macroheterocyclic compounds of ABBB type. *Russ. J. Gen. Chem.* **2010**, *80*, 1369-1372.
- (114) FRANCE, H. O. New dyestuff intermediates. United Kingdom GB19510030353 19511228, 1955.
- (115) Shirley, H. J.; Koyioni, M.; Muncan, F.; Donohoe, T. J. Synthesis of lamellarin alkaloids using orthoester-masked α -keto acids. *Chemical Science* **2019**, *10* (15), 4334-4338.
- (116) Goslinski, T.; Tykarska, E.; Kryjewski, M.; Osmalek, T.; Sobiak, S.; Gdaniec, M.; Dutkiewicz, Z.; Mielcarek, J. Potential aluminium (III)-and gallium (III)-selective optical sensors based on porphyrazines. *Analytical Sciences* **2011**, *27* (5), 511-515.
- (117) Liu, W. X.; Yan, F.; Qian, S. L.; Ye, J. Y.; Liu, X.; Yu, M. X.; Wu, X. H.; Le, M. L.; Zhou, Z. Y.; Liu, S. H. Electronic Structures of Divinylchalcogenophene-Bridged Biruthenium Complexes: Exploring Trends from O to Te. *Eur. J. Inorg. Chem.* **2017**, (43), 5015-5026.
- (118) Díaz-Moscoso, A.; Tizzard, G. J.; Coles, S. J.; Cammidge, A. N. Synthesis of meso-substituted tetrabenzotriazaporphyrins: easy access to hybrid macrocycles. *Angew. Chem., Int. Ed.* **2013**, *52* (41), 10784-10787.
- (119) Alsaiani, N. Multidecker assemblies from Porphyrin and Phthalocyanine derivatives. University of East Anglia, University of East Anglia, 2022.
- (120) Furuyama, T.; Ogura, Y.; Yoza, K.; Kobayashi, N. Superazaporphyrins: Meso-Pentaazapentaphyrins and One of Their Low-Symmetry Derivatives. *Angew. Chem., Int. Ed.* **2012**, *51* (44), 11110-11114.
- (121) Chambrier, I.; Cook, M. Reaction of phthalonitrile with alkoxide ions. *Journal of chemical research. Synopses (Print)* **1990**, (10), 322-323.
- (122) Alkorbi, F.; Díaz-Moscoso, A.; Gretton, J.; Chambrier, I.; Tizzard, G. J.; Coles, S. J.; Hughes, D. L.; Cammidge, A. N. Complementary Syntheses Giving Access to a Full Suite of Differentially Substituted Phthalocyanine-Porphyrin Hybrids. *Angew. Chem., Int. Ed.* **2021**, *60* (14), 7632-7636.
-

Appendices

1) 2.14 (Figure 2.18) .**Crystal structure analysis of 5-imino-3,4-bis(4-methoxyphenyl)-2,5-dihydro-1H-pyrrol-2-one**

Crystal data: C₁₈H₁₆N₂O₃, M = 308.33. Monoclinic, space group P2₁/n (equiv. to no. 14), a = 10.9813(4), b = 6.1585(2), c = 22.8069(8) Å, β = 97.332(3) °, V = 1529.78(9) Å³. Z = 4, D_c = 1.339 g cm⁻³, F(000) = 648, T = 99.99(11) K, μ(Cu-Kα) = 7.55 cm⁻¹, λ(Cu-Kα) = 1.54184 Å.

The crystal was a yellow needle. From a sample under oil, one, *ca* 0.021 x 0.042 x 0.413 mm, was mounted on a small loop and fixed in the cold nitrogen stream on a Rigaku Oxford Diffraction XtaLAB Synergy diffractometer, equipped with Cu-Kα radiation, HyPix detector and mirror monochromator. Intensity data were measured by thin-slice ω-scans. Total no. of reflections recorded, to θ_{max} = 72.5°, was 9533 of which 2942 were unique (R_{int} = 0.045); 2276 were 'observed' with I > 2σ_I.

Data were processed using the CrysAlisPro-CCD and -RED (1) programs. The structure was determined by the intrinsic phasing routines in the SHELXT program (2A) and refined by full-matrix least-squares methods, on F²'s, in SHELXL (2B). The non-hydrogen atoms were refined with anisotropic thermal parameters. The amino hydrogen atoms on N(1) and N(5) were located in a difference map and were refined freely. The remaining hydrogen atoms were included in idealised positions and their U_{iso} values were set to ride on the U_{eq} values of the parent carbon atoms. At the conclusion of the refinement, wR₂ = 0.117 and R₁ = 0.072 (2B) for all 2942 reflections weighted w = [σ²(F_o²) + (0.0299 P)² + 1.682 P]⁻¹ with P = (F_o² + 2F_c²)/3; for the 'observed' data only, R₁ = 0.049.

In the final difference map, the highest peak (*ca* 0.24 eÅ⁻³) was near C(3).

Scattering factors for neutral atoms were taken from reference (3). Computer programs used in this analysis have been noted above, and were run through WinGX (4) on a Dell Optiplex 780 PC at the University of East Anglia.

Legends for Figures

Figure 1. View of a molecule of 5-imino-3,4-bis(4-methoxyphenyl)-2,5-dihydro-1*H*-pyrrol-2-one, showing the hydrogen-bonded neighbours and indicating the atom numbering scheme. Thermal ellipsoids are drawn at the 50% probability level.

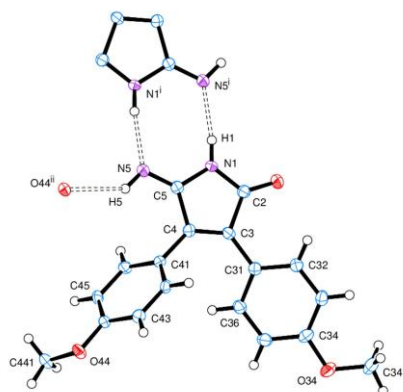


Figure 2. View along the *b* axis of the packing of molecules. Molecules are linked in pairs through N(1)-H(1)...N(5') hydrogen bonds about centres of symmetry, and through N(5)-H(5)...O(44'') bonds in chains around a 2_1 screw axis parallel to the *b* axis.

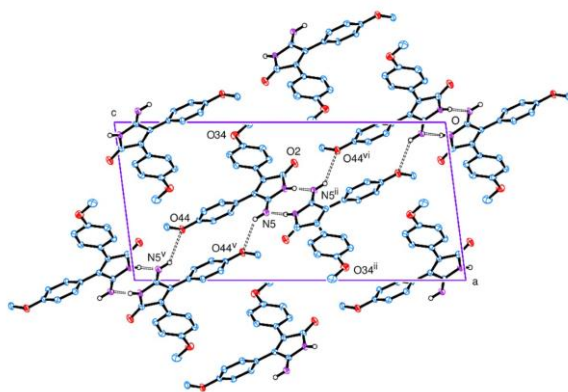


Figure 3. General view of the packing of molecules (omitting the methoxyphenyl group on the C(3) atom in each molecule).

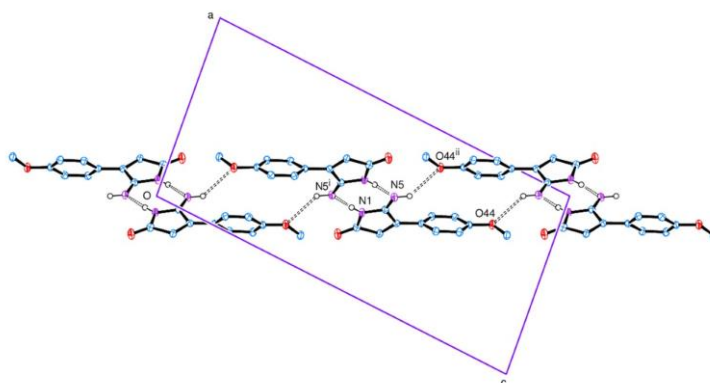


Figure 4. View along the *b* axis of a single hydrogen-bonded sheet, side-on, omitting the methoxyphenyl group on the C(3) atom in each molecule.

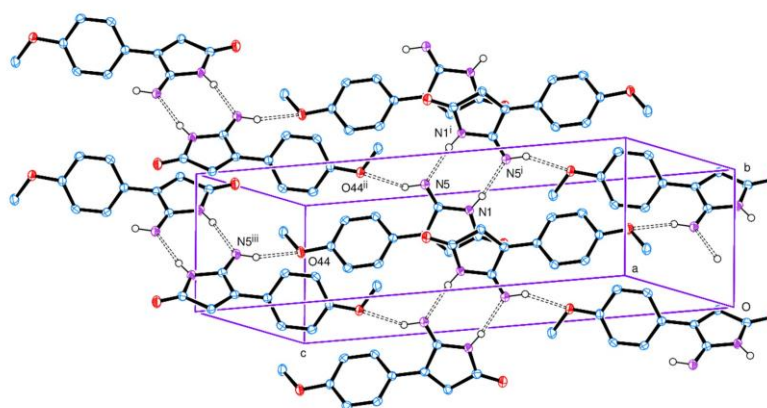
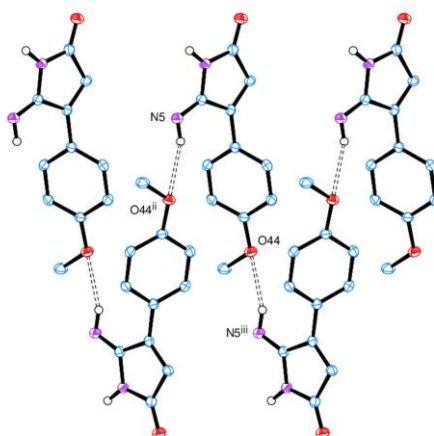


Figure 5. Linking of molecules around a 2_1 -screw axis which lies parallel to the *b* axis and horizontal in the plane of the paper.



Notes on the structure

The 5-imino-pyrrolone group is essentially planar, with the two phenyl rings rotated about the C(3)-C(31) and C(4)-C(41) bonds by 26.01(10) and 58.40(6) ° respectively, Figure 1.

The N(1)-H(1) group forms a good hydrogen bond with N(5ⁱ) of a molecule related by a centre of symmetry, with the corresponding N(1ⁱ)-H(1ⁱ)...N(5) bond completing an 8-membered ring and the formation of a hydrogen-bonded dimer unit, Figure 1. N(5) is also the donor atom of a secondary, rather weaker hydrogen bond to O(44ⁱⁱⁱ). The dimer units are thus linked in a two-dimensional sheets parallel to the 101 plane in which adjacent units are related by the *n*-glide symmetry, Figure 2.

Other views of the packing arrangements are shown in Figures 3-5.

2)2.18 (Figure 2.25).**Crystal structure analysis of an isoindole-3-amine derivative**

Crystal data: C₃₄H₂₇N₃O₄, M = 541.58. Monoclinic, space group P2₁/c (no. 14), a = 11.2245(6), b = 17.7373(8), c = 14.1554(8) Å, β = 109.248(6) °, V = 2660.7(3) Å³. Z = 4, D_c = 1.352 g cm⁻³, F(000) = 1136, T = 100.15(10) K, μ(Cu-Kα) = 7.04 cm⁻¹, λ(Cu-Kα) = 1.54184 Å.

The crystal was a dark orange block. From a sample under oil, one, ca 0.130 x 0.200 x 0.277 mm, was mounted on a small loop and fixed in the cold nitrogen stream on a Rigaku Oxford Diffraction XtaLAB Synergy diffractometer, equipped with Cu-Kα radiation, HyPix detector and mirror monochromator. Intensity data were measured by thin-slice ω-scans. Total no. of reflections recorded, to θ_{max} = 72.5°, was 21155 of which 5185 were unique (R_{int} = 0.063); 4422 were 'observed' with I > 2σ_I.

Data were processed using the CrysAlisPro-CCD and -RED (1) programs. The structure was determined by the intrinsic phasing routines in the SHELXT program (2A) and refined by full-matrix least-squares methods, on F²'s, in SHELXL (2B). The non-hydrogen atoms were refined with anisotropic thermal parameters. The hydrogen atom on N(1) was located in a difference map and was refined freely. The remaining hydrogen atoms were included in idealised positions and their U_{iso} values were set to ride on the U_{eq} values of the parent carbon atoms. At the conclusion of the refinement, wR₂ = 0.139 and R₁ = 0.057 (2B) for all 5185 reflections weighted w = [σ²(F_o²) + (0.0845 P)² + 0.6885 P]⁻¹ with P = (F_o² + 2F_c²)/3; for the 'observed' data only, R₁ = 0.050.

In the final difference map, the highest peak (ca 0.28 eÅ⁻³) was near C(53).

Scattering factors for neutral atoms were taken from reference (3). Computer programs used in this analysis have been noted above, and were run through WinGX (4) on a Dell Optiplex 780 PC at the University of East Anglia.

Legends for Figures

Figure 1. View of a molecule of the isoindole-3-amine derivative, indicating the atom numbering scheme. Thermal ellipsoids are drawn at the 50% probability level.

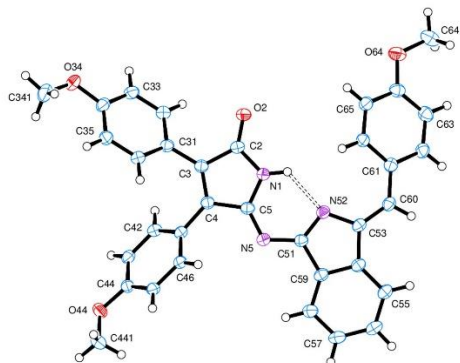


Figure 2. Two overlapping molecules, related by a centre of symmetry.

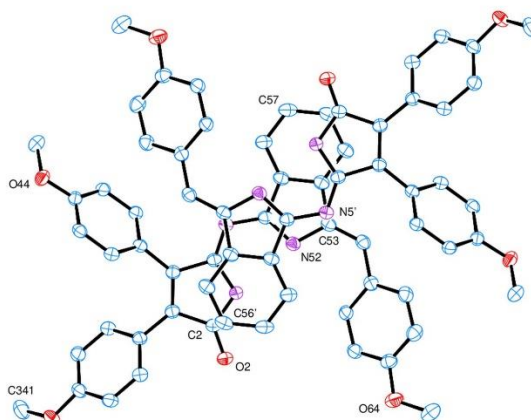


Figure 3. The overlap of the central core planes.

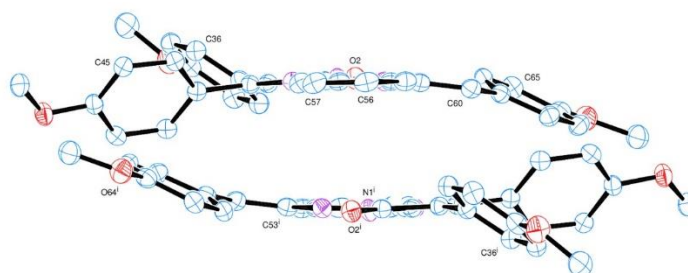
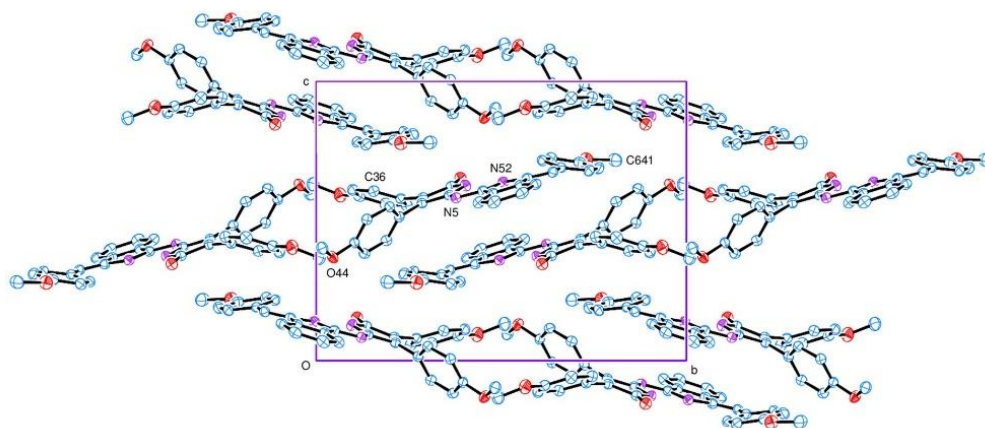


Figure 4. View of the packing of molecules, along the *a* axis.

Notes on the structure

The core of the molecule, *i.e.* the isoindole and linked pyrrole rings, form a planar system. The substituent phenyl rings are rotated away from this central plane, Figure 1. All the non-hydrogen atoms were clearly located and their elemental type assigned and confirmed in the refinement procedure. All the hydrogen atoms were identified in difference maps; the pyrrole H-atom was confirmed by its free refinement, while all the remaining hydrogen atoms were included in idealised positions and set to ride on the parent carbon atoms. There is a well-defined intramolecular hydrogen bond from the pyrrole N-H group to the isoindoline N-atom, Figure 1.

The central cores of a pair of molecules lie overlapping about a centre of symmetry, with the closest contacts between N(5)...C(53') at 3.301 Å and C(2)...C(56') at 3.341 Å, Figures 2 and 3. Other intermolecular contacts are at normal van der Waals' distances.

3) 2.19 (Figure 2.33).**Crystal structure analysis of [Mg (isoindole-N)-{pyrrole(methoxyphenyl)₂-N₃} (OH₂)], 1.5(thf)**

Crystal data: C₆₆ H₆₁ Mg N₈ O₈, 0.5(C₄ H₈ O), M = 1154.59. Triclinic, space group P-1 (no. 2), a = 8.74516(17), b = 16.4767(3), c = 20.6654(3) Å, α = 76.6464(13), β = 84.9397(13), γ = 87.5462(15) °, V = 2885.14(8) Å³. Z = 2, D_c = 1329. g cm⁻³, F(000) = 1218, T = 100(2) K, μ(Cu-Kα) = 8.13 cm⁻¹, λ(Cu-Kα) = 1.54184 Å.

The crystal was a purple block. From a sample under oil, one, *ca* 0.25 x 0.22 x 0.07 mm, was mounted on a small loop and fixed in the cold nitrogen stream on a Rigaku Oxford Diffraction XtaLAB Synergy diffractometer, equipped with Cu-Kα radiation, HyPix detector and mirror monochromator. Intensity data were measured by thin-slice ω-scans. Total no. of reflections recorded, to θ_{max} = 72.5°, was 39,029 of which 11,144 were unique (R_{int} = 0.031); 9,442 were 'observed' with I > 2σ_I.

Data were processed using the CrysAlisPro-CCD and -RED (1) programs. The structure was determined by the intrinsic phasing routines in the SHELXT program (2A) and refined by full-matrix least-squares methods, on F²'s, in SHELXL (2B). The magnesium centre is five-coordinate with a square pyramidal pattern; The square base comprises the four pyrrole/isoindole nitrogen atoms, with a water molecule at the apical site. The two hydrogen atoms of the water molecule were located in a difference map and were refined isotropically. The non-hydrogen atoms of the Mg complex were refined with anisotropic thermal parameters. Two thf molecules were identified, one of which was disordered about a centre of symmetry; the dimensions of this half-molecule were considered unreliable and the hydrogen atoms for C(54) and C(55) were not calculated for inclusion in the refinement process. The hydrogen atoms of the cyclic isoindole-tripyrrole compound and attached thf molecule were included in idealised positions and their U_{iso} values were set to ride on the U_{eq} values of the parent carbon atoms. At the conclusion of the refinement, wR₂ = 0.189 and R₁ = 0.071 (2B) for all 11,144 reflections weighted $w = [\sigma^2(F_o^2) + (0.1130 P)^2 + 1.4795 P]^{-1}$ with $P = (F_o^2 + 2F_c^2)/3$; for the 'observed' data only, R₁ = 0.062.

In the final difference map, the highest peak (*ca* 1.1 eÅ⁻³) was near O(41).

Scattering factors for neutral atoms were taken from reference (3). Computer programs used in this analysis have been noted above, and were run through WinGX (4) on a Dell Optiplex 780 PC at the University of East Anglia.

Legends for Figures

Figure 1. View of the magnesium isoindole-tripyrrole derivative molecule, with a hydrogen bonded the molecule attached. The atom numbering scheme is indicated. Thermal ellipsoids are drawn at the 20% probability level.

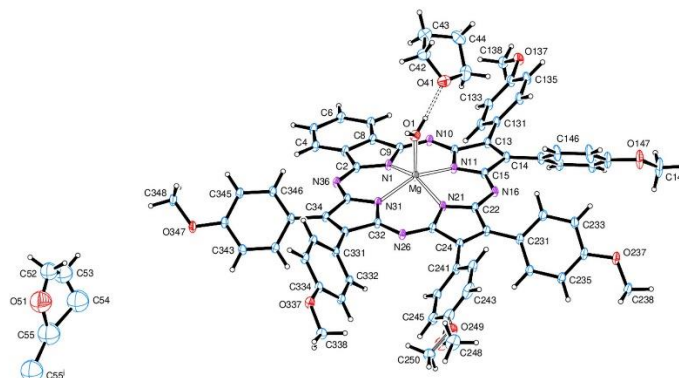


Figure 2. The hydrogen bonds about O(1) of the water molecule.

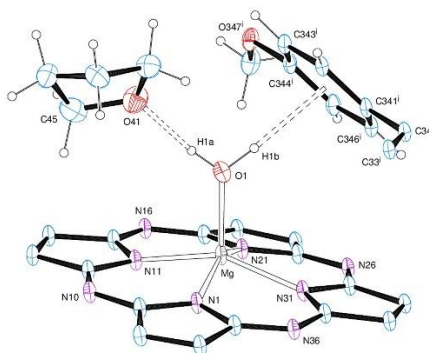


Figure 3. The pairing of two Mg complex molecules about a centre of symmetry.

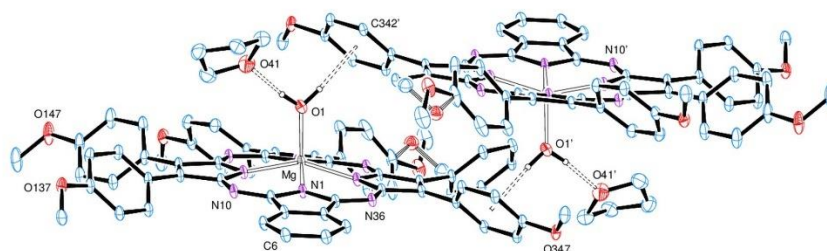
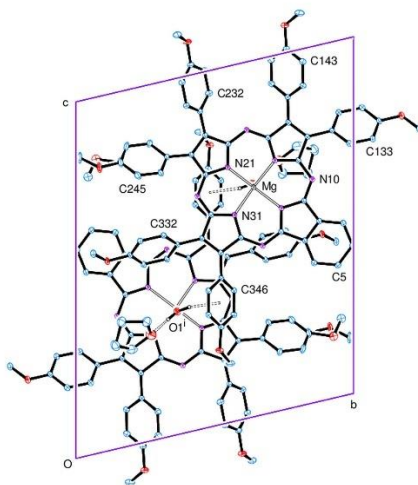


Figure 4. The dimer molecule of Figure 3 viewed along the *a* axis, showing the overlaying of the pyrrole group of N(31) with its inverted neighbour. The rings are *ca* 4.4 Å apart.



Notes on the structure

The diffraction analysis clarifies the molecular structure as shown in Figure 1. The Mg atom is at the centre of square pyramid in which the four atoms of the base are the N atoms of the isoindole and three pyrrole rings of the 1:3-phthal-porph cyclic system; the Mg atom is displaced 0.4999(12) Å from the mean-plane of the N₄ atoms. The apical site is occupied by an adventitious water molecule whose two hydrogen atoms form good hydrogen bonds (Figure 2) viz H(1a)...O(41) of a complete thf molecule, and H(1b)...Ct1 (where Ct is the centroid of the phenyl group of C(341)-346) of a related molecule), which thus forms a hydrogen-bonded dimer, Figure 3; the H...Ct distance is 2.20 Å.

There is a second thf molecule in this crystal; it lies disordered about a centre of symmetry, with unreliable dimensions; its only close interaction is between C(55) and H(24c) (also in a disordered group) at *ca* 2.42 Å.

The dimer molecules appear to be stacked along the *a* axis; however, C(33)-C(34) bonds at the centre of the overlaid N(31) pyrrole rings are *ca* 4.3 Å apart within the dimer and *ca* 4.4 Å between neighbouring dimers, Figure 4.

4) 2.22 (Figure 2.37).**Crystal structure analysis of [Zn (HOME) (3,4-benzo-13,14,23,24,33,34-hexamethoxyphenyl-C₁₆N₈)]**

Crystal data: C₆₃ H₅₀ N₈ O₇ Zn, M = 1096.48. Triclinic, space group P-1 (no. 2), a = 13.7702(4), b = 14.1242(3), c = 14.8649(3) Å, α = 66.896(2), β = 84.678(2), γ = 73.034(2)°, V = 2542.72(11) Å³. Z = 2, D_c = 1.432 g cm⁻³, F(000) = 1140, T = 100(2) K, μ(Cu-Kα) = 12.19 cm⁻¹, λ(Cu-Kα) = 1.54184 Å.

The crystal was a dark blue rhomboid. From a sample under oil, one, *ca* 0.25 x 0.07 x 0.02 mm, was mounted on a small loop and fixed in the cold nitrogen stream on a Rigaku Oxford Diffraction XtaLAB Synergy diffractometer, equipped with Cu-Kα radiation, HyPix detector and mirror monochromator. Intensity data were measured by thin-slice ω-scans. Total no. of reflections recorded, to θ_{max} = 70.0°, was 33,504 of which 9,504 were unique (R_{int} = 0.058); 7,951 were 'observed' with I > 2σ_I.

Data were processed using the CrysAlisPro-CCD and -RED (1) programs. The structure was determined by the intrinsic phasing routines in the SHELXT program (2A) and refined by full-matrix least-squares methods, on F²'s, in SHELXL (2B). The non-hydrogen atoms were refined with anisotropic thermal parameters. The hydroxyl hydrogen atom of the MeOH ligand was located in a difference map and was refined freely. The remaining hydrogen atoms were included in idealised positions and their U_{iso} values were set to ride on the U_{eq} values of the parent carbon atoms. At the conclusion of the refinement, wR₂ = 0.144 and R₁ = 0.060 (2B) for all 9,504 reflections weighted w = [σ²(F_o²) + (0.0825 P)² + 0.5855 P]⁻¹ with P = (F_o² + 2F_c²)/3; for the 'observed' data only, R₁ = 0.051.

In the final difference map, the highest peak (*ca* 0.7 eÅ⁻³) was near the zinc atom.

Scattering factors for neutral atoms were taken from reference (3). Computer programs used in this analysis have been noted above, and were run through WinGX (4) on a Dell Optiplex 780 PC at the University of East Anglia.

Legends for Figures

Figure 1. General view of the zinc complex molecule, indicating the atom numbering scheme. Thermal ellipsoids are drawn at the 50% probability level.

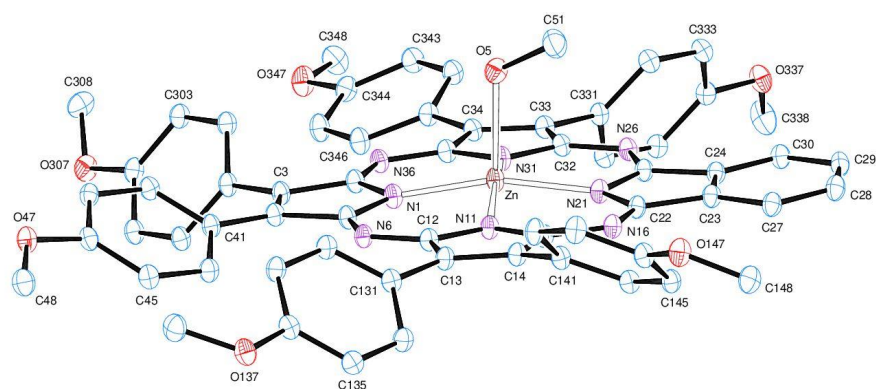


Figure 2. The zinc complex molecule viewed on to the coordinating N_4 plane.

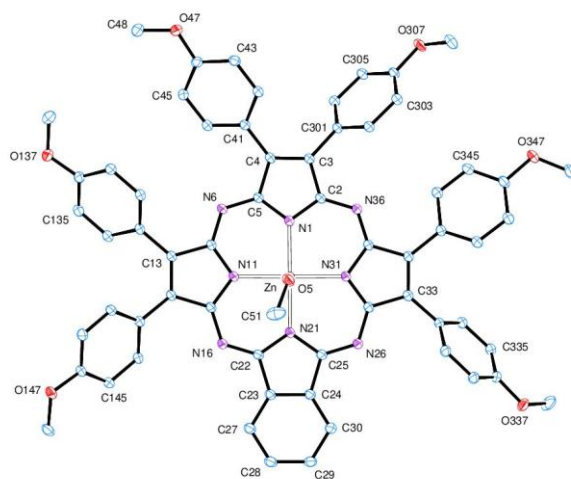


Figure 3. The methanol ligand and its hydrogen bond to a neighbouring phenyl ring.

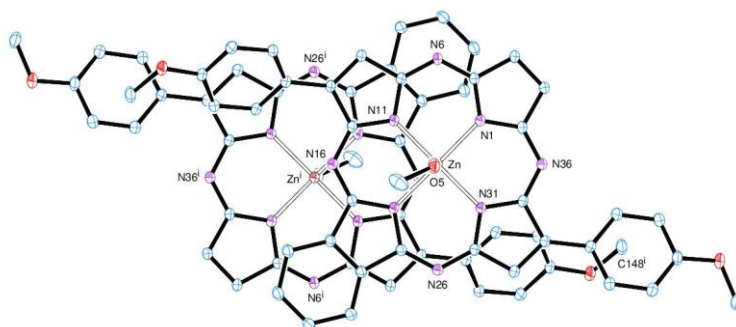


Figure 4. Overlap of the central, planar section of two adjacent molecules.

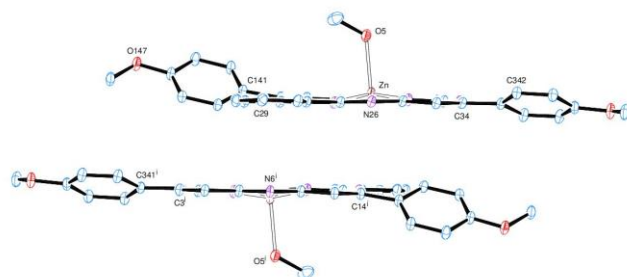


Figure 5. The two overlapping molecules viewed along the N(26)...N(6) vector.

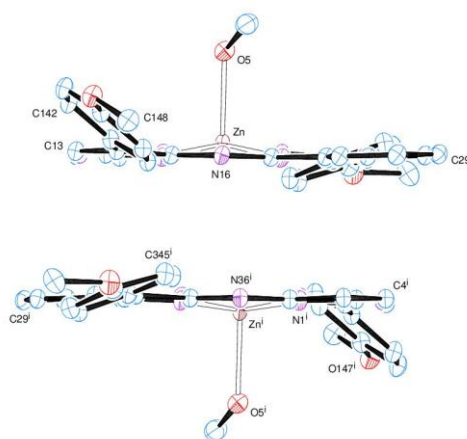
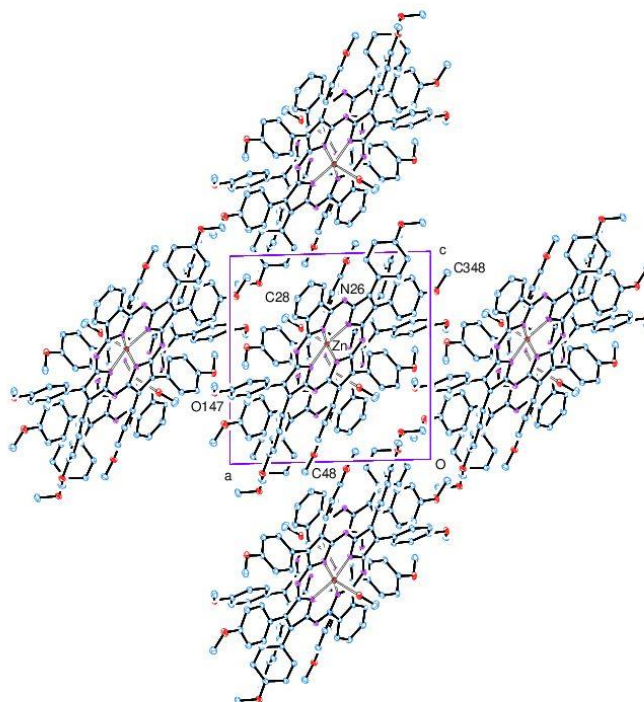


Figure 6. The two overlapping molecules viewed along the N(16)...N(36) vector.



Notes on the structure

This complex of a phthalocyanine derivative shows a zinc atom at the centre, coordinating a methanol ligand in the apex site of a square pyramidal pattern, Figures 1 and 2. The zinc atom is displaced 0.2755(4) Å towards the MeOH ligand from the planar N₄ group of coordinating atoms.

The hydroxyl hydrogen atom of the MeOH ligand showed up clearly in a difference map and was included in the refinement process. The O–H bond is directed face-on towards a phenyl ring, with the closest interactions at 2.65 and 2.67 Å for the H(5o)...C(303') and ...C(304') distances, Figure 3.

Pairs of the molecules lie back-to-back, with overlapping parallel planes related by a centre of symmetry, Figures 4-6. The planes are *ca* 3.3 Å apart.

5) 2.27 (Figure 2.43) .**Crystal structure analysis of 2-NH,3,4-bis-(^tbutylphenyl),5-N-isoindole-CH-methoxyphenyl-pyrrole**

Crystal data: C₄₀ H₃₉ N₄ O, 0.3(C), M = 595.35. Triclinic, space group P-1 (no. 2), a = 6.2107(3), b = 15.5071(4), c = 18.1783(5) Å, α = 109.543(3), β = 95.018, γ = 92.890(3) °, V = 1637.64(10) Å³. Z = 2, D_c = 1.209 g cm⁻³, F(000) = 636, T = 100(2) K, μ(Cu-Kα) = 5.67 cm⁻¹, λ(Cu-Kα) = 1.54184 Å.

The crystal was a red plate. From a sample under oil, one, *ca* 0.62 x 0.17 x 0.03 mm, was mounted on a small loop and fixed in the cold nitrogen stream on a Rigaku Oxford Diffraction XtaLAB Synergy diffractometer, equipped with Cu-Kα radiation, HyPix detector and mirror monochromator. Intensity data were measured by thin-slice ω-scans. Total no. of reflections recorded, to θ_{max} = 70.0°, was 17,986 of which 6078 were unique (R_{int} = 0.046); 5150 were 'observed' with I > 2σ_I.

Data were processed using the CrysAlisPro-CCD and -RED (1) programs. The structure was determined by the intrinsic phasing routines in the SHELXT program (2A) and refined by full-matrix least-squares methods, on F²'s, in SHELXL (2B). There is disorder of the Ph-OMe group in two distinct orientations. There is also a not-fully-resolved, partially occupied, solvent atom (or maybe two atoms) close to an inversion centre. The non-hydrogen atoms (except for the solvent atom) were refined with anisotropic thermal parameters. The hydrogen atoms were mostly included in idealised positions and their U_{iso} values were set to ride on the U_{eq} values of the parent carbon atoms; the hydrogen atom bonded to N(3), however, was located in a difference map and was refined freely. At the conclusion of the refinement, wR₂ = 0.189 and R₁ = 0.077 (2B) for all 6078 reflections weighted w = [σ²(F_o²) + (0.1006 P)² + 0.7268 P]⁻¹ with P = (F_o² + 2F_c²)/3; for the 'observed' data only, R₁ = 0.068.

In the final difference map, the highest peak (*ca* 0.5 eÅ⁻³) was near C(70).

Scattering factors for neutral atoms were taken from reference (3). Computer programs used in this analysis have been noted above, and were run through WinGX (4) on a Dell Optiplex 780 PC at the University of East Anglia.

Legends for Figures

Figure 1. View of the indole-pyrrole molecule, indicating the atom numbering scheme.

Thermal ellipsoids are drawn at the 20% probability level.

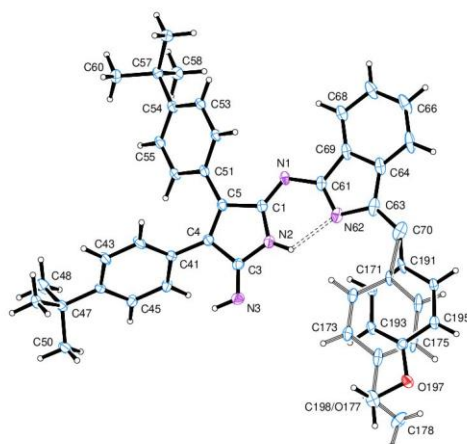
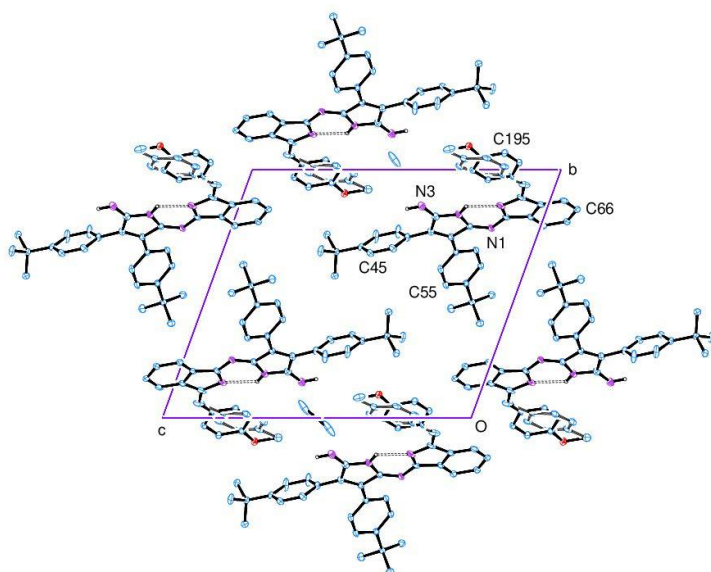


Figure 2. The packing of molecules, viewed along the *a* axis.



Notes on the structure

The pyrrole and isoindole rings each form good planes; the normals to these planes are 6.42° apart. The phenyl group of C(191-196) is essentially coplanar with these planes. The other ring planes are rotated distinctly out of this central plane. The hydrogen atoms on N(2) and N(3) were clearly identified in difference maps; that on N(2) forms a good, intramolecular hydrogen bond, whereas that on N(3) forms normal van der Waals', intermolecular contacts.

Around the pyrrole ring, bond lengths indicate double bonds C(1)=N(1) and C(3)=N(3). The methoxy phenyl group is disordered over two orientations with an occupation ratio of 0.44/0.56 for the rings of C(171)/C(191); the large thermal ellipsoid for C(70) suggests similar disorder. The O(177) and C(198) atoms occupy a common site.

6) 2.24 (Figure 2.51) .**Crystal structure analysis of {propyl-O-C₆H₄-C(CN)}₂**

Crystal data: C₂₂ H₂₂ N₂ O₂, M = 346. Monoclinic, space group P2₁/c (no. 14), a = 10.57118(17), b = 7.96264(10), c = 11.45121(18) Å, β = 111.4906(18) °, V = 896.88(3) Å³. Z = 2, D_c = 1.283 g cm⁻³, F(000) = 368, T = 100(2) K, μ(Cu-Kα) = 6.57 cm⁻¹, λ(Cu-Kα) = 1.54184 Å.

The crystal was a yellow plate. From a sample under oil, one, *ca* 0.08 x 0.28 x 0.42 mm, was mounted on a small loop and fixed in the cold nitrogen stream on a Rigaku Oxford Diffraction XtaLAB Synergy diffractometer, equipped with Cu-Kα radiation, HyPix detector and mirror monochromator. Intensity data were measured by thin-slice ω-scans. Total no. of reflections recorded, to θ_{max} = 72.5°, was 5705 of which 1719 were unique (R_{int} = 0.019); 1641 were 'observed' with I > 2σ_I.

Data were processed using the CrysAlisPro-CCD and -RED (1) programs. The structure was determined by the intrinsic phasing routines in the SHELXT program (2A) and refined by full-matrix least-squares methods, on F²'s, in SHELXL (2B). The molecules were shown to be dimeric, lying about centres of symmetry. They were also found to be disordered over two orientations with an occupation ratio of *ca* 0.80:0.20; some sites were common to both components, but in other cases, the minor components may be hidden in the electron clouds of a major component atom. The non-hydrogen atoms of the major component were refined with anisotropic thermal parameters. The hydrogen atoms of the major component were included in idealised positions and their U_{iso} values were set to ride on the U_{eq} values of the parent carbon atoms; those of the minor component were not included. At the conclusion of the refinement, wR₂ = 0.0890 and R₁ = 0.0349 (2B) for all 1719 reflections weighted w = [σ²(F_o²) + (0.0422 P)² + 0.3353 P]⁻¹ with P = (F_o² + 2F_c²)/3; for the 'observed' data only, R₁ = 0.0363.

In the final difference map, the highest peak (*ca* 0.2 eÅ⁻³) was on the C(4)-C(41) bond.

Scattering factors for neutral atoms were taken from reference (3). Computer programs used in this analysis have been noted above, and were run through WinGX (4) on a Dell Optiplex 780 PC at the University of East Anglia.

Legends for Figures

Figure 1. View of the dimeric molecule; a centre of symmetry on the C(41)-C(41') bond relates the two halves of the molecule. The atom numbering scheme is indicated. Thermal ellipsoids are drawn at the 50% probability level.

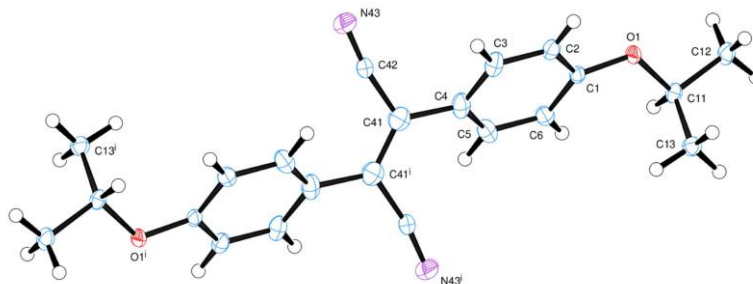


Figure 2. The overlaying of the major disordered component by the minor component (occupancy *ca* 0.20).

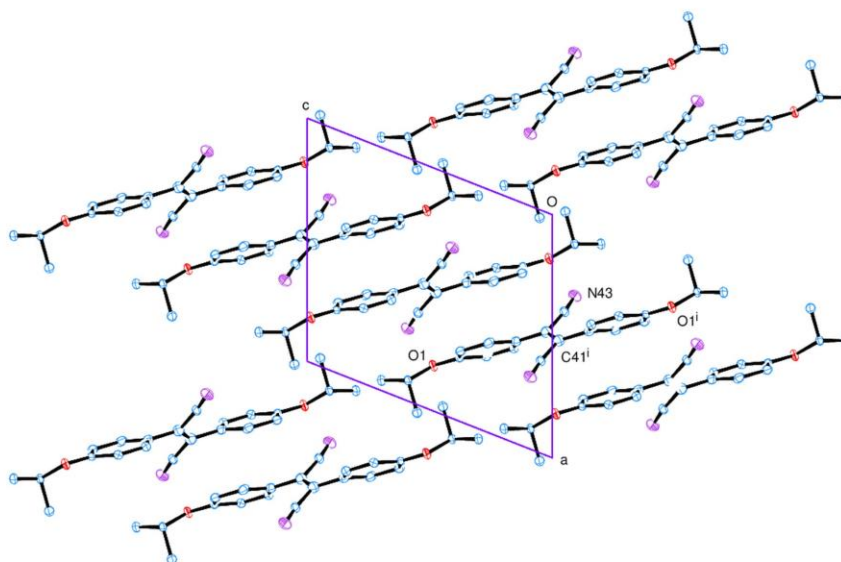
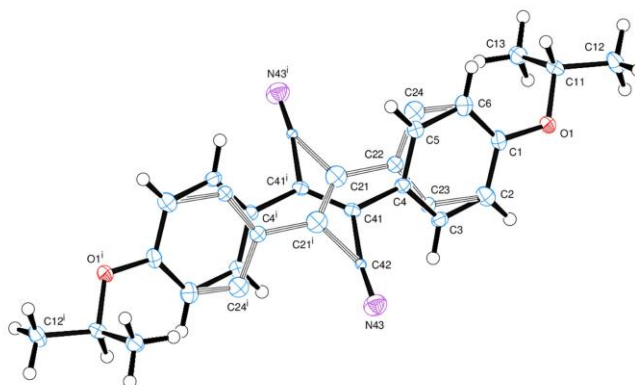


Figure 3. The packing of the major molecules, viewed along the *b* axis.



Notes on the structure

The molecule is a dimer, lying about a centre of symmetry on the C(41)–C(41') bond. The angle of rotation about the C(4)–C(41), *i.e.* between the phenyl ring and the connecting plane between the two phenyl rings is 40.86(4) °.

The molecule is disordered, with a minor component (occupancy *ca* 0.20) overlaying the major component.

Intermolecular contacts appear to be at van der Waals' distances.

7) 2.45 (Figure 2.63) .**Crystal structure analysis of (MeO-C₆H₄)₂NH-pyrrole-N-isoindole-CH-thiophene**

Crystal data: C₃₁ H₂₄ N₄ O₂ S, M = 516.60. Monoclinic, space group P2₁/c (no. 14), a = 10.48577(14), b = 6.48338(9), c = 36.8776(5) Å, β = 91.6325(11) °, V = 2506.06(6) Å³. Z = 4, D_c = 1.369 g cm⁻³, F(000) = 1080, T = 100(2) K, μ(Cu-Kα) = 14.5 cm⁻¹, λ(Cu-Kα) = 1.54184 Å.

The crystals were orange needles. From a sample under oil, one, *ca* 0.26 x 0.04 x 0.04 mm, was mounted on a small loop and fixed in the cold nitrogen stream on a Rigaku Oxford Diffraction XtaLAB Synergy diffractometer, equipped with Cu-Kα radiation, HyPix detector and mirror monochromator. Intensity data were measured by thin-slice ω-scans. Total no. of reflections recorded, to θ_{max} = 70.0 °, was 16,375 of which 4,682 were unique (R_{int} = 0.040); 4,131 were 'observed' with I > 2σ₁.

Data were processed using the CrysAlisPro-CCD and -RED (1) programs. The structure was determined by the intrinsic phasing routines in the SHELXT program (2A) and refined by full-matrix least-squares methods, on F²'s, in SHELXL (2B). The non-hydrogen atoms were refined with anisotropic thermal parameters. All the hydrogen atoms were located in difference maps and were refined freely and isotropically. At the conclusion of the refinement, wR₂ = 0.092 and R₁ = 0.040 (2B) for all 4682 reflections weighted w = [σ²(F_o²) + (0.0431 P)² + 0.890 P]⁻¹ with P = (F_o² + 2F_c²)/3; for the 'observed' data only, R₁ = 0.035.

In the final difference map, the highest peak (*ca* 0.24 eÅ⁻³) was near C(22).

Scattering factors for neutral atoms were taken from reference (3). Computer programs used in this analysis have been noted above, and were run through WinGX (4) on a Dell Optiplex 780 PC at the University of East Anglia.

Legends for Figures

Figure 1. View of the molecule with its intramolecular hydrogen bond, indicating the atom numbering scheme. Thermal ellipsoids are drawn at the 50% probability level.

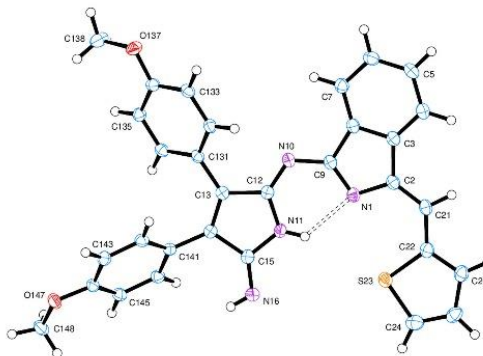


Figure 2. View of the molecule showing the tilting of the several aromatic planes.

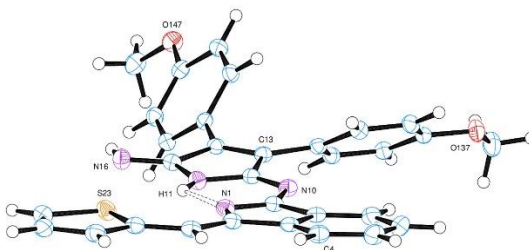
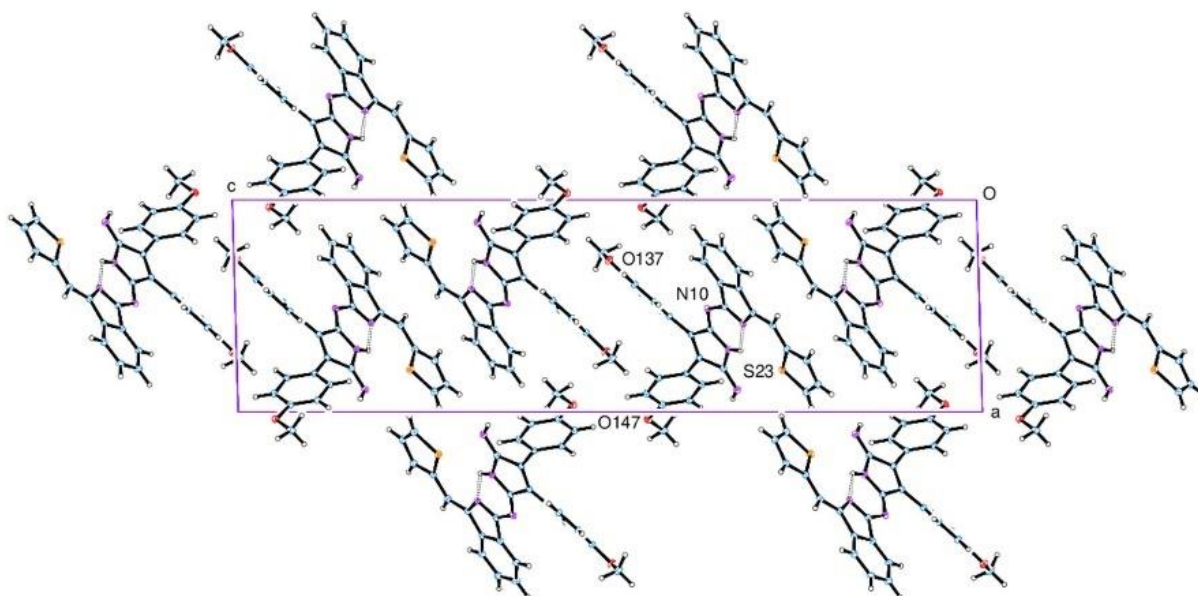


Figure 2. The packing of molecules, viewed along the *b* axis.



Notes on the structure

The structure comprises five planar aromatic rings, Figure 1. The thiophene and isoindole rings are essentially coplanar, Figure 2, and the remaining rings are tilted gradually away from that plane.

As noted above, all the hydrogen atoms were located in difference maps and were refined freely and isotropically. In particular, we note that the nitrogen atoms N(11) and N(16) have trigonal, planar geometries; H(11) is 2.18 Å from N(1), thus forming an intramolecular hydrogen bond, whereas the N(16)-H(16) group does not appear to have any neighbouring acceptor group within a hydrogen bonding distance.

8) 2.46 (Figure 2.63) .**Crystal structure analysis of *cyclo*-{HNCO(C₆H₄OMe)₂C}-N-isoindole-CH-thiophene**

Crystal data: C₃₁H₂₃N₃O₃S., M = 517.58. Monoclinic, space group P2₁/c (no. 14), a = 10.73807(15), b = 6.326701(8), c = 36.5838(5) Å, β = 90.9209(12) °, V = 2485.06(6) Å³. Z = 4, D_c = 1.383 g cm⁻³, F(000) = 1080, T = 100(2) K, μ(Cu-Kα) = 14.8 cm⁻¹, λ(Cu-Kα) = 1.54184 Å.

The crystal was a red needle. From a sample under oil, one, *ca* 0.04 x 0.11 x 0.78 mm, was mounted on a small loop and fixed in the cold nitrogen stream on a Rigaku Oxford Diffraction XtaLAB Synergy diffractometer, equipped with Cu-Kα radiation, HyPix detector and mirror monochromator. Intensity data were measured by thin-slice ω-scans. Total no. of reflections recorded, to θ_{max} = 72.5°, was 17,506 of which 4770 were unique (R_{int} = 0.036); 4285 were 'observed' with I > 2σ_I.

Data were processed using the CrysAlisPro-CCD and -RED (1) programs. The structure was determined by the intrinsic phasing routines in the SHELXT program (2A) and refined by full-matrix least-squares methods, on F²'s, in SHELXL (2B). The non-hydrogen atoms were refined with anisotropic thermal parameters. The hydrogen atoms were included in idealised positions and their U_{iso} values were set to ride on the U_{eq} values of the parent carbon atoms. At the conclusion of the refinement, wR₂ = 0.122 and R₁ = 0.043 (2B) for all 4770 reflections weighted w = [σ²(F_o²) + (0.0786 P)² + 0.5924 P]⁻¹ with P = (F_o² + 2F_c²)/3; for the 'observed' data only, R₁ = 0.0040.

In the final difference map, the highest peak (*ca* 0.45 eÅ⁻³) was near C(22).

Scattering factors for neutral atoms were taken from reference (3). Computer programs used in this analysis have been noted above, and were run through WinGX (4) on a Dell Optiplex 780 PC at the University of East Anglia.

Notes on the structure

The molecule, Figure 1, shows the structure of the right-hand ChemDRAW diagram, with conjugated double bonds for the C(5)=N(6), C(12)=N(11) and C(19)=C(20) bonds. Most of the molecule is close to being planar, except for the methoxyphenyl groups which are each rotated *ca* 40 ° from the general mean plane.

The hydrogen atom on N(1) was clear in a difference map and forms a good intramolecular hydrogen bond to N(11); its contact with S21) is weaker, but may be considered part of a bifurcated system.

From the packing diagram, Figure 2, we note that the phenyl ring of C(41–46) appears to be lying parallel to its symmetry related plane about the cell centre; in fact, C(44) lies over the C(44)–C(45) bond of the related molecule, with C...C distances 3.480 and 3.381 Å.

9) 2.47 (Figure 2.67).**Crystal structure analysis of a Zn-porph-like complex, with solvents**

Crystal data: C_{57.67} H₄₂ N₇ O₅ S Zn, *ca* (C_{7.35} O Cl_{0.6}), M = 1146.57. Triclinic, space group P-1 (no. 2), a = 11.9069(2), b = 13.1286(2), c = 16.8124(3) Å, α = 93.5790(14), β = 99.1372(16), γ = 94.9061(14)°, V = 2577.55(8) Å³. Z = 2, D_c = 1.477 g cm⁻³, F(000) = 1181, T = 100(2) K, μ(Cu-Kα) = 19.8 cm⁻¹, λ(Cu-Kα) = 1.54184 Å.

The crystals were dark blue plates. From a sample under oil, one, *ca* 0.47 x 0.33 x 0.14 mm, was mounted on a small loop and fixed in the cold nitrogen stream on a Rigaku Oxford Diffraction XtaLAB Synergy diffractometer, equipped with Cu-Kα radiation, HyPix detector and mirror monochromator. Intensity data were measured by thin-slice ω-scans. Total no. of reflections recorded, to θ_{max} = 70.0°, was 32,335 of which 9,608 were unique (R_{int} = 0.058); 8121 were 'observed' with I > 2σ_I.

Data were processed using the CrysAlisPro-CCD and -RED (1) programs. The structure was determined by the intrinsic phasing routines in the SHELXT program (2A) and refined by full-matrix least-squares methods, on F²'s, in SHELXL (2B). The principal molecule was clearly defined and refined well; in addition, there were disordered CH₂Cl₂ molecules and other unidentified molecules in the cell. In the principal molecule, the non-hydrogen atoms were refined with anisotropic thermal parameters; the remaining atoms were mostly refined isotropically. Hydrogen atoms were included in idealised positions and their U_{iso} values were set to ride on the U_{eq} values of the parent carbon atoms. At the conclusion of the refinement, wR₂ = 0.182 and R₁ = 0.071 (2B) for all 9608 reflections weighted w = [σ²(F_o²) + (0.1243 P)² + 3.968 P]⁻¹ with P = (F_o² + 2F_c²)/3; for the 'observed' data only, R₁ = 0.062.

In the final difference map, the highest peak (*ca* 1.0 eÅ⁻³) was near H(13c).

Scattering factors for neutral atoms were taken from reference (3). Computer programs used in this analysis have been noted above, and were run through WinGX (4) on a Dell Optiplex 780 PC at the University of East Anglia.

Legends for Figures

Figure 1. View of the principal molecule, Zn-porph-like complex, indicating the atom numbering scheme. Thermal ellipsoids are drawn at the 30% probability level.

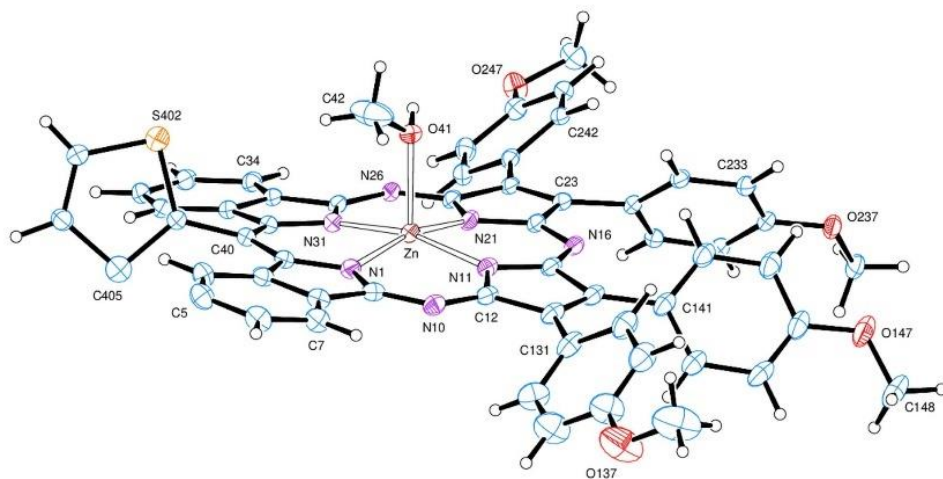
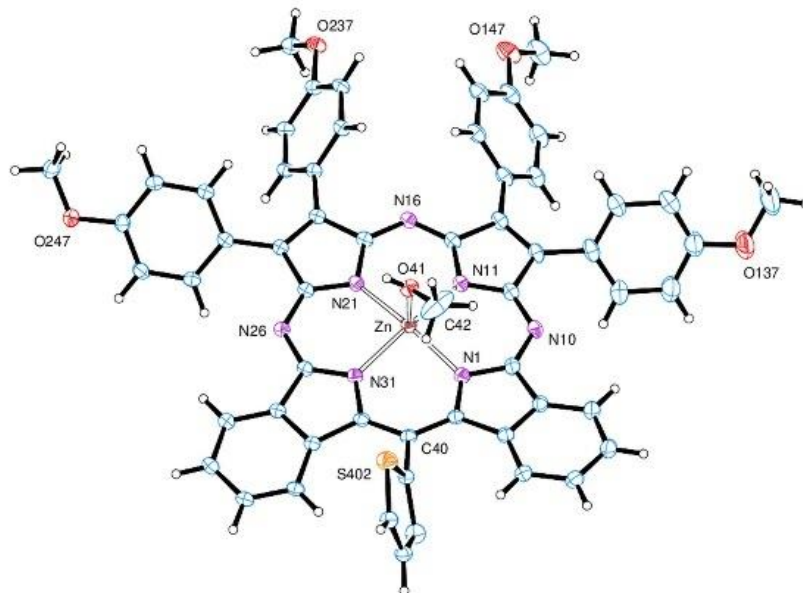


Figure 2. The packing of molecules, viewed along the *b* axis.



Notes on the structure

The principal molecule in this structure is almost as expected, with a methanol molecule attached in the apical site of the square pyramidal coordination pattern about the zinc atom, Figure 1. The central 16-membered has a slightly wavy shape about the zinc atom, with C(40) displaced 0.215(4) Å from the mean-plane of the four coordinated N atoms. There is a pseudo-mirror plane through the Zn, O(41), N(16) and C(40) atoms; the tilting of the methoxyphenyl rings and the orientation of the methoxy groups are related across this plane.

There appears to be some disorder in the thiophene group; the sulphur atom S(402) has typical S-C and C-S-C dimensions, viz 1.702(3) and 1.670(3) Å and 92.72(16)°. The thermal parameters of C(405) were smaller than expected, but gave more acceptable values when this atom was considered disordered between the C atom and an S atom at the same site; site occupancies for these atoms refined to 0.719(8) and 0.281(8). There is presumably a similar disorder at S(402), but this has not been examined, the smaller carbon atom having less influence on the overall geometry here.

The OH group of the coordinated MeOH molecule is directed towards the axis of the phenyl group of C(231-236) of a neighbouring molecule; the O-H bond appears short, at 0.70(4) Å but the H...C distances to C(233') and C(234') are also short at 2.67 and 2.68 Å.

There is also disorder in the 'solvent region' of this structure, mostly unresolved. We believe that most of the molecules in this region are disordered CH₂Cl₂; two major difference peaks were identified as chlorine atoms, and there are clusters of smaller peaks which might also be chlorine atoms. Also, on the periphery of these molecules there is a distinct five-membered ring, possibly of a thiophene molecule; this, however, appears uncomfortably close to C(42) of the coordinated MeOH molecule, with C(81)...C(42) at 1.510 Å.

References

- (1) Programs CrysAlisPro, Rigaku Oxford Diffraction Ltd., Abingdon, UK (2018).
- (2) G. M. Sheldrick, Programs for crystal structure determination (SHELXT), *Acta Cryst.* (2015) **A71**, 3-8, and refinement (SHELXL), *Acta Cryst.* (2008) **A64**, 112-122 and (2015) **C71**, 3-8.
- (3) '*International Tables for X-ray Crystallography*', Kluwer Academic Publishers, Dordrecht (1992). Vol. C, pp. 500, 219 and 193.
- (4) L. J. Farrugia, *J. Appl. Cryst.* (2012) **45**, 849–854.